Role of the immune system during the development of acute and chronic renal disease

Amy Fearn

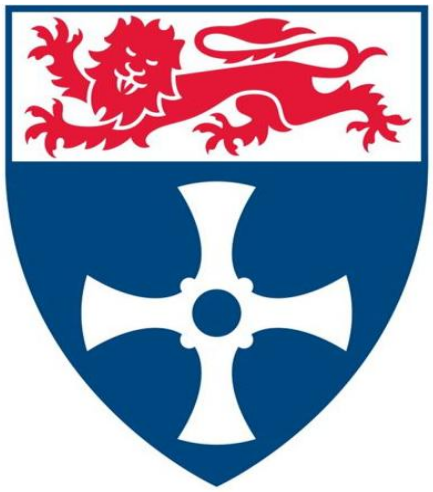

Institute of Cellular Medicine
Newcastle University

A thesis submitted in fulfilment of the
requirements for the degree of Doctor of Philosophy

March 2013

Acknowledgements

Firstly, I would like to thank my supervisor, Professor Neil Sheerin for giving me the opportunity to pursue a Ph.D. during my time working for him at Newcastle University. The encouragement, guidance, advice and support that I received from Neil during the last five years (in addition to my evenings, weekends and holiday days spent in the lab and in front of the computer producing this thesis), helped to make this thesis possible. I would also like to thank Neil for assisting me with the UUO surgeries, NTS injections and for his expert glomerular injury scoring and neutrophil counting in chapter five of this thesis. In addition, I am very grateful for the research funding, which was provided by Northern Counties Kidney Research.

I would also like to thank Professor Derek Mann and Dr Fiona Oakley for providing the *nfκb1*$^{-/-}$ mice and some of the primers used in this study as well as their input and advice on all things relating to the vastness that is NF-κB. I am also grateful to Dr Mike Robson for providing the steady supply of NTS used both in this study and for the additional research work arising from part of this study which is still ongoing in the lab today.

I thank Christopher Fox for assisting me with some of the UUO surgeries and for thoroughly checking (and subsequently assisting with the amendment of) some of the experimental methodology contained within this thesis. Thanks also for advice on current complement-related NF-κB literature. Your attention to detail and thorough planning always keeps me on my toes in the world of science! I also thank Dr Victoria Ingram for her assistance with UUO surgeries and the London group for their help with the C5a ELISA experiments.

I am particularly grateful to Dr Luca Ermini for his teaching and help with all things statistical. This has significantly helped to increase my understanding and application of statistics in scientific research ($p<0.05$)! I also thank my work colleagues (in order of chronological appearance) Dr Luca Ermini, Christopher Fox, Lucy Bates and Dr Ian Logan for all of their input and support during my Ph.D. studies and for the welcome distractions of regular visits to Costa, pineapple buns, cavies and Kings of Pastry!

I thank Professor John Kirby and Dr Kevin Marchbank for their input and guidance during the internal assessment stages of my Ph.D. I also thank Dr Alison Tyson-Capper for always making the time to listen to any Ph.D. related concerns, for enduring the reading of this colossal thesis and for finding a suitable location for my Ph.D. viva, in her capacity as internal examiner. As well, I thank my external examiner Dr Mark Dockrell for his many hours traversing the country to attend my viva examination during the most appalling of weather conditions.

Finally, I thank all of my close friends and loved ones for their emotional support and for providing kindness in many forms, including; homeopathy, massage, food, long chats, gin, cavies, tax returns, a roof over my head, phone calls at all hours, dragging me away from the writing for breaks, hugs and unexpected visits bearing cake. Thank you (ever so much) for still being around despite my frequent bouts of tiredness, grumpiness and asocial tendencies. ☺

Table of Contents

Abbreviations

ACE	Angiotensin-converting enzyme
a-GBM	Anti-glomerular basement membrane
AN	Adriamycin nephropathy
ANG II	Angiotensin II
BCIP	5-bromo-4-chloro-3'-indolyphosphate
BSA	Bovine serum albumin
BUMPT	Boston University Mouse Proximal Tubule
$C1qa^{-/-}$	Complement 1qa deficient
C3	Complement 3
$C3^{-/-}$	Complement 3 knock out
$C3aR^{-/-}$	C3a Receptor deficient
C4bp	Complement 4 binding protein
C57BL/6	C57 Black 6
$C6^{-}$	Complement 6 deficient
$C6^{+}$	Complement 6 sufficient
$CD59a^{-/-}$	CD59a deficient
cDNA	Copy deoxyribonucleic acid
cDNA	Complementary deoxyribonucleic acid
CKD	Chronic kidney disease
CR1	Complement receptor 1
CR2	Complement receptor 2
Crry	Complement receptor-1 related protein-y
C_T	Cycle threshold
CVD	Cardio-vascular disease
DAB	Diaminobenzidine
Daf-1	Decay accelerating factor-1
ddH_2O	Double distilled water
DEPC	Diethylpyrocarbonate
DIG	Digoxygennin
DMEM	Dulbecco's Modified Eagle's Medium
DMSO	Dimethylsulfoxide

DNA	Deoxyribonucleic acid
dsDNA	Double stranded deoxyribonucleic acid
ECM	Extracellular matrix
EDTA	Ethlyenediaminetetraacetic acid
eGFR	Estimated glomerular filtration rate
EMT	Epithelial mesenchymal transition
ESRD	End-stage renal disease
ESRF	End-stage renal failure
FB	Factor B
$FB^{-/-}$	Factor B deficient
FCS	Foetal calf serum
FD	Factor D
$FD^{-/-}$	Factor D deficient
FH	Factor H
FI	Factor I
FITC	Fluorescein isothiocyanate
FRMD7	FERM domain-containing protein 7
GBM	Glomerular basement membrane
GFR	Glomerular filtration rate
GN	Glomerular nephritis
HPF	High-powered field
HRP	Horseradish peroxidase
IHC	Immunohistochemistry
IKK	Inhibitory kappa-B kinase
IL-1β	Interleukin-1 beta
IL-6	Interleukin-6
IL-8	Interleukin-8
IRI	Ischaemia reperfusion injury
IκB	Inhibitory kappa-B
JNK	c-jun terminal kinase
KDOQI	National Kidney Foundation Disease Outcomes Quality Initiative
LPS	Lipopolysaccharide
MAC	Membrane attack complex

MBL	Mannose-binding lectin
MCP	Membrane cofactor protein
MCP-1	Monocyte chemoattractant protein 1
MOPS	3-(N-morpholino) propanesulfonic acid
mRNA	Messenger ribonucleic acid
NBT	Nitroblue tetrazolium
NEMO	Nuclear factor kappa-B essential modifier
NF-κB	Nuclear factor kappa-B
nfκb1$^{-/-}$	Nuclear factor kappa-B1 knock out
NIK	Nuclear factor kappa-B inducing kinase
NLS	Nuclear localisation sequence
NTS	Nephrotoxic serum
ObN	Obstructive nephropathy
OD	Optical density
PAS	Periodic acid Schiff's
PBS	Phosophate buffered saline
PBST	Phosophate buffered saline-Tween 20
PCR	Polymerase chain reaction
PDCT	Pyrrodidine dithiocarbonate
PMN	Polymorphonuclear
PTEC	Proximal tubular epithelial cell
RHD	Rel homology domain
RIP	Receptor interacting protein
RNA	Ribonucleic acid
ROI(s)	Region(s) of interest
ROS	Reactive oxygen species
RRT	Renal replacement therapy
RT	Room temperature
rtPCR	Real-time polymerase chain reaction
siRNA	Small interfering ribonucleic acid
SS	Two serine residues
SSC	Saline sodium citrate
ssRNA	Single stranded ribonucleic acid

TAD	Transcription activation domain
TBE	Tris-Boric acid EDTA
TGF-β	Tumour growth factor-beta
T_H	T helper
TNFR	Tumour necrosis factor receptor
TNF-α	Tumour necrosis factor-alpha
TRAF	Tumour necrosis factor receptor associated factor
UUO	Unilateral ureteric obstruction
VCAM	Vascular cell adhesion molecule
VSMC	Vascular smooth muscle cell
WT	Wild type
α-SMA	Alpha-smooth muscle actin

Abstract

The purpose of this thesis was to investigate the contribution of the inflammatory mediators Nuclear factor κB and complement during the progression of renal diseases. The first two results chapters in this thesis demonstrated a novel role for complement component 3 (C3) during the progression of chronic renal disease in the murine model of unilateral ureteric obstruction (UUO) C3 gene up-regulation and complement activation persisted throughout the course of UUO in wild type (WT) mice. *In situ* hybridisation showed that renal tubular epithelial cells were the primary site of C3 gene expression during early ureteric obstruction in the renal cortices of WT mice. Gene expression for transforming growth factor-beta (TGF-β) and collagen I in obstructed C3 deficient ($C3^{-/-}$) mouse kidneys was significantly reduced compared with obstructed kidneys from WT mice. The decrease in TGF-β and collagen I also coincided with a significant reduction in mRNA expression for alpha-smooth muscle actin (α-SMA) as well as a significant decrease in interstitial collagen deposition. In addition to these observations, the number of infiltrating $CD8^{+}$ T cells and $F4/80^{+}$ macrophages counted within the cortical tubulointerstitial compartment, was significantly higher in $C3^{-/-}$ mice.

Gene expression for the membrane-bound complement regulatory proteins complement receptor-related protein-y (crry), CD59a and decay accelerating factor 1 (DAF1) decreased in WT and $C3^{-/-}$ mice during the course of UUO. In particular, crry, CD59a and DAF1 mRNA expression was found to be much lower in $C3^{-/-}$ mice. A transition from membrane to cytoplasmic expression of crry protein was also demonstrated in tubular epithelial cells of obstructed WT mouse kidneys. In contrast to this, factor H gene expression was markedly elevated in WT mice, but not in $C3^{-/-}$ mice.

In vitro stimulation of mouse proximal tubular cells using lipopolysaccharide (LPS) resulted in complement activation, C3 gene up-regulation and production of C3 protein, providing an *in vitro* model to use for future targeting of proximal tubular epithelial cell C3 gene expression.

The final results chapter of this thesis demonstrated an important role for nuclear factor kappa-B (NF-κB) subunit nfκb1 during the progression of renal inflammation in the nephrotoxic serum nephritis model of acute renal injury. nfκb1 deficient mice developed significantly worse glomerular injury and proteinuria and displayed sustained up-regulation of interleukin-6 and S100 calcium binding proteins A8 and A9. Finally, in contrast to observations in the nephrotoxic serum model, fibrosis, immune cell infiltration and cytokine mRNA expression were all unchanged in nfκb1 deficient mice compared with WT mice after ten days of ureteric obstruction.

Index of Figures

Index of Tables

1 Introduction

1.1 The urinary tract

1.1.1 General anatomy of the kidney

The kidneys are paired lobular organs weighing 120-170g in adults. They are situated on the posterior abdominal wall either side of the vertebral column, with the right kidney normally lower than the left. Each kidney is covered in a thin uniform capsule which is surrounded by adipose tissue contained within the renal fascia. The kidney can be divided into two distinct regions, the cortex and the medulla. The medulla is made up of a number of renal pyramids, which then project into the renal pelvis (Figure 1.1).

1.1.2 The nephron

The basic functional unit of the kidney is the nephron and there are approximately one million nephrons in a human kidney. Each nephron consists of a cortical Bowman's capsule containing the glomerulus which then connects to a system of tubules delivering urine to the collecting ducts (Figure 1.2). The glomerulus itself is made up of a network of capillaries supplied by the afferent arteriole. The fenestrated endothelium, specialised endothelial basement membrane and epithelial podocytes of the glomerular capillaries allow selective ultrafiltration according to size and charge (Figure 1.3). Following passage through the glomerulus, the filtrate enters the tubular system and is subsequently modified by re-absorption and secretory processes.

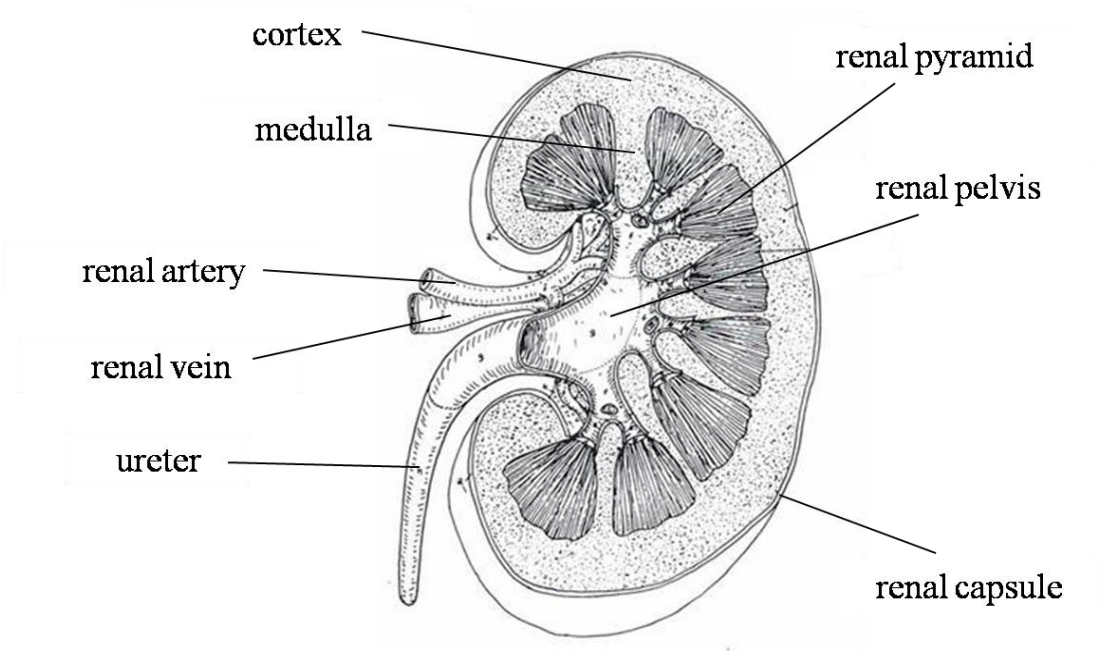

Figure 1.1. General anatomy of the kidney
Extracted from http://www.d.umn.edu

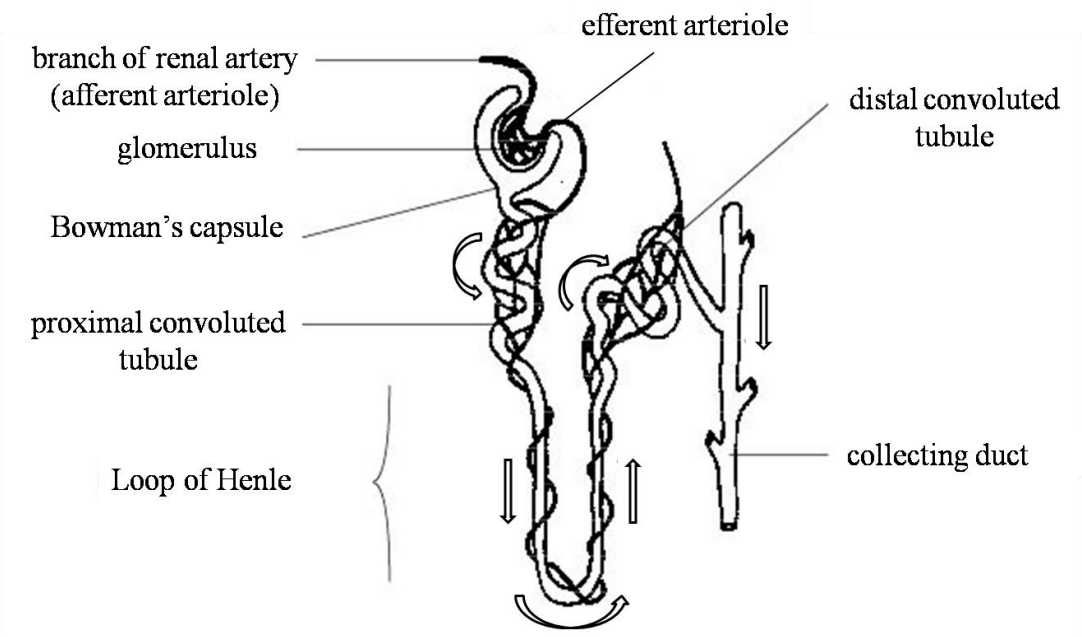

Figure 1.2. Structure of an individual nephron
Extracted from http://wikieducator.org

The tubular system is divided into functionally distinct regions known as the proximal tubule, loop of Henle, the distal tubule and collecting duct, each region differing functionally, structurally and cytologically. Re-absorption is enhanced by increased surface area due to the presence of cellular microvilli forming a characteristic apical brush border. The urine is then concentrated at the loop of Henle and collecting ducts before reaching the renal pelvis.

1.1.3 The ureters

The ureters originate from the renal pelvis of each kidney (Figure 1.1). Their structure consists of a hollow muscular tube lined with transitional epithelial cells and their function is to facilitate the movement of urine from kidney to bladder by ureteric peristalsis.

1.1.4 The bladder

The bladder is a highly distensible structure responsible for the short-term storage of urine. The wall of the bladder is made up of smooth muscle bundles and the lumen is lined with a multi-layered transitional epithelium attached to the bladder wall via a thin basement membrane. The upper layer of differentiated epithelial cells, secrete uroplakins to their apical surface which serve to strengthen the underlying epithelium and provide an impermeable barrier.

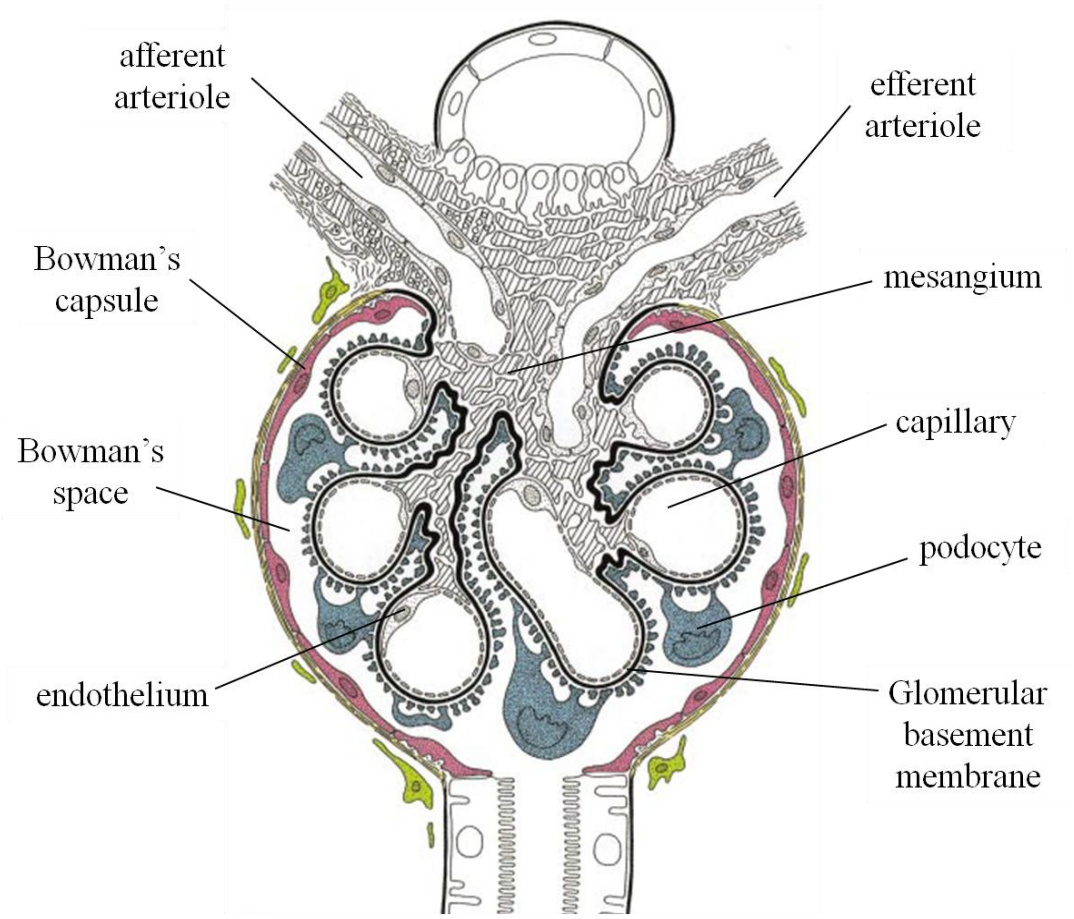

Figure 1.3. Anatomy of the glomerulus
Extracted from (Kriz et al., 1998).

1.1.5 Renal function

The kidney plays an important role in the maintenance of extracellular fluid and electrolyte homeostasis. This is achieved by ultrafiltration of blood plasma followed by the active and passive re-absorption of solutes along each distinct segment of the nephron. The kidney functions to excrete waste products, drugs and excess acid. It is also involved in the metabolism of small proteins and vitamin D as well as the production of erythropoietin and prostaglandins.

1.2 Chronic kidney disease

Chronic kidney disease (CKD) is a general term applied to an array of heterogeneous disorders affecting renal structure and function and is becoming increasingly recognised worldwide as a major public health problem. It is often asymptomatic and therefore not usually detected until later during disease progression. In the clinic, CKD is detected by testing for the presence of proteinuria or haematuria and by using serum creatinine to estimate glomerular filtration rate (Levey and Coresh, 2012). CKD is diagnosed when structural and functional abnormalities persist for >3 months and is categorised into five stages of increasing disease severity according to remaining kidney function; (Table 1.1; (Cirillo, 2010)). When remaining kidney function becomes insufficient to maintain homeostasis, renal failure occurs. Patients with end stage renal disease (ESRD) require renal replacement therapy (RRT) in the form of either dialysis or transplantation to survive. Over the last 20 years, the number of patients diagnosed with ESRD has continued to escalate, thereby increasing the cost of providing RRT (Zoccali et al., 2010; Zhang and Rothenbacher, 2008).

Stage	Description	eGFR (mL/min/1.73m^2)
1	Kidney damage with normal or raised GFR	>90
2	Kidney damage with mildly reduced GFR	60-89
3	Moderately reduced GFR	30-59
4	Severe reduction in GFR	15-29
5	Kidney failure	<15

Table 1.1. National kidney foundation KDOQI staging for CKD
Glomerular filtration rate (GFR). Extracted from Stevens et al., 2007

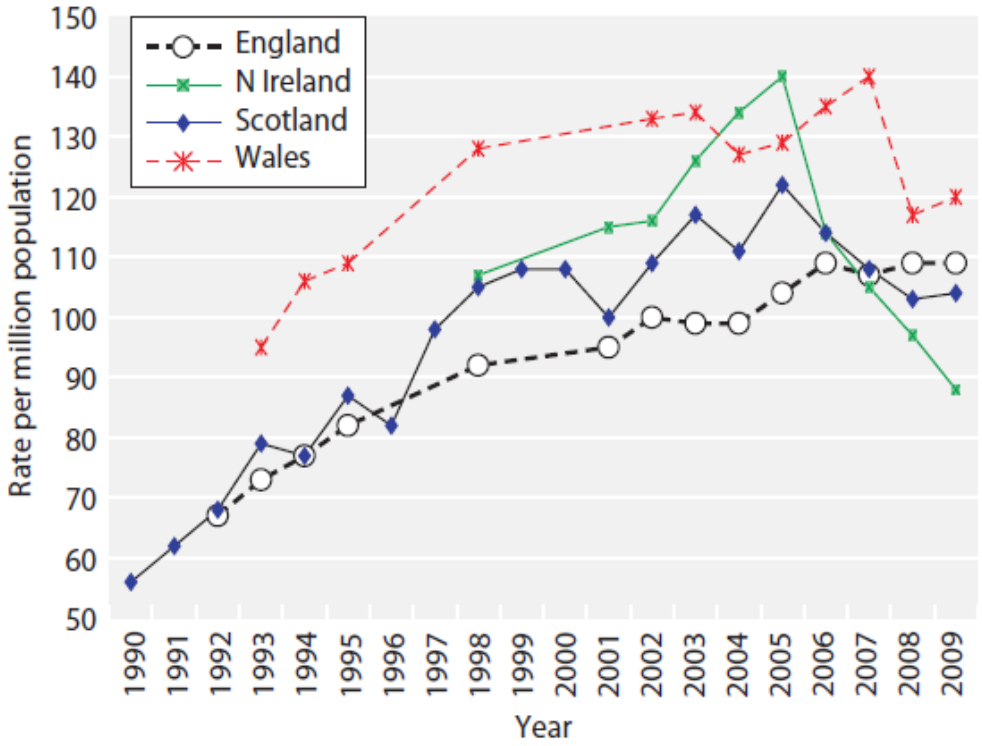

Figure 1.4. RRT incident rates in countries of the UK 1990-2009
Renal replacement therapy (RRT). Extracted from the UK Renal Registry 13th Annual Report 2010 (Caskey et al., 2011).

1.2.1 Prevalence of CKD

According to a large primary care study in 2007 the UK age-standardised prevalence of CKD stages 3-5 was 8.5% (10.6% in females and 5.8% in males; (Stevens et al., 2007)). In 2009, the number of new patients requiring RRT was 6,730 in the UK, equating to 109 patients per million population (Figure 1.4). The number of UK patients requiring some form of RRT has increased from approximately 7000 patients in 1982 up to almost 50,000 patients in 2009 and currently costs the NHS an estimated £30,000/patient/year (Figure 1.5). Research into CKD has intensified during the last 10 years and it is widely believed that early detection could delay or even prevent progression towards renal failure (Anderson and Glynn, 2011; Caskey et al., 2011).

1.2.2 Causes of CKD

In 2010, a national analysis of patients beginning RRT in the UK reported that diabetes and glomerulonephritis were the first two primary renal diagnoses, of which diabetic nephropathy was the most common, accounting for 25% of all incident diagnoses (Table 1.2; (Caskey et al., 2011)). Other research has suggested that co-morbidities such as hypertension, diabetes and obesity can significantly increase the chances of developing CKD (Levey et al., 2010). Diabetes mellitus is a chronic metabolic condition characterised by high blood sugar (hyperglycaemia) and is caused by either a resistance to or a deficiency of the hormone insulin. Prolonged hyperglycaemia leads to microangiopathy of small blood vessels, of which the glomerular arterioles are particularly susceptible.

Over time, glomerulosclerosis develops in many diabetic patients leading to proteinuria and progression toward ESRD (Levey et al., 2010). Glomerulonephritis (GN) is the general term ascribed to a group of different diseases targeting both kidneys, causing inflammation of the glomerulus and reduced renal function. It is characterised by the presence of haematuria and proteinuria and may have either primary (intrinsic) or secondary (systemic) causes (Vassalotti et al., 2007). Progression towards ESRD is often unavoidable, but the rate at which this occurs varies depending on the type of disease. CKD has been shown to have an inter-relationship with other diseases and is itself a risk factor for clinical complications and death from other chronic diseases and infections. A study by Levey and Coresh demonstrated that patients diagnosed with CKD (particularly the elderly) have an increased risk of cardiovascular complications (Levey and Coresh, 2012). The same study also showed that the risk of death arising from cardiovascular disease (CVD) in patients diagnosed with ESRD increased by 100 times. Another study showed that patients diagnosed with CKD at stages 4-5 had a 2-4 times greater risk of death (Zoccali et al., 2010).

1.2.3 End stage renal disease

It is well known that renal function is correlated to kidney architecture and the replacement of functioning nephrons with fibrotic scar tissue remains a strong indicator of renal disease progression in the clinical setting.

In healthy renal biopsies, tubules exist in close proximity to one another and are surrounded by a sparse extracellular matrix (ECM). ESRD is defined by the presence of extensive interstitial fibrosis (characterised by the deposition of collagen), infiltrating leukocytes and tubular atrophy. Patients diagnosed with ESRD have an estimated glomerular filtration rate (eGFR; mL/min/1.73m^2) of <15 and require RRT or a kidney transplant to survive.

1.3 Animal models of experimental renal injury

Animal models of experimental renal injury have been developed over time and are used to mimic the progression of numerous acute and chronic renal diseases encountered in the clinical setting. They are important for studying the mechanisms of renal fibrosis and provide a better understanding of the preceding pathophysiological events; assisting with the development of improved therapeutic interventions to help preserve renal function.

1.3.1 Obstructive nephropathy

Obstructive nephropathy (ObN) is a relatively common renal disease caused by the impaired flow of urine, resulting in hydronephrosis and tubulointerstitial injury. It is induced by the presence of functional or structural changes within the urinary tract that prevent the normal flow of urine. ObN can affect patients of all ages.

Diagnosis	Age <65	Age ⩾65	All patients	M:F
Diabetes	27.3	23.2	25.3	1.5
Glomerulonephritis	16.0	6.9	11.5	2.2
Pyelonephritis	7.1	7.6	7.3	1.4
Hypertension	6.0	7.9	6.9	2.0
Polycystic kidney	10.2	3.1	6.7	0.8
Renal vascular disease	2.0	10.4	6.1	2.0
Other	16.5	14.4	15.5	1.4
Uncertain aetiology*	15.0	26.6	20.7	1.8

Table 1.2. Primary renal diagnosis
Incidence rates per million population (2009), *includes presumed glomerulonephritis not biopsy proven.
Extracted from the UK Renal Registry 13th Annual Report 2010 (Caskey et al., 2011).

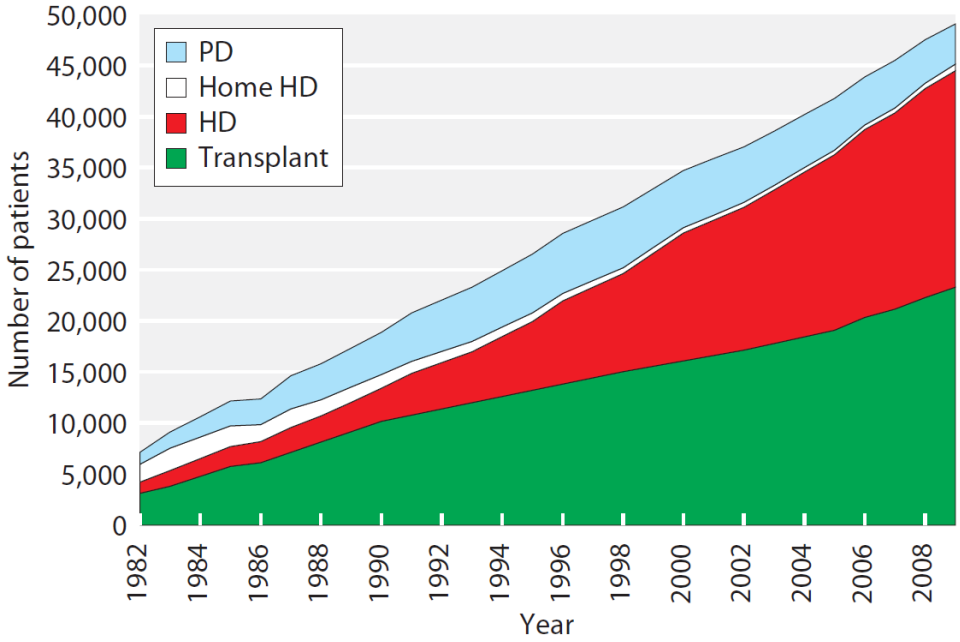

Figure 1.5. Growth in prevalent patients by treatment modality
Extracted from the UK Renal Registry 13th Annual Report 2010 (Caskey et al., 2011).

It may be asymptomatic, or present with a range of clinical symptoms such as hypertension, acute and chronic renal failure or an enlarged kidney (Klahr, 2000). The characteristic pathophysiological events of ObN include renal vasoconstriction, interstitial infiltration of macrophages and T cells, interstitial accumulation of ECM proteins, proliferation of intrinsic renal calls and eventual tubular cell atrophy (Guo et al., 2001; Truong et al., 1996).

The unilateral ureteric obstruction (UUO) experimental model of chronic renal injury is induced by surgical ligation of a single ureter (Klahr and Purkerson, 1994; Kuncio et al., 1991). It is a well characterised model of renal disease which is commonly used for studying the mechanisms of renal inflammation and fibrosis and to evaluate potential therapeutic approaches towards improving the outcome of renal disease (Wang et al., 2005a; Yang and Liu, 2002; Satoh et al., 2001). This model is characterised by the gradual development of interstitial inflammation and fibrosis, macrophage, T cell and fibroblast infiltration and eventual loss of functioning nephrons. Both infiltrating immune cells and resident renal cells are thought to be the source of pro-inflammatory and pro-fibrotic cytokine generation during ureteric obstruction.

1.3.2 Nephrotoxic serum nephritis

Anti-glomerular basement membrane (a-GBM) nephropathy is a rare but destructive glomerular disease caused by IgG antibodies which target and disrupt the α3 chain of type IV collagen present within the capillary walls of the GBM of the kidney.

Onset of disease is rapid and affected patients present with acute renal failure, haematuria, oedema and on biopsy have a crescentic glomerulonephritis. Occasionally the a-GBM antibody also targets the pulmonary alveolar basement membrane in a rare condition known as Goodpasteure's syndrome. Patients affected in this way present with concomitant pulmonary haemorrhage in addition to acute renal failure. Nephrotoxic serum (NTS) nephritis is an experimental model of renal injury used to study the development and progression of antibody-mediated glomerular injury. Nephrotoxic serum contains an anti-collagen antibody which binds to the GBM and induces a cascade of complement-mediated injury. In this model, renal injury following NTS injection is characterised by rapid neutrophil infiltration followed by glomerular thrombosis and proteinuria (Chen et al., 2002; Hebert et al., 1998).

1.4 Tubulointerstitial inflammation and fibrosis

The cortical region of the kidney is comprised of the tubulointerstitium (around 90%) and the glomeruli (remaining 10%). The tubulointerstitial compartment contains predominantly tubular epithelial cells, but also a small number of quiescent fibroblasts and immune cells. Tubulointerstitial inflammation and fibrosis is a major factor in the progressive loss of renal function in a variety of kidney diseases, including glomerulonephritis, chronic allograft nephropathy and ObN (Harris and Neilson, 2006). The process itself is particularly complex due to the number of interacting pathways which ultimately result in the replacement of functioning nephrons with scar tissue.

1.4.1 Mediators of inflammation and fibrosis during renal injury

Cellular stress and injury result in the generation of inflammatory and fibrogenic mediators including growth factors and pro-inflammatory cytokines as well as activation of the renin-angiotensin system.

1.4.1.1 Renin-angiotensin system

The progression of a number of renal diseases toward end-stage renal failure (ESRF) is driven by the multiple effects of angiotensin-II (ANG II). Following ureteric ligation, there is an alteration in renal haemodynamics resulting in significant vasoconstriction of the renal vasculature. These changes in renal blood flow are mediated by ANG II via the AT_1 receptor (Klahr and Morrissey, 2002b; Satoh et al., 2001). Angiotensinogen gene expression (a precursor to angiotensin) is stimulated by nuclear factor-κB (NF-κB). Other effects of ANG II are illustrated in Figure 1.6 (Guo et al., 2001; Klahr and Morrissey, 1998).

1.4.1.2 Pro-inflammatory cytokines

Numerous cytokines have been inferred in the progression of inflammation during renal disease. One of the most widely studied acute phase pro-inflammatory cytokines is tumour necrosis factor-α (TNF-α). Following its discovery, it was initially thought to be exclusively produced by macrophages; however fibroblasts and endothelial cells have since demonstrated their capacity to produce TNF-α in response to stimuli such as interleukins and bacterial LPS.

TNF-α mediates inflammation by binding to one of its specific TNF-α receptors (TNFR1 or TNFR2), subsequently inducing activation of a distinct cell signalling pathway, including the NF-κB pathway (Figure 1.6; (Grande et al., 2010)). Depending upon which pathway is activated, TNF-α signalling is capable of eliciting cell survival, proliferation, differentiation and apoptosis. In animal models of ureteric obstruction, ANG II mediated NF-κB signalling contributes towards an early increase in TNF-α mRNA expression (Ucero et al., 2010). The resulting inflammatory environment then stimulates the production of chemoattractants such as monocyte chemoattractant protein 1 (MCP-1), causing macrophages to migrate into the renal interstitium. Further, TNF-α production by macrophages and resident renal cells contributes towards increasing infiltration of leukocytes and mediates cellular changes such as apoptosis and necrotic cell death (Misseri et al., 2005).

Rodent studies using angiotensin-converting enzyme (ACE) inhibitors and angiotensin receptor knock-out mice (Khalil et al., 2012; Klahr and Morrissey, 2002a; Ishidoya et al., 1996; Kaneto et al., 1994), have demonstrated that TNF-α production is mediated at least in part, by ANG II signalling (Esteban et al., 2004; Dinh et al., 2001). TNF-α signalling via TNFRs is also an important contributor towards tubulointerstitial inflammation and fibrosis during UUO. Mice lacking TNFR1 exhibit decreased NF-κB activation, reduced collagen deposition and fewer alpha-smooth muscle actin (α-SMA) positive interstitial myfibroblasts (Guo et al., 1999).

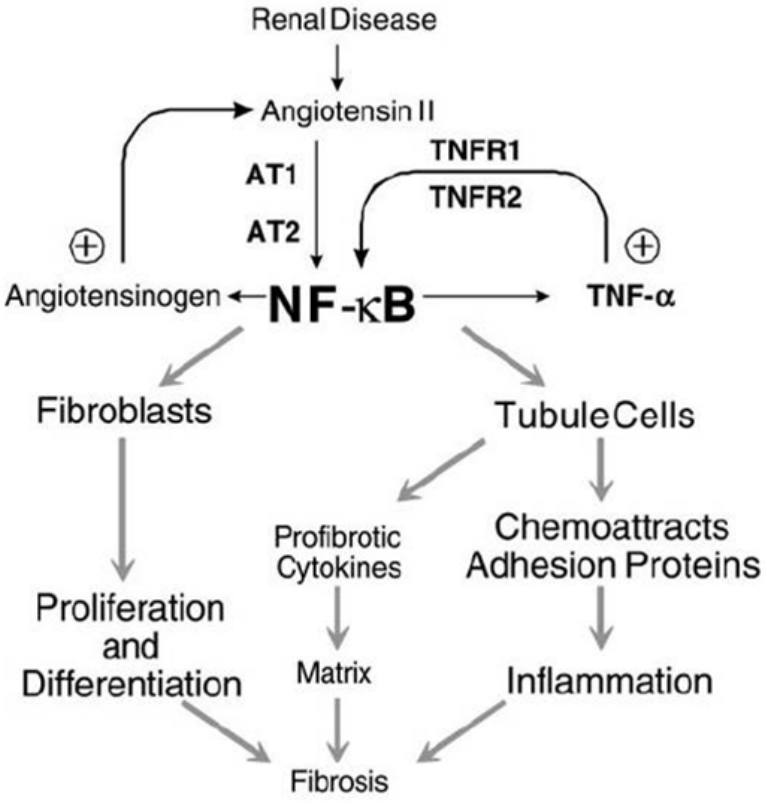

Figure 1.6. Angiotensin-II mediated activation of TNF-α and NF-κB
Taken from Klahr and Morrissey 2002.

Interleukin-6 (IL-6) is a pleiotropic cytokine that mediates the acute phase inflammatory response following tissue stress and trauma. It is produced by T cells, macrophages and endothelial cells and has an important role in T cell and B cell differentiation and the activation of other immune cells. IL-6 signalling pathways control the transcription of many proteins and may exert either pro or anti-inflammatory actions depending upon the nature of activation. A recent study by Zhang and co workers identified ANG II-mediated IL-6 signalling as a key contributor towards renal fibrosis in mice and demonstrated that IL-6 is mRNA also up-regulated in kidneys taken from CKD patients (Zhang et al., 2012). Earlier studies also showed that IL-6 receptor blockade significantly suppressed development of IgG class antibody autoimmune kidney disease and that production of IL-6 by macrophages in a mouse model of renal ischaemia reperfusion injury (IRI) exacerbated renal injury (Kielar et al., 2005). More recently, Buraczynska and co workers demonstrated a link between an IL-6 gene single nucleotide polymorphism and progression to ESRD in patients with chronic glomerulonephritis (Buraczynska et al., 2007).

1.4.1.3 Growth factors

There are several growth factors implicated in the development of tubulointerstitial fibrosis (Wang et al., 2005b; Bottinger and Bitzer, 2002; Yang and Liu, 2002). Perhaps the most important of these is Tumour growth factor-β (TGF- β). The role of TGF-β and its subsequent activation of down-stream signalling events leading to the progression of CKD have been investigated in detail (Oliver, 2002; Miyajima et al., 2000; Kaneto et al., 1999).

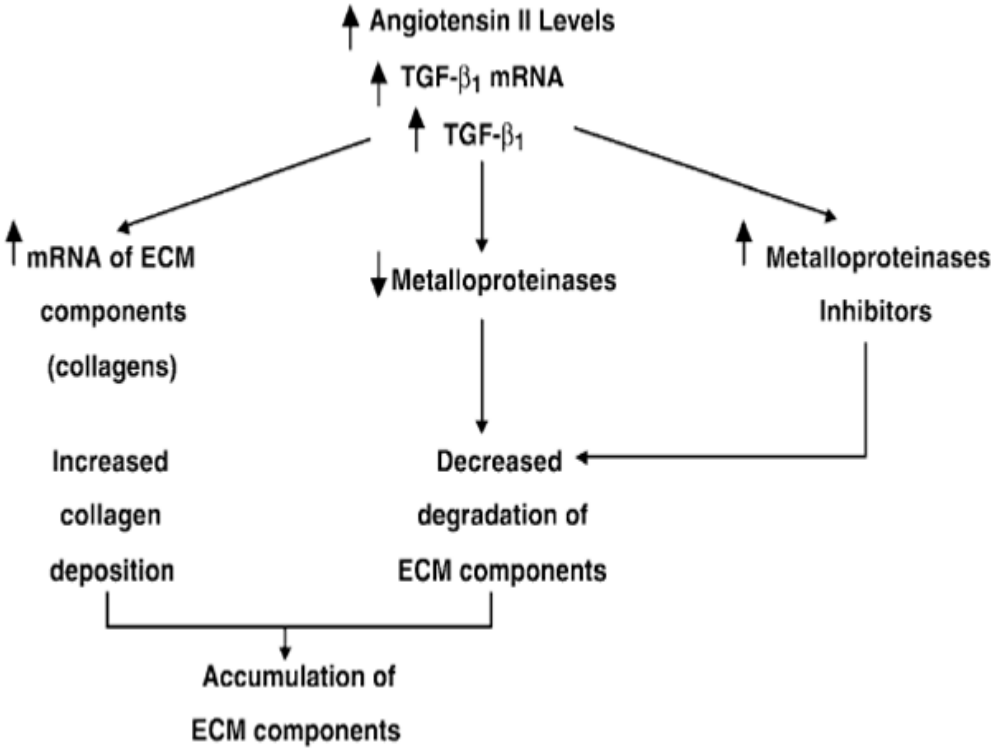

Figure 1.7. TGF-β mediated ECM deposition during renal injury
Taken from Klahr and Morrissey 2002.

TGF-β belongs to a multifunctional superfamily of regulatory cytokines produced in virtually all mammalian tissues. The TGF-β family of secreted peptides includes the three TGF-β isoforms (TGF-β1, -β2 and –β3), bone morphogenetic proteins (BMP) and activins. TGF-β isoforms are widely distributed and exert their effects on mammalian cells by ligand-induced activation of TGF-β receptors at the cell surface, triggering an intracellular signalling cascade of smad proteins. Depending on the physiological context of activation, smad proteins can directly influence the transcription of a number of different genes, including those associated with cellular homeostasis and development, apoptosis, immunological response and ECM re-modelling (Blobe et al., 2000). TGF-β1 plays an important role in inflammation by regulating the repair and regeneration of tissue following injury. It contributes to fibrogenesis through ECM re-modelling, fibroblast proliferation and migration, chemoattraction of macrophages and upregulation of gene expression for collagen, fibronectin, laminins and integrins (Grygielko et al., 2005).

1.4.2 The extracellular matrix

In the normal kidney, structural integrity and biological function are dependent upon a network of cellular and extracellular interactions. The ECM is an organised heterogeneous structure providing an architectural scaffold for cell-cell contact and cell-matrix adhesion (Kuncio et al., 1991; Lemley and Kriz, 1991). Alterations to the composition or topography of the ECM can have important consequences for normal functioning of nephrons and for the kidney as a whole. Fibrosis is characterised as the imbalance between ECM deposition and degradation and is a common histopathological feature of progressive renal diseases.

1.4.3 Source of renal fibroblasts in disease

A contributing factor to the progression of renal fibrosis is the proliferation of fibroblasts in the interstitial compartment. The precise origin of these fibroblasts remains controversial, though several mechanisms that may contribute towards their increasing numbers during fibrogenesis have been suggested (Iwano and Neilson, 2004). One hypothesis is that bone marrow derived cells (fibrocytes) circulate to peripheral organs where they act as progenitors for resident tissue fibroblasts (Bucala et al., 1994). A different hypothesis suggests that interstitial fibroblasts, resident in the normal kidney around blood vessels (pericytes), are stimulated to divide by the presence of cytokines and growth factors originating from injured renal epithelial cells (Klahr and Morrissey, 2002b; Strutz et al., 2000). These intrinsic renal fibroblasts subsequently transform into myofibroblasts during the early stages of injury and contribute to the development of renal fibrosis (Picard et al., 2008). Finally, there is the hypothesis that renal epithelial cells can themselves transdifferentiate into myofibroblasts by a process known as epithelial to mesenchymal transition (EMT; (Iwano et al., 2002; Strutz et al., 2002). This change from an epithelial to mesenchymal phenotype is thought to be driven by a number of different factors including TGF-β (Yang and Liu, 2002; Stahl and Felsen, 2001).

1.5 The role of the immune system during renal injury

Recently, excessive immune activation has been shown to play an important role in the development of tubulointerstitial injury. The pathophysiological events following ObN include infiltration of macrophages, monocytes and T-lymphocytes into areas of interstitium surrounding the renal tubules.

It has been suggested that following tubular injury, renal epithelial cells release inflammatory mediators and chemokines that in turn stimulate infiltration and proliferation of lymphocytes and macrophages in the affected area (Lange-Sperandio et al., 2002). $CD4^+$ lymphocytes have an important role in disease progression. In particular T helper 2 (T_H2) cells are strongly linked to the development of a pro-fibrotic phenotype (Wynn, 2004). In addition, T_H1 $CD4^+$ T-cells induce a potent inflammatory response by producing interferon-γ (IFN-γ). The direction of disease progression therefore depends upon the phenotype of the T_H response. $CD8^+$ T-lymphocytes play more of an effector role in that they may directly target native renal cells and induce phenotypic changes such as EMT or apoptosis (Robertson et al., 2004; Wynn, 2004). Knowledge surrounding the mechanism by which activation of invading lymphocytes takes place remains incomplete, but another area which may be of interest is the interaction between the adaptive and innate immune systems. A component of the innate immune system that may be important in this is the complement system, since complement is able to directly influence the adaptive immune response.

1.6 The complement system

The complement system is a biochemical cascade made up of approximately 30 serum and membrane-bound proteins which constitute almost 10% of all serum proteins and make up part of one of the major defence systems within the body, the innate immune system. Complement was identified in the late 19th century by German scientist Paul Ehrlich as a heat-labile blood serum component with non-specific antimicrobial activity. The heat-sensitive component observed by Ehrlich was named "complement" due to the observation that it complemented other elements of the immune system. As part of the innate immune system, the complement system responds rapidly to defend the host against a variety of invading microorganisms (Morgan and Walport, 1991). The complement system can also participate during the inductive phase of the acquired immune response by contributing to the recognition and presentation of non-self antigen, triggering B-cell activation, maturation and proliferation (Carroll, 2004; Nielsen et al., 2000). In addition to this, the complement system also plays a role in the solubilisation of immune complexes and the control of inflammatory reactions (Frank and Fries, 1991; Atkinson, 1988).

The components of the complement system exist as inactive pro-enzymes which require proteolytic cleavage in order to become biologically active. Regulatory molecules including; complement receptor 1 (CR1), membrane cofactor protein (MCP), decay accelerating factor (DAF), C4 binding protein (C4bp), Factor H (FH) and Factor I (FI), target complement activation to non-self targets to prevent damage to neighbouring host cells (Liszewski et al., 1996).

1.6.1 Complement production

The primary location for biosynthesis of complement is the liver. Although Erlich and Morgenroth suggested the liver as the main source of complement production in 1900, it was only confirmed by Alper and Rosen in recipient to donor allotype conversion during liver transplantations in 1976. Further support for this initial observation came from studies of primary human hepatocyte cultures, rodent hepatoma cell lines and the human hepatoma derived cell line HepG2 (Morris et al., 1982). In addition, at a similar time, studies supporting the extrahepatic synthesis of complement began to emerge and have continued to do so up to the present day. It is now widely acknowledged that extrahepatic complement synthesis contributes approximately 10% of circulating C3, the pivotal component of the complement cascade. These alternative sites for complement production include epithelial cells, fibroblasts, lymphocytes and macrophages derived from different organs, including the kidney (Naughton et al., 1996). In the kidney, local complement production has been shown to occur at different sites along the nephron and may be further enhanced by the presence of cytokines and infiltrating immune cells during acute infection (Sheerin et al., 1997; Sacks et al., 1993; Brooimans et al., 1991).

1.6.2 Activation of the complement system

Activation of the complement cascade is triggered by one of three distinct pathways: the classical pathway, the alternative pathway and the mannose-binding lectin (MBL) pathway (Figure 1.8). All three pathways converge to cleave complement component C3, which subsequently initiates activation of the terminal complement pathway and formation of the membrane attack complex (MAC).

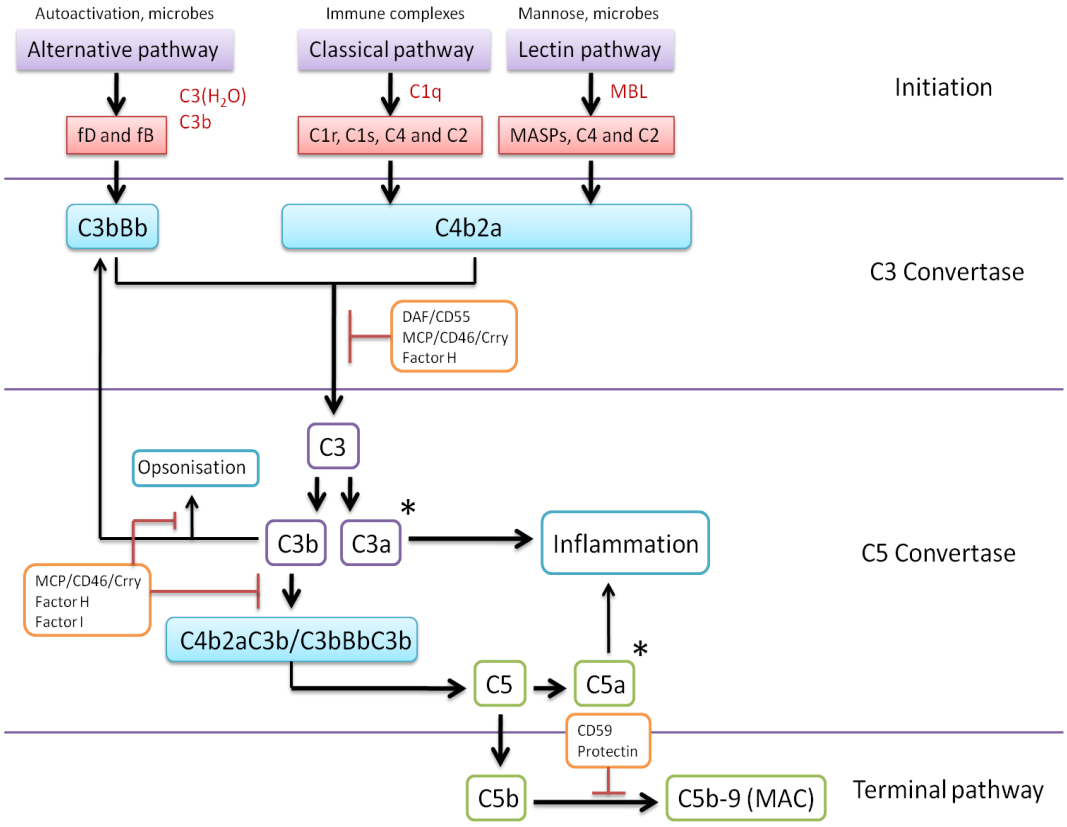

Figure 1.8. Complement activation pathways
Complement activation is triggered via activation of either the alternative, classical or lectin pathways, all three of which converge to cleave central component C3. Briefly, activation of the alternative pathway occurs following the spontaneous hydrolysis of C3 to C3(H_2O). C3(H_2O) binds factor B (FB) to form C3bB which is then cleaved by factor D (FD) leaving the C3bBb complex. C3bBb is stabilised by properdin to form the alternative pathway C3 convertase. C3 is subsequently cleaved to C3a and C3b to form the C5 convertase C3BbC3b. Activation of the classical complement pathway occurs when immunoglobulin-bound antigens bind to and activate the C1 complex (consisting of C1qr2s2). Activated C1qr2s2 cleaves C4 to C4a and C4b. C4b becomes membrane-bound and binds to pro-enzyme C2, which is then cleaved to C2a and C2b fragments by C1s. C2a remains bound to C4b, forming the classical C3 convertase C4b2a. C3 is cleaved to C3a and C3b to form the C5 convertase C4b2aC3b. The lectin complement pathway is homologous to the classical pathway, with the exception that it is activated by the binding of lectin to microbial cell surface carbohydrates (mannose). Surface-bound lectin activates MBL-associated serine proteases (MASPs), which directly activate C3 and directly cleave C2 and C4. Activation of the terminal complement pathway occurs when the alternative and classical C5 convertases C3bBbC3b or C4b2aC3b cleave C5 in to C5a and C5b. C5b binds to C6 and C7, forming C5b67, which associates with an adjacent membrane. C5b67 then binds to C8 and multiple C9 molecules forming the transmembrane pore C5b-9, also known as the MAC. *denotes the analphyatoxins C3a and C5a. Orange boxes highlight regulatory complement proteins.

1.6.2.1 The classical pathway

The classical pathway is initiated by the activation of the C1 complex (one molecule of the hexameric C1q and two molecules each of C1r and C1s forming C1qr2s2). Activation of C1qr2s2 usually occurs when C1q binds to IgG or IgM bound antigens, however activation may also occur independently of antibody in the presence of nucleic acids and damaged cellular components. Activated C1q undergoes a conformational change, inducing auto-activation of the pro-enzyme C1r which then cleaves the remaining C1s molecules. The activated C1qr2s2 molecule then cleaves C4 which releases a small C4a fragment and a large C4b fragment. The exposed thioester group in C4b is then able to bind covalently and irreversibly with membrane or activating surface amino or hydroxyl groups. In the presence of Mg^{2+} ions membrane-bound C4b is able to bind and present pro-enzyme C2. Bound C2 is cleaved to C2a and C2b fragments by adjacent C1s. The larger C2a fragment remains bound to C4b to form C4b2a, the classical pathway C3 convertase. C3 binds to the C2a part of C4b2a where it is cleaved, releasing the small C3a fragment. The exposed thioester bond on the remaining C3b fragment allows the binding of C3b to the C4b2a complex forming the C5 convertase C4b2a3b (Figure 1.8).

1.6.2.2 The alternative pathway

Activation of the alternative pathway is dependent on the spontaneous low level hydrolysis of the internal thioester bond of C3 to C3(H_2O). C3(H_2O) resembles C3b and can bind to factor B (FB). C3(H_2O)B or C3bB, is cleaved by factor D (FD), releasing the smaller fraction Ba.

The resulting complex is further stabilised by properdin, forming the alternative pathway C3 convertase C3bBb. C3bBb cleaves C3 to form C3a and C3b. Binding of C3b to C3bBb forms the alternative pathway C5 convertase C3bBbC3b. C3bBb is also able to cleave more C3 to C3b, creating a positive feedback loop and increasing deposition of C3b at the target surface. Bound C3b in turn acts as a receptor for C5 which is then cleaved by Bb in an adjacent C3bBb complex (Figure 1.8).

1.6.2.3 The lectin-binding pathway

The third complement activation pathway, the lectin-binding pathway, is homologous to the classical pathway except that it is activated by the binding of lectin to carbohydrates on microbial surfaces. Binding of lectin activates the MBL-associated serine proteases MASP-1 and MASP-2. MASP-1 is able to directly activate C3 and MASP-2 is able to directly cleave C2 and C4 (Figure 1.8; (Thiel et al., 1997)).

1.6.2.4 The terminal complement pathway

Complement components C6 and C7 bind to C5b, releasing C5b67 which is then able to form a stable association with an adjacent membrane, resulting in the binding of C8 and multiple C9 molecules. The C9 molecules associate with one another to form a barrel-like structure which traverses the membrane to form a C5b-9 pore also known as the MAC (Figure 1.8).

1.6.3 Consequences of complement activation

The main purpose of complement activation is to remove invading pathogenic organisms such as bacteria. This may be achieved directly through the formation of the MAC (sections 1.6.2.4 and 1.6.3.2) or indirectly via the activation of phagocytosis and removal of immune complexes.

1.6.3.1 Opsonisation

Opsonisation is important in the defence against infection. It involves the binding of IgG antibody or complement proteins to the surface of foreign particles such as micro-organisms, to facilitate their removal by phagocytosis (Ehlenberger and Nussenzweig, 1977). The major complement opsonin is activated C3 (C3b). C3b and the C3b breakdown product C3bi are recognised by the complement receptors CR1 and CR3 present on phagocytic cell membranes, leading to phagocytosis of the opsonised target.

1.6.3.2 Cell lysis

The complement-mediated direct killing of micro-organisms occurs via activation of the terminal complement pathway and subsequent formation of MAC (section 1.6.2.4). These membrane traversing barrel-like complexes are inserted into the lipid bi-layers of target cells to create pores allowing diffusion of cellular solutes and ions resulting in cell lysis.

1.6.3.3 Generation of anaphylatoxins

Complement activation results in cleavage of the complement proteins C3 and C5 to form the small, biologically active molecules C3a and C5a (Figure 1.8). These readily diffusible complement components have a variety of functions, including cellular chemotaxis during inflammation and the ability to stimulate release of histamine from mast cells. Their inflammatory effects are mediated by receptor specific binding to C3aR and C5aR (Wetsel, 1995).

1.6.3.4 Augmentation of the acquired immune response

Complement receptor 2 (CR2) provides one link between innate and acquired immunity. CR2 is present on B-cells and promotes their uptake of C3 opsonised antigen for processing and subsequent presentation to T-lymphocytes (Jacquiersarlin et al., 1995). It is also present on dendritic cells where it is able to interact with B-cells and allow the complement system to play a role in B-cell maturation (Fischer et al., 1998).

1.6.4 Regulation of complement

In humans, the complement system contains proteins which regulate it at different stages of activation (Figure 1.8). These regulatory proteins function to prevent uncontrolled activation of complement, maintain homeostasis, and prevent host damage by restricting the effects of complement to target antigen.

The regulators of complement activity are segregated into two distinct groups; fluid phase complement regulators (factor H, C4 binding protein, S-protein and clusterin) and membrane-bound regulators (CR1, MCP, DAF and CD59). Of the fluid phase regulators, S-protein and clusterin prevent MAC insertion by binding terminal complement components, thus preventing cell lysis. C4bp accelerates the dissociation of the C3 convertase during classical pathways activation. FH protects self-cells from complement activation by accelerating dissociation of the C3 convertase of the alternative pathway. FH also has co-factor activity for FI mediated C3b cleavage.

The membrane bound regulator CR1 acts on both alternative and classical pathway convertases through binding and subsequent dissociation. DAF prevents assembly of the C3 convertase C3bBb and can also accelerate the decay of pre-formed C3bBb, subsequently inhibiting formation of the MAC. CD59 (CD59a and CD59b isoforms in mice) inhibits formation of the MAC by binding to C5b678, preventing binding and polymerisation of C9. CD46 and CR1 in conjunction with FI, inhibit formation of the MAC by promoting enzymatic cleavage of C3b thus restricting C3/C5 convertase activity. FI cleaves both cell-bound and fluid phase C3b and C4b. In mice, CR1 related protein-y (crry), a membrane-bound complement regulator, inhibits classical and alternative complement pathways by binding to C3b and C4b. Crry-bound C3b and C4b is then cleaved by FI (Lesher and Song, 2010; Sjoberg et al., 2009; Zipfel and Skerka, 2009).

1.6.5 Complement receptors

The binding of complement components to specific receptors on target cells is important in mediating the variety of effects of the complement system including activation of phagocytosis and cell lysis, enhanced antibody responses, presentation of immune complexes and local inflammation. The specificities and properties of the main complement receptors are summarised in Table 1.3.

1.6.6 Complement in renal injury

1.6.6.1 Renal ischaemia reperfusion injury

Ischaemia reperfusion injury (IRI) occurs when tissues are temporarily deprived of a blood supply after which perfusion is restored eliciting an intense inflammatory response. IRI is common after tissue transplantation and is an important factor in determining graft survival. It is a common cause of acute renal failure in native kidneys and allografts and when present is associated with high mortality. Renal IRI causes activation and subsequent migration of neutrophils to the site of tissue injury and is also characterised by cytokine release, formation of reactive oxygen species (ROS), acute tubular necrosis and activation of complement. The role of complement during the progression of renal IRI has been debated for some time. Studies using $C3^{-/-}$ $C4^{-/-}$ and C6 deficient ($C6^{-}$) mice have demonstrated that $C3^{-/-}$ and $C6^{-}$ mice are significantly protected from IRI (Lien et al., 2003; Thurman et al., 2003). The contribution of locally produced C3 during IRI has been demonstrated *in vivo* (Zheng et al., 2006) and is discussed in more detail in section 1.6.6.3.

Receptor	Alternative name(s)	Location	Specificity	Role
CR1	CD35	Macrophages Neutrophils B-cells Some T-cells Renal epithelium	C3b C4b	Binding of opsonised immune complexes for transport to phagocytes
CR2	CD21	B-cells Some T-cells Dendritic cells Epithelia	C3d	Link between innate and acquired immune response on B-cells. Presentation of immune complexes to B-cells
CR3	CD11b/18	Macrophages Natural killer cells Neutrophils	iC3b	Cellular-extracellular matrix linkage. Promotes phagocytosis of opsonised complexes
CR4	CD11c	Macrophages Neutrophils	iC3b C3dg	Receptor for iC3b-opsonised particles
C3aR	-	Renal epithelium Macrophages Neutrophils	C3a	Mediation of inflammation
C5aR	-		C5a	
C1qR	-	Leukocytes Platelets Monocytes Neutrophils	Collagen	Up-regulation of phagocytic capacity Protein chaperone

Table 1.3. Properties of complement receptors
Adapted from Morgan and Harris 1999.

Further evidence for the involvement of the alternative complement pathway in IRI was provided in studies using FB deficient ($FB^{-/-}$) mice. 24 hours after reperfusion of $FB^{-/-}$ mice, serum urea nitrogen and infiltrating neutrophils were significantly lower and the levels of functional and morphological injury appeared less severe in comparison to FB sufficient mice. In addition, C3 and C9 staining was not present within renal tissues of $FB^{-/-}$ mice following IRI (Lien et al., 2003; Thurman et al., 2003). Other studies have performed IRI in rodents lacking components of the classical complement pathway and have not shown significant reductions in ischaemic injury. The ability to regulate formation of the MAC during complement activation appears to be of importance in renal IRI. A study in which mice deficient in CD59a ($CD59a^{-/-}$) were subjected to renal IRI demonstrated that a lack of CD59a resulted in more severe polymorphonuclear (PMN) leukocyte infiltration, enhanced tubular injury and increased apoptosis. Compared with WT mice, $CD59a^{-/-}$ mice also had increased interstitial deposits of C9 and affected kidneys did not show recovery from IRI (Turnberg et al., 2004).

1.6.6.2 Proteinuric renal disease

Adriamycin nephropathy (AN) is a non-immune mediated experimental model of acute glomerular injury leading to proteinuria and progressive loss of renal function. Intravenous administration of adriamycin rapidly induces podocyte damage, causing glomerulosclerosis, proteinuria, tubulointerstitial damage and tubular atrophy. The hallmark development of interstitial fibrosis and accumulation of myofibroblasts during AN closely resembles the final common pathway observed in human glomerular disease.

Complement-mediated tubulointerstitial injury caused by heavy proteinuria is not completely understood. A recent study suggested a pivotal role for C3 in the progression of proteinuric disease. Approximately 48 hours after induction of AN, C3 protein was present within the glomerulus. Glomerular deposition of C3 increased up to day 10. C3 deposition was also observed in the damaged tubulointerstitial compartment of the kidney and was significantly elevated compared with saline injected WT mice (Sheerin et al., 2008). Another study demonstrated that $C3^{-/-}$ mice exhibited less damage to glomerular podocytes and had significantly reduced histological glomerular and tubulointerstitial injury compared with WT mice. Similarly, $FD^{-/-}$ mice exhibited preserved renal function and were protected from early proteinuria. In the same study, AN-induced renal injury in WT and $C1qa^{-/-}$ mice was equivalent, demonstrating that complement activation via the alternative complement pathway was contributing towards disease progression in this model (Turnberg et al., 2006).

The terminal complement pathway has also been shown to be an important mediator of renal damage. One study showed that compared to WT mice, $CD59a^{-/-}$ mice had increased levels of C9 within glomeruli and significantly more interstitial collagen and α-SMA deposition during AN (Turnberg et al., 2006). In a second study, researchers evaluated adriamycin-induced renal injury in C6 sufficient ($C6^{+}$) and $C6^{-}$ rats and discovered that both interstitial ECM deposition and peritubular myofibroblast accumulation at days 21 and 42 were attenuated in $C6^{-}$ rats. In addition, no C5b-9 deposition was observed in $C6^{-}$ rats (Rangan et al., 2004).

In the AN model of renal disease it is apparent that deficiency of various complement components can offer some protection from progression towards renal insufficiency. A more recent *in vivo* study using the AN model of glomerular injury, complement C3a receptor deficient ($C3aR^{-/-}$) mice had reduced albuminuria and histological injury compared to WT mice and saline controls, suggesting that an absence of complement receptors may protect against disease progression. Interestingly, $C3aR^{-/-}$ mice in this study also exhibited fewer infiltrating macrophages and less fibrosis (measured by collagen-I and α-SMA deposition) compared with that observed amongst WT mice (Tang et al., 2009; Tang et al., 1999).

1.6.6.3 Renal complement synthesis

Liver hepatocytes are the primary source of plasma complement, however, there is increasing evidence that smaller amounts of complement proteins are synthesised by other cell types and organs, including bone marrow cells, adipocytes, the brain and the kidney (Zhou et al., 2001). The contribution of complement towards renal injury is well documented (Welch and Blystone, 2009; Welch, 2001). The majority of components from each complement activation pathway can be synthesised by the kidney and under different inflammatory conditions, complement synthesis is stimulated in distinct regions including the glomerular mesangium, endothelium and epithelium and the tubular epithelium (Marsh et al., 2001).

Several studies have highlighted the importance of intrarenal synthesis of complement component C3 as an important mediator of local tissue injury (Quigg, 2003; Springall et al., 2001; Daha and van Kooten, 2000; Welch et al., 2000). One study of AN in mice showed that WT mice receiving $C3^{-/-}$ mouse kidney transplants prior to induction of AN had improved renal function and reduced mortality, demonstrating that renal synthesis of C3 was in part responsible for complement-mediated injury in this model (Sheerin et al., 2008). The contribution of C3 towards progression of renal disease *in vivo* was confirmed in a renal IRI study utilising C3 specific small interfering RNA (siRNA). This study showed that administration of C3 siRNA prior to induction of IRI inhibited C3-mediated progression of standard and severe IRI. 24 hours post-IRI, reductions in serum creatinine and blood urea nitrogen were observed. In addition, neutrophil infiltration, C9 deposition and infarction of tissues were reduced compared with mice not given C3 siRNA (Zheng et al., 2006).

Renal synthesis of C3 has also been shown to affect long term graft survival following transplantation. In one study, C57BL/6 $C3^{-/-}$ mouse kidneys transplanted into B10.Br recipient mice demonstrated long term graft function with 8/10 mice surviving to 100 days. Conversely, C57BL/6 mouse kidneys transplanted into B10.Br mice were acutely rejected with a mean graft survival of just 12.5 days (Pratt et al., 2002).

1.6.6.4 The role of complement in unilateral ureteric obstruction

The role of complement in non-proteinuric renal disease is not understood. A recent study demonstrated that mice deficient in C5 were protected from renal injury during the acute phase of ureteric obstruction (Boor et al., 2007). Studies in other animal models of renal disease have demonstrated that animals deficient in either complement components or complement receptors also show a reduction in renal injury. It is becoming increasingly apparent that manipulation of the complement system could provide an alternative therapeutic strategy capable of treating renal inflammation and fibrosis in the future.

1.7 Nuclear factor kappa-B

NF-κB was identified approximately 25 years ago in eukaryotes as a transcription factor regulating the expression of the kappa-B (κB) light chain in B cells. In response to numerous different exogenous and endogenous stimuli, NF-κB signalling has since been shown to induce and repress the expression of many genes, including cytokines, chemokines and adhesion molecules. During normal physiological conditions, NF-κB regulates critical cellular processes such as development, cell growth, apoptosis and cellular immunogenic and inflammatory responses (Kucharczak et al., 2003; Chen et al., 2001). As well as regulating normal cellular activities, NF-κB has been shown to have an important role in the progression of a number of pathological states including asthma, arthritis, heart disease, neurological degeneration and cancer. Owing to its highly conserved role in signalling pathways of the innate and adaptive immune systems and its diverse biological role in other cellular signalling mechanisms, inappropriate activation of NF-κB causes a broad range of harmful effects (Ghosh et al., 1998).

1.7.1 NF-κB/Rel protein family

NF-κB regulated gene expression is mediated by NF-κB and Rel proteins which belong to a structurally related, dimer-forming family of transcription factors (Figure 1.9). NF-κB/Rel proteins are separated into two classes or subfamilies; the NF-κB subfamily (class one) and the Rel subfamily (class two). Both NF-κB and Rel proteins share a homologous and highly conserved DNA binding and heterodimerisation 'Rel homology domain' (RHD; (Gilmore, 2006; Bonizzi and Karin, 2004).

1.7.1.1 Rel sub-family

The Rel protein subfamily consists of RelA (also known as p65), RelB, c-Rel, Drosophila dorsal and dif (Figure 1.9, top row). In contrast to their NF-κB subfamily counterparts, Rel proteins are defined by their C-terminal transcriptional activation domains (TAD). In vertebrates, Rel proteins are able to form hetero and homodimers with one another with the exception of RelB, which does not form homodimer complexes (Hayden and Ghosh, 2008). Rel proteins also dimerise with NF-κB subfamily proteins, indeed the major NF-κB/Rel complex present in most cells is the p50/RelA heterodimer. The combinational diversity of NF-κB and Rel homo and heterodimers serve to regulate very distinct, but overlapping sets of genes. In addition, individual dimmers also have distinct DNA binding site specifications for a group of related κB binding sites (Ghosh et al., 1998).

1.7.1.2 NF-κB sub-family

The proteins categorised within the NF-κB subfamily are p105, p100 and Drosophila relish (Figure 1.9, second row). Each NF-κB protein has a characteristic long C-terminal domain containing inhibitory ankryin repeat sequences rendering them unable to activate gene transcription in their monomeric form. p105 and p100 NF-κB proteins are synthesised as inactive precursor proteins and are subsequently converted to the shorter DNA binding proteins p50 (nfκb1) and p52 (nfκb2) respectively, following proteolysis of their C-terminal domains.

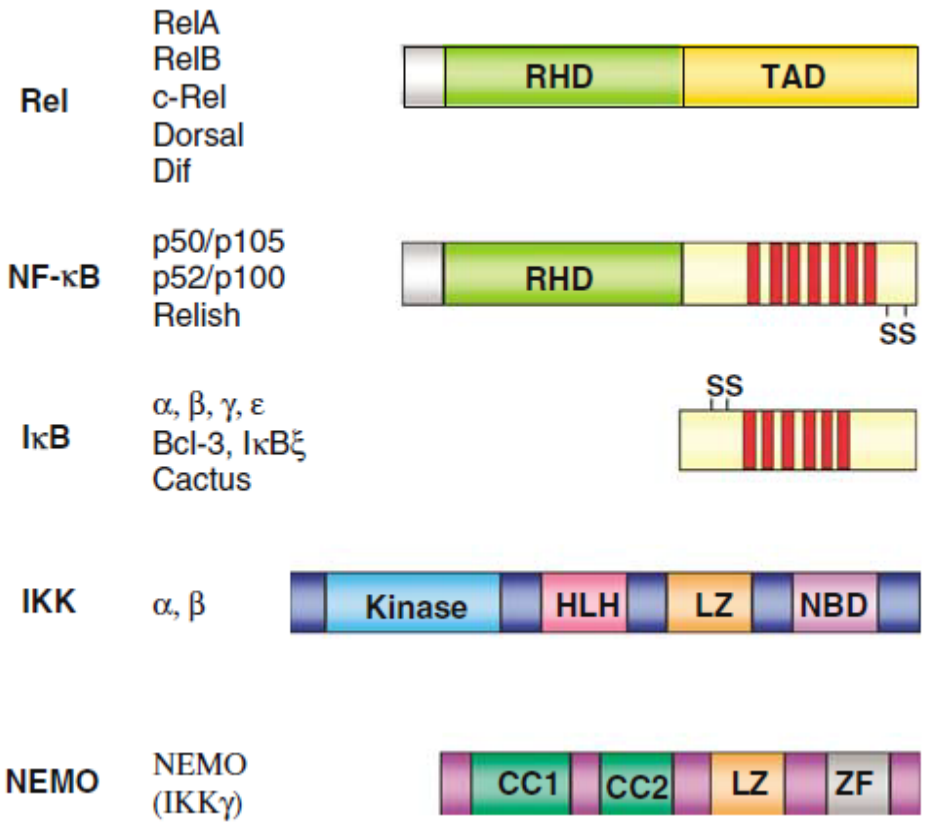

Figure 1.9. The Rel/NF-κB family of proteins
Generalised structures of the NF-κB and Rel transcription factor subfamilies. NF-κB and Rel proteins both have a highly conserved DNA binding domain known as the Rel homology domain (RHD). The C-terminal portions of Rel proteins contains a transcriptional activation domain (TAD), whereas the C-terminal portion of NF-κB proteins has an inhibitory domain containing ankyrin repeats and two serine residues (SS). Similarly, the majority of inhibitory κB (IκB) proteins contain a series of inhibitory ankyrin repeats and N-terminal SS residues. The SS residues on NF-κB and IκB proteins function as phosphorylation sites for inhibitory κB kinase (IKK) proteins. In general, IKK α and β consist of a kinase domain, a helix-loop-helix (HLH), leucine zipper (LZ) and NEMO binding domain (NBD). NF-κB essential modifier protein (NEMO) consists of two coiled coils (CC), a LZ and a zinc finger (ZF) domain.
Taken from TD Gilmore (2006).

nfκb1 and nfκb2 typically form transcriptionally active dimmers with Rel subfamily proteins, nfκb1 is also able form dimmers with other nfκb1 molecules (Hayden and Ghosh, 2008; Perkins and Gilmore, 2006; Ghosh et al., 1998).

1.7.2 Regulation of NF-κB

NF-κB activity is tightly regulated by inhibitory κB (IκB) proteins. Following activation of the NF-κB pathway, IκB proteins become targets for either proteolysis or phosphorylation, subsequently permitting NF-κB to translocate to the nucleus and regulate target genes. Upstream signalling events preceding the regulation of IκB, involve the activity of a myriad of adaptor proteins and kinases, whose role it is to determine precisely which NF-κB dimer is activated and, subsequently, which genes are targeted for transcription.

1.7.2.1 IκB proteins

Rel homo and heterodimers and NF-κB heterodimers are maintained in an inactive state in the cytoplasm through interactions with IκB. nfκb1 and nfκb2 homodimers are an exception to this as they are not regulated by IκB proteins and are frequently found within the nucleus. One of the functions of IκB proteins is to mask highly conserved nuclear localisation sequences (NLS) present in the RHDs of NF-κB subunits, preventing nuclear accumulation and DNA binding. Several IκB proteins have been identified, each with a different affinity for discrete dimer complexes.

In addition, IκB proteins are regulated slightly differently from one another and exhibit different tissue-specific patterns of expression (Figure 1.9, third row; (Wan and Lenardo, 2009; Hayden and Ghosh, 2008).

1.7.2.1.1 IκBα, IκBβ and IκBε

Inhibitory κB proteins IκBα, IκBβ and IκBε each possess different functional characteristics and activation kinetics, of which IκBα and its role in the conanical NF-κB activation pathway has been most widely studied. The nfκb1/RelA NF-κB heterodimer is largely bound to IκBα and during periods of inactivity, IκBα prevents NF-κB activation of gene transcription by two means; firstly, by masking the NLS on RelA to prevent nuclear localisation and secondly by the binding of its own nuclear export sequence (NES) to the exposed NLS of nfκb1, resulting in a constant shuttling of the IκBα-nfκb1/RelA complex between the nucleus and cytoplasm. Upon activation of the canonical pathway, IκBα is rapidly degraded by proteosomes resulting in nuclear translocation and DNA binding of nfκb1/RelA, inducing transcription of target genes. IκBα transcription is also included and the subsequent increase in expression of IκBα provides a negative feedback loop for NF-κB signalling. In addition to nfκb1/RelA, other NF-κB dimmers have been shown to bind IκBα and when IκBα is not present, the termination of NF-κB activation is markedly prolonged. Unlike IκBα, IκBβ and IκBε exhibit considerably slower degradation and re-synthesis during NF-κB signalling. IκBβ has been shown to associate with NF-κB dimers already bound to κB sites on target genes within the nucleus, suggesting a regulatory role for IκBβ at the site of DNA binding (Hayden and Ghosh, 2008; Perkins, 2007; Hayden and Ghosh, 2004).

1.7.2.1.2 p100 and p105

The nfκb1 and nfκb2 precursor proteins p105 and p100 respectively, are important for the regulation of NF-κB. nfκb2 has been shown to induce and regulate activity of NF-κB complexes including RelB dimer dependent gene expression. Another study has demonstrated that upon activation of the canonical NF-κB pathway the nfκb1 precursor protein p105 is degraded, suggesting that p105 may behave in a similar way to IκB proteins. In mice, the 3' end of the p105 gene also encodes the inhibitory IκB protein IκBγ, though its precise role in the mouse is not presently clear (Perkins, 2007).

1.7.2.1.3 Bcl-3 and IκBζ; atypical IκB proteins

The behaviour and mode of action of the atypical IκB proteins, Bcl-3 and IκBζ, is yet to be completely clarified, though the two proteins do share greater homology to one another than to the above-mentioned IκB proteins. Bcl-3 has been located within the nucleus of cells in association with nfκb1 and nfκb2 homo and heterodimers. It possesses a TAD that may act to both stabilise repressive NF-κB dimers such as nfκb1/nfκb1 (inhibiting NF-κB activation by preventing dimer access to κB sites) and to remove repressive NF-κB dimers bound to κB sites on target genes, allowing access to other NF-κB dimers. IκBζ is the least homologous out of all of the IκB proteins. Depending upon how IκBζ is activated, it is thought to either associate with nfκb1 homodimers in the nucleus or negatively regulate activity of RelA NF-κB dimmers (Wan and Lenardo, 2009; Hayden and Ghosh, 2008).

1.7.2.2 TNF receptor associated factor (TRAF) adaptors

TRAF proteins have been identified as intermediate adaptors in the canonical and non-canonical NF-κB signalling pathways. In all, seven TRAF protein family members have been identified, and are distinguishable by their homologous C-terminal TRAF domains. In canonical and non-canonical NF-κB activation pathways, the key role for TRAF adaptors appears to be the mediation of receptor induced IKK activation via protein-protein interaction, though the precise mechanisms by which TRAF adaptors contribute to IKK activation remain unclear (Hayden and Ghosh, 2008).

1.7.2.3 Receptor interacting proteins (RIP)

RIP proteins belong to a family of kinases whose role in most canonical NF-κB signalling pathways is to interact with TRAF proteins in order to activate IKK. RIP is thought to recruit IKK complexes via the binding of NEMO proteins, a process which is required for TNF-α and toll-like receptor induced NF-κB signalling as well as IKK activation following T cell and B cell antigen receptor activation (Hayden and Ghosh, 2008).

1.7.2.4 NF-κB inducing kinase (NIK)

NIK is regulated by TRAF proteins during the activation of non-canonical NF-κB signalling pathways and is thought to directly phosphorylate and activate IKKα independently of NEMO (Hayden and Ghosh, 2008).

1.7.2.5 NF-κB essential modifier protein (NEMO)

NEMO (also known as IKKγ), belongs to the IKK family of proteins, and is present as a multimer of either dimeric and/or trimeric molecules (Figure 1.9, bottom row). Following ubiquitinylation, NEMO is thought to activate and recruit IKK during classical NF-κB signalling, as well as functioning independently of IKK. Although classified within the IKK family, NEMO does not have kinase activity and is not related to the two other family members, IKKα and IKKβ (Perkins and Gilmore, 2006).

1.7.2.6 Inhibitory κB kinases (IKK)

IKK proteins are an important regulatory step in determining NF-κB response and commonly exist as dimmers containing the catalytic subunits IKKα and/or IKKβ which may or may not associate with the regulatory IKK protein NEMO (Figure 1.9, fourth row). IKKα and IKKβ are classified as serine/threonine kinases and each possess an N-terminal kinase domain, a C-terminal helix-loop-helix (HLH) domain (required for complete IKKβ activity and down regulation of kinase activity) and a leucine zipper domain (required for kinase activity). *In vivo*, IKKα and IKKβ can form homodimers, but preferentially form the heterodimeric IKKα/IKKβ complex, which has the greatest catalytic efficiency. IKK complexes become active following phosphorylation of at least one subunit and subsequently activate NF-κB by phosphorylating IκB family members, a common step in all NF-κB activation pathways. Regulation of IKK activity is thought to be mediated by adaptor proteins such as RIP and TRAF and also through autophosphorylation of its own C-terminal domain as part of a negative feedback loop.

Following activation of the canonical NF-κB pathway, IKKβ is necessary for the subsequent phosphorylation of IκBα, whereas during non-canonical pathway stimulation, NF-κB activation occurs by NIK mediated activation of IKKα (Hayden and Ghosh, 2008; Perkins, 2007; Perkins and Gilmore, 2006; Hayden and Ghosh, 2004; Karin and Delhase, 2000).

1.7.3 Activation of NF-κB

NF-κB activation is triggered by numerous stimuli including ANG II, oxidative stress, haemodynamic changes and endogenous/exogenous ligand-receptor binding. The phosphorylation, ubiquitination and proteolysis of specific inhibitory-κB (IκB) proteins results in dissociation of NF-κB. Un-bound NF-κB then freely translocates to the nucleus where it binds to κB sites to induce the transcription of target genes (Bonizzi and Karin, 2004). Of the many distinct, but overlapping, NF-κB activation pathways described in the literature, the two most studied pathways are the canonical and non-canonical pathways (Gilmore, 2006).

1.7.3.1 The canonical pathway

The canonical pathway is thought to be the most frequently observed NF-κB activation pathway and is induced in response to inflammatory stimuli such as TNF-α binding to its cell surface receptor TNFR1. In this case, the binding of TNF-α to its receptor causes the recruitment of TRAF adaptor proteins to the cytosolic domain of the receptor, which in turn recruit and phosphorylate the IKK complex (IKKα/IKKβ/NEMO).

The activated IKK complex subsequently phosphorylates IκBα, resulting in the ubiquitinylation and proteosomal degradation of IκBα, releasing nfκb1/RelA NF-κB dimers. Free nfκb1/RelA dimers translocate to the nucleus where they bind to κB sites on target genes to elicit the production of specific cytokines, growth factors and MHC antigens (Figure 1.10, left panel). Another target gene activated by nfκb1/RelA DNA binding is the IκBα gene. The increased production of IκBα forms an autoregulatory feedback loop resulting in the re-sequesteration of active nfκb1/RelA dimmers and their subsequent removal from the nucleus (Gilmore, 2006; Perkins, 2006).

1.7.3.2 The non-canonical pathway

During T cell and B cell development, the alternative NF-κB activation pathway is stimulated by the binding of specific receptor ligands such as CD40 and B cell activating factor respectively. This activates NIK which subsequently phosphorylates and activates the IKKα/IKKα complex. Activated IKKα/IKKα in turn phosphorylate the IκB domain of the p100/RelB NF-κB dimer liberating nfκb2/RelB (Figure 1.10, right panel; (Gilmore, 2006; Perkins, 2006).

1.7.4 Terminating NF-κB activation

The mechanism by which NF-κB pathway activation is terminated remains poorly understood. One possible mechanism is the re-synthesis of IκB proteins and subsequent re-sequesteration of active NF-κB.

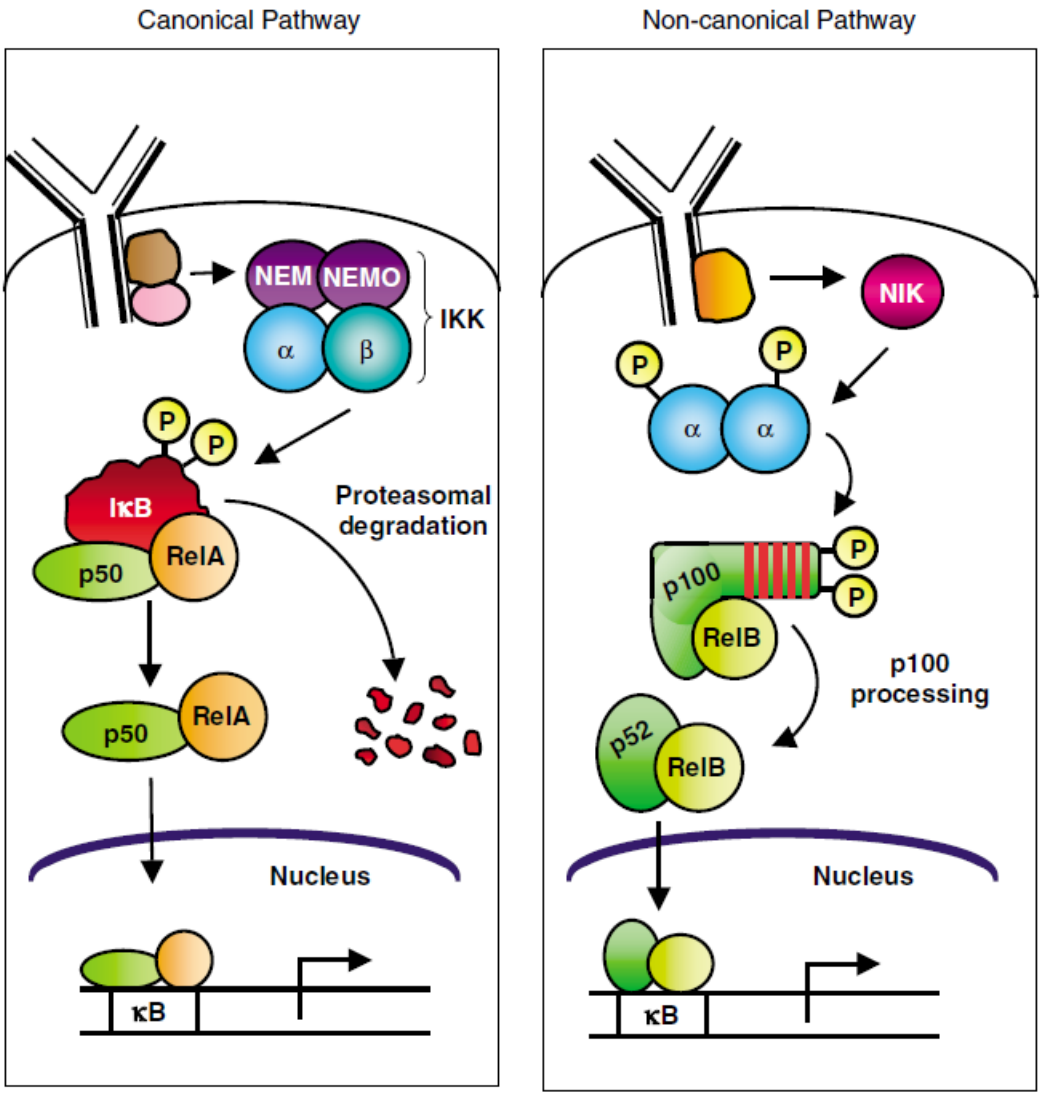

Figure 1.10. Canonical and non-canonical NF-κB activation pathways
NF-κB activation and signalling via canonical and non-canonical pathways. Activation of both pathways is initiated by the binding of a ligand to its specific cell surface receptor. Upon activation of both pathways, adaptor proteins are recruited to the cytosolic receptor domain. After binding to receptors, adaptor proteins recruit and phosphorylate the canonical pathway inhibitory κB (IκB) kinase complex (IKK; consisting of IKKα, IKKβ and NEMO). During non-canonical pathway activation, adaptor proteins activate NF-κB inducing kinase (NIK) which subsequently phosphorylates and activates the non-canonical IKK complex (IKKα/IKKα). Subsequent phosphorylation of canonical IκB and non-canonical p100 inhibitory domains by activated IKK complexes causes ubiquitinylation and degradation of IκB and p100 inhibitory domains, releasing nfκb1/RelA (p50/RelA) and nfκb2/RelB (p52/RelB) dimmers. Free NF-κB dimmers translocate to the nucleus where they bind κB sites on target genes.
Taken from TD Gilmore (2006).

Alternatively, the synthesis of other gene products inhibiting the upstream components of the NF-κB signalling pathway may also contribute towards terminating NF-κB activity (Wan and Lenardo, 2009; Saccani et al., 2004).

1.7.5 NF-κB in disease

Since its discovery, NF-κB signalling is increasingly being implicated in the development and progression of a number of pathophysiological states, such as those preceding the development of colorectal cancer and hepatitis-induced hepatocellular carcinomas. Whilst NF-κB may not play a role in the initiation of tumour cell expansion and subsequent metastasis it has been shown to promote tumour survival and expansion through stimulating the expression of anti-apoptotic proteins (Karin, 2006; Mann and Oakley, 2005).

In experimental atherosclerosis and wounded aortic endothelium models, systemic infusion of ANG II stimulates NF-κB activity in vascular smooth muscle cells (VSMC) causing up regulation of IL-6, vascular cell adhesion molecule 1 (VCAM-1) and MCP-1; (Guzik and Harrison, 2007). ANG II also induces the generation of ROS, another known stimulant for NF-κB (Pueyo et al., 2000). Antioxidant treatment of an angiotensin-stimulated rat aortic endothelial cell line demonstrated a reduction in IκB degradation and ANG II-induced VCAM-1 expression (Muller et al., 2000a).

In vitro administration of ACE inhibitors and angiotensin receptor antagonists to VSMCs also demonstrated that NF-κB activation and IκB degradation were dependent upon ANG II mediated angiotensin receptor stimulation (primarily via AT_1 receptors) indicating a potential role for NF-κB in the pathogenesis of cardiovascular and renal diseases (Henke et al., 2007; Ruiz-Ortega et al., 2001; Ruiz-Ortega et al., 2000). In contrast to its role during inflammation, there is increasing evidence to suggest that NF-κB may be involved in mediating resolution from inflammation (Lawrence and Fong, 2010; Oakley et al., 2005; Lawrence et al., 2001).

1.7.6 NF-κB signalling in renal disease

NF-κB activation leading to inflammatory injury has been implicated in both acute and chronic renal disease (Sanz et al., 2010; Guijarro and Egido, 2001). In previous studies, pro-inflammatory stimulation of cultured mesangial cells induced phosphorylation of IκB and activation of NF-κB, switching on expression of VCAM-1, MCP-1, IL-6, IL-8 and ROS. Inhibition of NF-κB subsequently decreased the expression of IL-8 and MCP-1 in human and mouse mesangial cell cultures (Massy et al., 1999). In a model of immune-mediated mesangial cell injury, NF-κB activity during acute and chronic injury was shown to be biphasic. Following complement-mediated lysis of mesangial cells in the rat anti-Thy 1 model, monocytes and macrophages were recruited to the site of injury and deposition of ECM components within the glomerulus increased between 24 hours and seven days.

Resolution of glomerular injury started from day eight and was monitored up until day 14. During this time, MCP-1 expression returned to control levels and both glomerular damage and macrophage infiltrate resolved.

To determine whether different NF-κB subunits were activated in a time-dependent manner, anti-nfκb1 and anti-RelA antibodies were used to stain renal tissues from anti-Thy 1 irradiated rats. nfκb1 and RelA were present in glomerular nuclei at 24 hours post-ATS however by day ten, only nfκb1 could be detected, suggesting a role for p50 in the resolution of glomerular injury (Panzer et al., 2009). In an accelerated model of acute immune-mediated glomeular injury, activation of NF-κB also occurred during the resolution phase (*in vivo* and *in vitro* data). In this model, injection of LPS (a classical activator of NF-κB), induced significant interstitial oedema and infiltration of $CD3^+$ T cells and $F4/80^+$ macrophages by three hours (first NF-κB peak). However by 48 hours, oedema and immune cell infiltrates had returned to control levels (second NF-κB peak; (Panzer et al., 2009)). Using nfκb1 deficient mice (*nfκb1*$^{-/-}$), the authors demonstrated a reduction in the first peak for NF-κB activity and a complete absence of a second NF-κB activity peak. In addition, LPS-treated *nfκb1*$^{-/-}$ mice also had significantly elevated levels of cytokines and pro-inflammatory mediators compared with WT mice after three hours. In *nfκb1*$^{-/-}$ mice, infiltrating $CD3^+$ T cells and $F4/80^+$ macrophages persisted at 48 hours and a more severe pathological phenotype was apparent (Panzer et al., 2009).

1.7.6.1 Activation of NF-κB during UUO

The changes in haemodynamics following ureteric obstruction are mediated through the effects of ANG II signalling via AT_1 and AT_2 receptors, inducing activation of NF-κB signalling and subsequent stimulation of angiotensinogen gene transcription.

In mice, administration of ACE inhibitors such as Enalapril or the use of individual AT_1/AT_2 receptor antagonists have been shown to reduce the activity of NF-κB (and subsequent up-regulation of NF-κB-related pro-inflammatory genes), prevent infiltration of monocytes and immune cells into renal tissues and slow renal disease progression during UUO (Esteban et al., 2004; Nakatani et al., 2002; Morrissey and Klahr, 1997). In another study of AT_1 and AT_2 receptor deficient mice, it was shown that each receptor played a different role in controlling NF-κB signalling by activating different NF-κB dimmers (Klahr, 2000). TNF-α signalling via TNFR1 and TNFR2 receptors has also been shown to contribute towards early NF-κB activation in rodent models of ureteric obstruction. Mice deficient in either TNFR1 ($TNFR1^{-/-}$) or TNFR2 ($TNFR2^{-/-}$) displayed significantly less NF-κB activation during UUO than TNFR sufficient animals. In particular, $TNFR1^{-/-}$ mice had significantly reduced TNF-α mRNA expression as well as marked reduction in the deposition of collagen IV and α-SMA compared to their WT counterparts (Guo et al., 1999).

During the early stages of UUO (10-12 hours post-obstruction), oxidative stress is induced by the physiological effects of fluid dynamic alterations within renal tissue. This in turn increases ANG II production and the subsequent synthesis of ROS, which increase the activity of NF-κB.

When applied experimentally, antioxidant compounds such as pyrrolidine dithiocarbamate (PDCT), have been shown to restore the redox equilibrium by ameliorating ANG II mediated NF-κB activity. In the UUO model, an attenuation in UUO-induced increases in NF-κB DNA binding was observed rats treated with PDCT and candesartan. MCP-1 gene expression and macrophage infiltration were also attenuated and renal interstitial fibrosis was ameliorated (Nakatani et al., 2002).

1.7.6.2 NF-κB activation during NTS glomerulonephritis

The role of NF-κB in NTS glomerulonephritis has received some attention. In one study, NF-κB DNA binding activity was detected in the glomerular nuclear extracts of rats injected with NTS. In the same study, administration of the antioxidant PDCT inhibited albuminuria, NTS-induced NF-κB DNA binding activity and mRNA expression of; MCP-1, intracellular adhesion molecule-1, interleukin-1β (IL-1β) and inducible nitric oxide synthase (Sakurai et al., 1996). Another study investigated the effects of administering glucocorticoids to NTS-injected rats and reported that therapeutic doses of prednisolone suppressed NF-κB activity, reduced proteinuria and decreased mRNA expression of IL-1β, MCP-1, and TGF-β (Sakurai et al., 1997). *In vitro* studies using mesangial cell cultures have also demonstrated that LPS and pro-inflammatory molecules such as IL-1β and TNFα can induce measurable NF-κB activation. In addition to this, the application of NF-κB inhibitors to stimulated mesangial cells significantly reduced IL-1β, IL-8 and MCP-1 gene expression. A more recent study used gene expression profiling to identify the presence of the active NF-κB target genes IL-1β, Il-6 and C3 during NTS glomerulonephritis (Kim et al., 2004).

1.8 Aims

Multiple factors including complement activation and NF-κB signalling, have been shown to contribute towards the progression of many renal diseases. Of the numerous components belonging to each of the complement and NF-κB systems, it is thought that the central complement component C3 and the NF-κB family protein nfκb1 may each be involved during the progression of injury in experimental models of acute and chronic renal disease.

In the first part of this study, UUO will be induced in WT and $C3^{-/-}$ mice to determine the contribution of complement component C3 towards the progression of tubulointerstitial injury, including analyses of; histological examination, immune cell infiltration, cytokine expression, ECM deposition and gene up-regulation of key ECM components after three, five and ten days of UUO. Following on from this, complement activation and deposition will be measured in WT and $C3^{-/-}$ mice where appropriate. mRNA expression of C3 and regulatory complement components will be compared in WT and $C3^{-/-}$ mice at time points of three, five and ten days post-UUO to determine the mechanism of complement activation in this disease model. The site of C3 up-regulation will be determined using *in situ* hybridisation.

In the second part of this study, NTS nephritis and UUO will be induced in WT and $nf\kappa b1^{-/-}$ mice to compare the contribution of nfκb1 during the progression of acute and chronic renal disease. Histological analyses will be used to determine neutrophil infiltration and glomerular injury at two and 24 hours post-NTS administration and interstitial expansion and tubular dilatation after three and ten days of ureteric obstruction.

Renal injury during NTS nephritis will be determined by urinary albumin output and gene expression of known pro-inflammatory mediators. Disease progression in obstructed WT and *nfκb1*$^{-/-}$ mice will be analysed in an identical manner as set out in the previous paragraph.

2 Materials and Methods

2.1 Materials

General chemicals and histological stains were purchased from Sigma Aldrich, Poole, UK. Cell culture reagents were purchased from; PAA Laboratories, Yeovil, UK, Invitrogen, Paisley, Scotland and Sigma Aldrich, Poole, UK. General consumables and cell culture consumables were purchased from; Gibco Life Sciences, Paisley, Scotland, Scientific Laboratory Supplies, Nottingham, UK, Starlab, Milton Keynes, UK and VWR International, Lutterworth, UK. Unless otherwise stated, the general chemicals used for *in situ* hybridisation were purchased from Sigma Aldrich and BDH Prolab, VWR International, Lutterworth, UK.

GoTaq DNA polymerase was purchased from Promega, Southampton, UK. Reverse transcription reagents were purchased from Invitrogen, Paisley, Scotland and Agilent Technologies, Wokingham, UK. DyNAmo HS SYBR green PCR kit was purchased from New England Biolabs, Hitchin, UK. All primers were purchased from Eurofins MWG Operon, Ebesberg, Germany.

2.1.1 General buffers

Phosphate buffered saline	1.15g of Na_2HPO_4, 8.0g of NaCl, 0.2g of KCl and 0.2g of KH_2PO_4 in 1000ml dH_2O with pH adjusted to 7.4

Sodium phosphate buffer (0.2M)	1.18g of Na_2HPO_4 and 1.61g of NaH_2PO_4 in 100ml dH_2O with pH adjusted to 6.5
Carbonate buffer (0.1M)	1.06g of Na_2CO_3 and 0.85g of $NaHCO_3$ in 100ml dH_2O with pH adjusted to 9.5
Formal saline (3.8%)	10ml of 38% formaldehyde in 90ml PBS

2.1.2 DNA buffers

Tris-Boric acid EDTA	10.8g of Tris-base, 5.5g of boric acid and 9.3g of EDTA in 1000ml dH_2O with pH adjusted to 8.3

2.1.3 *In situ* hybridisation buffers

20x SSC	3M NaCl, 0.3M sodium-citrate with pH adjusted to 7.2. diluted to 5x and 2x SSC with ddH_2O
Buffer 1	0.1M Tris (pH 7.6), 0.15M NaCl. Made up to 1000ml with ddH_2O

Buffer 2	0.1M Tris (pH 9.5), 0.1M NaCl. Made up to 1000ml with ddH_2O

2.1.4 Other buffers and wash solutions

Destain solution for RIA	450ml H_2O, 450ml absolute ethanol and 100ml acetic acid
1% coomassie blue	10g of coomassie blue powder dissolved in1 litre of destain solution

2.2 Animals

All animals were used in accordance with the Animals (Scientific Procedures) Act 1986 and were housed under pathogen-free conditions. C3 and nfκb1 sufficient C57BL/6 wild type mice (WT) were purchased from Charles River UK Ltd, Kent.

2.2.1 $C3^{-/-}$ mice

C3 deficient ($C3^{-/-}$) mice were produced using homologous recombination in embryonic stem cells. Briefly, disruption of the C3 coding sequence was achieved by the targeted deletion of nucleotides spanning the N-terminal region of the β chain and the C-terminal region of the α chain (Wessels et al., 1995). $C3^{-/-}$ homozygous mice were phenotypically normal, had no antigenic or functional C3 and were backcrossed onto a C57BL/6 background for >7 generations.

2.2.2 *nfκb1*$^{-/-}$ mice

nfκb1$^{-/-}$ mice were originally formed by the targeted disruption of the *NFKB1* gene at exon 6. *NFKB1* encodes p105, the precursor of the shorter DNA binding protein p50. p105 and p50 proteins produced by *nfκb1*$^{-/-}$ mice are functionally inactive and are unable to bind DNA or dimerise with other Rel/NF-κB proteins (Sha et al., 1995). *nfκb1*$^{-/-}$ mice were backcrossed onto a C57BL/6 background for at least 5 generations and were kindly provided by Professor Derek Mann, Newcastle University.

2.2.3 Experimental unilateral ureteric obstruction

Experimental UUO was induced in male WT and C3$^{-/-}$ mice aged 6-8 weeks and female *nfκb1*$^{-/-}$ mice aged 8-10 weeks. Mice were anaesthetised by inhalation using 2-3% isofluorane mixed in oxygen. Small clippers were used to remove fur from the abdominal area and then mice were injected subcutaneously with 250µL of 6µg/ml buprenorphine. The abdominal area was cleaned using a sterile wipe. A ventral laparotomy incision was made along the linea alba, extending from just above the symphysis pubis to the xyphi sternum. To gain access to the left kidney, the bowels were reflected upwards outside of the abdomen onto a piece of gauze moistened with saline. Under an operating microscope, the left ureter was located and tied twice with waxed 7/0 silk in double-knots approximately 3 mm apart then a cut was made between the two ties (Figure 2.1). The bowels were replaced and the abdomen was closed with 5/0 vicryl. Anaesthetic was reversed by removing isofluorane and leaving on oxygen for a few minutes. Mice were allowed to recover over night in an incubator set to 30°C before being transferred back to their standard housing to following day.

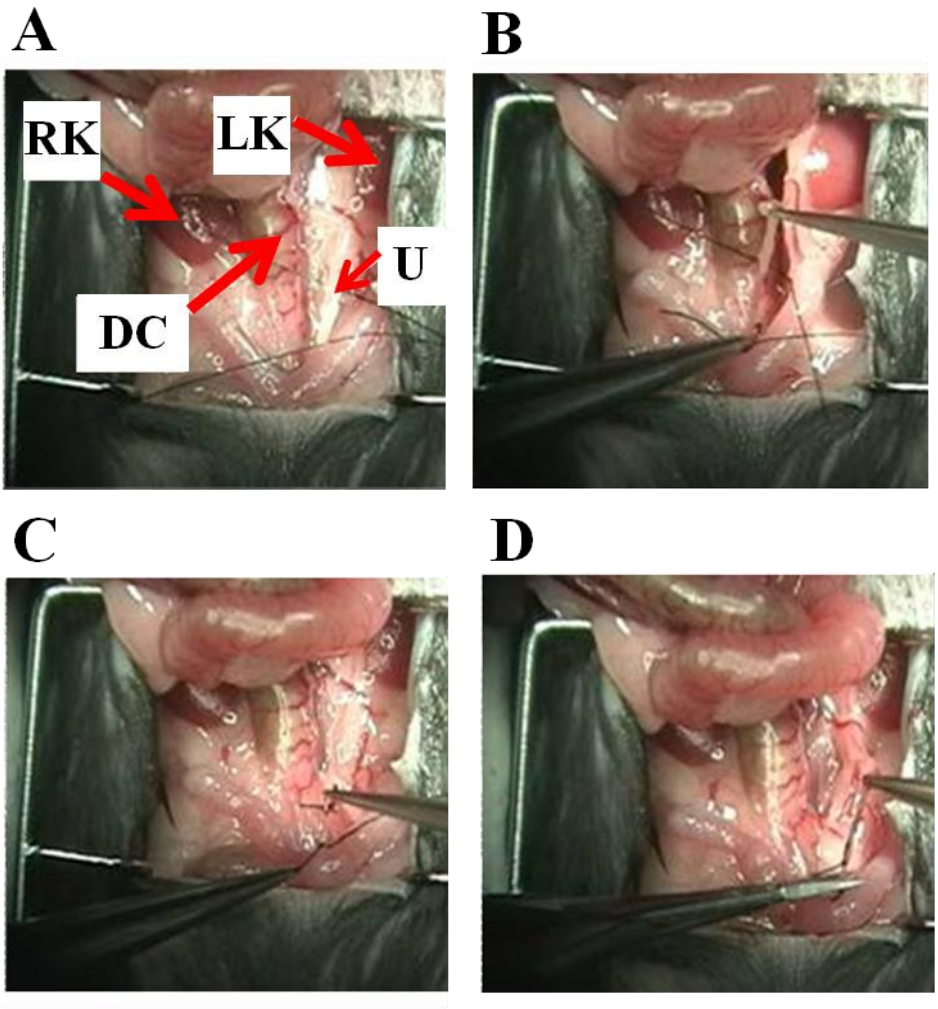

Figure 2.1. Unilateral ureteric obstruction (UUO) procedure.
Following anaesthesia and a ventral laparotomy incision, the left ureter was tied twice and then cut between the ties. The left ureter was dissected and two 7/0 silk sutures were placed underneath (A). R, right kidney; L, left kidney; DC, descending colon; U, left ureter. The first knot was tied and moved to a distal position (B). The second knot was tied and positioned further distal in close proximity to the bladder (C). The left ureter was cut between the two ties (D). Following this the laparotomy incision was closed using 5/0 vicryl. *Images obtained with kind permission from the Ph.D. Thesis of Dr. Thomas Tapmeier.*

2.2.4 Induction of nephrotoxic serum (NTS) nephritis

NTS nephritis was induced in 8 week old female WT and *nfκb1*$^{-/-}$ mice by injecting 200µl of NTS containing 0.5ng/µl LPS via the tail vein. Sheep anti-mouse nephrotoxic serum was a kind gift from Dr Mike Robson, King's College London. After NTS injection, mice were housed in standard metabolic cages for a period of 24 hours so that urine samples could be collected.

2.2.5 Harvesting of tissues post-ureteric obstruction

Prior to harvesting tissues blood samples were obtained by cardiac puncture under terminal anaesthesia. Both kidneys were excised and urine was extracted from the dilated pelvis of obstructed kidneys. Each kidney was bisected along its longitudinal axis and a small part of the cortex removed and snap-frozen in liquid nitrogen for RNA extraction. One half of each kidney was fixed in 3.8% formal saline (section 2.1.1), then processed and embedded in paraffin for histological analysis. The other half was snap-frozen in isopentane over liquid nitrogen and then stored at -80°C for immunohistochemical analyses. Blood samples were allowed to clot at room temperature before centrifugation at 10,000rpm to obtain serum. Urine and serum samples were stored at -20°C.

2.2.6 Harvesting of tissues following NTS administration

Mice were killed at 2 and 24 hours post-NTS injection. Blood samples and renal tissues were harvested, processed and stored as described in section 2.2.5.

The volume of urine produced in each 24 hour period was recorded and urine samples were stored at -20°C.

2.3 Histology and immunochemistry analyses

2.3.1 Periodic acid Schiff's histology

Periodic acid Schiff's (PAS) histology is a technique used to visualise pathological changes in tissues during disease. It works by staining large carbohydrate structures found in connective tissues & basement membranes, the latter of which surrounds renal tubules. Paraffin blocks containing formalin-fixed embedded kidney tissues were sectioned at 2µm intervals using a Leica Microtome. Sections were transferred to a 40°C water bath to be stretched out, then collected onto superfrost plus slides and dried at 37°C over night. Following this, sections were de-paraffinised by immersion in 100% xylene for 10 minutes. Tissue sections were rehydrated through graded ethanol (100%, and 95%) to deionised water (dH_2O). Tissue sections were incubated in 1% periodic acid for 6 minutes at room temperature (RT) then washed three times for two minutes in dH_2O. Schiff's reagent was applied to all sections for 10 minutes at RT then slides were washed under running tap water for 12 minutes. Sections were counterstained with Mayer's haematoxylin for 1 minute then blued under running tap water for 5 minutes. Finally, slides were dehydrated through graded ethanol washes (50%, 75%, 95% and 100%) and two final xylene washes before mounting in DPX.

2.3.1.1 Histological scoring of kidney sections

PAS histology was examined by bright field microscopy at x250 magnification using a Leica DMR microscope. For each contralateral and obstructed kidney section, 20 cortical field images were acquired and the percentage of interstitial expansion and tubular dilatation was calculated. Briefly, a 10 x 10 grid was superimposed onto each image and the number of grid intersections overlaying areas of interstitium and tubular luminae were counted and expressed as a percentage of the total area containing 81 grid intersections (excluding glomeruli), for each image (**Figure 2.2**). All counts were preformed in a blinded manner.

Glomerular thrombosis (identified as PAS positive material) in the lumen of glomerular capillaries 24 hours post-NTS injection was scored in 30 glomeruli per tissue section and classified as either '0' (no injury), '1' (<25% injury), '2' (25-50% injury), '3' (50-75% injury) and '4' (75-100% injury). 2 hours after NTS injection, the number of infiltrating neutrophils (identified by their typical multi-lobulated nuclear morphology), were counted in 15 glomeruli per tissue section. Glomerular thrombosis and neutrophil counts were both carried out in a blinded manner.

2.3.2 Sirius red histology

Paraffin-embedded renal tissue sections of 3µm in thickness were prepared as described previously (section 2.3.1). Tissue sections were washed under running tap water for 2 minutes then washed briefly in 0.1% acetic acid.

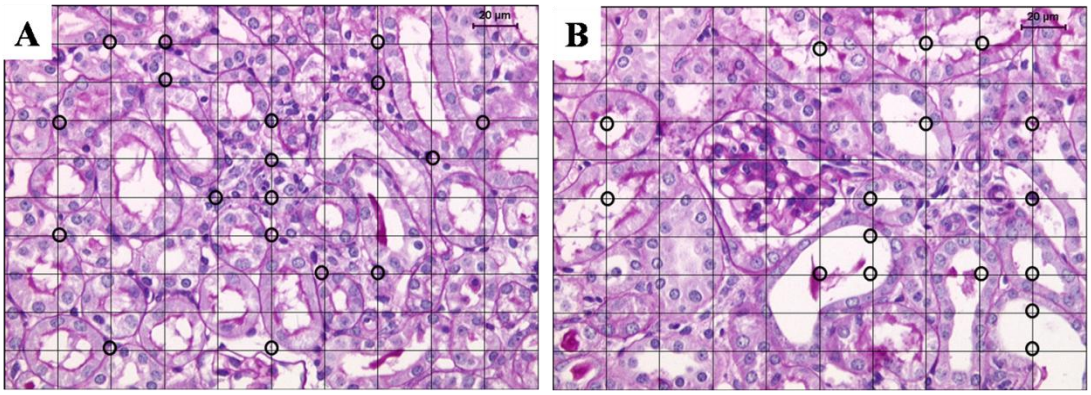

Figure 2.2. Manual scoring of periodic acid Schiff's stained renal tissues.
Counting of grid intersections over areas of interest to measure interstitial expansion (A), and tubular dilatation (B), then expressing these as a percentage of the total number of grid intersections per high powered field. Small black circles highlight grid intersections falling over areas of interstitium (A) and dilated tubules (B). Magnification is x250.

Slides were incubated in 0.1% Sirius red F3B for 1 hour at RT after which, sections were washed twice in 0.1% acetic acid. Finally, slides were rapidly dehydrated through three 100% ethanol washes and then cleared in xylene before mounting in DPX. For day 3 and day 10 UUO analyses, histological staining was examined in a blinded manner at 125x magnification using a Leica DMR microscope and accompanying Leica QWin computer software. For each slide, 20 random cortical field images (0.143mm^2 each) were acquired. For each field the percentage area of Sirius red staining was determined using Leica Q-win analysis software. Day 5 UUO tissues were analysed using an Aperio slide scanner and accompanying Scanscope software.

2.3.3 Immunohistochemical staining for CD4, CD8 and F4/80

Cryo-preserved kidneys from all animals were sectioned at 5µm using a Leica cryostat. Sections were collected on to Superfrost plus slides (VWR International, UK), dried for 24 hours at RT and then stored at -80°C. Prior to immunohistochemical staining, slides were thawed to RT for 1 hour. Slides were fixed for 5 minutes in ice cold acetone (-20°C), left to air dry for 5 minutes and then washed once in PBS for 5 minutes. Endogenous peroxidase activity was blocked by immersing slides in 0.3% H_2O_2 in PBS for 10 minutes, after which, slides were washed once in PBS for 5 minutes. Endogenous avidin & biotin were blocked using a streptavidin and biotin blocking kit (Vector Labs). Briefly, slides were first incubated with streptavidin blocking solution for 15 minutes then washed once in PBS for 5 minutes.

Following this, slides were incubated with biotin blocking solution for 15 minutes then washed once in PBS for 5 minutes. Slides were then incubated with primary antibodies (**Table 2.1**); rat anti-mouse CD4 and CD8 antibodies (1:20 dilution in PBS) and a rat anti-mouse F4/80 antibody (1:50 dilution in PBS), for 1hr at RT, then washed in PBS for 3 x 5 minutes. Following this, slides were incubated with a biotinylated goat anti-rat secondary antibody (1:100 dilution; **Table 2.1**), for 30 minutes at RT, then washed three times in PBS each for 5 minutes. Next, slides were incubated with pre-diluted streptavidin-conjugated horse radish peroxidise (BD Biosciences) for 30 minutes at RT. After this slides were washed twice in PBS each for 3 minutes. During this time, 3,3-diaminobenzidine (DAB) solution was prepared according to manufacturer's instructions and kept in the dark.

Slides were covered with excess DAB solution and incubated for 5 minutes in the dark until sections had developed. After DAB detection, slides were washed once in dH_2O for 5 minutes. Slides were then counterstained with Mayer's haematoxylin for 5 minutes and 'blued' for 5 minutes under running tap water. Finally, slides were taken through a series of alcohol dehydration steps (50%, 75%, 95% and 100%), cleared with xylene, then mounted in DPX and left to dry overnight. Slides were analysed using an Aperio slide scanner and Scanscope software. Images were taken using a Leica LCM microscope and accompanying computer software.

Table 2.1. Primary antibodies

Protein	Antibody	Clone	Source	Application	Dilution	Secondary antibody
α-SMA	Anti-mouse α-smooth muscle actin	1A4	Sigma Aldrich, UK	IHC	1:10,000	1
C3	Goat anti-mouse C3 FITC-conjugate	-	Cappel	IF	40µg/ml	-
Anti-NTS	Donkey anti-sheep FITC-conjugate	-	JIR Labs Inc.	IF	7.5µg/ml	-
F4/80 antigen	Rat anti-mouse F4/80	Cl:A3-1	AbD Serotec	IHC	1:50	2
CD8 antigen	Rat anti-mouse CD8a	53-6.7	BD Parmingen	IHC	1:20	2
CD4 antigen	Rat anti-mouse CD4	H129.19	BD Parmingen	IHC	1:20	2
Collagen type 1	Rabbit anti-mouse collagen type 1	-	Millipore	IHC	1:200	3
C3a	Rat anti-mouse C3a	I87-1162	BD Parmingen	ELISA	4µg/ml	4 and 7
C5a	Rat anti-mouse C5a	I52-1486	BD Parmingen	ELISA	1µg/ml	5 and 7
C3	Goat anti-mouse C3	-	MP Biomedicals	ELISA	8µg/ml	6
Crry	Rat anti-mouse crry	IF2	BD Parmingen	IF	0.25µg/ml	8
Mouse albumin	Rabbit polyclonal to mouse serum albumin	-	Abcam	RID	15µl/ml	-

Table 2.2. Secondary and capture antibodies

Number	Antibody	Source	Application	Dilution
1	Anti-mouse Envision^{+}	Dako	IHC	Manufacturer's instructions
2	Biotinylated goat anti-rat	BD Parmingen	IHC	1:100
3	Goat anti-rabbit HRP-conjugate	Dako	IHC	1:200
4	Biotinylated rat anti-mouse C3a	BD Parmingen	ELISA	1µg/ml
5	Biotinylated rat anti-mouse C5a	BD Parmingen	ELISA	1µg/ml
6	Goat anti-mouse C3c HRP-conjugate	Autogen Bioclear Ltd	ELISA	2µg/ml
7	Streptavidin HRP	BD Parmingen	IHC	1:1000
8	Goat anti-rat FITC-conjugate	Sigma Aldrich	IF	0.5µg/ml

2.3.4 Immunohistochemical staining for collagen I

Kidneys were cryo-sectioned, acetone-fixed and blocked with H_2O_2 using methods outlined previously in section 2.3.3. Non-specific binding of the secondary antibody was reduced by incubating slides in 20% goat serum in PBS for 1 hour at RT. Slides were then incubated with rabbit anti-mouse collagen type I primary antibody (1:200 dilution in PBS; **Table 2.1**), for 1hr at RT, then washed three times in PBS each for 5 minutes. Following this, slides were incubated with a horse radish peroxidase (HRP) conjugated goat anti-rabbit secondary antibody (diluted 1:200 in PBS; **Table 2.2**), for 1 hour at RT, then washed three times in PBS each for 5 minutes. During this time, DAB solution was prepared as outlined in section 2.3.3. Slides were covered with excess DAB solution and incubated for 12-13 minutes in the dark until sections had developed and turned brown. After DAB detection, slides were counterstained, dehydrated, imaged and analysed as outlined in section 2.3.3.

2.3.5 Immunohistochemical staining for alpha-smooth muscle actin

Paraffin-embedded renal tissue sections 3µm in thickness were prepared as described in section 2.3.1. Endogenous peroxidise activity was blocked by immersing slides in 0.3% H_2O_2 in PBS for 15 minutes, after which, slides were washed once in PBS for 5 minutes. Slides were then incubated with anti-mouse α-smooth muscle actin (α-SMA) primary antibody (diluted 1:10,000 in PBS; **Table 2.1**), for 1hr at RT and then washed three times in PBS each for 5 minutes. An Envision$^+$ System-HRP kit (**Table 2.2**) purchased from DAKO specifically for the detection of mouse primary antibodies, was used to detect the presence of anti-mouse α-SMA antibody.

Briefly, the kit consists of an HRP-labelled avidin and biotin-free polymer which is conjugated to a secondary antibody. Applied in the same way as a secondary antibody, the Envision^{+} system provides higher specificity, enhanced signal generation of antigens present at low concentrations and elimination of nonspecific endogenous avidin and biotin activities. Slides were covered with excess DAB solution and incubated for 15 minutes in the dark until sections had developed and turned brown. After DAB detection, slides were counterstained, dehydrated, imaged and analysed as outlined in section 2.3.3.

2.3.6 Immunofluorescence staining for anti-GBM antibody

Control staining to verify equal distribution of bound anti-GBM antibody was performed on un-fixed frozen kidney sections. 24 hour cryo-preserved NTS kidneys were sectioned and collected onto slides as described previously (section 2.3.3). Following 1 x 5 minute wash in PBS, sections were blocked in 5% horse serum (diluted in 1x PBS), for 1 hour at room temperature, followed by incubating with a FITC-conjugated donkey anti-sheep antibody (**Table 2.1**) for 1 hour at room temperature. Finally, slides were washed 3 x 5 minutes in PBS before mounting with fluorescent mounting medium (DAKO, UK) and glass cover slips. After 12 hours drying at RT, cover slips were sealed with nail varnish and slides stored at 4°C. Slides were imaged using a Leica LMD microscope.

2.3.7 Immunofluorescence staining for crry

Immunofluorescent staining was used to determine the distribution of crry within the renal cortex. Day three and day ten contralateral and UUO kidneys were cryo-sectioned using methods outlined previously in section 2.3.3. Sections were then washed 3 x 2 minutes with PBS to remove residual OTC compound. Slides were incubated with 0.25µg/ml rat anti-mouse antibody to crry/p65 (**Table 2.1**) for 1 hour at RT, before washing 3 x 5 minutes with PBS. Slides were then incubated in the dark at RT for 1 hour with 0.5µg/ml of FITC-conjugated goat anti-rat secondary antibody (**Table 2.2**). Slides were washed in the dark for 3 x 5 minutes with PBS before mounting with cover slips and storing as described previously (section 2.3.6). Slides were imaged using a Leica LMD microscope.

2.3.8 Immunofluorescence staining for C3

Immunofluorescent staining was used to determine the renal distribution of C3. Day three and day ten contralateral and UUO kidneys were cryo-sectioned using methods outlined previously in section 2.3.3. Sections were then washed 3 x 2 minutes with PBS to remove residual OCT compound. Following this, sections were blocked with 20% goat serum (Sigma Aldrich, UK) for 1 hour at RT. Serum block was removed by gently tapping slides onto the lab bench. Slides were then incubated in the dark at RT for 1 hour with 40µg/ml goat anti-mouse FITC-conjugated antibody (**Table 2.1**). Slides were washed in the dark for 3 x 5 minutes with PBS before mounting with cover slips and storing as described previously (section 2.3.6). Slides were imaged using a Leica confocal microscope.

2.3.9 Aperio and grid-based immunohistochemical analyses

Automated immunohistochemical analyses were performed using the Aperio Scanscope system (Staniszewski, 2009). Digital bright field images of renal tissues were captured using an Aperio Scanscope slide scanner at x20 magnification. For each tissue section, a region of interest (ROI) was selected and highlighted. The ROI was restricted to the renal cortex, which was itself defined by the presence of glomeruli. Automated analyses of all ROIs were performed using Aperio image analysis algorithms, which were modified for the purpose of this study (**Figure 2.4**, **Figure 2.5** and **Figure 2.6**). A non-automated counting method was used to verify automated analyses and to assess whether the results generated from using a less time-consuming automated method correlated with results obtained from quantifying observations using a non-automated counting method (Figure 2.3). For each animal, ten random screen shots of Aperio-scanned renal cortices at x20 magnification were captured and saved as image files. Images were then exported to Adobe Photoshop CS3 and a 10 x 10 grid was superimposed over each image. To analyse F4/80, collagen-1 and α-SMA immunohistochemical (IHC) staining, grid intersections present over areas of positive staining were counted and expressed as a percentage of the total number of grid intersections for each image (Figure 2.3B-C). Analysis of CD4 and CD8 positive T-cells was performed by counting the number of positively stained cells per high power field (HPF) image (Figure 2.3A). All Aperio and non-automated counts were carried out in a blinded manner.

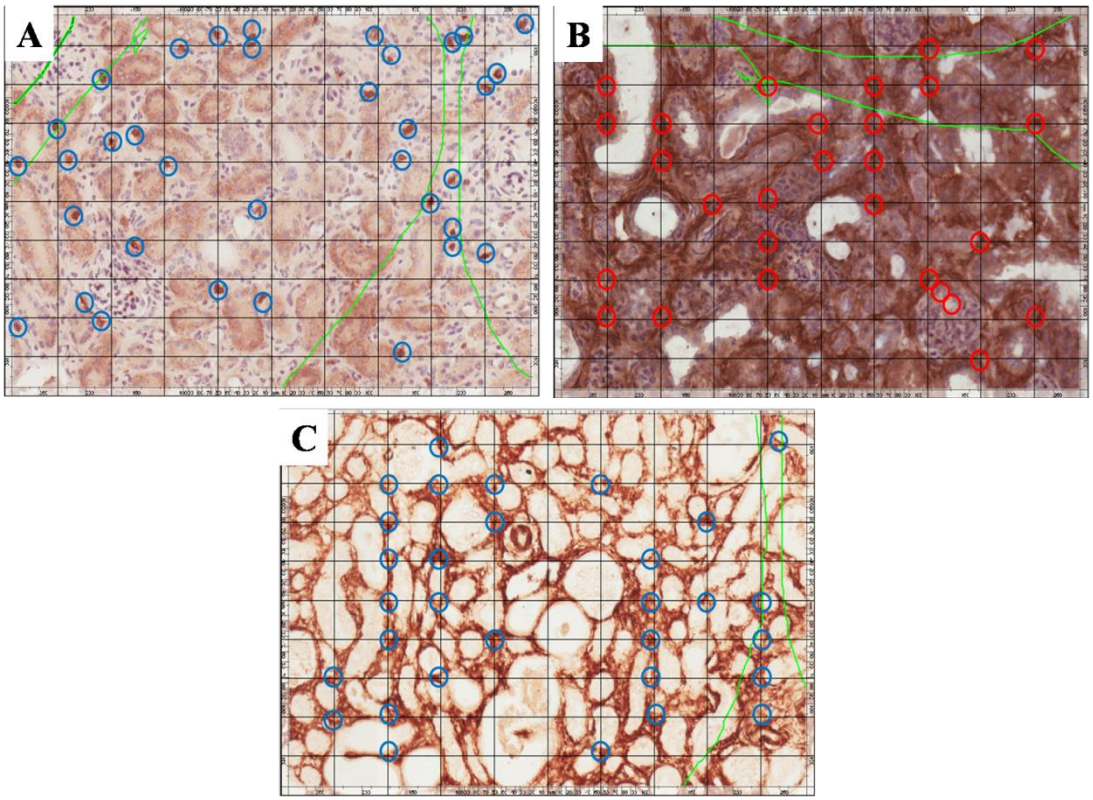

Figure 2.3. Manual scoring of immunohistochemically stained renal tissues
CD4 and CD8 positively stained T-cells in each HPF were counted (A). F4/80 macrophage staining was quantified by counting the number of grid intersections over areas of positive staining in each HPF (B). Collagen I and α-SMA staining was quantified in the same way as for F4/80 macrophage staining (C). Magnification x250.

2.3.9.1 Immunohistochemical nuclear algorithm

The IHC nuclear algorithm was used to count CD4 and CD8 positive T-cells within the renal cortices of day 10 WT and $C3^{-/-}$ mice (**Figure 2.4**). The algorithm was modified to account for a range of acceptable cell shapes and sizes and to detect only those cells with strong positive staining. The number of positive cells for each ROI (**Figure 2.4**A) were summed and expressed as the total number of positive cells per mm^2 of renal cortex.

2.3.9.2 Positive pixel count algorithm

The positive pixel count algorithm was used to measure the area of positive staining for F4/80, α-SMA and collagen-1 within the cortical interstitium of day 10 WT and $C3^{-/-}$ mice and for Sirius red histological staining in day 5 WT and $C3^{-/-}$ mice. For Sirius red and α-SMA staining, the algorithm measured the number of weak-positive, positive and strong-positive pixels (**Figure 2.5**A-D). For collagen I IHC, the algorithm measured the number of positive and strong positive pixels and for F4/80 IHC staining, the algorithm measured only the number of strong positive pixels (**Figure 2.6**A-B). The number of positive pixels for each ROI was converted to mm^2 and then expressed as a percentage of the overall area measured for each tissue section.

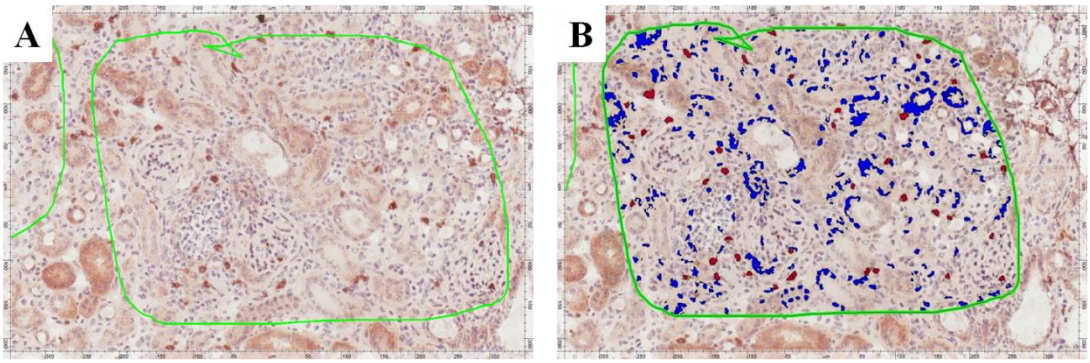

Figure 2.4. Automated immunohistochemistry cell count
A region of interest is selected (A). The IHC nuclear algorithm is used to count the number of positively stained cells (red) within the region of interest (B). The algorithm can also be used to identify negatively stained cells (blue). Magnification x150.

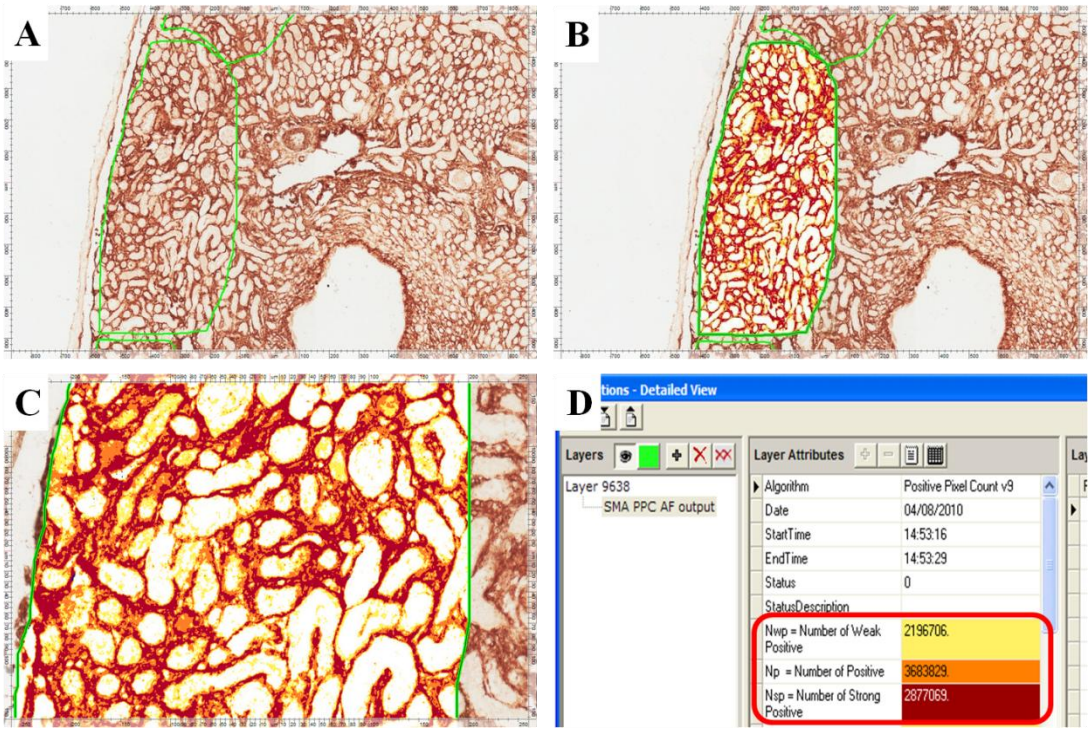

Figure 2.5. Automated α-SMA immunohistochemistry scoring
A region of interest is selected (A), x 60 magnification. The positive pixel count algorithm is used to count the number of strongly stained positive pixels (red), the number of positively stained pixels (orange) and the number of weakly stained positive pixels (yellow) within the region of interest (B and C), at x60 and x200 magnification respectively. A numerical read out for the selected region of interest in A, B and C (D). The same version of this algorithm was used for the automated analysis of day 5 UUO tissues stained for Sirius red.

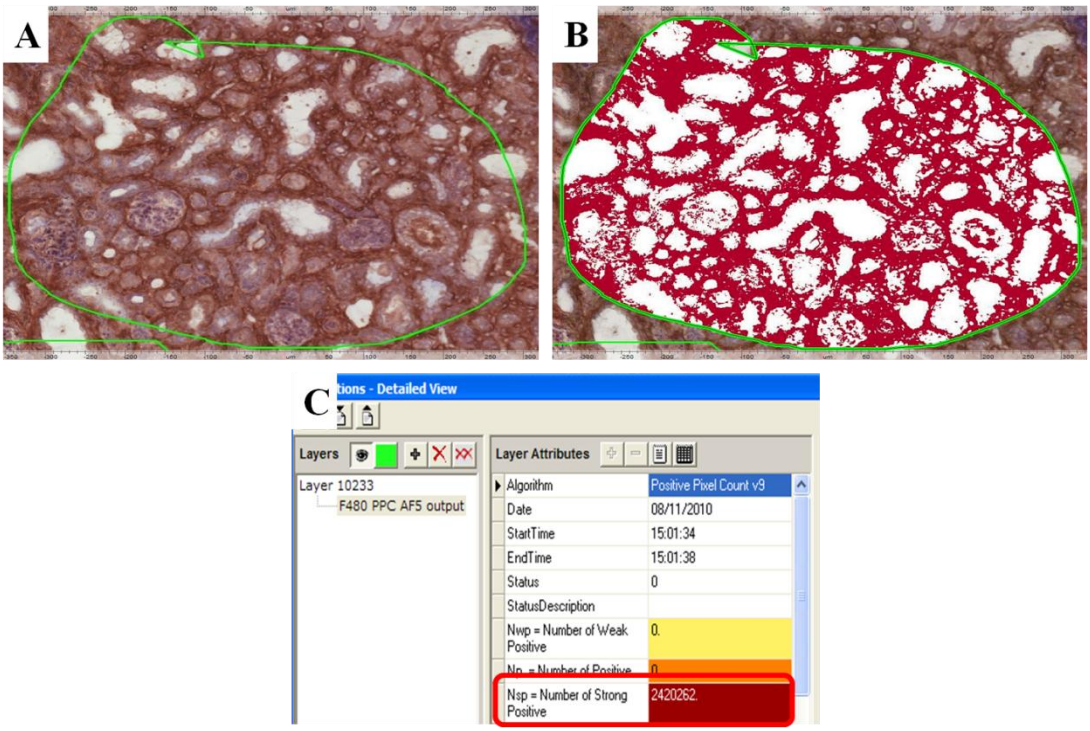

Figure 2.6. Automated F4/80 immunohistochemistry scoring
A region of interest is selected (A). The positive pixel count algorithm is used to count the number of strongly stained positive pixels (red) within the region of interest (B). A numerical read out for the selected region of interest in A and B (C). Magnification x120.

2.4 Molecular biology

2.4.1 Total RNA extraction from whole kidney

Total RNA was extracted from whole kidney tissue by phenol chloroform extraction and isopropanol precipitation. Unless otherwise stated, all centrifugation steps were carried out at 4°C. Snap frozen fragments of kidney cortex were transferred to 800µl of TRIzol reagent in a 1.5ml RNase free microcentrifuge tube without allowing the tissue to defrost. The tissue was homogenised for 2-3 minutes using a plastic RNase free pestle and then centrifuged at 8161g for 10mins. The supernatant was transferred to a phase lock gel tube (Eppendorf UK Limited) into which 160µl of chloroform was added and the solutions mixed by vigorous shaking.

Samples were left at RT for 2-3mins before centrifugation at 8161g for 15 minutes. The top aqueous phase was then transferred to a new tube into which 640µl of isopropanol was added. Samples were incubated at -20°C for 60 minutes to allow the RNA to precipitate out. Following further centrifugation at 8161g for 10 minutes, the supernatant was removed leaving the RNA pellet. After washing in 75% ethanol, the RNA pellet was dried at RT for up to 60 minutes to allow evaporation of excess ethanol and then re-suspended in 25µl nuclease-free water. All RNA samples were stored at -80°C until required.

2.4.2 Extraction of RNA from cells

RNA was extracted from cells using an RNeasy mini kit purchased from Qiagen Ltd, Crawley, Sussex according to manufacturer's instructions.

Briefly, cells were lysed in their culture vessels by addition of 600µl of guanidine-thiocyanate buffer (buffer RLT). An equal volume of 70% ethanol was added to the lysate and the solution mixed by pipette aspirating. The resulting suspension was transferred to an RNeasy spin column and centrifuged at 8000g for 15 seconds. The flow-through was discarded and RNA which had bound to the column was washed twice each with buffers RW1 and RPE. RNeasy spin columns were centrifuged between each wash as before. Finally, RNA was eluted by the addition of 25µl nuclease-free water.

2.4.3 Quantification and integrity of RNA from tissues and cells

The quantity and purity of whole RNA was measured using a Nanodrop spectrophotometer. Briefly, a 1µl RNA sample was loaded on to the platform of the Nanodrop and the ratio of absorbance at 260 and 280nm for each sample was calculated. Ratios in the range of 1.8-2.0 were accepted as 'pure' RNA for this study. The ratio of absorbance at 260 and 230nm was also used as a secondary measure of RNA purity, with ratios in the range of 1.8-2.2 accepted for this study. In addition to this, RNA integrity and genomic DNA contamination were determined by RNA gel electrophoresis. Briefly, a 1.2% native agarose gel was prepared in 1 x TBE buffer by heating with ethidium bromide (EtBr) added to give a final concentration of 0.5µg/ml. The ssRNA ladder (New England Biolabs, UK), RNA samples and loading buffer mixes were prepared and heated to 65ºC for 5 minutes before cooling on ice. Once the gel had set, it was transferred to an electrophoresis gel tank and submerged in 1 x TBE buffer. The ssRNA ladder and RNA samples were added to the wells and the gel was resolved at 90V for 40 minutes.

Discrete bands for 18s and 28s ribosomal RNA were detected under UV light using an Alpha Innotech gel doc and accompanying computer software (Alpha Innotech, CA).

2.4.4 Reverse transcription reactions

Before mRNA can be amplified using primers and measured in a PCR reaction it must first be reverse transcribed to obtain cDNA. In this study, two different methods of reverse transcription were used. In the first method, cDNA synthesis was carried out according to the method of Sambrook *et al* (1989) using the RNA extracted in section 2.4.1. RNA samples were denatured by heating to 90^{o}C for 5 minutes and then transferred to ice. A master mix containing reverse transcription reagents in the following quantities (excluding RNA and nuclease-free water), was prepared in a nuclease-free microcentrifuge tube kept on ice:

Reverse transcriptase buffer (5×)	4 μl
DTT (100mM)	2 μl
RNAsin (40U/μl)	0.75 μl
dNTP mixture (5mM each)	2 μl
oligo $(dT)_{15}$ (0.5 μg/μl)	0.32 μl
Superscript reverse transcriptase III (200U/μl)	1 μl

250ng of total RNA

Nuclease-free water (up to total volume of 20μl)

The resulting 20µl reaction mixture was incubated at 37^{o}C for 90 minutes using. The cDNA product was diluted in nuclease-free water and then stored at -20^{o}C. In the second cDNA synthesis method, RNA extracted in sections 2.4.1 and 2.4.2 was reverse transcribed using a cDNA synthesis kit purchased from Agilent Technologies, Wokingham, UK. Briefly, 250ng of RNA was combined with nuclease-free water up to a final volume of 15.7µl and then 1µl of 0.5µg/µl oligo (dT) primer was added. The RNA-oligo (dT) mix was heated to 65°C for 5 minutes and then gradually cooled to 22ºC using a G-storm 482 thermal cycler. The RNA-oligo (dT) samples were transferred to ice and the following reagents were added in the order set out below:

10 x AffinityScript buffer	2µl
100mM dNTPs (25mM each dNTP)	0.8µl
RNase Block Ribonuclease inhibitor (40U/µl)	0.5µl
AffinityScript Multiple temperature Reverse Transcriptase	1µl

The final reaction mixture was transferred to a thermal cycler and heated to 45°C for 5 minutes, 55°C for 1 hour and 70°C for 10 minutes, then cooled to 4°C. The cDNA product was diluted and stored as described previously.

2.4.5 Real time PCR

Real time PCR (rtPCR) is a quantitative method used for precisely measuring the mRNA expression of different genes.

For conventional PCR, amplification of the correct product can only be visualised as bands on an agarose gel at the end point of the reaction. In contrast to this, an rtPCR reaction can be monitored during the early (exponential) stages of amplification, prior to the reaction slowing down (linear stage) and reaching the final end point (plateau). It is during the exponential phase of an rtPCR reaction that the quantity of a product can be determined, since doubling of the product is occurring at each cycle at this time.

2.4.5.1 SYBR green I chemistry

In this study, SYBR green I fluorescent dye was used to quantify the amount of cDNA in each reaction. SYBR green is highly specific for dsDNA. It binds to the minor-groove of a DNA template and increases its fluorescence once bound. For each new copy of dsDNA, a proportionate increase in fluorescence occurs. A disadvantage to SYBR green chemistry is that it is also possible for non-specific dsDNA products such as dimerised primers to be amplified, giving a false positive signal. To overcome this, a dissociation curve analysis is run after the rtPCR reaction to determine the melting temperatures of all dsDNA products. For each primer set, it is expected that the amplified product in all sample wells will have the same melting temperature. Amplification of non-specific products using SYBR green can be determined in this way and further confirmed by agarose gel electrophoresis.

Table 2.3. rtPCR primers

Name	Sequence	Amplicon size, reference	rtPCR cycle conditions
β-actin forward	5'- GAT CAA GAT CAT TGC TCC TCC TG -3'	182bp NM_007393.3 GI:145966868	40 cycles: 95°C for 15 seconds 60°C for 45 seconds 72°C for 45 seconds
β-actin reverse	5'- GGG TGT AAA ACG CAG CTC AGT -3'		
C3 forward	5'- TCA CAC ACC GAA GAA GAC TGC C -3'	408bp NM_009778.2 GI:126518316	40 cycles: 94°C for 15 seconds 60°C for 60 seconds 72°C for 20 seconds
C3 reverse	5'- GTG GCT GAT GAA CTT GCG TTG C -3'		
FB forward	5'- ACA AGC CAG TTG TGA GAG AGA TG -3'	195bp NM_001142706.1 GI:218156290	50 cycles: 94°C for 15 seconds 60°C for 60 seconds 72°C for 60 seconds
FB reverse	5'- ATC ACA CCA ACT TGA ATG AAG CGG -3'		
FH forward	5'- TGC TGT GAC CAC AGT TCA TAG C -3'	162bp NM_009888.3 GI:109627651	40 cycles: 95°C for 15 seconds 54°C for 60 seconds 72°C for 45 seconds
FH reverse	5'- GAG GAC CTT TAC AAT CTT CTG CTG C -3'		
FI forward	5'- TTT CCA CTG GGT GTT CGT GAC -3'	105bp NM_007686.2 GI:110347405	40 cycles: 95°C for 15 seconds 56°C for 45 seconds 72°C for 45 seconds
FI reverse	5'- GGT CTC TAC TCC CCG GCA AT -3'		
CD59a forward	5'- GAG CAT GAG CAC AGT CAC TGG CG -3'	259bp NM_001111060.1 GI:161484615 (Var-1) 139bp NM_007652.4 GI:161484614 (Var-2)	40 cycles: 95°C for 15 seconds 60°C for 45 seconds 72°C for 45 seconds
CD59a reverse	5'- GAA CAC AGC CAG AAG CAG CAG GAG -3'		

Crry forward	5'- GGC AGC TGG AAT CCT CTT CTG GC -3'	258bp NM_013499.2 GI:52426749	40 cycles: 95°C for 15 seconds 62°C for 60 seconds 72°C for 20 seconds
Crry reverse	5'- TGC TGG GCT AGT GGT ACT GCT GTT -3'		
CD55 forward	5'- AGC CTA ACA CAG GTG GTG ACC G -3'	111bp NM_010016.2 GI:114326521	50 cycles: 95°C for 15 seconds 60°C for 45 seconds 72°C for 45 seconds
CD55 reverse	5'- TCT TCG TTG GCT ATG TCA AGT AGC C -3'		
TNF-α forward	5' - ATC CGC GAC GTG GAA CTG GC -3'	279bp NM_013693.2 GI:133892368	40 cycles: 95°C for 15 seconds 60°C for 45 seconds 72°C for 45 seconds
TNF-α reverse	5'- GTG GTT TGC TAC GAC GTG GGC T -3'		
TGF-β forward	5'- CCT GAG TGG CTG TCT TTT GAC G -3'	91bp NM_011577.1 GI:6755774	40 cycles: 95°C for 15 seconds 58°C for 60 seconds 72°C for 20 seconds
TGF-β reverse	5'- AGT GAG CGC TGA ATC GAA AGC -3'		
IL-6 forward	5'- GAG GAT ACC ACT CCC AAC AGA -3'	141bp NM_031168.1 GI:13624310	40 cycles: 94°C for 15 seconds 55°C for 60 seconds 72°C for 20 seconds
IL-6 reverse	5'- AAG TGC ATC ATC GTT GTT CAT A -3'		
Collagen -I(a1) forward	5'- GAG CGG AGA GTA CTG GAT CG -3'	204bp NM_007742.3 GI:118131144	40 cycles: 94°C for 15 seconds 53°C for 60 seconds 72°C for 20 seconds
Collagen -I(a1) reverse	5'- TAC TCG AAC GGG AAT CCA TC -3'		

Collagen -III(a1) forward	5'- CTA GTG GCT TCC GAG GAC CT -3'	65bp NM_009930.2 GI:226423932	40 cycles: 95°C for 15 seconds 55°C for 60 seconds 72°C for 20 seconds
Collagen -III(a1) reverse	5'- CTC TCC GGG AGG ACC CTT TT -3’		
α-SMA forward	5'- CTG ACA GAG GCA CCA CTG AA -3'	160bp NM_007392.2 GI:31982518	40 cycles: 95°C for 15 seconds 60°C for 45 seconds 72°C for 45 seconds
α-SMA reverse	5'- CAT CTC CAG AGT CCA GCA CA -3'		
S100a8 forward	5'- TGC GAT GGT GAT AAA AGT GG -3'	69bp NM_013650.2 GI:113930764	40 cycles: 95°C for 10 seconds 55°C for 30 seconds 72°C for 30 seconds
S100a8 reverse	5'- GGC CAG AAG CTC TGC TAC TC -3'		
S100a9 forward	5'- CAC CCT GAG CAA GAA GGA AT -3'	95bp NM_009114.2 GI:133893069	40 cycles: 95°C for 10 seconds 55°C for 30 seconds 72°C for 30 seconds
S100a9 reverse	5'- TGT CAT TTA TGA GGG CTT CAT TT -3'		

2.4.5.2 Setting up a qPCR reaction

In this study, rtPCR was performed on all cDNA samples using SYBR green I. Prior to using in rtPCR, primers were diluted to 1.25pmol/µl in nuclease-free water. All rtPCR reactions were performed in triplicate in a 20µl reaction mixture containing the following reagents:

SYBR green master mix (2x)	10µl
Forward and reverse primer mix (0.3125pmol/µl each)	5µl
ROX passive reference dye (50x)	0.4µl
Nuclease-free water	0.6µl
cDNA	4µl

An ABI Prism 7000 Sequence Detection System and a StepOnePlus Real-Time PCR System were used to measure expression of all genes of interest relative to the housekeeping gene. A housekeeping gene is defined as a gene which is present at the same level of expression during both normal and disease states. In some studies the expression of genes of interest are calculated relative to the average expression of a panel of different housekeeping genes. For the purpose of this study, gene of interest expression was calculated relative to that of the housekeeping gene β-actin. Following an initial denaturation period at 95°C for 15 minutes, primer-specific cycles of denaturation, annealing and extension were run as set out in **Table 2.3**. At the end of each cycle, SYBR green fluorescence was measured. After the last rtPCR cycle, a melt curve analysis was performed on all samples, before cooling to 4°C.

Amplification data and melt curve recordings were collated using accompanying computer software programmes for each detection system and then interpreted using Microsoft Excel and GraphPad Prism 5 software packages. rtPCR products were confirmed visually by agarose gel electrophoresis to verify amplification of the correct product. Briefly, a 2 or 2.5% agarose gel (depending upon predicted size of rtPCR product) was prepared by the addition of 1 or 1.25g agarose to 50ml 1x TBE buffer (pH8.3). The solution was heated in a microwave for up to two minutes to facilitate the agarose to dissolve. 50µl of EtBr was added to give a final concentration of 0.5µg/ml. When the agarose gel had cooled slightly, it was poured into a running chamber which had been sealed at the top and bottom. One or more combs were placed onto the running chamber, creating small wells into which samples would be loaded once the gel had set (after 30-40 minutes). The solidified gel was placed into an electrophoresis gel tank containing 1x TBE running buffer and then PCR product samples were added directly to wells at a volume of 10µl each. 10µl of a 50-1000 bp DNA ladder (Geneflow Ltd, Staffordshire, UK) was added to one of the wells on the gel to assist with identification of PCR products according to their size. Gels were resolved for 30-45 minutes at 100V and then imaged using an Alpha Innotech gel doc with accompanying computer software. All melt curve abnormalities, were confirmed by agarose gel electrophoresis and subsequently excluded from relative quantification of gene expression calculations.

2.4.5.3 Relative quantification of gene expression ($\Delta\Delta C_T$ method)

The comparative C_T method ($\Delta\Delta C_T$) is a type of analysis used to quantify the expression of a target gene relative to the expression of a control (reference) gene.

During exponential amplification, the number of PCR cycles required for a fluorescent signal to cross a threshold that exceeds background fluorescence levels is known as the cycle threshold (C_T). Unlike the target gene, the reference gene (usually a housekeeping gene) maintains a constant level of expression during healthy and diseased states. Comparative expression of the target gene relative to an endogenous reference is calculated as $2^{-\Delta\Delta CT}$ .Where $\Delta\Delta C_T = \Delta C_T$ target gene - ΔC_T reference gene.

2.4.5.4 Primer efficiencies

To calculate the efficiency and sensitivity of all primer pairs used in rtPCR reactions, a series of 1:5 serial dilutions of affected cDNA were prepared and added to the SYBR green reaction mixture as described previously (section 2.4.5.2). The rtPCR cycle conditions for each primer pair are described in **Table 2.3**. For a given primer pair, the C_T values obtained for each sample dilution were used to calculate the efficiency of the PCR reaction and the samples resolved on an agarose gel to verify correct amplicon size.

2.5 *In situ* hybridisation

In situ hybridisation (ISH) is a method used to visualise the precise location of target nucleic acid sequences within morphologically identifiable structures such as tissues and cells. It is based on the principle that labelled nucleic acid probes will pair with complementary nucleic acids present in target tissues.

2.5.1 Design and synthesis of PCR-derived RNA probes

A sequence of bases specific to the RNA polymerases SP6 and T7 were added to the beginning of forward and reverse C3 primer sequences as set out below:

Probe	**Sequence**
SP6 ‘sense’	5’ – AAT ACG ATT TAG GTG ACA CTA TAG ATT ACC TTG TGT GGG GCT GTT AAA TG – 3’ (50 bases)
T7 ‘anti-sense’	5’ – TAA GTT AAT ACG ACT CAC TAT AGG GCG ACA AGG CTT GGA ATA CCA TGA AGG – 3’ (51 bases)

Sequences in RED represent SP6 and T7 binding sites, sequences in GREEN represent C3 forward and reverse primer sequences. Three rounds of conventional PCR with the above designed primers were used to amplify part of mouse complement C3 which was 598 base pairs in length, using day 10 WT UUO mouse cDNA as a template. The purpose of performing multiple rounds of conventional PCR was to generate a highly purified cDNA product from which high quality RNA probes could be synthesised later. Following the first round of PCR amplified product was resolved by electrophoresis on a 2% agarose gel, at 100V for 30 minutes (section 2.4.5.2) and then extracted using a QIAquick gel extraction kit (Qiagen, Crawly, UK), according to the manufacturer’s instructions The amount of PCR product was quantified using a Nanodrop spectrophotometer. Purified PCR product derived from the first round of PCR amplification was diluted 1:10 and 1:100 and used as a template for two individual second round PCR reactions.

The resulting second round PCR products were resolved by agarose gel electrophoresis then purified and quantified. The second round PCR products were used as a template for third round PCR reactions, from which the resulting products were purified and quantified in the same way as for first and second round PCR reactions. Purified PCR products were stored at -20°C.

PCR cycle conditions: 94°C for 2 minutes

94°C for 30s, 55°C for 30s, 68°C for 30s(x 30)

72°C for 10 minutes

First, second and third round PCR reaction mixes were made as outlined below. Note that second and third round PCR reactions were performed twice, each using different dilutions (1:10 and 1:100) of first and second round PCR reaction products:

Reagents (stock concentration)	**1st round PCR**	**2nd round PCR**	**3rd round PCR**
Sense primer (100µM)	0.2µl	0.1µl	0.1µl
Anti-sense primer (100µM)	0.2µl	0.1µl	0.1µl
DEPC H_20	11.6µl	17.8µl	17.8µl
PCR mix	80µl	80µl	80µl
cDNA template (4ng/µl)	8µl	-	-
PCR product (1:100)	-	1µl	1µl
PCR product (1:1000)	-	1µl	1µl

2.5.1.1 In vitro transcription of DIG-UTP labelled RNA probes

During RNA probe synthesis, T7 and SP6 RNA polymerases are to be used to produce "run-off" transcripts which incorporate digoxigenin (DIG)-UTP into the newly synthesised RNA probes at approximately every 20-25th nucleotide. Single stranded complementary RNA probes were synthesised by *in vitro* transcription using reagents purchased from Roche Applied Science, Burgess Hill, UK:

PCR DNA probe	75ng
Transcription buffer (10x)	2µl
Digoxigenin (DIG) labelling mix	2µl
RNAsin	1µl
RNA polymerase	2µl
ddH_2O	Up to 20µl

The above reaction mixture was incubated at 37°C for 2 hours. To remove template DNA, 2µl of DNase 1 from the same kit was added to the reaction mixture and then incubated for a further 15 minutes at 37°C. Following the second incubation, DEPC H_2O was added to the reaction mixture up to a final volume of 50µl. Unincorporated NTPs were removed from the mixture by spin column purification using Spin ProbeQuant G-50 Micro Columns (GE Healthcare, Buckinghamshire, UK), centrifuged at 2500rpm for 2 minutes. Probes were quantified using a Nanodrop spectrophotometer.

2.5.1.2 Dot blot verification of Dig-labelled RNA probes

Following *in vitro* transcription of RNA probes, a dot blot was used to verify DIG labelling of the probes. Briefly, 1:10, 1:100, 1:1000 and 1:10.000 dilutions of labelled probe and control RNA (Roche Applied Science) were prepared in sterile water. 1µl of each dilution was blotted onto a piece of Hybond nitrocellulose membrane (GE Healthcare), air-dried and then cross-linked by exposure to UV at 125Mj. The membrane was washed in PBS Tween 20 (PBST) containing 0.3% Tween 20 for 2 minutes and then blocked with 1% blocking solution (Sigma Aldrich) for 30 minutes. Following this, the membrane was incubated with an alkaline phosphate-labelled Anti-Digoxygenin (anti-Dig) antibody (Roche Applied Science) diluted 1:5000 in PBS for 20 minutes. The blot was then washed with 0.3% PBST for 5 minutes. The above incubations and washes were carried out at RT with agitation. Nitro-blue tetrazolium (NBT) and 5-bromo-4-chloro-3'-indolyphosphate (BCIP) chromogen solution (Roche Applied Science) was prepared in buffer 2 (20µl NBT-BCIP/ml). The blotting membrane was immersed in NBT-BCIP solution for 1 hour in the dark at RT. Following this, the membrane was washed in ddH_2O for 5 minutes with agitation at RT and then air dried.

2.5.1.3 Formamide gel resolution of RNA probes

Using RNase-free glassware, 5ml of 10x 3-(N-morpholino) propanesulphonic acid (MOPS) was added to 36ml of diethylpyrocarbonate (DEPC)-treated ddH_2O. 1g of agarose was added to the above solution which was then microwaved for 1 minute. The agarose solution was made up to 41 ml by addition of DEPC ddH_2O and then up to a final volume of 50 ml using 37% formamide.

The gel was poured into a cast and left to set at RT. Once set, the gel was transferred to a gel electrophoresis tank and immersed in 1 x MOPS EDTA running buffer. The RNA samples and RNA ladder (Fermentas GMBH, St. Leon-Rot, Germany) were heated to 70°C for 10 minutes and then cooled for 2 minutes on ice before loading on to the gel.

RNA samples	**RNA ladder**
5µl H_2O	3µl H_2O
6µl loading dye	6µl loading dye
1µl RNA	1µl ladder

The RNA formamide gel was run at 50V for approximately 2 hours. After this time, the gel was stained with SYBR green II dye (Invitrogen) in Tris-EDTA buffer for 15 minutes in the dark with agitation. Finally, the gel was washed briefly in ddH_2O, before visualisation.

2.5.2 Pre-hybridisation

Under RNase-free conditions, paraffin blocks containing formalin-fixed embedded kidney tissues were sectioned at 7µm intervals using a Leica Microtome. Sections were carefully transferred to RNase-free slides covered in DEPC-treated dH_2O. When all sections had been mounted on to slides, excess dH_2O was removed and slides were then allowed to dry at 37°C over night.

All solutions were made using DEPC treated H_2O or PBS and all glass ware was baked at 180° for 4 hours prior to use. Slides were taken through a series of rehydration steps consisting of three 5 minute washes in xylene, one 5 minute wash in 50% xylene:50% ethanol, two 3 minute washes in 100% ethanol and one wash each in 90%, 70% and 50% ethanol for 3 minutes. Slides were then washed twice for 2 minutes in PBS, before RNA was exposed by incubating with 20µg/ml proteinase K (Sigma Aldrich) in PBS for 8 minutes at 37°C. As a control, one slide was also treated with RNase. The purpose of this was to verify mRNA-specific binding of DIG-labelled probes during hybridisation. Slides were washed briefly in PBS before fixation in 4% paraformaldehyde in PBS for 20 minutes at RT. Following fixation, slides were washed twice with PBS each for 2 minutes. Slides were treated with 0.1M triethanolamine (Sigma Aldrich, pH 8.0) containing 0.25% acetic anhydride (Sigma Aldrich) in DEPC PBS for 10 minutes at RT and then washed twice in PBS. Acetic anhydride acetylates any amines that are present, neutralising their positive charge and subsequently preventing the binding of any DIG-labelled probes by electrostatic interaction. Sections were then dehydrated in the reverse order to which they were hydrated, for the same incubation times and using the same solutions as detailed above for the rehydration process. Once dehydrated, slides were air dried in a filtered air stream for 1 hour.

2.5.3 Hybridisation

Slides were transferred to a DEPC ethanol-treated hybridisation chamber containing slide trays and paper towel soaked in 50% 2x saline-sodium citrate buffer (2x SSC).

Slides were transferred onto the slide trays and then 100µl of probe-hybridisation mix (Roche Applied Science) containing 3ng/µl DIG-labelled probe was added to each slide before gently covering with a glass cover slip. Slides were incubated in the hybridisation chamber over night at 68°C.

2.5.4 Post-hybridisation

Following over night hybridisation, cover slips were removed by rinsing slides in 5x SSC which was pre-warmed to 60°C. Slides were then washed twice in 5x SSC and once in 2x SSC each for 10 minutes at 60°C, followed by a final wash in 2x SSC heated to 60°C, but incubated at room temperature on a shaker for 10 minutes. Prior to detection of the Dig-labelled probe, slides were washed three times in buffer 1 (section 2.1.3) each for 10 minutes and then transferred to a humidity chamber containing paper towels soaked in buffer 1. Dig-labelled probe was detected by incubating tissue sections with 150µl anti-Dig (Roche Applied Science, diluted 1:1000 in buffer 1, containing 2% foetal calf serum) at 4°C over night. Tissue sections were covered in parafilm cover slips for the duration of the above incubation. The following day, slides were washed three times in buffer 1 and then equilibrated in buffer 2 (section 2.1.3) by washing three times, each for 5 minutes. Slides were then transferred to a tray before being flooded with NBT/BCIP (Roche Applied Science; diluted to 20µl/ml in buffer 2). Slides were left to develop in the dark at room temperature over night. When slides had developed, further staining was inhibited by rinsing slides in buffer 2, followed by several changes of deionised water.

Slides were then mounted in Aquatex aqua mount (BDH Prolab) and sealed using nail polish. Slides were imaged using a Leica LCM microscope and accompanying computer software.

2.6 Cell culture

2.6.1 Boston University mouse proximal tubule cells

Boston University mouse proximal tubule cells (BUMPTs) were a generous gift form Professor John Schwartz.

2.6.2 Maintenance of BUMPT cells

Cells were cultured in high-glucose Dulbecco's Modified Eagle's Medium (DMEM) containing 100U/ml penicillin, 100µg/ml streptomycin and 10% foetal calf serum (FCS) and were maintained at 37°C with 5% CO_2 under constant humidity.

2.6.3 Passage of BUMPT cells

On reaching confluence (**Figure 2.7**A), cells were passaged and split 1:8 (**Figure 2.7**B). The supernatant was removed and the cells washed twice in PBS without Mg^{2+} and Ca^{2+}. Pre-diluted Trypsin-EDTA containing 0.5g/L trypsin and 0.2g/L EDTA, was added to the cell monolayer and the culture vessel incubated at 37°C for 5 minutes. Trypsinisation was stopped by the addition of one volume of complete culture medium.

The resulting cell suspension was centrifuged at 1000rpm for 5 minutes and the cell pellet re-suspended in complete medium. Cells were cultured in 75cm^2 culture flasks. Unless otherwise stated, cells were used at passage 15.

2.6.4 Preparation of frozen stocks of BUMPT cells

Frozen stocks of cells were prepared in DMEM containing FCS and dimethyl sulfoxide (DMSO). Cells used to produce frozen stocks were in the log phase of growth and were detached from culture vessels as described previously. Following centrifugation, cells were re-suspended in DMEM containing 10% FCS and 10% DMSO at a maximum concentration of 2x 10^6 cells/ml. 2ml aliquots of cell suspension were transferred to cryo-vials and cooled at a rate of 1°C/minute using an isopropyl alcohol bath placed in a -80°C freezer. Cells were then transferred to liquid nitrogen for long-term storage.

2.6.5 Revival of cryo-preserved BUMPT cells

Cells were warmed to room temperature as quickly as possible by removing from liquid nitrogen and transferring to a 37°C water bath until fully thawed. To prevent osmotic lysis, 5ml of culture media was added to the cell suspension very slowly drop-wise. The resulting cell suspension was centrifuged at 1000rpm for 5 minutes and the cell pellet re-suspended in 10ml complete medium before transferring to a 75cm^2 cell culture vessel. Cells were maintained as described in section 2.6.2.

2.6.6 Lipopolysaccharide stimulation of BUMPT cells

On reaching confluence, cells cultured in 75cm^2 culture flasks were passaged as described previously (2.6.3). Cells were seeded at a density of 60,000/cm^2 in 6-well plates. After 3 days, culture medium was replaced with fresh serum-free culture medium and left for 24 hours. The following day, cells were stimulated with lipopolysaccharide (LPS; Sigma Aldrich, UK) at 10ng/ml, 100ng/ml and 1000ng/ml, in triplicate wells under serum-free conditions for 12, 24 and 48 hour time points. Triplicate wells of un-stimulated cells were also established for each time point and LPS concentration. Following stimulation for each time point, 1ml of supernatant was removed for ELISA analysis and stored at -20°C. RNA was extracted from lysed cells using an RNeasy mini kit from Qiagen and following manufacturer's instructions. cDNA was synthesised as described previously (section 2.4.2). rtPCR was used to determine changes in C3 gene expression following LPS stimulation. An ELISA assays were used to measure C3 and C3a protein present in the supernatant.

2.7 Protein methodology

2.7.1 C3a ELISA

Corning EIA/RIA medium-binding 96 well plates were coated with 4µg/ml purified rat anti-mouse C3a (**Table 2.1**; BD Biosciences, UK) in 0.2M sodium phosphate buffer (pH 6.5) overnight at 4°C. Excess antibody was removed by washing three times with PBS. The plates were blocked by the addition of 1% bovine serum albumin (BSA) in PBS for 2 hours then washed three times with PBST containing 0.05% Tween 20 (0.05% PBST).

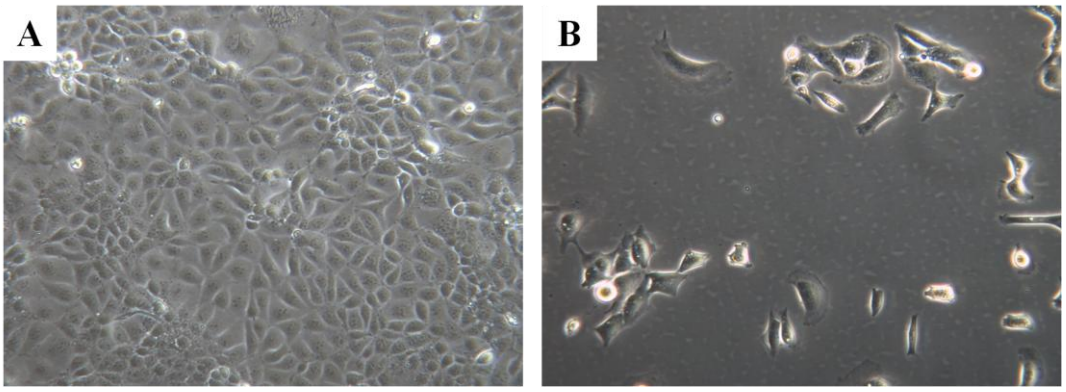

Figure 2.7. Boston University mouse proximal tubule (BUMPT) cells.
Confluent and sub-confluent BUMPT cells at passage 15 (A and B respectively). BUMPT cells displayed typical 'cobble stone' epithelial morphology. Magnification x200.

Mouse urine samples and BUMPT cell supernatants were diluted 1:25 and 1:10 respectively in 0.5% BSA-PBS and then added to wells and incubated for 2 hours. Similarly, BUMPT cell supernatants were diluted 1:10. Purified mouse C3a protein (BD Biosciences, UK) was selected as a standard control and diluted to 50, 25, 12.5, 6.25, and 3.125ng/ml in 0.5% BSA-PBS before adding to wells and incubating as for the urine samples above. Following this, plates were washed five times with PBST before incubating with 1µg/ml biotinylated rat anti-mouse C3a (BD Biosciences, UK; **Table 2.2**) in PBS for 1 hour. Plates were again washed five times with 0.05% PBST and then incubated with streptavidin-HRP (BD Biosciences, UK; **Table 2.2**) diluted 1:1000 in PBS for 1 hour. Plates were once again washed five times with 0.05% PBST. HRP was detected by the addition of O-Phenylenediamine dihydrochloride substrate (SigmaFast-OPD) for 30 minutes in the dark.

The reaction was stopped by the addition of 50µl 2M H_2SO_4 and the optical density (OD) measured at 490nm using an OpsysMR plate reader (Dynex Technologies Limited, UK). Unless otherwise stated, all antibody incubations were carried out at RT. A standard curve for OD of known C3a concentrations was plotted and urinary C3a concentrations were then calculated.

2.7.2 C3 ELISA

Corning EIA/RIA medium-binding 96 well plates were coated with 8µg/ml purified goat anti-mouse C3 (MP Biomedicals Inc, Ohio; **Table 2.1**) in PBS (pH 7.4) overnight at 4°C. Excess antibody was removed by washing twice with PBST and twice again with PBS.

The plates were blocked by the addition of 2% BSA-PBST for 1 hour at RT then washed twice with PBST and then twice again with PBS. Mouse serum collected by cardiac puncture was diluted to 1:1000, 1:2000, 1:4000, 1:8000, 1:16,000, 1:32,000, 1:64,000, 1:128,000, 1:256,000, 1:512,000, 1:1024,000 in 2% BSA-PBST then added to wells and incubated for 1 hour at 37ºC. Following this, plates were washed twice with PBST and twice again with PBS before incubating with HRP-conjugated goat anti-mouse C3c (Autogen Bioclear Ltd, UK; **Table 2.2**) diluted to 2µg/ml in 2% BSA in PBST for 1 hour at 37ºC. Plates were once again washed twice with PBST and then twice again with PBS. HRP was detected by the addition of O-Phenylenediamine dihydrochloride (SigmaFast-OPD) substrate for 7.5 minutes at RT in the dark. The reaction was stopped by the addition of 50µl 2M H_2SO_4 and the OD measured at 490nm using an OpsysMR plate reader (Dynex Technologies Limited, UK). Initial serum C3 concentration was assumed to be 1mg/ml.

2.7.3 C5a ELISA

Corning EIA/RIA medium-binding 96 well plates were coated with 100µl/well 1µg/ml purified rat anti-mouse C5a (BD Biosciences, UK; **Table 2.1**) in 0.2M sodium phosphate buffer (pH 6.5) overnight at 4°C. Excess antibody was removed by washing three times with PBST. The plates were blocked by the addition of 200µl/well 10% FCS in PBS for 1 hour and then washed three times with PBST. Mouse urine collected from the dilated pelvis of day 3 and day 10 obstructed kidneys was diluted 1:25 in 0.5% BSA-PBS then added to wells and incubated for 2 hours.

Purified recombinant mouse C5a protein (BD Biosciences, UK), was selected as a standard control and diluted to 200, 100, 50, 25, 12.5, 6.25, 3.125, 1.5626pg/ml in 0.5% BSA-PBS before adding to wells and incubating as for the urine samples above. Following this, plates were washed five times with PBST before incubating with biotinylated rat anti-mouse C5a (BD Biosciences, UK; **Table 2.2**) diluted 1:500 in PBS for 1 hour. After washing five times with PBST, the plates were incubated with the streptavidin-HRP used in section 2.7.1 under identical conditions. Plates were once again washed five times with PBST. HRP was detected by the addition of 3,3',5,5'-tetramethylbenzidine substrate (Sigma Aldrich) for 10 minutes in the dark.

The reaction was stopped by the addition of 50µl 2M H_2SO_4 and the OD measured at 450nm using a Dynatech MRX microplate reader (Dynatech Laboratories Inc, Chantilly, VA) standard curve for OD of known C5a concentrations was plotted and urinary C5a concentrations were then calculated. Unless otherwise stated, antibody incubations were carried out at RT.

2.7.4 Radial immunodiffusion assay to detect urinary albumin

Urine albumin concentration was measured by radial immunodiffusion in 1.2% agarose gels containing 150µl of rabbit anti-mouse albumin antibody (Abcam, Cambridge, UK; **Table 2.1**) per 10ml of gel. The agarose/antibody solution was carefully poured onto a 10x10cm glass plate on a flat surface and left to set at RT. Once set, 3mm wells were cut in to the gel and the plugs removed by suction. Standard solutions of mouse albumin measuring 1.6, 0.8, 0.4, 0.2, 0.1 & 0.05mg/ml and test urine samples (diluted 1:10), were prepared in dH_2O and added to the agarose gels in duplicates each containing 4µl/well.

The agarose-coated glass plates were incubated in a humidified box for 24 hours at 4°C to equilibrate. The next day, gels were transferred on to the hydrophilic side of a piece of gel-bond membrane (Lonza Biologics plc, Tewkesbury, UK) and detached from the glass plates. Filter papers were then stacked on top of the non-membrane side of the gel and a small weight placed on top for 1-2 hours to facilitate absorption of excess moisture. Following this the gels were dried using a hairdryer. The albumin diffusion rings on the membrane were visualised by staining with 1% coomassie blue (section 2.1.4) for 20 minutes, after which, the membranes were repeatedly washed with destain solution (section 2.1.4) and then allowed to air dry. Coomassie-stained membranes were scanned to obtain computerised image files. Triplicate measurements for each standard solution diameter ring were obtained using ImageJ (v.1.45) software and then averaged to construct a standard curve of known albumin concentrations. The albumin concentration for each urine test sample was extrapolated from the standard curve using an averaged triplicate measurement for each urine test diffusion ring.

2.8 Statistical analyses

Data were analysed using an unpaired t-test, a Mann-Whitney U-test (with Bonferroni Correction) or a Wilcoxon Signed Rank test as appropriate and were expressed as either the mean + the standard error of the mean (SEM) or as median values. All statistical analyses were performed using Graphpad Prism 5.0 computer software. Data were considered statistically significant where $p<0.05$.

3 Characterisation of renal injury in WT and C3$^{-/-}$ mice during UUO

3.1 Introduction

The first stage in determining the role of complement during obstructive nephropathy was to characterise the progression of renal tissue injury in WT and C3$^{-/-}$ mice at early and advanced time points during the course of disease progression. The histological and pathological hallmarks of obstructive renal disease were compared in WT and C3$^{-/-}$ mice to determine the role of complement towards progression of fibrosis. For this study the model of UUO was chosen as it has been extensively studied and leads to the development of fibrosis, a common feature in the development of many human renal diseases leading to decline in renal function and subsequent ESRD.

3.2 Scoring of histological injury in WT and C3$^{-/-}$ mice following UUO

Interstitial expansion and tubular dilatation were evident in the renal cortices of WT and C3$^{-/-}$ mice following three days of UUO. In both experimental animal groups, epithelial cells lining dilated tubules had lost their characteristic apical membrane brush boarder and appeared flattened (Figure 3.1A and B). Some of the dilated tubules contained debris.

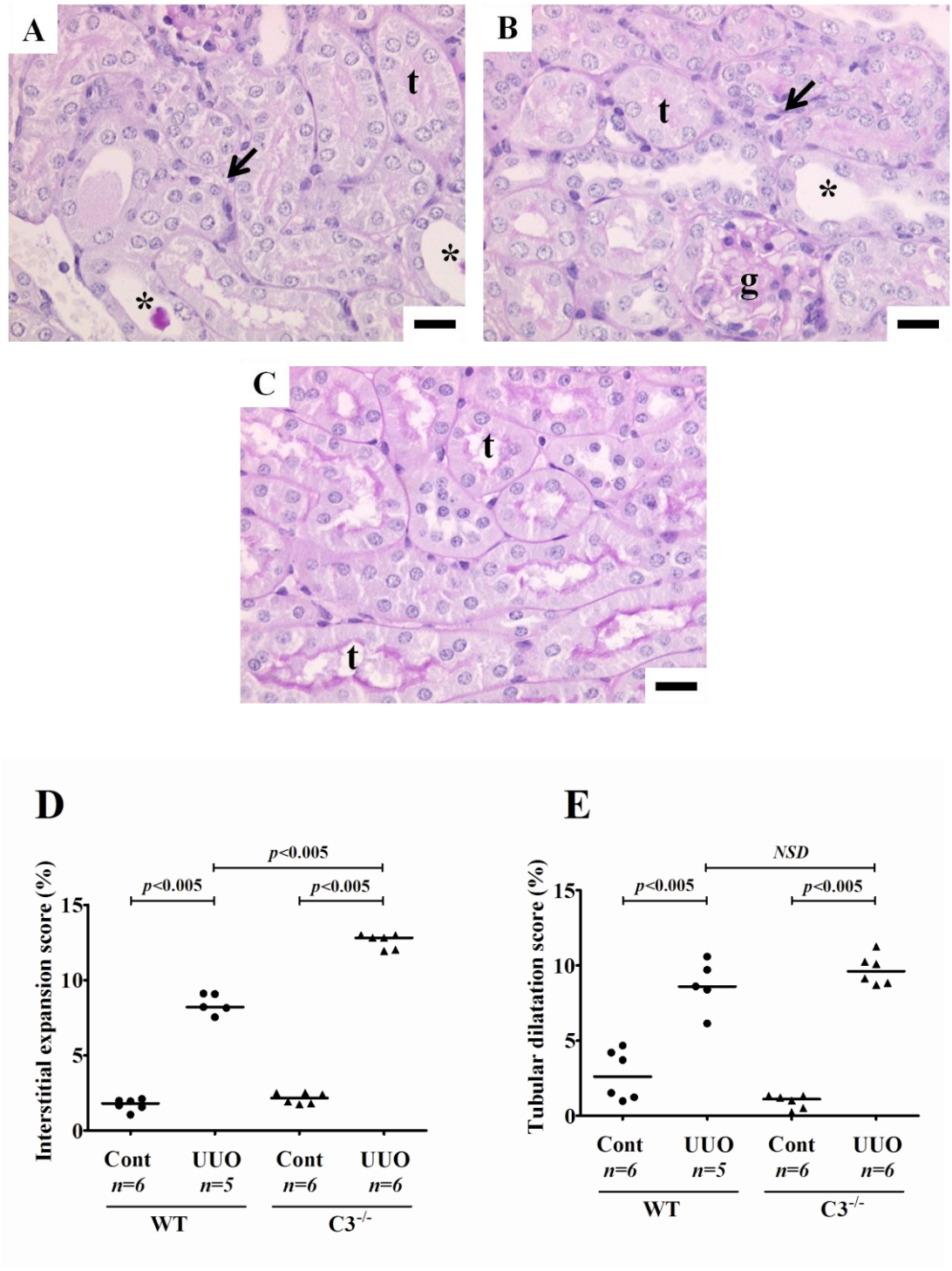

Figure 3.1. Histological injury at day three UUO
Histological injury in WT and C3$^{-/-}$ mice after three days of UUO. PAS staining of obstructed WT (A) and C3$^{-/-}$ (B) renal cortices. Representative image of contralateral renal cortex illustrating normal renal morphology (C). Arrows indicate areas of interstitial expansion. Asterisks identify dilated tubules. Tubules (t), glomerulus (g). Scoring of interstitial expansion (D) and tubular dilatation (E) using a grid based counting method. Scale bars on A-C represent 20µm. Bars on graphs D and E represent median values.

Three days post UUO, the tubular interstitium had expanded, forcing tubules apart, and contained a small number of cells as indicated by haematoxylin-stained nuclei. The glomeruli were unaffected at this stage and displayed normal glomerular morphology. In order to semi-quantify tubular and interstitial injury, a grid was superimposed onto each acquired image and the number of intersections over areas of interest counted and expressed as a percentage area. After three days of UUO, interstitial volume (Figure 3.1D), was significantly greater in obstructed groups compared with the contralateral kidney (median values of 8.21% vs. 1.81% and 12.81% vs. 2.17% in WT and $C3^{-/-}$ UUO groups respectively; $p<0.005$). The interstitial compartment of $C3^{-/-}$ UUO mice had expanded more than that of their WT counterparts ($p<0.005$). Tubular dilatation (Figure 3.1E) was also found to have increased in WT and $C3^{-/-}$ UUO groups compared with contralateral kidneys (median values of 8.60 vs. 2.62% and 9.62% vs. 1.12% respectively; $p<0.005$). The extent of tubular dilatation representing mechanical injury was equivalent for both UUO groups, although the median value for $C3^{-/-}$ UUO mice was numerically higher. Unaffected (contralateral) kidneys in WT and $C3^{-/-}$ mice displayed normal renal morphology, with no interstitial expansion or tubular dilatation.

Following ten days of ureteric obstruction, interstitial expansion and tubular dilatation had continued to develop in the renal cortices of obstructed WT and $C3^{-/-}$ mice (Figure 3.2A and B). At this time, injury had progressed to such an extent that some tubules had become atrophic in appearance. Such tubules were identifiable by their marked reduction in size and the presence of an irregular basement membrane.

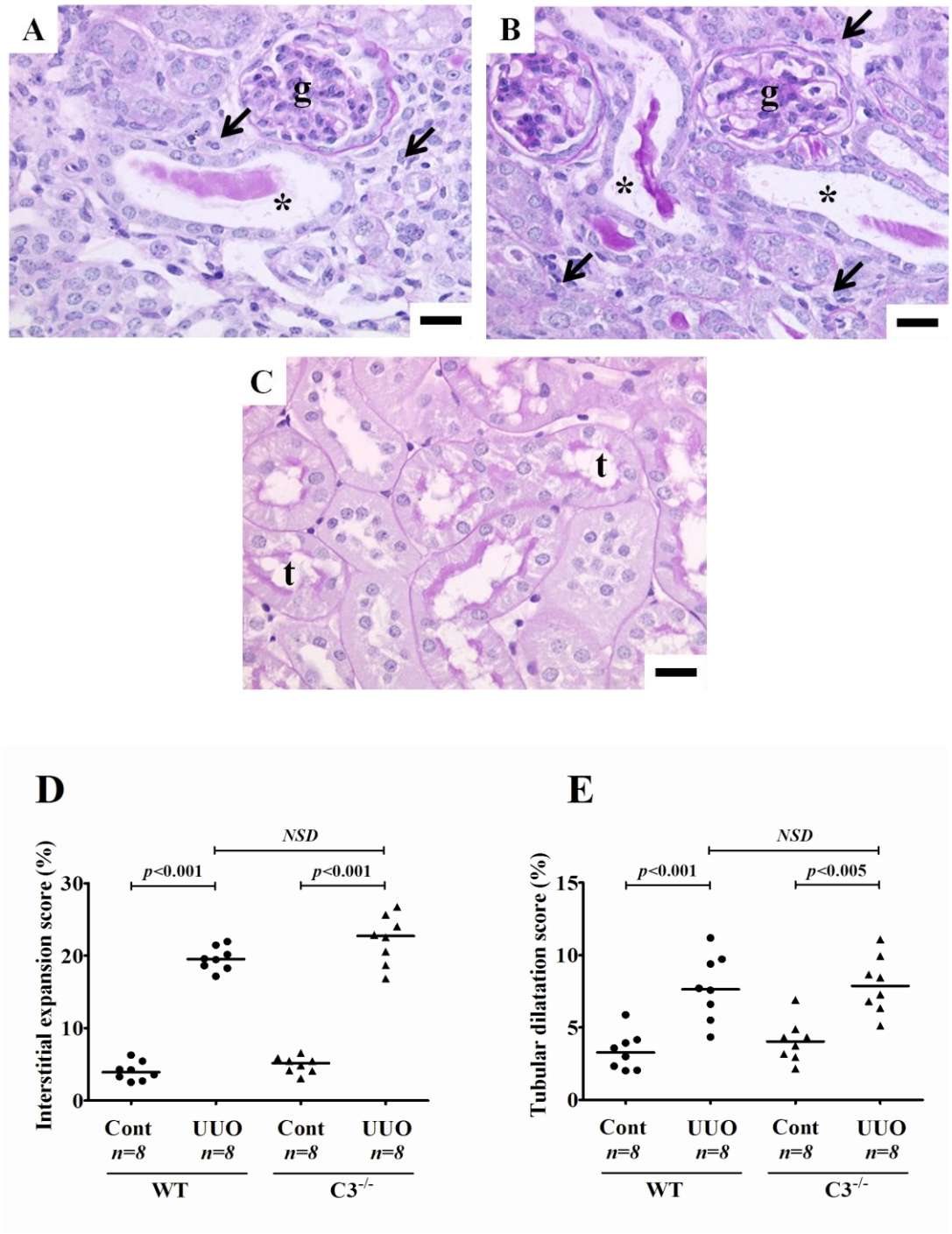

Figure 3.2. Histological injury at day ten UUO
Histological injury in WT and $C3^{-/-}$ kidneys following ten days of ureteric obstruction. PAS staining of WT UUO (A), $C3^{-/-}$ UUO (B) and representative contralateral renal cortices (C). All tissues were formalin-fixed and then paraffin-embedded. Arrows show areas of expanded interstitium. Asterisks highlight severely dilated tubules. Glomerulus (g), tubule (t). Scale bars on A-C represent 20µm. Interstitial expansion (D) and tubular dilatation (E) scoring carried out using a grid-based counting method. Bars on graphs represent median values.

Cortical interstitial volume (Figure 3.2D) had increased in obstructed WT and $C3^{-/-}$ groups compared with contralateral kidneys (median values 19.52% vs. 3.90% and 22.72% vs. 5.16% respectively; $p<0.001$). The interstitial volumes of WT and $C3^{-/-}$ UUO mice, was equivalent. Renal tubule dilation (Figure 3.2E) compared to the contralateral kidney was greater in WT and $C3^{-/-}$ UUO groups compared with contralateral kidneys (median values 8.54% vs. 3.46% and 8.55% vs. 4.03% respectively; $p<0.001$ and $p<0.005$ respectively). As with interstitial expansion, tubular dilatation in obstructed WT and $C3^{-/-}$ mice was equivalent. Contralateral kidneys remained unchanged.

3.3 Infiltration of lymphocytes into obstructed kidneys during UUO

To identify the presence of infiltrating leucocytes, obstructed kidneys were harvested from WT and $C3^{-/-}$ mice following ten days of ureteric obstruction and indirect IHC was used to stain $CD4^+$ (Figure 3.3A and B) and $CD8^+$ T cells (Figure 3.4A and B) and $F4/80^+$ macrophages (Figure 3.5A and B). In the obstructed kidneys of WT mice, there was a pronounced and significant infiltration of $CD4^+$ and $CD8^+$ T cells (median numbers of cells per HPF of 37.52 and 15.20 respectively; $p<0.001$). Numerically, fewer $CD4^+$ T cells were present at day ten in the obstructed cortices of $C3^{-/-}$ mice (median number of cells was 24.11 per HPF; Figure 3.3D). There was greater variability within the $C3^{-/-}$ UUO group, nevertheless $CD4^+$ cell infiltration was significant when compared with contralateral $C3^{-/-}$ kidneys ($p<0.001$). The median number of $CD4^+$ T cells in obstructed WT and $C3^{-/-}$ kidneys was not statistically different.

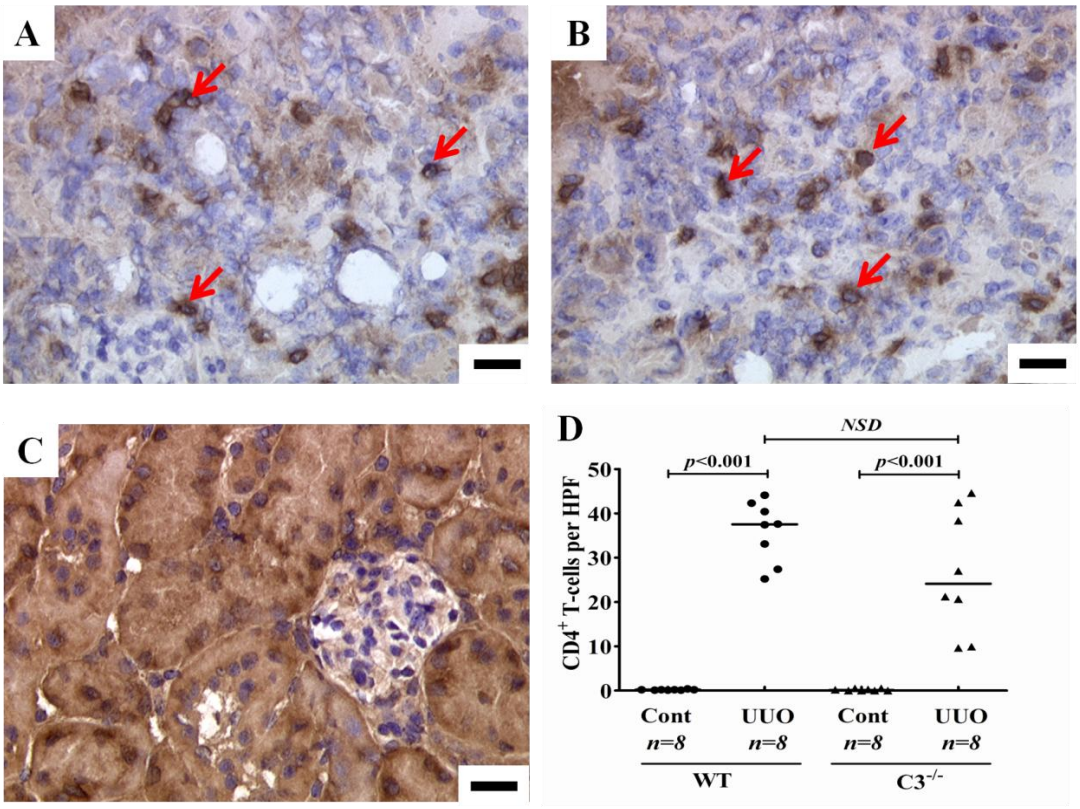

Figure 3.3. CD4^{+} T cell infiltration at day ten UUO
Indirect IHC was used to detect CD4^{+} T cells in cryo-preserved renal tissues. WT obstructed (A), C3$^{-/-}$ obstructed (B) and a representative unaffected contralateral kidney (C). Bars on A-C represent 20µm. For each animal, ten randomised cortical HPFs were acquired using an Aperio scanner and accompanying computer software. Positively stained cells (indicated by red arrows) present in each HPF field were manually counted. CD4^{+} cells were compared in WT and C3$^{-/-}$ obstructed renal cortices (D). Bars on graph represent median values.

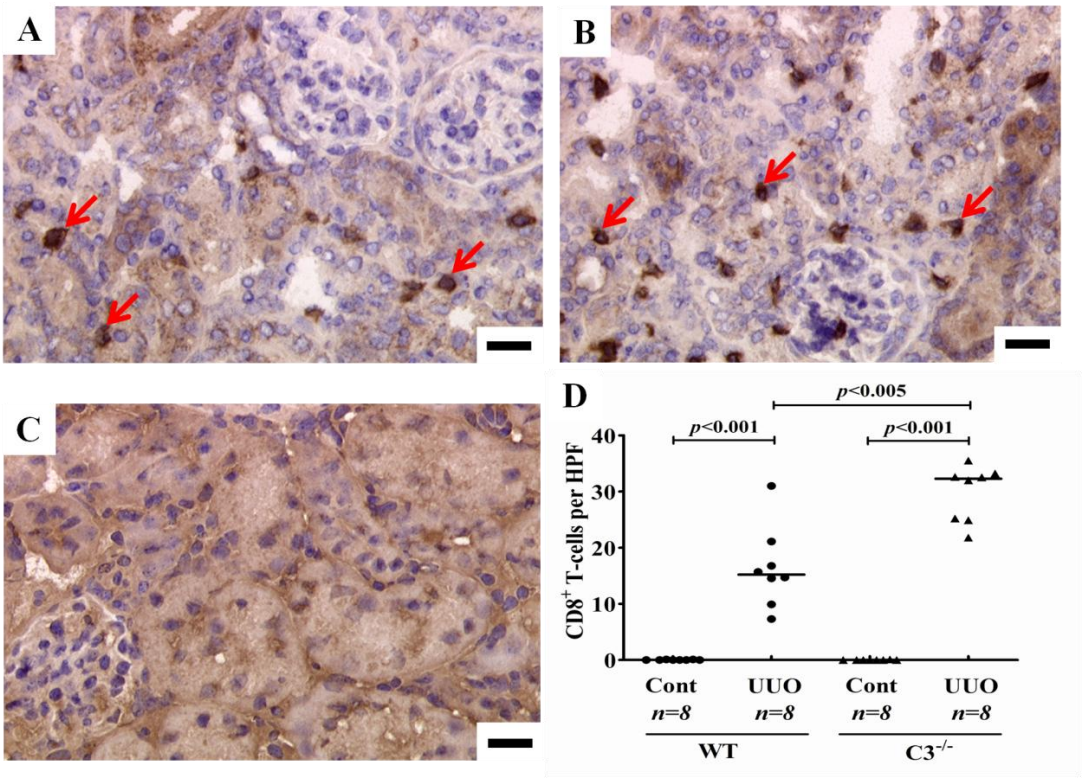

Figure 3.4. CD8$^+$ T cell infiltration at day ten UUO

CD8$^+$ T cells present in frozen renal tissues of day ten obstructed mice were determined using indirect IHC. WT obstructed (A), C3$^{-/-}$ obstructed (B) and a representative contralateral kidney (C). Scale bars on A-C represent 20µm. An Aperio scanner and accompanying computer software were used to capture ten cortical HPFs at random for each animal. Cells present in each HPF field which had stained positive for CD8$^+$ (indicated by red arrows), were manually counted (D). CD8$^+$ cells were present in obstructed WT kidneys and were more abundant in C3$^{-/-}$ obstructed kidneys. Bars on graph represent median values.

Similarly, $CD8^+$ T cells had also significantly increased in obstructed $C3^{-/-}$ mice (median number of cells was 32.28 per HPF; $p<0.001$), however, more than twice as many $CD8^+$ cells were present in $C3^{-/-}$ UUO mice ($p<0.005$; Figure 3.4D). Although no $CD4^+$ and $CD8^+$ cells were observed in the interstitium of contralateral WT and $C3^{-/-}$ renal cortices (Figure 3.3C and Figure 3.4C respectively), on rare occasions positively-stained cells were observed in glomeruli. Macrophage infiltration was quantified by scoring areas of interstitium which had positive staining for F4/80 (Figure 3.5A and B). In obstructed WT and $C3^{-/-}$ renal cortices, $F4/80^+$ cells occupied a median of 21.24% and 27.18% of the tubulointerstitial compartment vs. 0% in WT and $C3^{-/-}$ contralateral kidneys ($p<0.01$ for WT and $C3^{-/-}$ obstructed kidney groups). Interestingly, as observed with infiltrating $CD8^+$ T cell numbers, $F4/80^+$ macrophages were significantly elevated in the obstructed kidneys of $C3^{-/-}$ mice compared with the WT obstructed group ($p<0.005$; Figure 3.5D). No $F4/80^+$ areas of interstitium were present in the un-obstructed renal cortices of WT and $C3^{-/-}$ mice (Figure 3.5C).

3.4 Expansion of the interstitial compartment by collagen deposition and alpha-SMA^+ myofibroblasts

Sirius red is a histological technique which allows the visualisation of collagen fibres within tissues. Following treatment with Sirius red F3B dye, collagen fibres are stained red, distinguishing them from other structures. Leica QWin software was used to generate a macro capable of counting red coloured pixels.

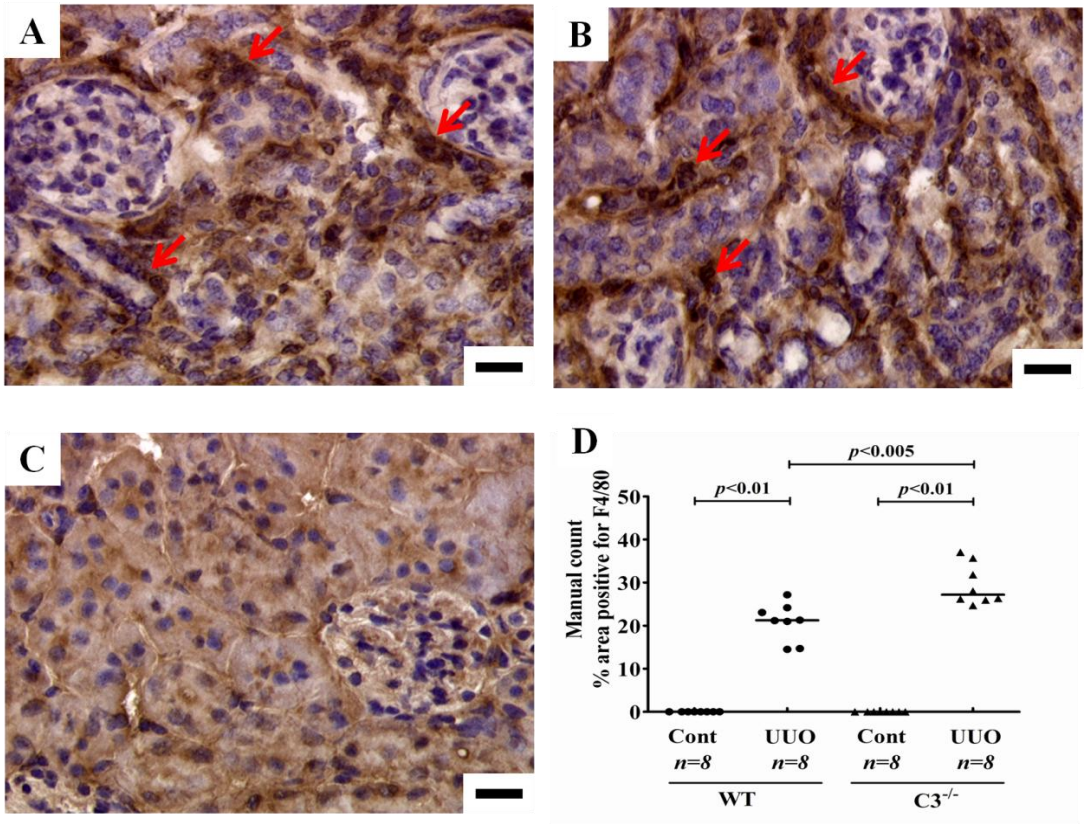

Figure 3.5. F4/80^{+} macrophage infiltration at day ten UUO
Indirect IHC was used to semi-quantify F4/80^{+} macrophages present in cryo-preserved kidneys of day ten obstructed mice. WT UUO (A), C3$^{-/-}$ UUO mice (B) and a representative unaffected contralateral kidney (C). Scale bars on A-C represent 20µm. Ten random cortical HPFs were acquired for each experimental group using an Aperio scanner and accompanying computer software. Areas of F4/80^{+} cells present in each HPF field (as indicated by red arrows), were manually counted using a grid-based method (D). F4/80^{+} macrophages were elevated in the renal cortices of all mice which had undergone UUO however a greater area of positive staining was present in C3$^{-/-}$ UUO mice. Bars on graph represent median values.

In contralateral and obstructed kidneys harvested at three and ten days post-UUO, the number of positively stained (red) pixels was expressed as a percentage of the total area measured for each animal. In WT mice interstitial collagen staining, was significantly greater after ureteric obstruction compared with contralateral kidneys (Figure 3.6A) with median values of 5.75% vs. 0.61% and 10.45% vs. 1.28% in obstructed vs. contralateral kidneys at day three and day ten respectively ($p<0.005$ and $p<0.001$ respectively; Figure 3.6D). Collagen deposition within the cortical interstitium of day three obstructed $C3^{-/-}$ mice (Figure 3.6B and D) was also significantly higher when compared with unobstructed kidneys (median values of 2.76% vs. 0.90 respectively; $p<0.005$). Interestingly, interstitial collagen staining in day three obstructed $C3^{-/-}$ mice was significantly lower ($p<0.05$) when compared with day three WT UUO mice. Following ten days of UUO, collagen deposition had increased to 9.03% in obstructed vs. 0.85% contralateral kidneys of $C3^{-/-}$ mice (Figure 3.7A, B and D). At this time, collagen staining was statistically equivalent in obstructed kidneys of WT and $C3^{-/-}$ mice. Collagen staining was also detected around glomeruli, tubules and blood vessels in the contralateral kidneys of WT and $C3^{-/-}$ groups (Figure 3.7C).

Specific identification of collagen I fibres was achieved using IHC staining in renal tissues harvested after ten days of ureteric obstruction. In the obstructed kidneys of WT and $C3^{-/-}$ mice, collagen I fibres were abundant throughout the expanded interstitium (Figure 3.8A and B). Median values for collagen I deposition in obstructed kidneys was higher than in unobstructed kidneys; 21.79% compared with 4.69% and 15.71% compared with 4.07% in WT and $C3^{-/-}$ mice respectively ($p<0.001$ and $p<0.01$ respectively; Figure 3.8D). Interestingly, cortical interstitial staining of collagen I was significantly lower in obstructed $C3^{-/-}$ mice ($p<0.05$).

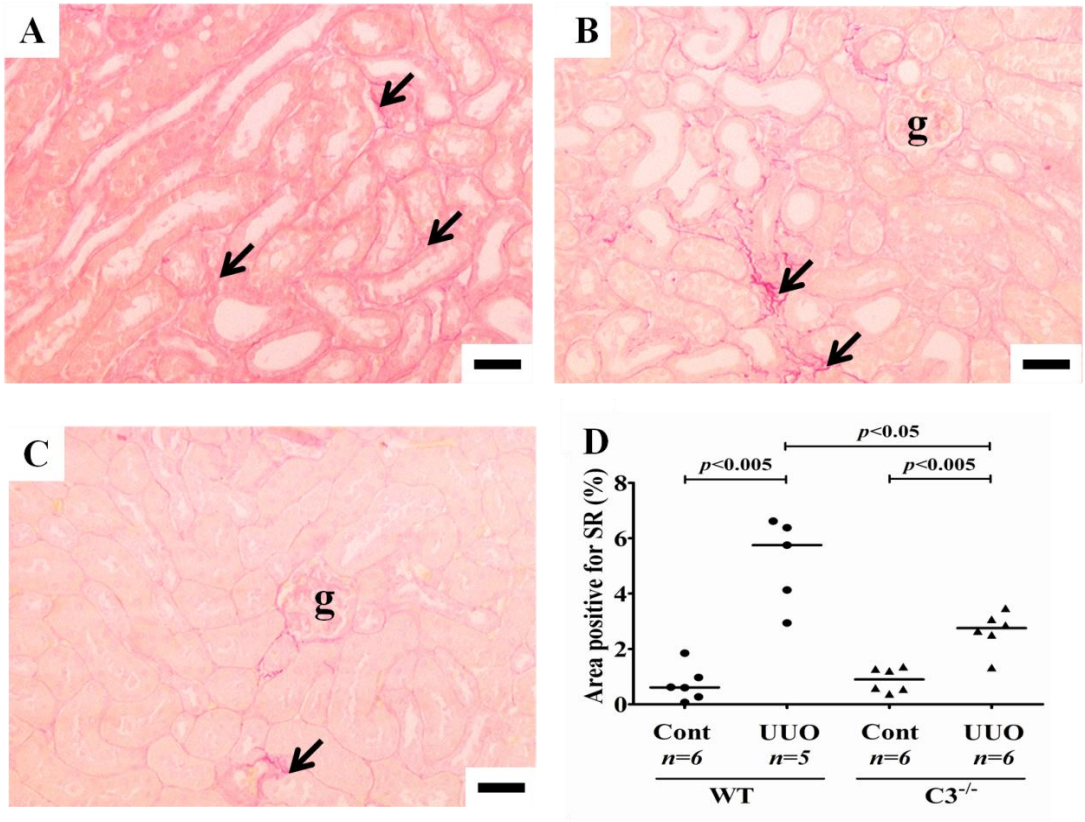

Figure 3.6. Interstitial collagen deposition at day three UUO
Following three days of ureteric obstruction, formalin-fixed paraffin embedded renal tissues were stained with Sirius red. Collagen fibres stained an intense red colour in WT (A) and $C3^{-/-}$ (B) renal cortices. An image of a representative unobstructed kidney (C). Collagen was present around glomerular and vascular structures in contralateral kidneys. Arrows indicate collagen fibres and (g) indicates a glomerulus. Scoring for collagen deposition was performed by a computer macro specifically designed to detect red pixels which was created using LeicaQwin software (D). Scale bars on A-C represent 40µm. Bars on graph represent median values.

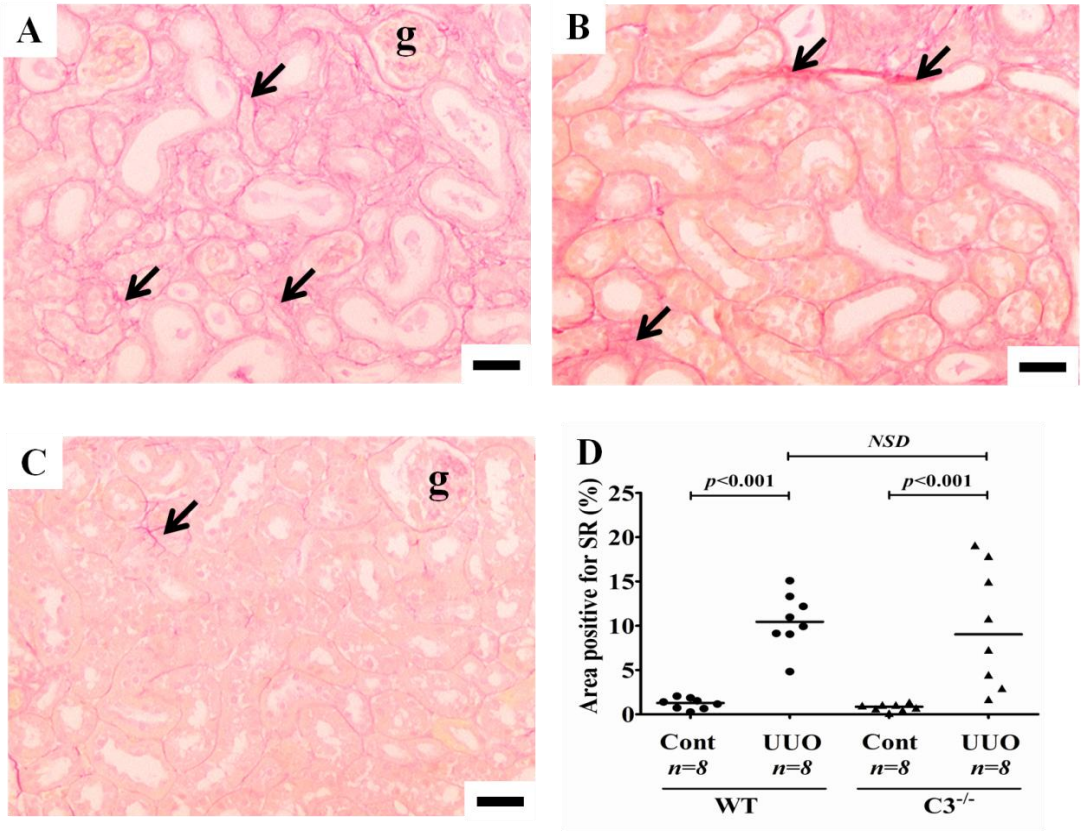

Figure 3.7. Interstitial collagen deposition at day ten UUO
Ten days post-UUO, paraffinised renal tissues were stained with Sirius red. In WT (A) and $C3^{-/-}$ (B) renal cortices, collagen fibres were stained an intense red colour. Collagen was also present around tubules, blood vessels and glomeruli in contralateral renal cortices of WT and $C3^{-/-}$ mice (C). Arrows illustrate collagen fibres and 'g' identifies glomeruli. Collagen deposition was measured using a LeicaQwin software macro which was specifically designed to detect red pixels (D). Scale bars on A-C represent 40µm. Bars on graph represent median values.

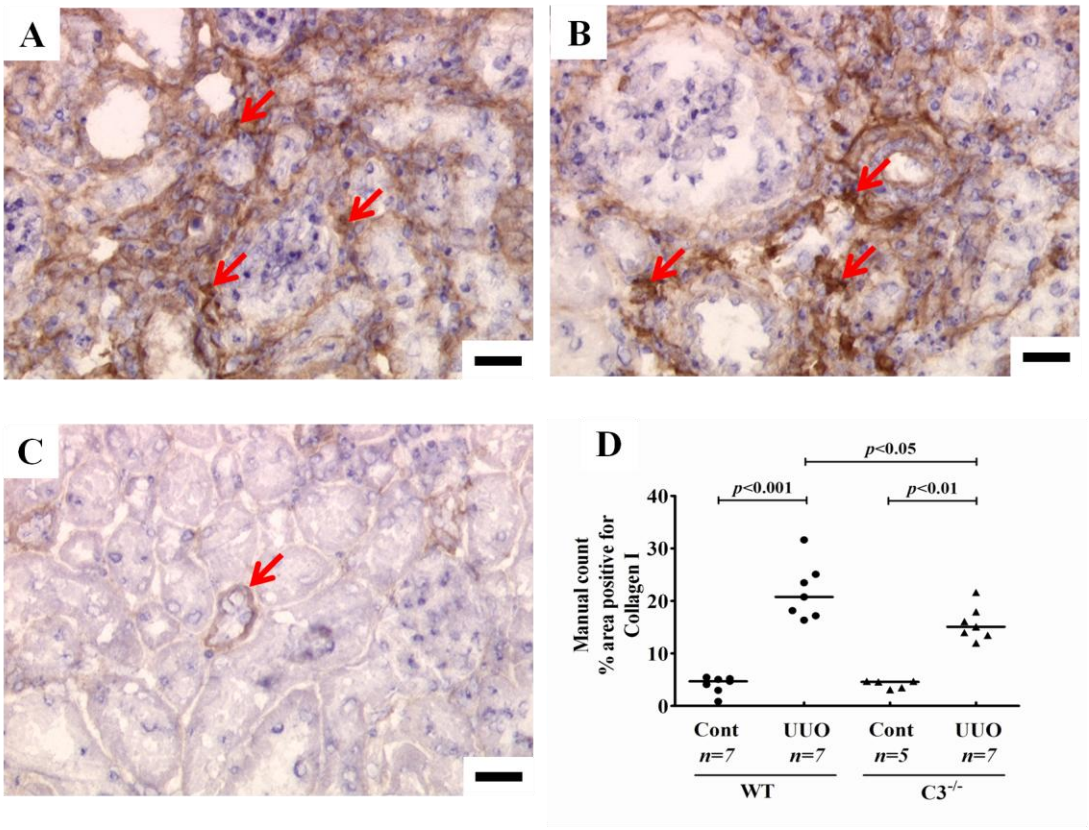

Figure 3.8. Collagen I deposition at day ten UUO

Following ten days of ureteric obstruction, immunohistochemical staining was used to semi-quantify collagen I deposition within the renal cortices of cryo-preserved kidneys. WT UUO (A), $C3^{-/-}$ UUO (B) and a representative contralateral kidney (C). Scale bars on A-C represent 20µm. For each experimental group, ten random cortical HPFs were acquired. Areas staining positive for collagen I fibres within each HPF field (as indicated by red arrows), were manually counted using a grid-based method (D). Collagen I deposition was observed in the obstructed renal cortices of WT and $C3^{-/-}$ mice, but was less severe in the absence of C3. Bars on graph represent median values.

Contralateral kidneys from WT and $C3^{-/-}$ mice exhibited weak collagen I staining around blood vessels (Figure 3.8C). α-SMA^{+} myofibroblasts present within the renal cortex after ten days of ureteric obstruction were identified by IHC staining (Figure 3.9A and B). Obstructed WT and $C3^{-/-}$ kidneys exhibited extensive α-SMA deposition within the tubulointerstitial compartment (Figure 3.8D) compared with unobstructed kidneys (66.91% vs. 2.59% and 63.46% vs. 2.59% respectively; $p<0.005$ and $p<0.001$ respectively). Median values for day ten obstructed WT and $C3^{-/-}$ groups were equivalent. Positive α-SMA staining was also present around blood vessels in all obstructed and contralateral WT and $C3^{-/-}$ kidneys (Figure 3.9C).

3.5 Cytokine gene expression during UUO

rtPCR was used to analyse changes in gene expression following UUO. RNA was extracted from the renal cortex and reverse transcribed. The resulting cDNA was analysed in a rtPCR reaction and the relative expression for each gene of interest was calculated by comparing expression to that of the house keeping gene β-actin. In the kidneys of day three obstructed WT mice, no significant increase in TNF-α mRNA expression was observed compared with unobstructed kidneys (2.82 vs. 1.34; Figure 3.10A), however TNF-α was significantly up-regulated after three days of UUO in kidneys of $C3^{-/-}$ mice compared with contralateral kidneys (4.30 vs. 1.80; $p<0.05$). By day ten, TNF-α gene expression in obstructed WT and $C3^{-/-}$ kidneys was significantly up-regulated (Figure 3.10B) compared with contralateral kidneys (5.65 vs. 0.86 and 12.58 vs. 1.93 respectively; $p<0.001$ and $p<0.005$ respectively).

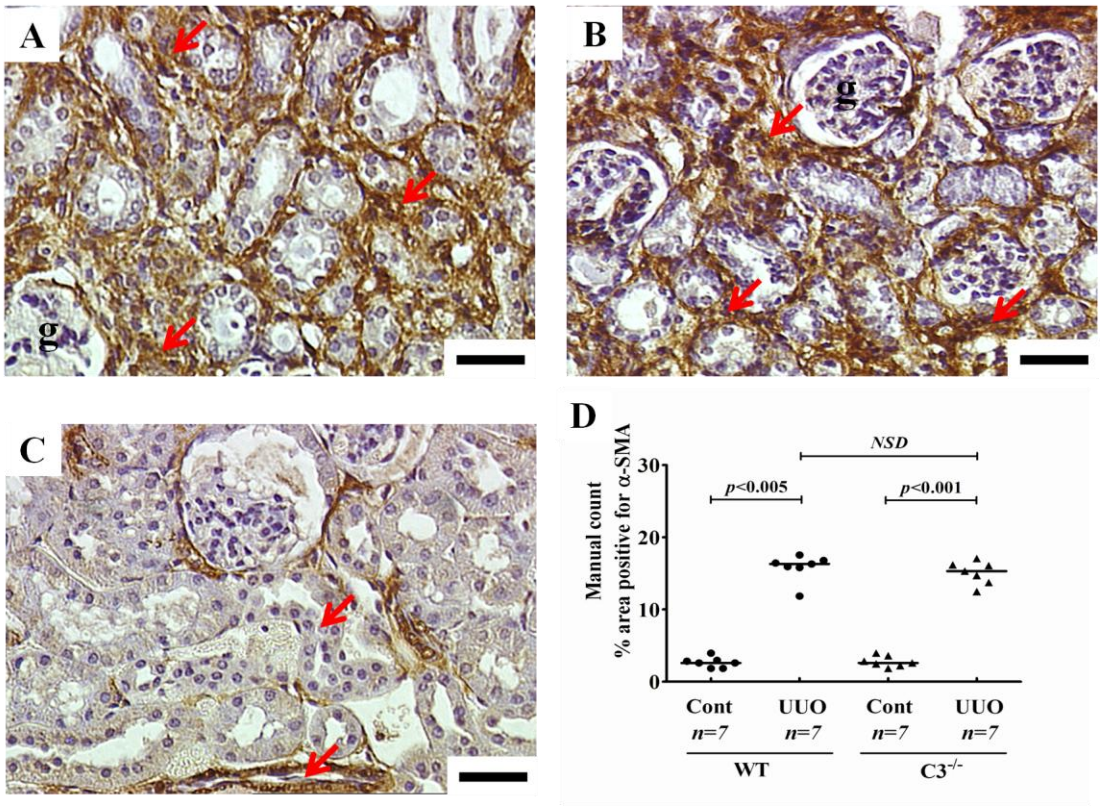

Figure 3.9. α-SMA^{+} myofibroblasts at day ten UUO
Following ten days of ureteric obstruction, α-SMA^{+} myofibroblasts present in the renal cortices of paraffinised kidneys were detected by IHC and semi-quantified. WT UUO (A), C3$^{-/-}$ UUO mouse kidney (B) and representative contralateral kidneys (C). Scale bars on A-C represent 40μm. Ten random cortical HPFs for each experimental group were selected in a blinded fashion. Areas containing α-SMA^{+} myofibroblasts (as indicated by red arrows), were counted using a grid-based method (D). Myofibroblasts staining positive for α-SMA were observed in the obstructed renal cortices of WT and C3$^{-/-}$ mice. Bars on graph represent median values.

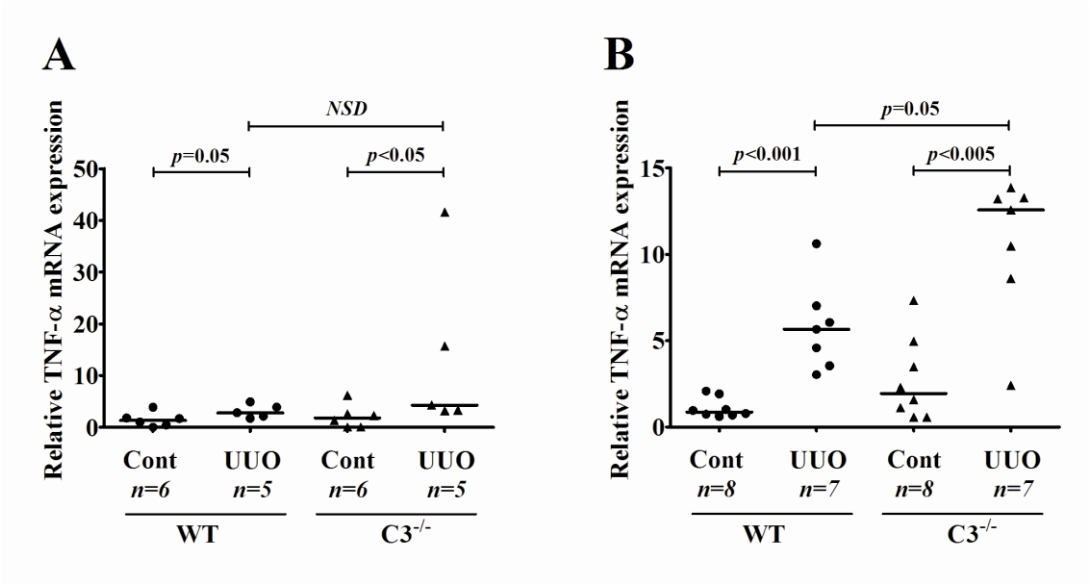

Figure 3.10. TNF-α gene expression at day three and day ten UUO
Gene expression of TNF-α in contralateral (cont) and obstructed (UUO) renal cortices three (A) and ten (B) days post-ureteric obstruction was quantified by rtPCR. TNF-α mRNA expression was first normalised to that of the house-keeping gene β-actin and then the relative mRNA expression of TNF-α was calculated. TNF-α was significantly elevated to boarder line significance in the obstructed renal cortices $C3^{-/-}$ mice and was elevated to boarder line significance in obstructed WT mouse kidneys. By day ten, TNF-α was significantly up-regulated in WT and $C3^{-/-}$ UUO mice. Bars on graphs represent median values. rtPCR was performed in triplicate for each animal.

There were no significant differences in TNF-α expression for WT and $C3^{-/-}$ obstructed kidneys at day three. However by day ten UUO, TNF-α gene expression in the obstructed kidneys of $C3^{-/-}$ mice was of boarder line significance compared with obstructed WT mice (p=0.05). Following three days of UUO, there was no significant change in the amount of TGF-β gene expression observed in obstructed WT and $C3^{-/-}$ kidneys (Figure 3.11A). After ten days of ureteric obstruction, median TGF-β expression in obstructed WT renal cortices was significantly elevated (Figure 3.11B) compared to unobstructed renal cortices (2.23 vs. 1.06; p<0.05). Similarly, median expression of TGF-β in day ten obstructed $C3^{-/-}$ kidneys was significantly higher compared with contralateral kidneys (1.04 vs. 0.54; p<0.001). Interestingly, TGF-β gene expression in obstructed $C3^{-/-}$ mice was significantly lower than that observed in WT UUO kidneys (p<0.01).

The median value for IL-6 expression in day three obstructed WT mice was 0.64, a significant increase of almost 18 times the median of $3.5x10^{-3}$ detected in contralateral kidneys of WT mice (p<0.005, Figure 3.12A). Similarly, in kidneys harvested from $C3^{-/-}$ mice, IL-6 mRNA expression was increased from a median of $4.6x10^{-3}$ to 0.57, although this increase was not statistically significant. The level of IL-6 gene expression in obstructed WT and $C3^{-/-}$ mice was not statistically different at this time point. After ten days of ureteric obstruction, IL-6 mRNA expression had continued to increase in obstructed WT and $C3^{-/-}$ kidneys. In WT mice, median IL-6 gene expression had increased 85.59 fold in obstructed kidneys vs. 0.95 in contralateral kidneys (p<0.001; Figure 3.12B).

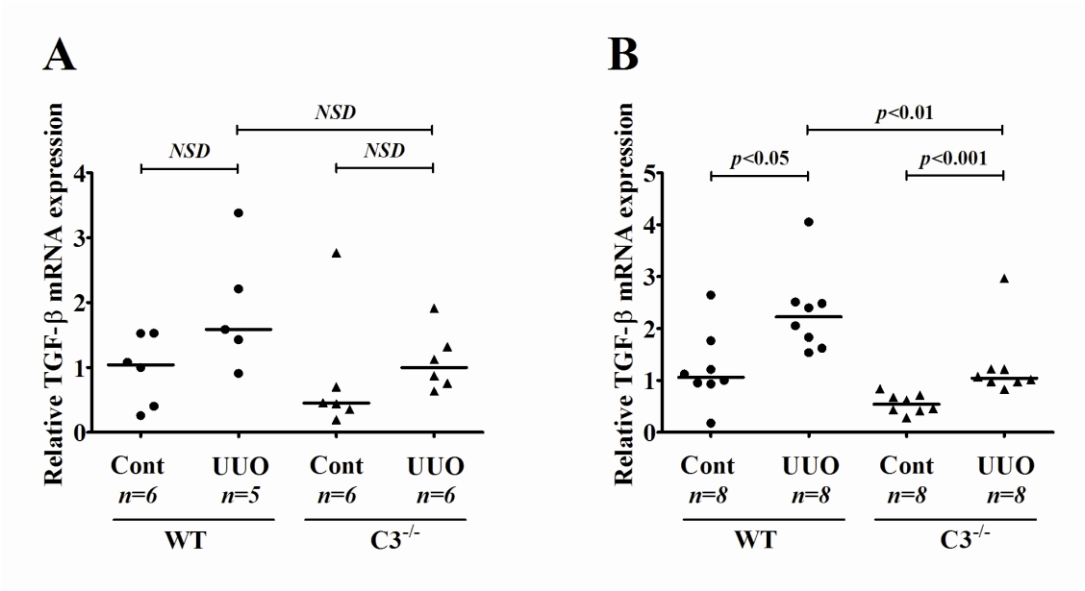

Figure 3.11. TGF-β gene expression at day three and day ten UUO
rtPCR was used to quantify gene expression of TGF-β in contralateral (cont) and obstructed (UUO) renal cortices three (A) and ten (B) days post-ureteric obstruction. Gene expression levels were first normalised to β-actin and then the relative mRNA expression of TGF-β was calculated. Following statistical analysis, TGF-β expression was found to have increased significantly in the obstructed kidneys of WT and $C3^{-/-}$ mice by day ten. Bars on graphs represent median values. rtPCR was performed in triplicate for each animal.

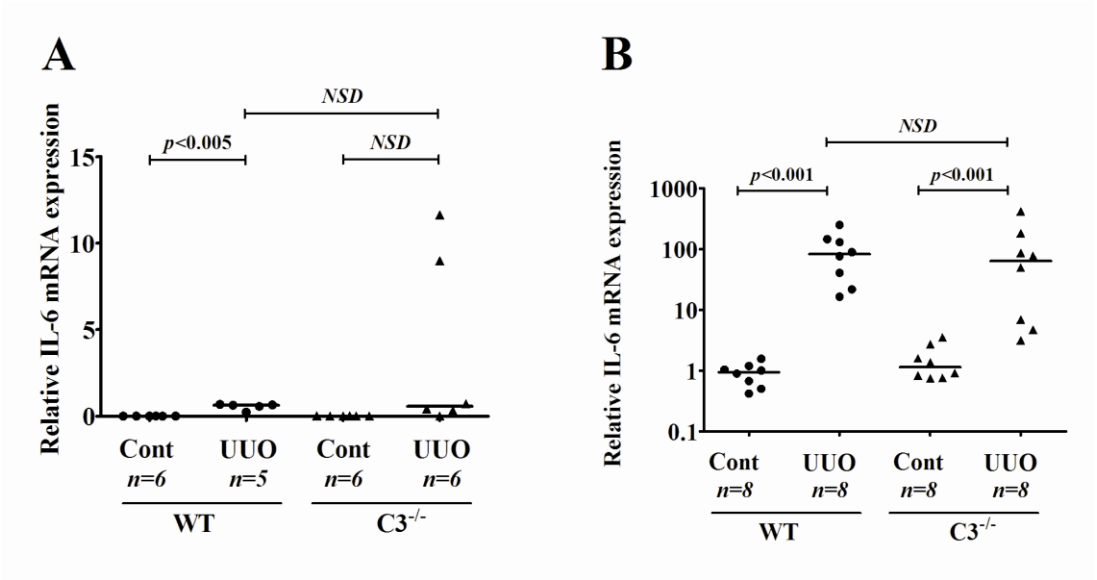

Figure 3.12. IL-6 gene expression at day three and day ten UUO
Quantification of IL-6 gene expression in obstructed (UUO) and contralateral (cont) renal cortices was performed by rtPCR following three (A) and ten (B) days of UUO. mRNA expression was normalised to the house-keeping gene β-actin, after which, the relative expression of IL-6 compared to β-actin was determined. IL-6 mRNA levels increased in obstructed WT and $C3^{-/-}$ kidneys during the latter stages of UUO. Bars on graphs represent median values. rtPCR was performed in triplicate for each animal.

Similarly, median IL-6 mRNA expression had significantly increased in the renal cortices of obstructed $C3^{-/-}$ mice to a median value of 63.73 vs. 1.14 in contralateral kidneys ($p<0.005$). IL-6 gene expression remained equivalent in obstructed WT and $C3^{-/-}$ kidneys.

3.6 Collagen and α-SMA gene expression during UUO

After three days of ureteric obstruction, median values for collagen I gene expression in WT mice was 1.18 in contralateral kidneys vs. 7.78 in obstructed kidneys ($p<0.005$; Figure 3.13A). A significant elevation in median collagen I mRNA expression was also present in $C3^{-/-}$ mice (3.77 in obstructed kidneys vs. 0.57 in contralateral kidneys; $p<0.005$). Despite the median level of collagen I gene expression in day three WT UUO kidneys being approximately twice as high as that observed in $C3^{-/-}$ UUO kidneys, this difference did not reach statistical significance. Following ten days of UUO, median collagen I mRNA expression in obstructed WT mice remained significantly elevated at 4.98 compared with 0.82 in contralateral kidneys ($p<0.001$; Figure 3.13B). The median expression of collagen I in day ten obstructed $C3^{-/-}$ mice was 2.72 fold and remained significantly higher than that of contralateral $C3^{-/-}$ kidneys (median value of 0.58; $p<0.001$). Interestingly, collagen I mRNA expression in day ten $C3^{-/-}$ UUO kidneys was significantly lower than that observed in WT UUO kidneys ($p<0.01$). Three days post-UUO, there was no significant change in the level of collagen III gene expression in obstructed WT and $C3^{-/-}$ kidneys (Figure 3.14A).

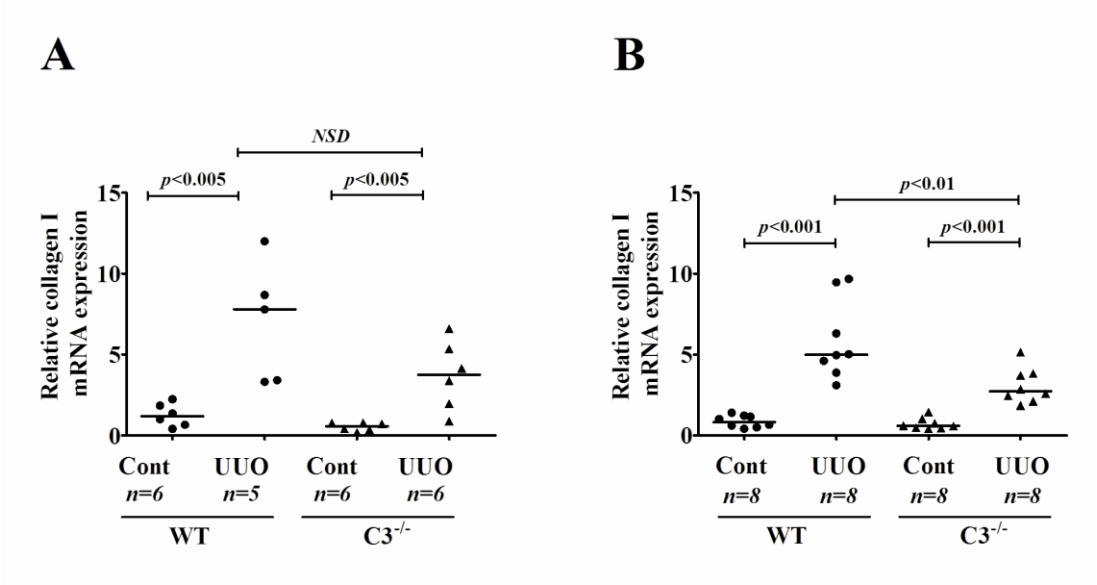

Figure 3.13. Collagen I gene expression at day three and day ten UUO
Collagen I mRNA expression was quantified by rtPCR in obstructed (UUO) and contralateral (cont) renal cortices following three (A) and ten (B) days of ureteric obstruction. Gene expression was normalised to β-actin, then the relative expression of collagen I was calculated. Collagen I gene expression was elevated in obstructed WT and $C3^{-/-}$ kidneys during the early and late stages of UUO, but was only significantly elevated in WT mice ten days post-obstruction. rtPCR was performed in triplicate for each animal. Bars on graphs represent median values.

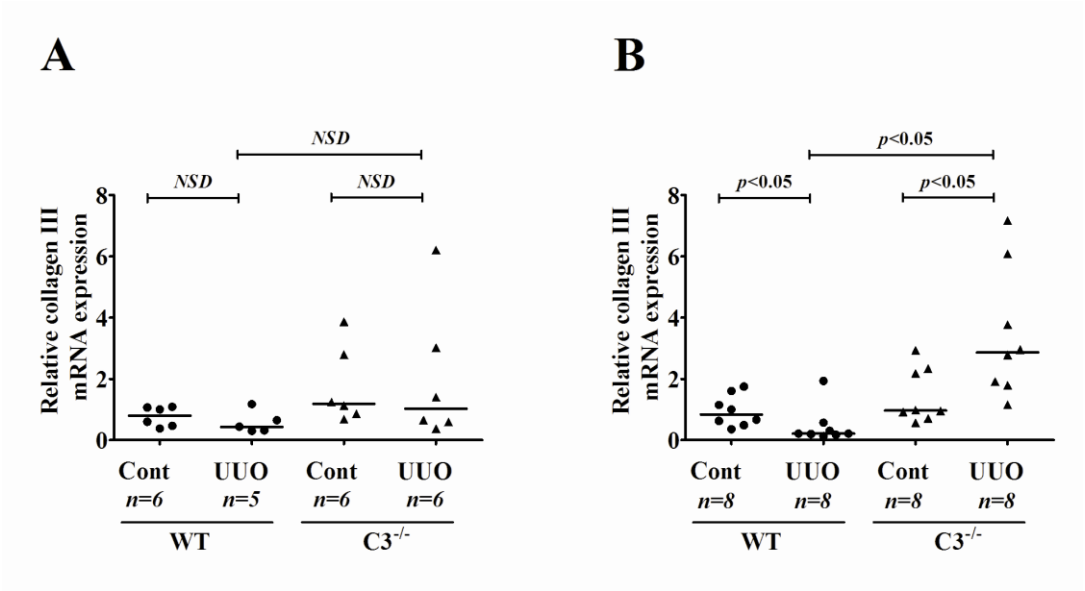

Figure 3.14. Collagen III gene expression at day three and day ten UUO
rtPCR was used to measure gene expression of collagen-III in obstructed (UUO) and contralateral (cont) renal cortices at three (A) and ten (B) days post-ureteric obstruction. Collagen III gene expression levels were normalised to the house-keeping gene β-actin. After ten days of UUO, collagen III gene expression had significantly decreased in WT obstructed kidneys, whereas a significant increase in expression was observed in $C3^{-/-}$ UUO kidneys. Overall, obstructed $C3^{-/-}$ kidneys had significantly higher collagen III expression compared with obstructed kidneys from WT mice. rtPCR was performed in triplicate for each animal. Bars on graphs represent median values.

Following ten days of UUO, collagen III gene expression (Figure 3.14B) as significantly lower in obstructed WT kidneys compared to contralateral kidneys (0.21 vs. 0.83; $p<0.05$). In the obstructed kidneys of $C3^{-/-}$ mice, median collagen III mRNA expression was significantly elevated compared with contralateral kidneys (2.87 vs. 0.97; $p<0.05$). Compared with WT UUO kidneys, collagen III gene expression was significantly elevated in obstructed $C3^{-/-}$ kidneys after ten days of ureteric obstruction ($p<0.05$).

Following three days of ureteric obstruction, α-SMA expression in obstructed kidneys from WT mice was significantly higher than in contralateral kidneys (5.56 vs. 1.20; $p<0.05$). Although α-SMA expression was elevated in obstructed kidneys of $C3^{-/-}$ mice, this was not significantly different from expression in unobstructed kidneys (3.64 vs. 1.11; Figure 3.15A). There were no significant differences in the levels of α-SMA mRNA expression observed in obstructed WT and $C3^{-/-}$ kidneys. After ten days of ureteric obstruction median α-SMA gene expression in obstructed kidneys of WT mice remained significantly elevated at 4.71 compared with 1.04 in contralateral kidneys ($p<0.05$; Figure 3.15B). Median mRNA expression of α-SMA in day ten $C3^{-/-}$ UUO mice had decreased to 0.81 and was statistically equivalent to the median α-SMA gene expression of 0.48 in contralateral $C3^{-/-}$ kidneys. Median day ten α-SMA expression in $C3^{-/-}$ UUO kidneys was significantly lower than that observed in WT UUO kidneys ($p<0.001$).

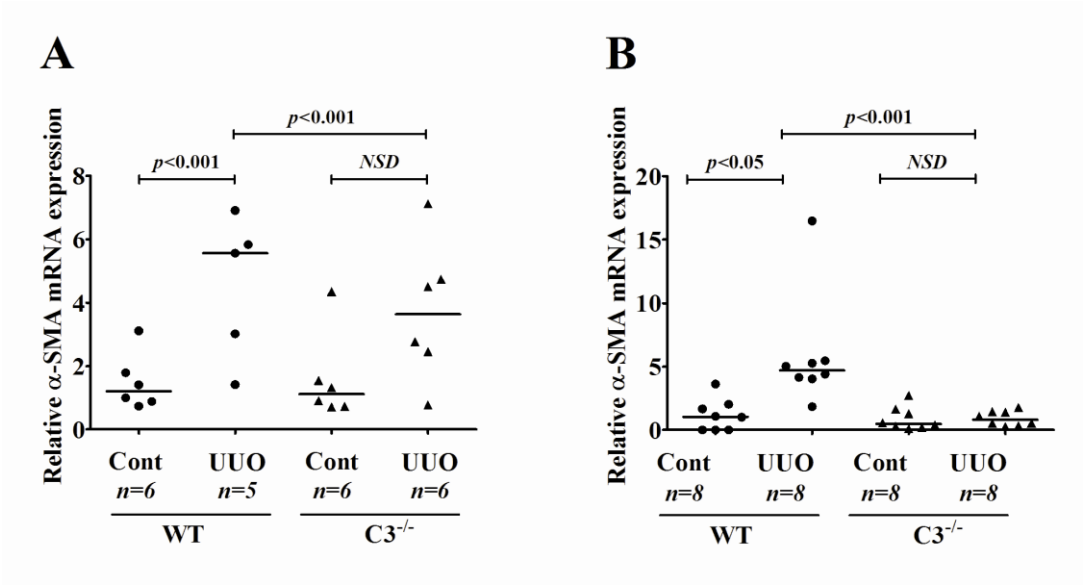

Figure 3.15. α-SMA gene expression at day three and day ten UUO
α-SMA gene expression in obstructed (UUO) and contralateral (cont) renal cortices three (A) and ten (B) days post-UUO was measured using rtPCR. α-SMA gene expression was normalised to β-actin, and the relative expression of α-SMA compared to β-actin was deduced. α-SMA mRNA expression increased in obstructed WT and $C3^{-/-}$ kidneys during the early stages of UUO, but only remained elevated in WT mice at day ten. Bars on graphs represent median values. rtPCR was performed in triplicate for each animal.

3.7 Analysis of renal injury following five days of UUO

After day three and day ten analyses had been conducted, it was decided that a sub-acute UUO time point should be included in the study. Day five UUO was chosen because it had been used in a previous study investigating the role of complement C5 during UUO (Boor et al., 2007). The same study had used day ten UUO as their final time point and so it was decided that inclusion of day five UUO in this study would allow a more direct comparison of the two studies. The day five UUO experiments in this study were conducted at a later time and so the findings are discussed separately to those of day three and day ten.

3.7.1 PAS and Sirius red histology

Expansion of the cortical tubular and interstitial compartments was evident after five days of ureteric obstruction. A number of tubules were dilated and the surrounding interstitium had distended in WT and $C3^{-/-}$ UUO groups as illustrated by asterisks and arrows respectively (Figure 3.16A and B). Expansion of the cortical interstitium was increased in WT and $C3^{-/-}$ obstructed mice respectively, with medians of 11.38% and 10.95% vs. 1.07% and 1.12% in contralateral kidneys ($p<0.005$ for both groups; Figure 3.16D). Tubular dilatation was also evident and had increased in WT and $C3^{-/-}$ UUO groups to medians of 5.01% and 5.41% compared to with medians of 1.48% and 0.93% respectively in unobstructed kidneys ($p<0.005$ for both groups; Figure 3.16E). Tubular dilatation and interstitial expansion in WT and $C3^{-/-}$ mice were both equivalent at this time. Contralateral kidneys belonging to both experimental groups displayed normal renal morphology with no visible tubular or interstitial expansion (Figure 3.16C).

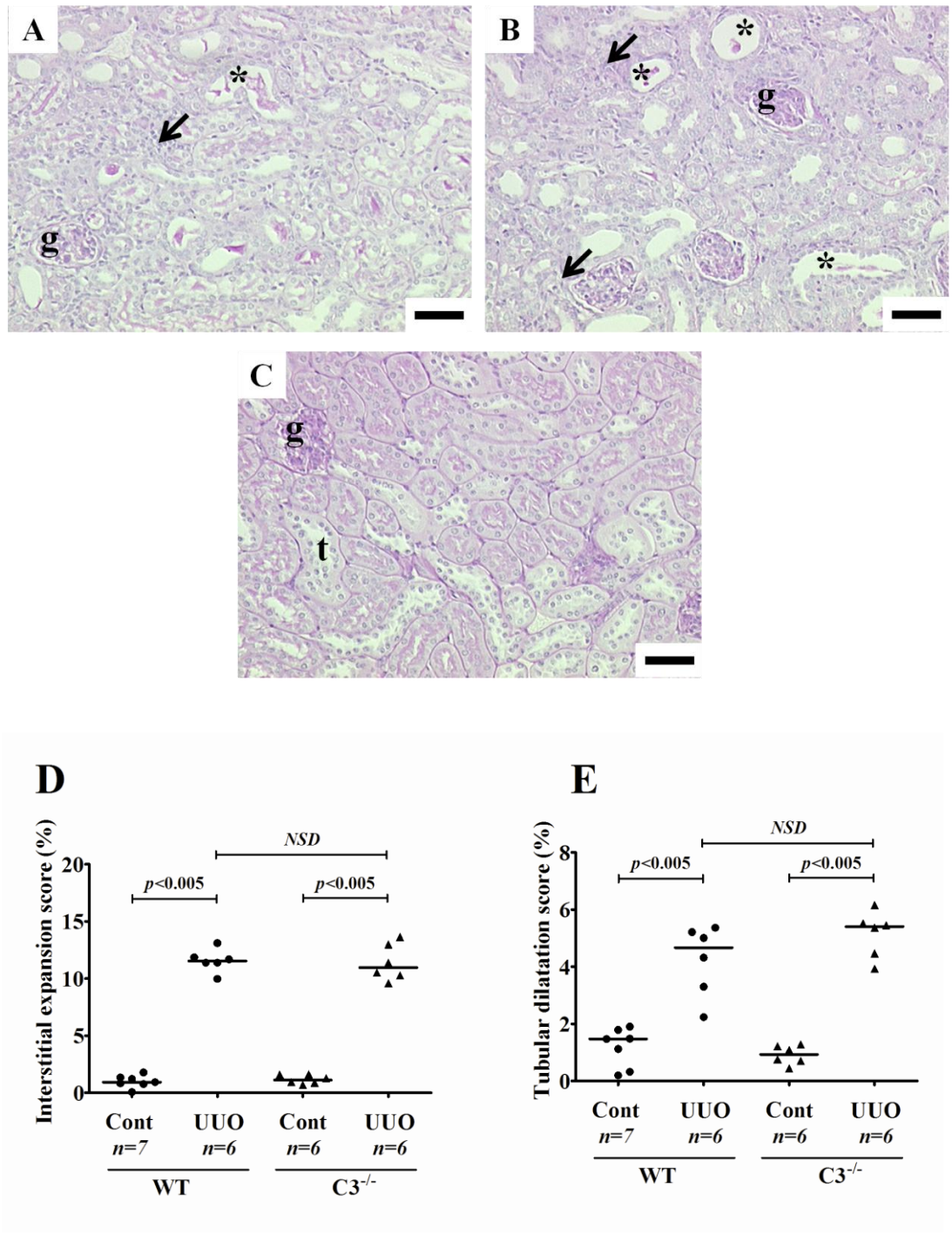

Figure 3.16. Histological injury at day five UUO
After five days of ureteric obstruction, paraffinised renal tissues were stained with PAS. Tubular basement membrane staining was evident in WT UUO (A), $C3^{-/-}$ UUO (B) and unaffected (C) renal cortices. Arrows on A and B show areas of expanded interstitium. Tubules (t), glomeruli (g). Asterisks indicate dilated tubules. Scale bars on A-C represent 50µm. Interstitial expansion (D) and tubular dilatation (E) were semi-quantified using a grid based counting method. Bars on graphs D and E represent median values.

WT and $C3^{-/-}$ day five contralateral and obstructed kidneys were harvested and stained with Sirius red as described previously (section 3.4.) Images used for measuring Sirius red staining were captured using an Aperio scanner and Scanscope software. And the number of positively stained (red) pixels within the renal cortex was determined using a modified positive pixel counting algorithm. Following five days of UUO, collagen deposition in obstructed WT mice was 0.60% compared with 0.14% in contralateral kidneys (Figure 3.17A and D). There was significantly more collagen staining in obstructed $C3^{-/-}$ kidneys (Figure 3.17B and D) compared with unobstructed kidneys (1.30% vs. 0.39%; $p<0.05$). This was not statistically significant compared to observations in the WT obstructed group. Contralateral kidneys from WT and $C3^{-/-}$ mice exhibited weak collagen staining around blood vessels and glomeruli (Figure 3.17C).

3.7.2 F4/80, Collagen I and alpha-SMA immunohistochemistry

Following five days of UUO, $F4/80^{+}$ macrophages (Figure 3.18A and B), collagen I fibres (Figure 3.19A and B) and α-SMA^{+} myofibroblasts (Figure 3.20A and B) were identified in obstructed renal tissues of WT and $C3^{-/-}$ mice using methods described previously (section 3.3 and 3.4) By day five, median values for $F4/80^{+}$ staining occupied 13.35% and 13.43% of the obstructed cortices of WT and $C3^{-/-}$ mice respectively (Figure 3.18C). The quantity of $F4/80^{+}$ macrophages in both experimental groups was equivalent. Interstitial deposition of collagen I fibres in WT and $C3^{-/-}$ day five obstructed kidneys , had increased significantly to median values of 20.75% and 17.47% respectively (Figure 3.19C).

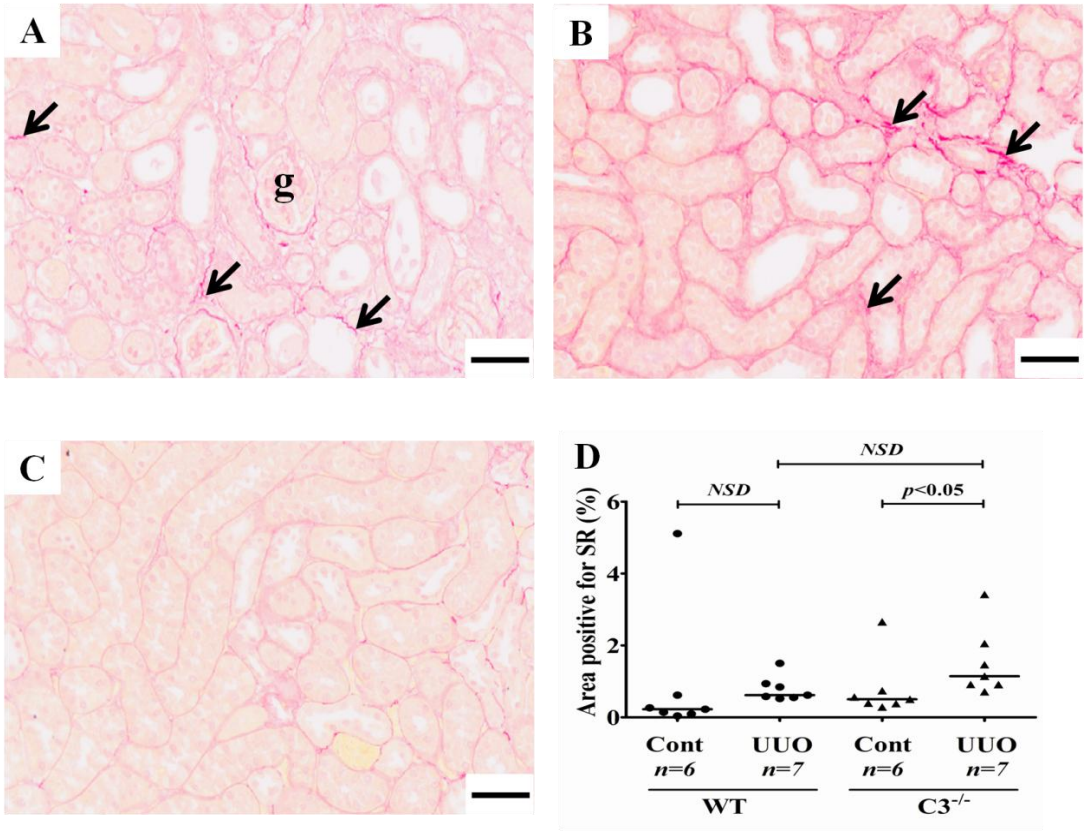

Figure 3.17. Interstitial collagen deposition at day five UUO
Sirius red was used to detect collagen deposition in paraffin-embedded renal tissues five days after unilateral ureteric obstruction. In WT (A), $C3^{-/-}$ (B) and contralateral renal cortices (C), collagen fibres present in vascular structures and within the interstitium. Arrows illustrate areas of collagen deposition and 'g' identifies a glomerulus. A computer macro created using LeicaQwin software detected Sirius red staining by counting red pixels (D). Scale bars on A-C represent 50µm. Bars on graph represent median values.

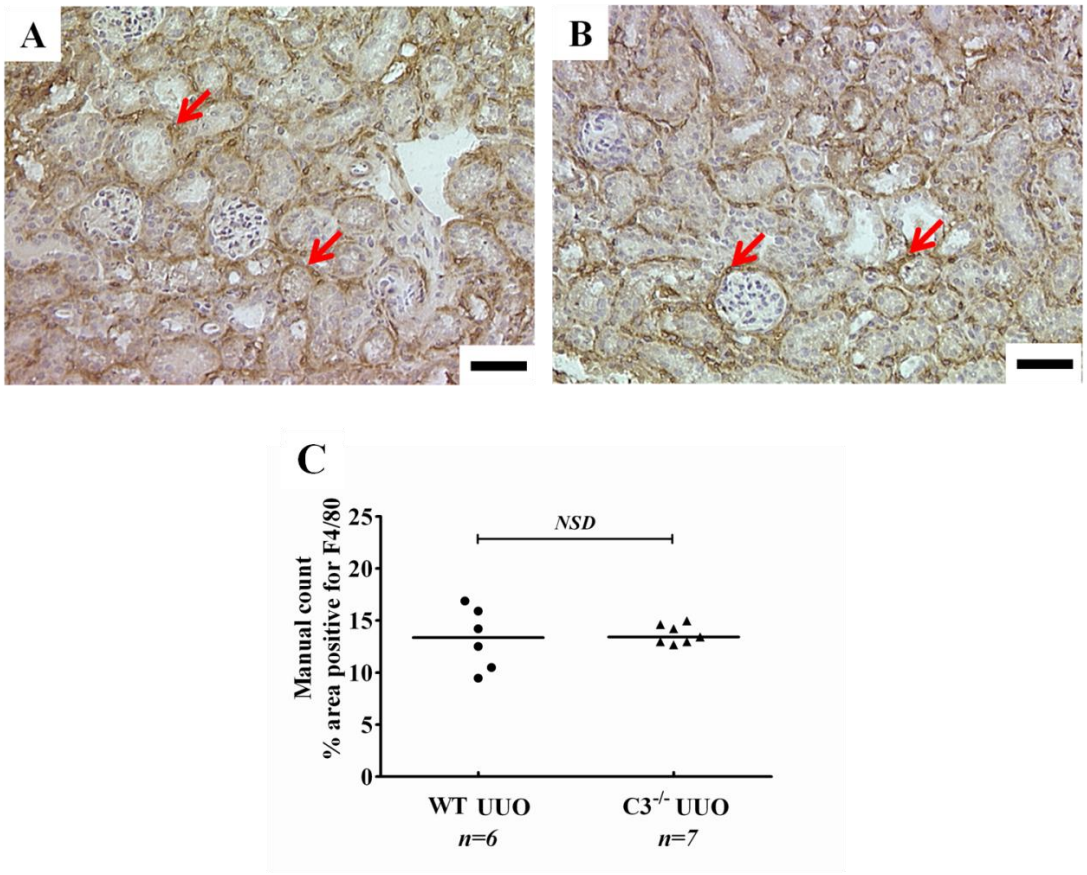

Figure 3.18. F4/80^{+} macrophage infiltration at day five UUO
Infiltrating F4/80^{+} macrophages present in frozen renal tissues of day five obstructed mice were semi-quantified by indirect IHC. WT and C3$^{-/-}$ obstructed mice (A and B respectively) contralateral kidneys not shown. Scale bars on A and B represent 50µm. An Aperio scanner and Scanscope software were used to capture ten random cortical HPFs for each experimental group. Areas present in each HPF field which were positive for F4/80^{+} (as indicated by red arrows), were manually counted using a grid-based method (C). Bars on graph represent median values.

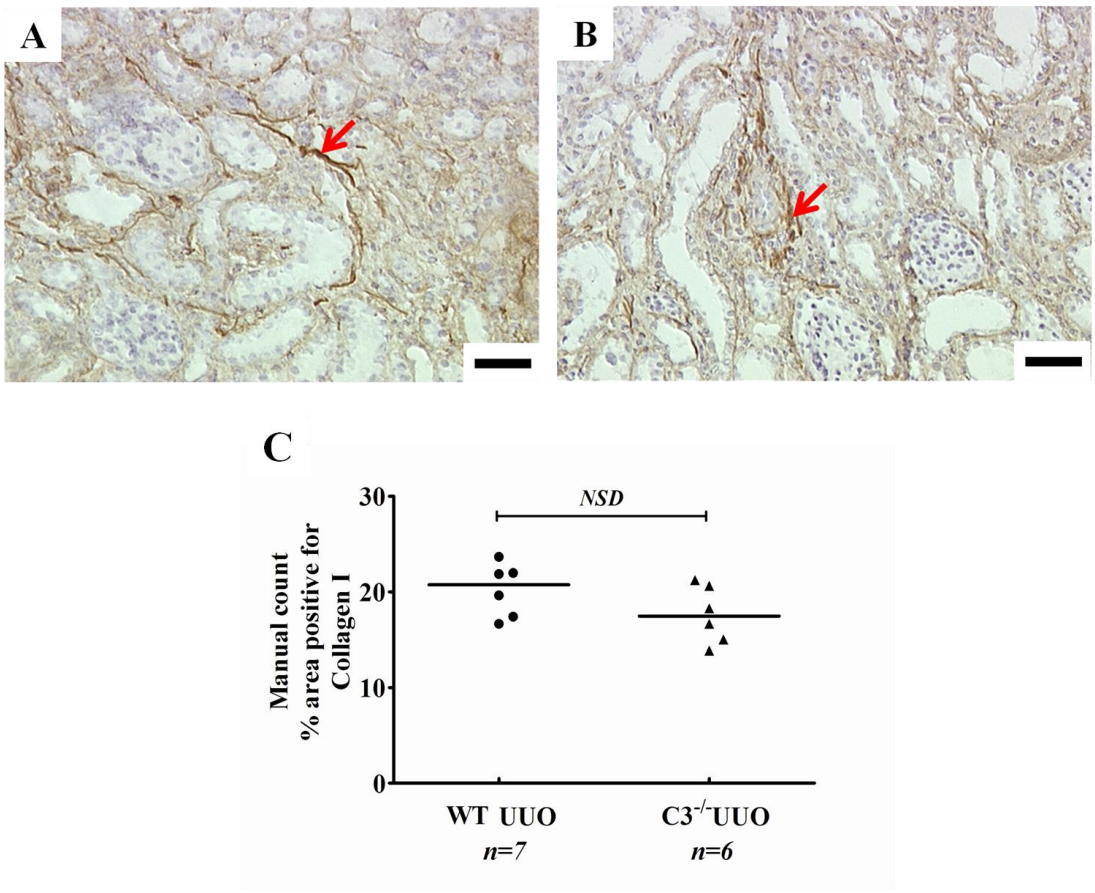

Figure 3.19. Collagen I deposition at day five UUO
The interstitial deposition of collagen I in frozen renal tissues of day five obstructed mice was semi-quantified by indirect IHC. WT and $C3^{-/-}$ UUO mice (A and B respectively). Scale bars on A and B represent 50µm. An Aperio scanner and Scanscope software were used to select ten random cortical fields for both experimental groups. Areas stained positive for collagen I fibres (as indicated by red arrows), were then manually counted using a grid-based method (C). Bars on graph represent median values.

Numerically, collagen I scoring in the kidneys of obstructed $C3^{-/-}$ mice was lower, however, this was not statistically different to collagen-I deposition observed in the renal cortices of obstructed WT mice. The median area occupied by α-SMA^{+} myofibroblasts in day five obstructed WT and $C3^{-/-}$ was 11.73% and 11.60% respectively (Figure 3.20C). There were no statistical differences between these values.

3.7.3 Gene expression

Following five days of UUO, TNF-α gene expression in WT and $C3^{-/-}$ obstructed kidneys (Figure 3.21A) was significantly elevated compared with contralateral kidneys (2.87 vs. 1.00 and 4.50 vs. 1.29 respectively; $p<0.001$ and $p<0.005$ respectively). TNF-α mRNA expression in obstructed WT and $C3^{-/-}$ UUO kidneys was equivalent.

Five days post-UUO, TGF-β mRNA levels in obstructed WT and $C3^{-/-}$ had increased (Figure 3.21B). Median TGF-β gene expression in obstructed WT mice was significantly elevated by almost three-fold to 2.86 compared with 1.00 in contralateral WT kidneys ($p<0.001$). Similarly, median expression of TGF-β in day five obstructed $C3^{-/-}$ mice was elevated approximately two-fold to 1.85 compared to a median of 0.93 in contralateral $C3^{-/-}$ kidneys ($p<0.05$). TGF-β mRNA expression in $C3^{-/-}$ UUO kidneys was significantly lower compared with levels observed in WT UUO kidneys ($p<0.05$).

IL-6 gene expression in obstructed WT and $C3^{-/-}$ kidneys was elevated after five days of UUO (Figure 3.21C). In WT obstructed kidneys, median IL-6 expression had increased compared with contralateral kidneys (25.00 vs. 0.44; $p<0.001$).

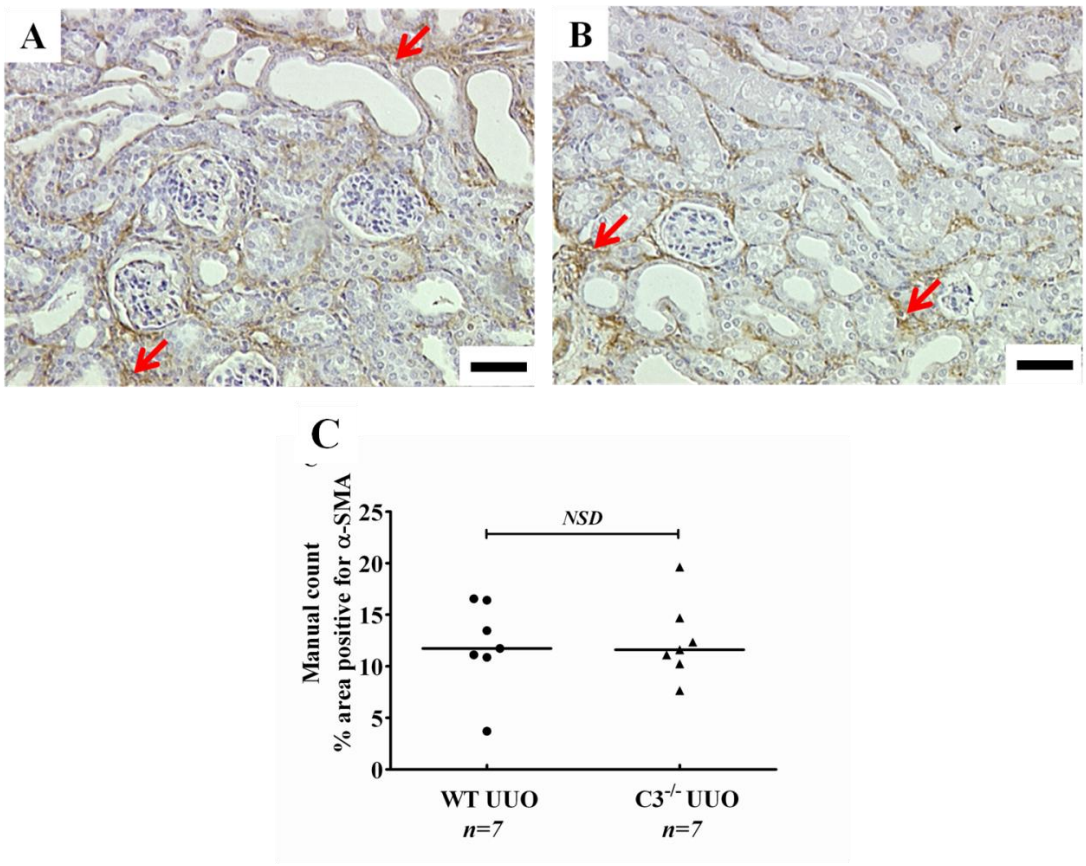

Figure 3.20. α-SMA^{+} myofibroblasts at day five UUO
Immunohistochemistry was used to semi-quantify the presence of α-SMA^{+} myofibroblasts in cryo-preserved renal tissues of day five WT and C3$^{-/-}$ UUO mice (A and B respectively). Scale bars on A and B represent 50µm. For both experimental groups, ten random cortical HPFs were acquired using an Aperio scanner and accompanying computer software. Areas of positive staining for α-SMA (as indicated by red arrows), were manually counted using a grid-based method, (C). Bars on graph represent median values.

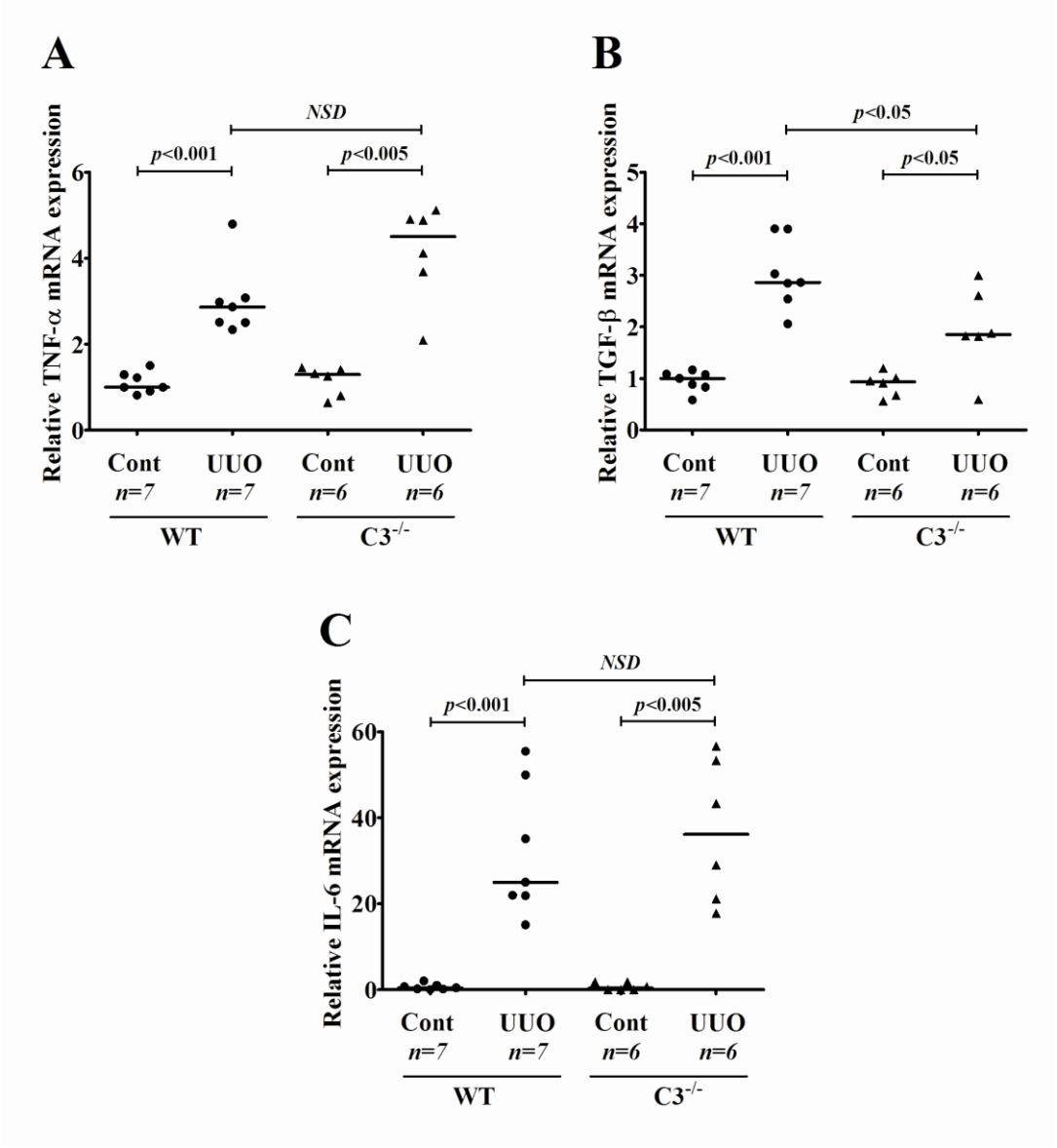

Figure 3.21. TNF-α, TGF-β and IL-6 gene expression at day five UUO
rtPCR was used to quantify levels of mRNA for TNF-α (A), TGF-β (B) and IL-6 (C) in obstructed (UUO) and contralateral (cont) renal cortices five days following ureteric obstruction. Gene expression was normalised to β-actin and the relative expression of TNF-α, TGF-β and IL-6 compared with that of β-actin was deduced. Elevated TNF-α, TGF-β and IL-6 gene expression was observed in WT and $C3^{-/-}$ obstructed renal cortices. TGF-β mRNA expression was significantly reduced in obstructed $C3^{-/-}$ kidneys. Bars on graphs represent median values. rtPCR was performed in triplicate for each animal.

Similarly, median IL-6 mRNA expression was elevated in renal cortices of obstructed $C3^{-/-}$ mice compared with unobstructed kidneys (36.15 vs. 0.35; $p<0.005$).

The median value for collagen I expression in day five obstructed WT mice was 5.31, a significant increase compared to the median of 1.1 in contralateral kidneys of WT mice ($p<0.001$; Figure 3.22A). Similarly, in obstructed kidneys harvested from $C3^{-/-}$ mice, median collagen I gene expression was higher compared to unobstructed kidneys (3.73 vs. 0.80), though this was not statistically significant. Collagen I gene expression in obstructed WT and $C3^{-/-}$ mouse kidneys was equivalent at this time. Five days post-UUO, there were no significant differences in the levels of collagen-III gene expression in obstructed WT and $C3^{-/-}$ kidneys compared with contralateral kidneys (0.81 and 1.50 vs. 0.60 and 0.85 respectively; Figure 3.22B).

Following five days of ureteric obstruction, there were no significant differences in the levels of α-SMA mRNA expression observed in obstructed WT and $C3^{-/-}$ kidneys (Figure 3.22C). In obstructed kidneys harvested from WT mice, median α-SMA expression was elevated compared with unobstructed kidneys (1.62 vs. 1.00). Similarly, median α-SMA mRNA expression in obstructed $C3^{-/-}$ mice was also higher compared with unobstructed kidneys (0.71 vs. 0.55). Interestingly, α-SMA expression in $C3^{-/-}$ UUO kidneys was significantly lower than that observed in WT UUO kidneys ($p<0.05$).

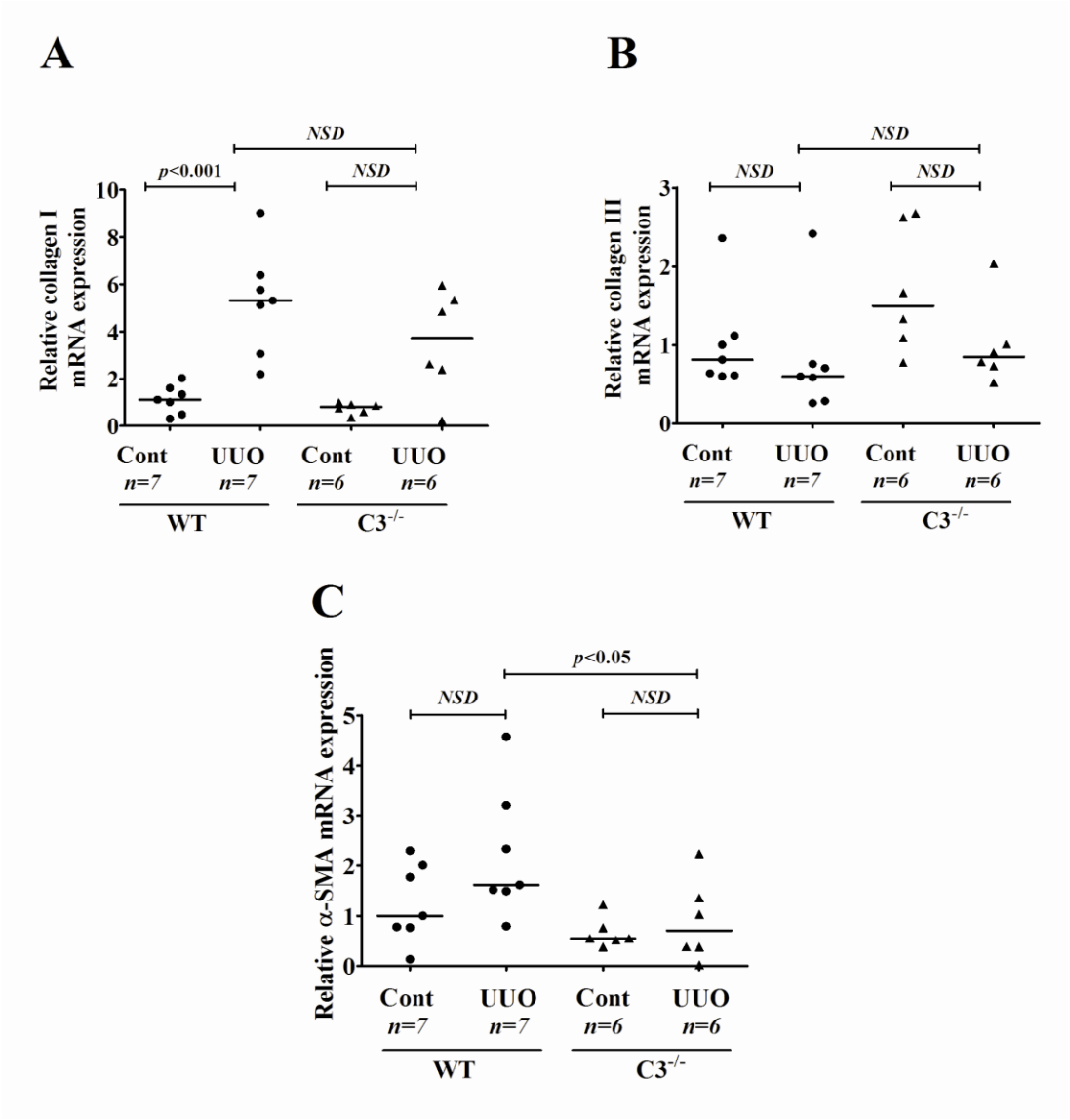

Figure 3.22. Collagen I & III and α-SMA gene expression at day five UUO
rtPCR was used to quantify gene expression of collagen I (A), collagen III (B) and α-SMA (C) in obstructed (UUO) and contralateral (cont) renal cortices five days after induction of ureteric obstruction. Gene expression was normalised to β-actin and the relative expression for collagen I, collagen III and α-SMA were calculated. At this time, collagen I expression was elevated in WT and $C3^{-/-}$ obstructed renal cortices. Collagen III expression remained unchanged. α-SMA mRNA expression was significantly lower in obstructed $C3^{-/-}$ mouse renal cortices. Bars on graphs represent median values. rtPCR was performed in triplicate for each animal.

3.8 A comparison of manual and automated immunohistochemical scoring methods in the murine model of ureteric obstruction

Immunohistochemically stained kidney sections taken from the obstructed kidneys of WT and $C3^{-/-}$ mice were imaged using an Aperio slide scanner. Accompanying Apreio Scanscope computer software was used to apply cell-count and positive pixel detection algorithms (modified for use in this study) to scanned renal tissue sections. Subsequent automated read-outs for number of cells per mm^2 and the percentage area occupied by positive pixels were obtained and analysed. To determine the effectiveness of the Aperio counting method against the manual counting method, the Pearson product-moment correlation coefficient (PPMCC) was used to test the linear dependence between the two methods. PPMCC regression ranges from -1 to 1, where +/-1 implies a perfect linear relationship between *X* and *Y*. An *r* value of zero indicates no linear correlation between the two variables.

In obstructed kidneys of WT and $C3^{-/-}$ mice Aperio software detected a median of 252.70 and 225.7 $CD4^+$ T cells per mm^2 respectively (Figure 3.23A). Although these median values were not considered statistically different from one another, the general trend was toward fewer $CD4^+$ cells being present in obstructed $C3^{-/-}$ kidneys, as in keeping with the outcome of the manual count method described previously (section 3.3). Compared with the manual counting method, the Aperio cell count algorithm for $CD4^+$ cell detection correlated very well (r=0.80; p<0.001; Figure 3.24A) The median number of $CD8^+$ T cells per mm^2 of renal cortex in obstructed WT and $C3^{-/-}$ mice were calculated to be 131.60 and 176.03 respectively (Figure 3.23B).

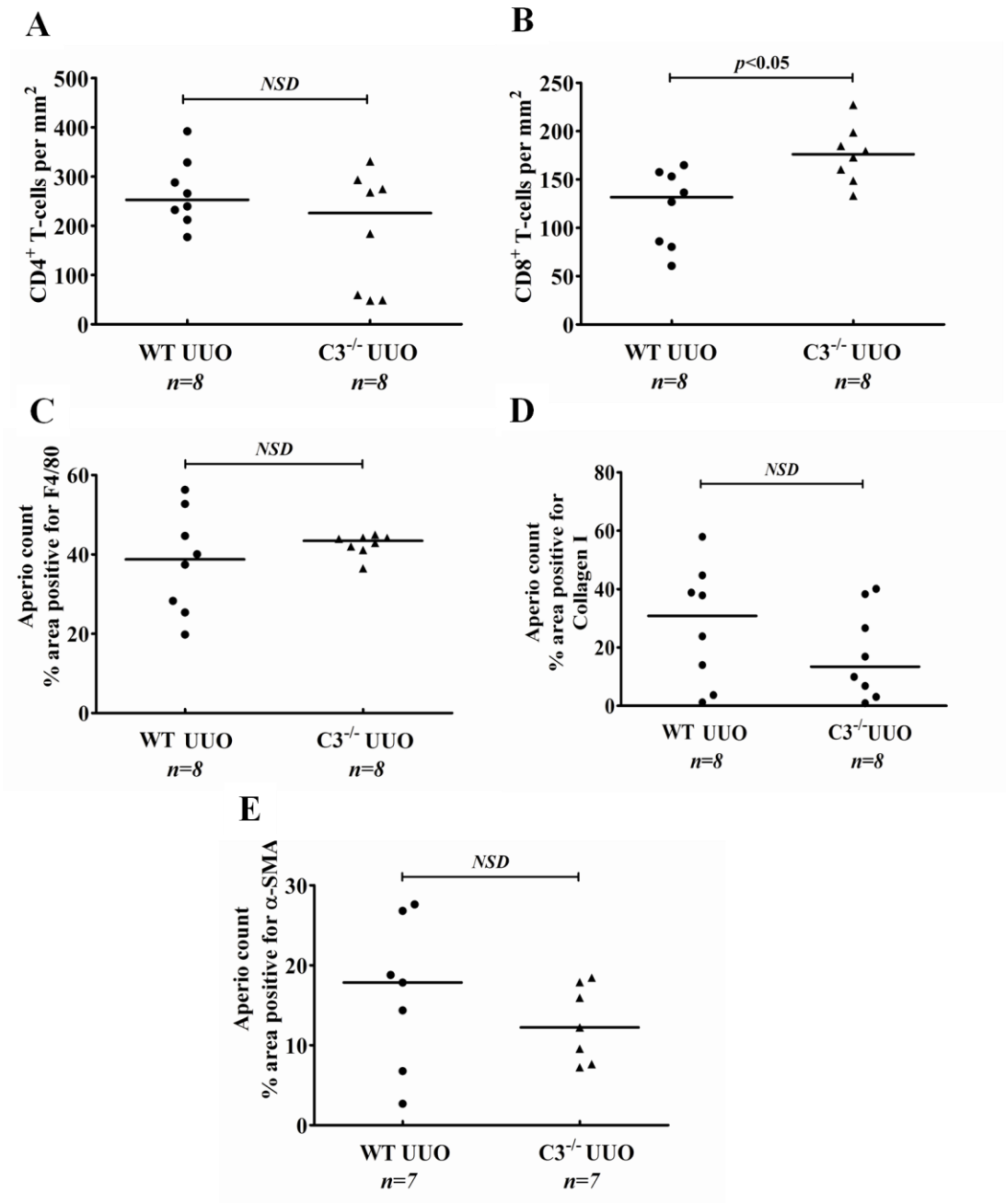

Figure 3.23. Aperio analysis of IHC staining at day ten UUO
IHC staining for CD4, CD8, F4-80 collagen I and α-SMA was visualised using the Aperio scanner and Scanscope software and regions of interest (ROI) were selected in a blinded manner. The IHC nuclear algorithm was used to count the number of positively stained CD4 (A) and CD8 (B) cells present. IHC positive pixel count algorithms were used to detect F4/80 (C), collagen I (D) and α-SMA (E) positive staining.

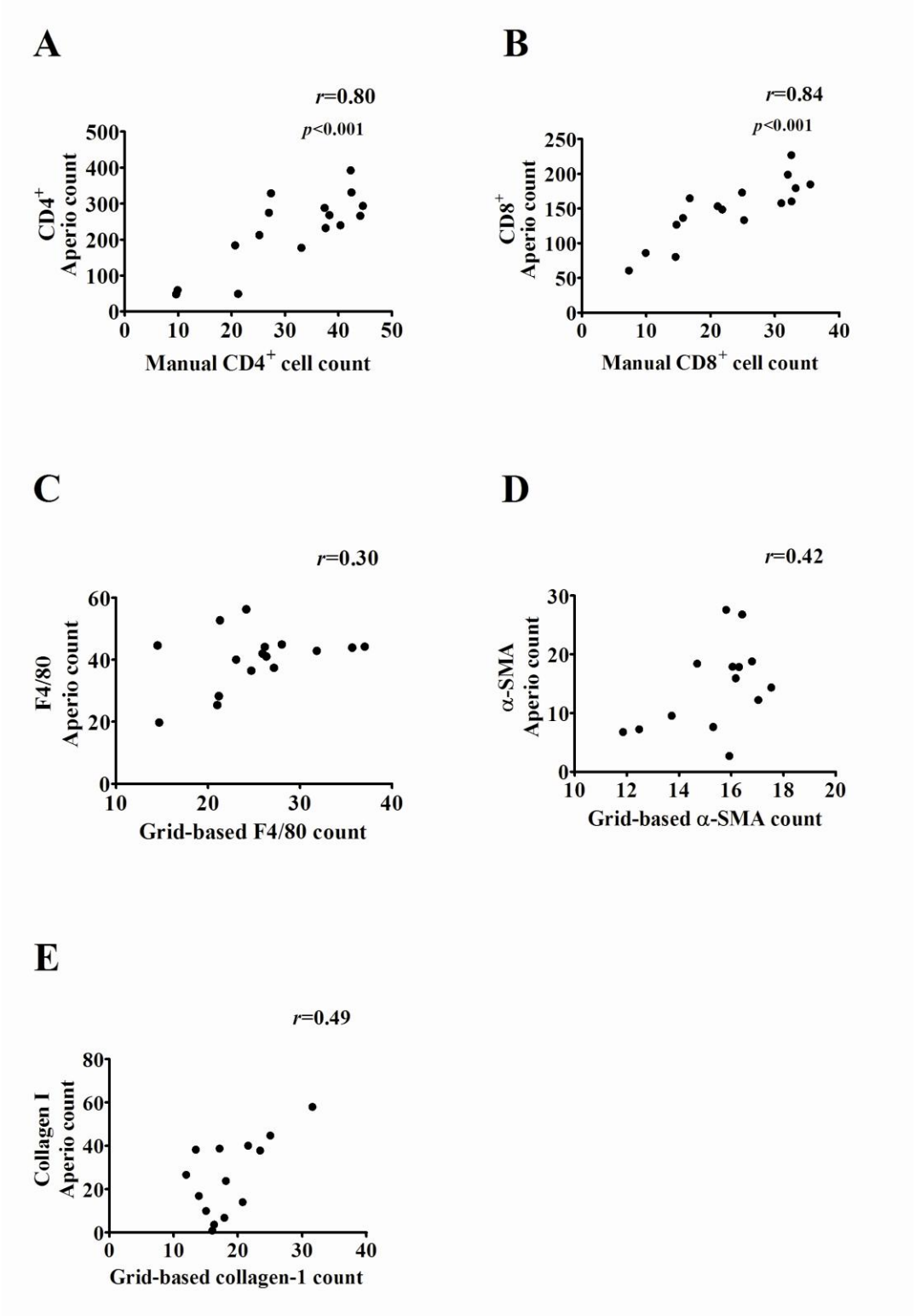

Figure 3.24. Comparison of day ten UUO Aperio and manual IHC counts
A statistical comparison of manual and automated immunohistochemical analyses to examine correlation between the two methods. $CD4^+$ (A) and $CD8^+$ (B) cell counts. F4/80 (C), α-SMA (D) and collagen I (E) positive staining.

The Aperio counting method detected significantly more $CD8^+$ cells in obstructed $C3^{-/-}$ kidneys ($p<0.05$). A comparison of the two different counting methods demonstrated strong correlation between the two data sets ($r=0.84$; $p<0.001$; Figure 3.24B). The Aperio positive pixel counts for $F4/80^+$ macrophages (Figure 3.23C), interstitial staining of collagen I (Figure 3.23D) and α-SMA (Figure 3.23E) in obstructed WT and $C3^{-/-}$ kidneys were; 38.74% and 43.41%, 31.12% and 17.83% and 65.77% and 44.45% respectively. Statistically, there were no significant differences between obstructed WT and $C3^{-/-}$ renal tissues expressing infiltrating $F4/80^+$ macrophages. Collagen I fibre deposition and $\alpha\text{-SMA}^+$ myofibroblasts were also equivalent in obstructed WT and $C3^{-/-}$ renal cortices. In general, there was significantly more variability in the data sets for F4/80, α-SMA and collagen I. However, numerical differences between the two groups do follow a similar pattern to that observed for the corresponding manual counts, despite their linear correlation being weak. The correlation between Aperio and manual $F4/80^+$ macrophage counts was very weak ($r=0.30$; $p>0.05$; Figure 3.24C) and although the correlation between Aperio and manual counts for α-SMA deposition were better ($r=0.45$; Figure 3.24D), neither were statistically significant. Similarly, the correlation between Aperio and manual counts for collagen I deposition in obstructed kidneys was weak ($r=0.49$; Figure 3.24E).

3.9 Discussion

Interstitial renal fibrosis is the characteristic hallmark of and common endpoint for many progressive kidney diseases. A more complete understanding of the mechanisms which contribute towards tubulointerstitial pathophysiology will assist with the future development of therapeutic strategies directed at preventing progressive loss of kidney function leading to renal insufficiency. Recent studies have demonstrated a pivotal role for complement during the progression of fibrosis in rodent models of proteinuric and ischaemic renal injury. Only one other study has addressed the contribution of complement towards the development of tubulointerstitial fibrosis in rodent models of ureteric obstruction. In the aforementioned study, Boor and co-workers demonstrated that after the induction of UUO, $C5^{-/-}$ mice and C5a receptor antagonist treated WT mice both had reduced ECM deposition and decreased mRNA levels for growth factors important in mediating renal fibrosis (Boor et al., 2007). Following on from the preliminary results of Boor *et al*, part of this study sought to further define the contribution of complement towards the progression of renal fibrosis in UUO, by investigating the role of the central complement pathway component C3.

During the course of UUO, interstitial expansion and tubular dilatation significantly increased in WT and $C3^{-/-}$ mice. Equivalent scores for tubular dilatation in both UUO groups for each time point demonstrated robustness of the UUO model in terms of consistent mechanical injury to tubules arising from surgical ligation of the ureter. Interestingly, the tubular interstitium of $C3^{-/-}$ mice was significantly more expanded at 3 days post-UUO compared with WT mice. This could have been caused by oedema, since interstitial volume at days 5 and 10 was equivalent in $C3^{-/-}$ and WT mice.

These initial findings contrasted with previous histological observations in a study of adriamycin nephropathy in mice, which demonstrated that mice deficient in C3 had significantly reduced tubulointerstitial injury (Turnberg et al., 2006). UUO and adriamycin nephropathy are different models of renal disease, however, both share a common fibrotic and inflammatory endpoint. Adriamycin targets the glomerular podocyte inducing heavy proteinuria and subsequent activation of tubular epithelial cells. During UUO, the back pressure caused by filtrate in the tubules and the ensuing compensatory changes to renal heamodynamics cause mechanical and hypoxic stress (Yeh et al., 2011; Dendooven et al., 2010). The different mechanisms of injury may influence the outcome of early histological observations using a semi-quantitative method of analysis. In an effort to detect more subtle differences in interstitial expansion in this study, the manual grid-counting method was modified by increasing the number of grid intersections and then applied in the same way. The outcome of this was that increasing the number of grid intersections counted over areas of interest only increased the variability of results.

During UUO, expansion of the interstitial compartment is an indicator of ECM re-modelling and cell proliferation. Several cytokines and growth factors have been implicated in ECM homeostasis (Yang and Liu, 2002; Matsumoto and Nakamura, 2001; Strutz et al., 2000), of particular importance is the regulatory pro-fibrotic cytokine TGF-β (Moon et al., 2006; Wang et al., 2005a; Muller et al., 2000b). Under normal physiological conditions, TGF-β is sequestered in an inactive form bound to an inhibitory latency associated peptide (LAP). Under permissible conditions, the integrin αvβ6 binds to LAP and TGF-β becomes activated. TGF-β is then free to bind receptors on target cells and trigger an intracellular signalling cascade.

Evidence for TGF-β activation during UUO was illustrated in a study by Ma and co-workers using β6 deficient mice. In the absence of β6, mice developed less severe tubulointerstitial fibrosis, demonstrating that αvβ6 integrin is an important mediator of TGF-β activation during UUO (Ma et al., 2003). A number of studies have previously demonstrated increased TGF-β mRNA expression during UUO (Misseri and Meldrum, 2005; Yamamoto et al., 1994). In this study, TGF-β gene expression was significantly elevated in the renal cortices of WT and $C3^{-/-}$ mice after 5 and 10 days of UUO. In addition to this, significantly elevated collagen I and α-SMA mRNA levels were observed in day 10 WT and $C3^{-/-}$ obstructed kidneys. Interestingly, in obstructed $C3^{-/-}$ mice, TGF-β mRNA levels were significantly lower at day 5 and day 10. Reduced TGF-β expression in the kidneys of obstructed $C3^{-/-}$ mice also coincided with significantly less collagen I and α-SMA gene expression after 10 days of UUO as well as significantly reduced levels of collagen I protein deposition within the interstitium.

These results suggest that during UUO, $C3^{-/-}$ mice are partially protected from TGF-β mediated ECM collagen deposition. Although collagen deposition was quantified as part of this study, TGF-β protein levels were not measured. Previous studies have demonstrated a poor relationship between active TGF-β and total TGF-β. It would be interesting to see if both urinary and tissue TGF-β protein levels in $C3^{-/-}$ mice during UUO reflected the changes in gene expression observed and if this gave some indication as to the site of TGF-β activation. Previous studies have demonstrated that up-regulation of TGF-β receptors occurs at the cell surface of tubular epithelial cells supporting the hypothesis that TGF-β mediated epithelial activation or transition to a mesenchymal phenotype may contribute towards an increase in myofibroblasts during renal fibrosis (Bottinger and Bitzer, 2002; Iwano et al., 2002).

Following the process of EMT, tubular epithelial cells no longer express characteristic markers of epithelial phenotype such as E-cadherin. With this in mind it would be intriguing to look at the expression and distribution of TGF-β receptors and characteristic epithelial cell markers during the progression of UUO in WT and $C3^{-/-}$ mice to see if the absence of C3 affected the transition of different resident renal cells into myofibroblasts.

The observations for collagen III gene expression in obstructed WT and $C3^{-/-}$ mouse kidneys in this study were unexpected. In WT mice, collagen III mRNA was lower in obstructed kidneys compared with unaffected contralateral kidneys throughout UUO. Similarly, collagen III gene expression after three and five days UUO in $C3^{-/-}$ mouse kidneys was lower than it was in contralateral kidneys. However, by day ten collagen III mRNA levels in the obstructed kidneys of $C3^{-/-}$ mice were significantly elevated. Collagen III is usually present within healing wounds and is synthesised by immature fibroblasts. In this study, the increase in collagen III seen in obstructed $C3^{-/-}$ mouse kidneys during the latter stages of UUO appears to coincide with lower α-SMA and collagen I gene expression as well as reduced interstitial collagen I deposition. Since collagen I accumulation was higher in the presence of C3, any changes to collagen III gene expression may have taken place prior to day three obstruction in WT mice. Another explanation could be that the presence of more macrophages in the absence of C3 may be occurring more rapidly. Interestingly, the significant increase in collagen III gene expression in the absence of C3 also coincided with an increase TNF-α gene expression and is discussed in more detail in paragraph on page 162.

α-SMA is a marker of myofibroblasts. Whilst α-SMA mRNA expression in WT and $C3^{-/-}$ mice at day 5 UUO was not significantly elevated compared to contralateral kidneys, α-SMA mRNA levels were significantly lower in $C3^{-/-}$ UUO mice at this time. One reason for this could be that myofibroblast proliferation is reduced in the absence of C3.

A general marker of cell proliferation such as Ki-67 could be used to identify populations of actively proliferating cells during the progression of UUO which may assist with identifying the source of interstitial fibroblasts and perhaps their upstream activators. In this study, deposition of Sirius red positive collagen fibres was significantly elevated in WT and $C3^{-/-}$ mice after 3 days of UUO. Interestingly collagen was less abundant in the tubular interstitium of $C3^{-/-}$ mice at this time. Since TGF-β mRNA expression was not significantly up-regulated at this time, the early decrease in collagen expression observed may be due to the activation of latent TGF-β. Activation of other fibrotic mediators may also have contributed towards these early differences. One candidate for this could be NF-κB, since NF-κB is known to induce the expression of inflammatory genes and participate in the progression of numerous pathophysiological states (discussed in chapter 1). In obstructive nephropathy, ANG-II has been shown to activate NF-κB signalling which then regulates downstream fibrotic responses.

NF-κB can also contribute to activation of angiotensinogen gene expression, a precursor to ANG-II production (Grande et al., 2010). One reason for reduced collagen deposition at this time could be that ANG-II mediated NF-κB pro-inflammatory/pro-fibrotic signalling during acute UUO-mediated injury is blunted in the absence of C3.

TNF-α is an important activator of NF-κB and during UUO, ANG-II mediated activation of NF-κB also contributes towards an early increase in TNF-α gene expression. Activation of NF-κB in response to ureteric ligation results in the formation of two autocrine reinforcing loops which amplify the production of ANG-II and TNF-α (Grande et al., 2010). In this study, TNF-α gene expression was significantly elevated in WT and $C3^{-/-}$ mouse renal cortices throughout ureteric obstruction. Interestingly, the amount of TNF-α mRNA in $C3^{-/-}$ mice after three and five days of UUO was numerically greater compared to WT mice and by day ten, the obstructed kidneys of $C3^{-/-}$ mice had significantly more TNF-α mRNA present compared with kidneys taken from obstructed WT mice. The increase in TNF-α gene expression that was observed in $C3^{-/-}$ mice could imply that in the absence of C3, TNF-α plays a more dominant role in driving tubulointerstitial inflammation and fibrosis during UUO. It would be interesting to see if a reduced TNF-α signal (perhaps achieved using TNFR antagonists or TNFR deficient mice) combined with the absence of C3 would further decrease interstitial and fibrosis. Future work could also explore the combined effects of blocking NF-κB activity or using ACE inhibitors in the absence of C3.

As a mediator of acute inflammatory response following injury to tissues, IL-6 can exert either anti- or pro-inflammatory responses depending on the nature of activation (Kayama et al., 1997). Expression of IL-6 mRNA in $C3^{-/-}$ mice was equivalent to expression in WT mice. In this study, persistent IL-6 gene expression in the kidneys of WT and $C3^{-/-}$ mice would suggest pro-inflammatory activity that is not altered in the absence of C3.

Infiltration of T cells and macrophages is a characteristic feature of renal fibrosis during obstructive nephropathy (Tapmeier et al., 2010).

In this study, $CD4^+$ T cells were seen in the renal interstitium of WT and $C3^{-/-}$ mice 10 days post-UUO and the number of cells was equivalent. A significant number of $CD8^+$ T cells and $F4/80^+$ macrophages were present in $C3^{-/-}$ and WT mouse kidneys at day 10 UUO. Interestingly, there were significantly higher numbers of $CD8^+$ T cells and $F4/80^+$ macrophages in the absence of C3.

Both monocytes and macrophages can express the F4/80 antigen on their cell surface. Other antigen presenting cells (APCs) such as dendritic cells (DCs) also express F4/80 on their cell surfaces, therefore IHC staining used in this study to detect F4/80 antigen is could be detecting the presence of a combination of different APCs. An additional degree of complexity arises from the different sub-divisions, classes and populations of DCs, macrophages and monocytes respectively. Stimulated macrophages and DCs can activate $CD4^+$ T cells and so a greater number of $F4/80^+$ APCs in day 10 UUO $C3^{-/-}$ mice might have been expected to elicit an exaggerated $CD4^+$ T cell response. This was not the case and so it is possible that the macrophages present within $C3^{-/-}$ mouse kidneys could have a different phenotype compared with those present in WT mice.

For example, M2 macrophages are known to promote wound healing and tissue repair by producing anti-inflammatory cytokines. In turn, the absence of complement activation within the interstitial compartment may confer more favourable conditions for the proliferation of anti-inflammatory mediators, reducing the severity of injury. In addition to elevated numbers of $F4/80^+$ macrophages in $C3^{-/-}$ mice at day 10 UUO, $CD8^+$ T cells were significantly elevated in this experimental group. Previous studies have suggested that $CD8^+$ T cells play more of an effector role during renal disease by directly targeting damaged or dysfunctional renal cells (Robertson et al., 2004).

However the presence of more $CD8^+$ T cells in a less fibrotic environment as shown in this current study would suggest that these cells are not causing tubular injury. $CD8^+$ T cells become activated when they encounter major histocompatibility complex I (MHC I) presentation of degraded cytosolic protein fragments. It is plausible that MHC I presentation of antigens from stressed/wounded cells could increase during renal injury, thus increasing the number of $CD8^+$ T cells.

On this basis more $CD8^+$ T cells would be expected in WT mice during the progression of UUO, since this study has demonstrated that $C3^{-/-}$ mice are partially protected from progression of tubulointerstitial fibrosis. It is evident that in the absence of complement activation the trafficking or proliferation of $CD8^+$ T cells is altered. A future study employing the depletion of macrophages prior to induction of UUO in $C3^{-/-}$ mice may assist with understanding how the recruitment process of $CD8^+$ T cells differs in complement deficient mice.

The analysis of renal tissues stained immunohistochemically for interstitial collagen I and α-SMA deposition and $CD4^+$, $CD8^+$ and $F4/80^+$ immune cell infiltrates was conducted using automated and non-automated counting methods. The purpose of testing an automated method was to attempt to increase the reproducibility of results whilst simultaneously reducing the time spent on IHC analysis in future projects. An Aperio Scanscope XT slide scanner was used to capture digital images of renal tissues using brightfield imaging at x20 magnification. Following this, Imagescope software was used to select regions of interest and then apply automated analyses in the form of algorithms. ImageScope software analyses for $CD4^+$ and $CD8^+$ cell counts in Aperio-scanned tissue sections correlated strongly with analyses obtained using non-automated counting methods.

As with the manual grid-counting method of analysis, the nuclear counting algorithm detected an equivalent number of $CD4^+$ T cells in day 10 WT and $C3^{-/-}$ obstructed mouse kidneys and a greater number of $CD8^+$ T cells present in day 10 $C3^{-/-}$ UUO kidneys than in WT UUO kidneys. Conversely, application of the positive pixel counting algorithm to quantify $F4/80^+$ cells, α-SMA^+ myofibroblasts and collagen I deposition did not correlate with non-automated analyses of obstructed kidneys of WT and $C3^{-/-}$ mouse kidneys at day 10.

It is plausible that non-specific background staining of endogenous biotin and avidin in renal tissues had more of an effect on the outcome of results obtained using the positive pixel counting algorithm, since the algorithm's parameters were less specific. It is not always possible to completely omit background staining when applying mathematical formulae to analyse areas of positive IHC staining that are in close proximity. In this study, the interference of background staining was partially overcome by selecting only strong positive pixels to undergo further analysis, as was the case for $F4/80^+$ staining. However this could not be applied to α-SMA and collagen I automated IHC analyses, since there was more variation in the intensity of positive staining. Non-specific staining for endogenous biotin and avidin did not impede when using the nuclear counting algorithm to count $CD4^+$ and $CD8^+$ cells in obstructed renal tissues, since the parameters for this algorithm included size and shape restrictions.

The Aperio slide scanner provides a less time-consuming and more consistent method of acquiring suitable images for semi-quantitative IHC analysis. Instead of focusing on a restricted number of images acquired using standard bright field microscopy, the Aperio slide scanner has the capacity to capture an entire tissue section, or even numerous sections on the same slide and save these in digital format.

This is particularly useful for providing the option of selecting a larger area to analyse at a later date. The ImageScope analysis software nuclear counting algorithm proved to be a reliable method for counting IHC-stained cells, but the positive pixel counting algorithm does not correlate with non-automated methods.

The results from this chapter provide evidence that complement is involved in the mediation of fibrosis during obstructive nephropathy. The mechanism by which complement becomes active following the induction of UUO is not known, however evidence from studies of other models of progressive renal disease have shown that complement is activated via the alternative pathway (Turnberg et al., 2006; Lien et al., 2003). The contribution of activated complement and other components of the complement system towards the progression of renal disease during ureteric obstruction is addressed in the following chapter.

4 The role of complement during UUO

4.1 Introduction

In the previous chapter, absence of C3 was found to reduce interstitial collagen deposition during UUO and attenuate collagen I and TGF-β gene expression during the later stages of UUO. This chapter examines C3 and crry protein expression, complement activation and gene expression of different components of the complement system, including regulatory proteins.

4.2 C3 protein detection in contralateral and obstructed renal tissues

A fluorescein isothiocyanate (FITC) conjugated polyclonal antibody was used to detect C3 protein deposition in frozen WT contralateral and obstructed renal tissue sections. C3 protein was abundant around the glomeruli and renal tubules of unaffected kidneys at both day three and day ten (Figure 4.1A and C). Three days following UUO, there appeared to be less C3 protein present around renal tubules (Figure 4.1B). A similar pattern of staining was observed following ten days of ureteric obstruction, though by this time, it was possible that C3 protein may have been subject to degradation as positive C3 staining appeared more fragmented and less specifically bound to structures such as tubules in the renal cortex (Figure 4.1D). In addition to this, infiltrating cells may also be contributing towards the production and expression of C3 at day ten UUO.

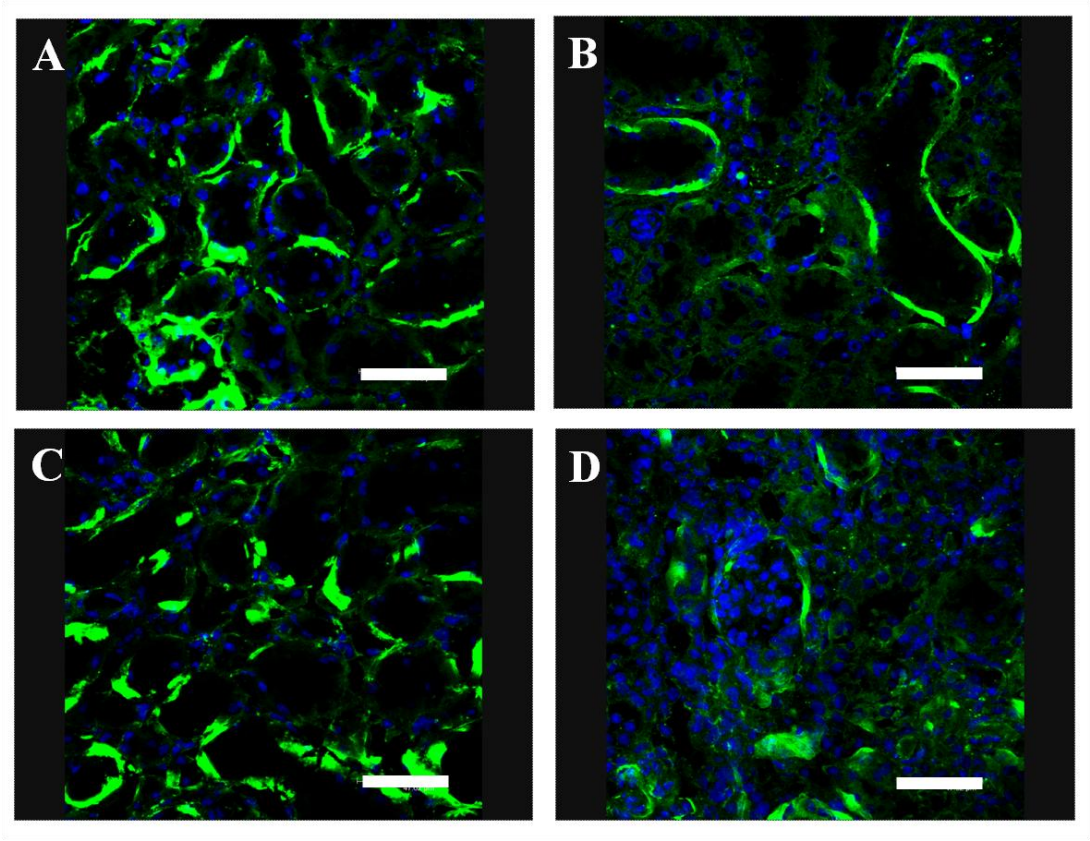

Figure 4.1. Immunofluorescence staining for C3.
Distribution of C3 within cryo-preserved renal cortices of WT mice before and during UUO (FITC=green, DAPI=blue). Day 3 and day 10, WT contralateral kidneys respectively (A and C). Day 3 and day 10, WT UUO kidneys respectively (B and D). Above images are representative of renal tissue sections from n=6 (day three) and n=8 (day ten) mice. Magnification for all images was x630, scale bar is 50μm.

4.3 Crry protein detection in contralateral and obstructed renal tissues

Crry protein was detected in cryo-preserved obstructed and contralateral renal cortices of WT mice at three and ten days post-UUO using indirect immunofluorescence. In unobstructed kidneys, crry staining was present within glomerili and also appeared to be localised to the basolateral membrane of renal tubules (Figure 4.2A, B, E and F). Three days following ureteric obstruction, the majority of crry seemed to have disappeared from the tubular basolateral membrane and instead seemed to show a more diffuse pattern of cytoplasmic staining. Glomerular crry staining remained unchanged at this time. After ten days of ureteric obstruction, crry staining appeared to be present in cells located in the expanded renal interstitium, but remained absent from the tubular basolateral membrane. Glomerular crry staining appeared to be more diffuse after ten days of UUO (Figure 4.2G and H). This part of the work was carried out by Mr Kittiphat Chanthong.

4.4 Complement activation in mice following UUO

Activation of complement in WT and $C3^{-/-}$ following ureteric obstruction was determined using an ELISA test and standard curve of known C3a concentration to measure the amount of C3a present in the urine collected from the dilated renal pelvis of obstructed kidneys (Figure 4.3D). Complement activation was evident after three days of ureteric obstruction and the median concentration of C3a in urine collected from WT mice at this time was 6344ng/ml ($p<0.005$; Figure 4.3A).

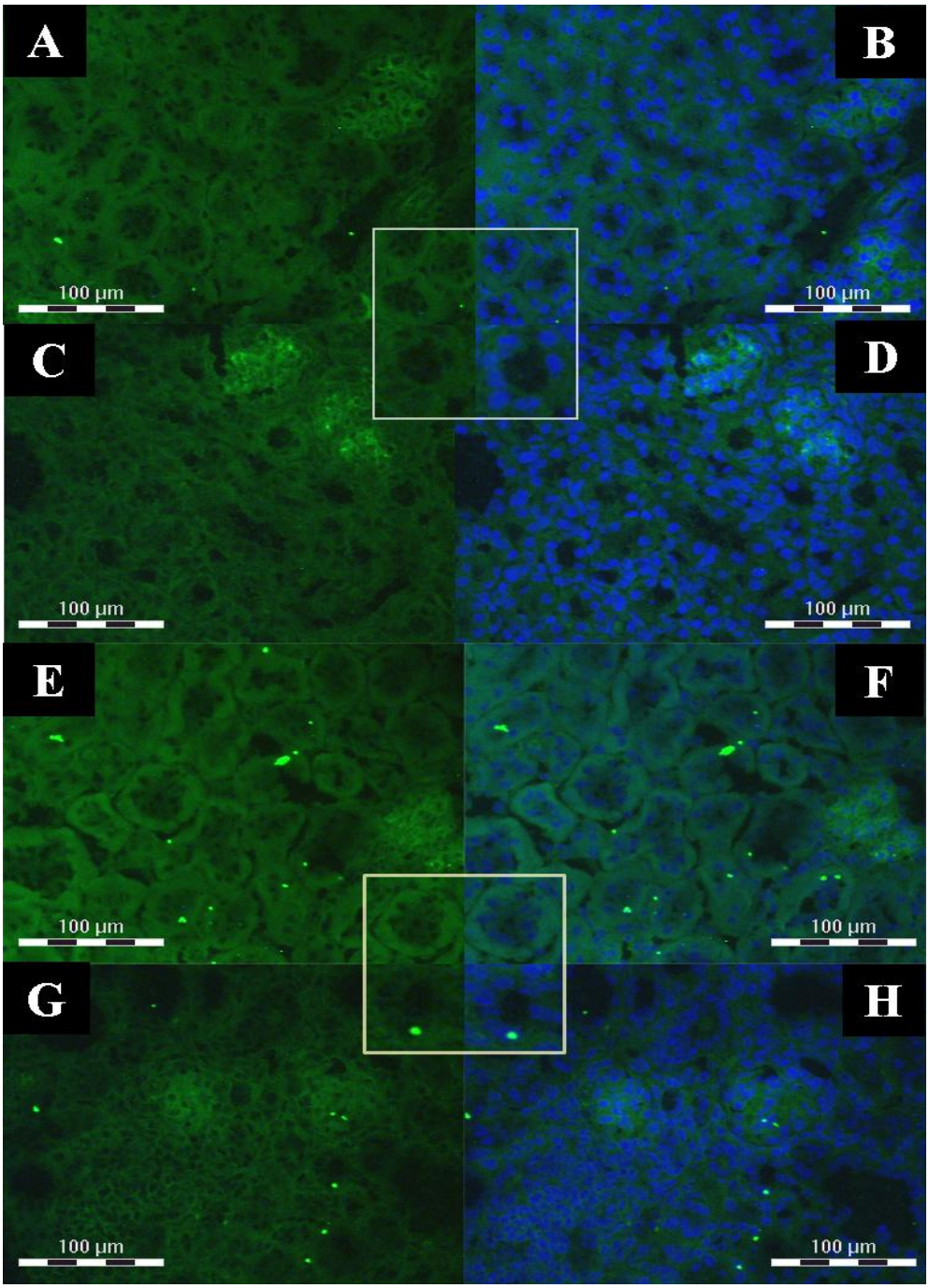

Figure 4.2 Immunofluorescence staining for crry.
Distribution of crry within the cryo-preserved renal cortices of WT mice before and during UUO (FITC=green, DAPI=blue). Day 3 (A and B) and day 10 (E and F), WT contralateral kidneys respectively. Day 3 (C and D) and day 10 (G and H), WT UUO kidneys respectively. Magnification for all images was x200, scale bar is 100µm.

C3a was significantly elevated to 8661ng/ml in urine taken from day 5 obstructed mice (p<0.001), demonstrating sustained complement activation during sub-acute ureteric obstruction (Figure 4.3B). Complement activation remained significantly elevated in WT mice following ten days of UUO, with a median value of 4457ng/ml (p<0.001; Figure 4.3C). C3a was not detected in the urine taken from the obstructed kidneys of $C3^{-/-}$ mice. C5 convertase activity, which occurs at the beginning of the terminal complement pathway prior to the membrane attack complex formation, was tested by measuring the amount of C5a protein present in urine derived from obstructed kidneys by ELISA. It was not possible to detect C5a in the urine taken from the renal pelvis (data not shown). Although the ELISA was able to detect C5a at concentrations above 1.56ng/ml based on the standard curve, the presence of urinary C5a at concentrations below this cannot be excluded.

4.5 Complement gene expression in WT and $C3^{-/-}$ mice during UUO

4.5.1 C3

4.5.1.1 C3 gene expression

After three days of UUO, median C3 mRNA expression in the obstructed kidneys of WT mice was significantly elevated compared with contralateral WT kidneys (102.30 vs. 0.98; p<0.005). In obstructed WT kidneys, C3 gene expression was significantly elevated (p<0.005) compared with obstructed kidneys from $C3^{-/-}$ mice (Figure 4.4A).

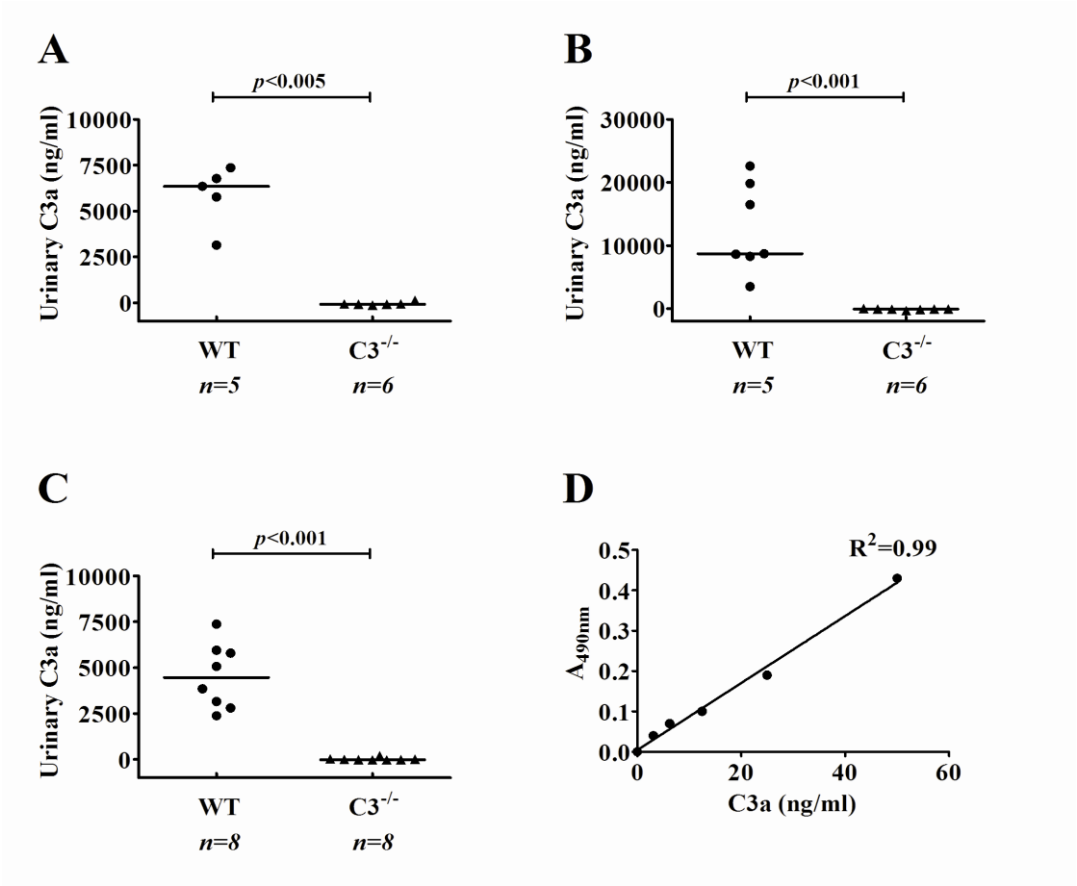

Figure 4.3. Urinary C3a after three, five and ten days of UUO
Urinary fluid which had accumulated within the renal pelvis of obstructed kidneys was removed and analysed for the presence of C3a protein (a marker of complement activation) by ELISA assay. Urinary concentrations for WT and $C3^{-/-}$ groups at three (A), five (B) and ten days post-UUO (C) were calculated from a standard curve of known C3a concentrations (D). Bars in graphs represent median values. R^2 indicates linear correlation between optical density (A_{490mm}) and C3a concentration in the range used.

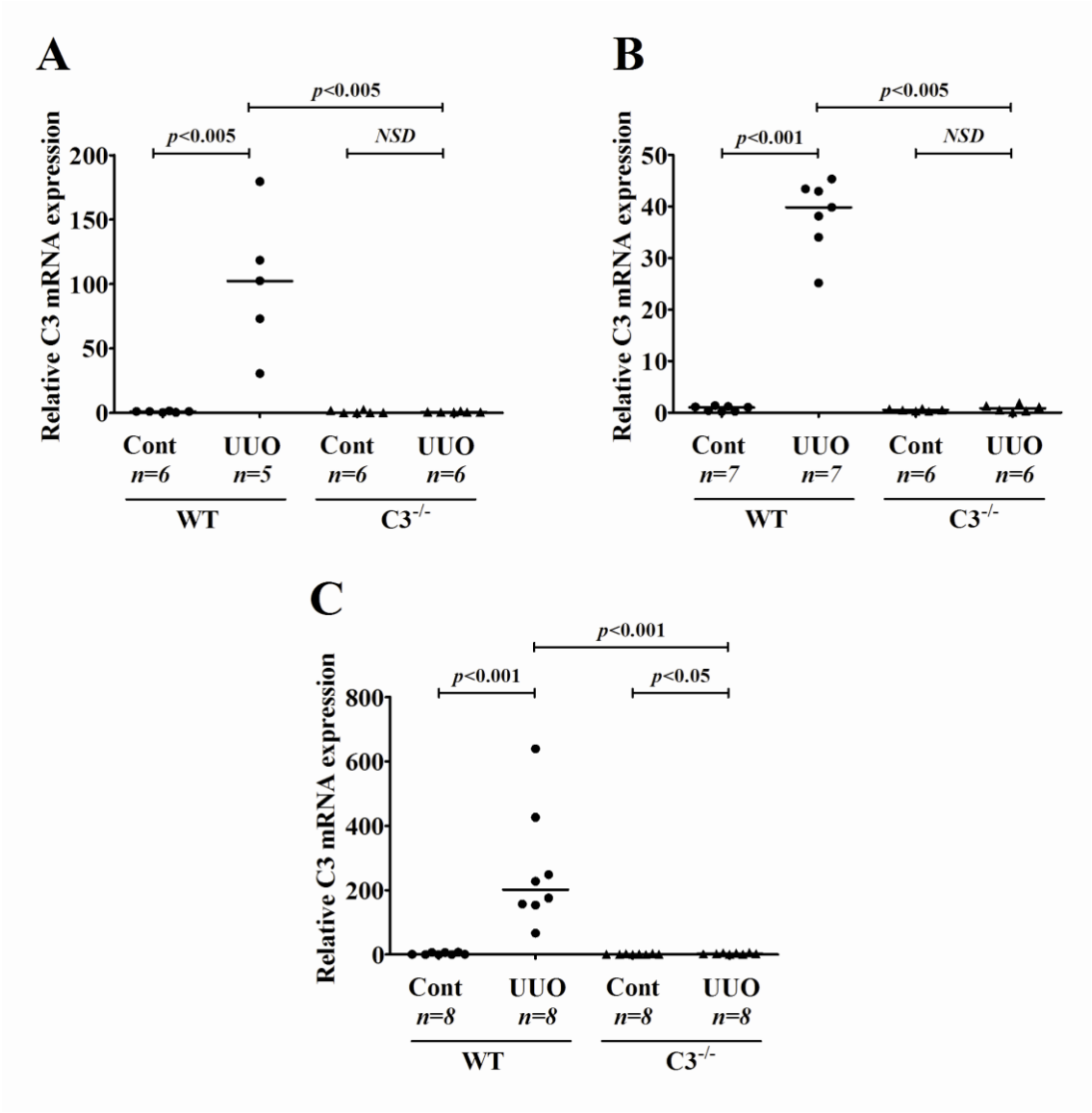

Figure 4.4 C3 gene expression after three, five and ten days of UUO
Expression of C3 mRNA was measured by rtPCR in UUO and contralateral renal cortices following three (A), five (B) and ten (C) days of UUO. Gene expression was normalised to β-actin. C3 was highly expressed in the obstructed renal cortices of WT mice at all time points. A Mann-Whitney U-test was used to calculate statistical significance. Bars on graphs represent median values. rtPCR was performed in triplicate for each animal.

After five days of ureteric obstruction, C3 gene expression in the affected (UUO) kidneys of WT mice had increased significantly to a median value of 39.82 fold (p<0.001), compared to a median value of 1.00 in unaffected WT kidneys (Figure 4.4B). By day ten, up-regulation of C3 gene expression persisted in the UUO kidneys of WT mice compared to unaffected contralateral kidneys (201.53 vs. 0.90; p<0.001; Figure 4.4C). No C3 gene expression was detected in $C3^{-/-}$ mouse kidneys (Figure 4.4A-C).

4.5.1.2 Spatial distribution of C3 gene expression in WT mice during early UUO

The site of C3 gene up-regulation was determined by *in situ* hybridisation. After three days of ureteric obstruction, C3 gene expression in WT mouse kidneys appeared to be restricted to tubular epithelial cells, with expression noticeably higher in some tubules than others (Figure 4.5A). C3 was not detected in unobstructed kidneys (Figure 4.5B). Similarly, C3 was not detected in obstructed or contralateral kidneys treated with SP6 sense probe (Figure 4.5C and D respectively). FERM domain-containing protein 7 (FRMD7) was used as a positive internal control and was expressed in contralateral and obstructed kidneys (Figure 4.5E and F respectively).

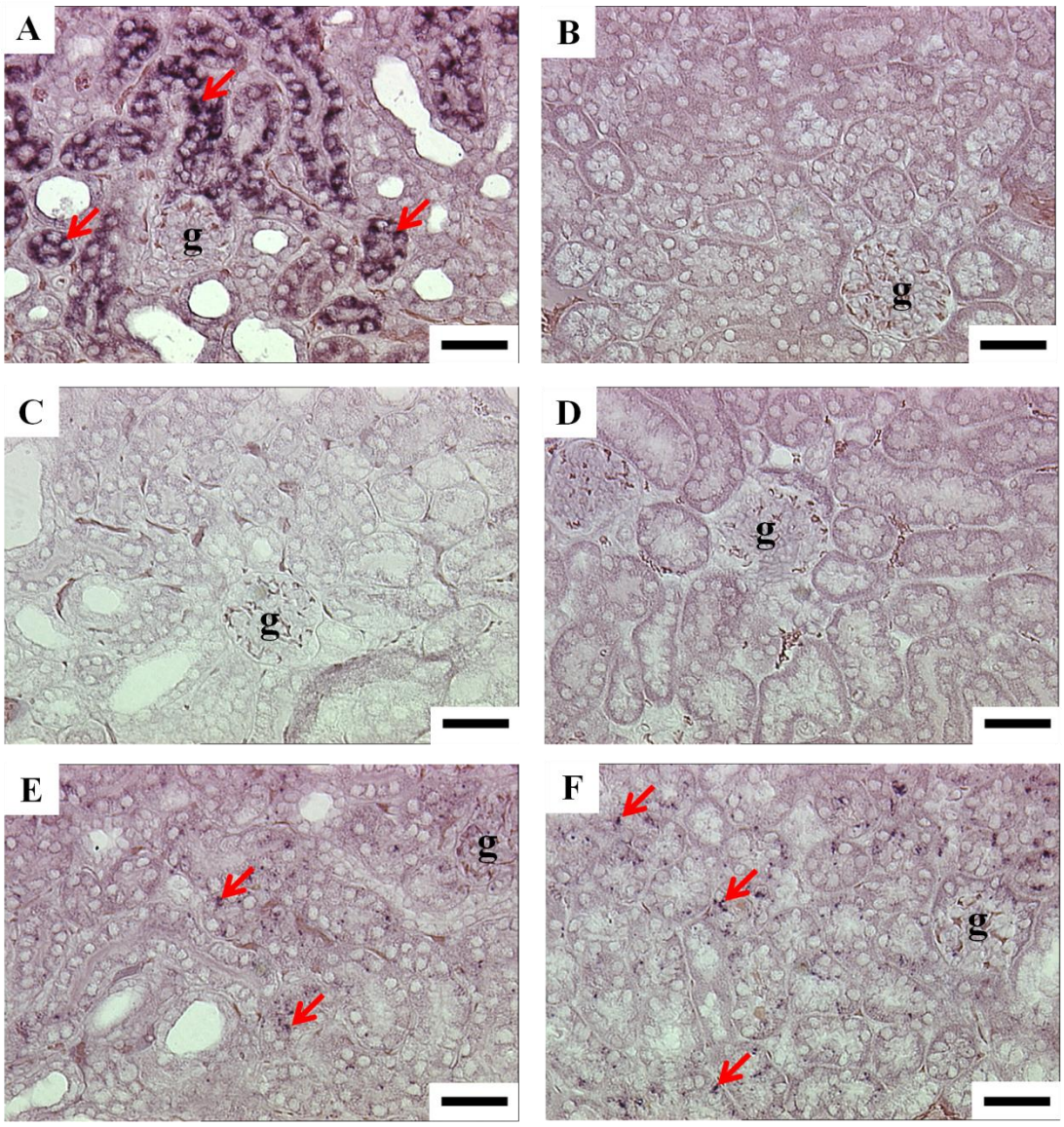

Figure 4.5. C3mRNA distribution in WT mice after three days of UUO
Detection of T7 anti-sense C3 probe in obstructed (A), but not contralateral (B) WT kidneys. No *in situ* hybridisation of SP6 sense C3 probe in obstructed or contralateral kidneys of WT mice (C and D respectively). Positive *in situ* hybridisation of FRMD7 probe in obstructed and contralateral kidneys of WT mice (E and F respectively). After three days of UUO, the T7 anti-sense probe detected varying amounts of C3mRNA within some renal tubular epithelial cells. Scale bar on images measures 50µm.

4.5.2 Crry

Crry is a murine membrane regulator of complement. It binds to C3b and C4b to inhibit classical and alternative pathways. Three days following UUO, there were no significant changes to the levels of crry mRNA expression in kidneys of obstructed WT and $C3^{-/-}$ mice. (Figure 4.6A). Five days post-ureteric obstruction, median mRNA expression for crry in obstructed WT and $C3^{-/-}$ mouse kidneys was significantly lower compared with contralateral kidneys ($p<0.001$ and $p<0.005$ respectively; Figure 4.6B). Median crry mRNA expression in day five $C3^{-/-}$ UUO kidneys was significantly lower than that observed in WT UUO kidneys ($p<0.01$; Figure 4.6B). The observations for crry gene expression after ten days of ureteric obstruction was similar to day five UUO. Crry mRNA was significantly reduced in both WT and $C3^{-/-}$ obstructed kidneys compared with unaffected contralateral kidneys ($p<0.05$ and $p<0.005$; Figure 4.6C). Crry gene expression was significantly reduced in obstructed $C3^{-/-}$ kidneys compared with WT UUO kidneys ($p<0.05$).

4.5.3 DAF1

DAF1 is a cell surface regulator of complement. It prevents the assembly of and accelerates the disassembly of the alternative pathway C3 convertase C3bBb. Three days post-UUO, no significant differences were observed in expression of DAF1 mRNA in WT and $C3^{-/-}$ kidneys when obstructed and contralateral kidneys were compared (Figure 4.7A).

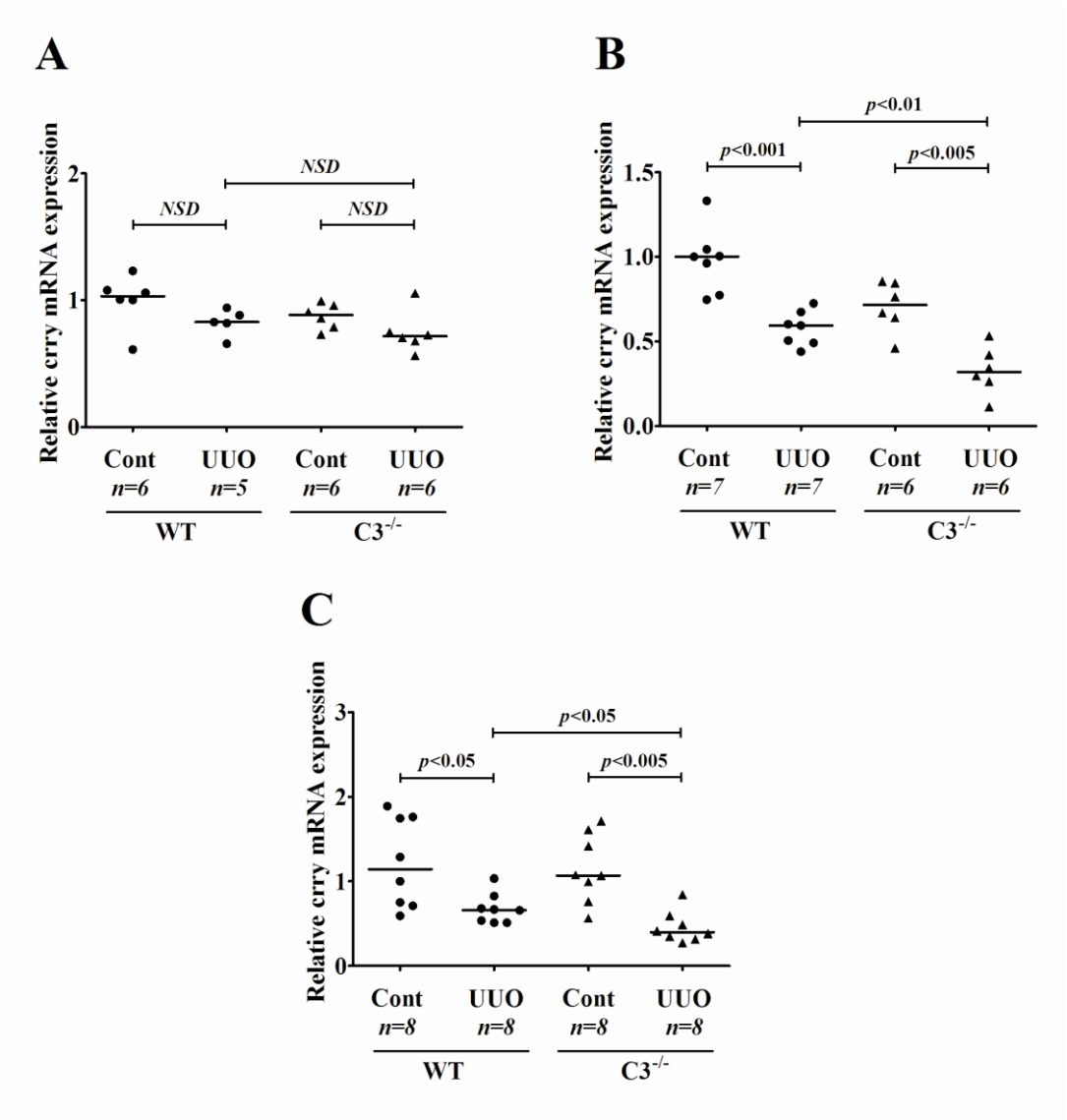

Figure 4.6. Crry gene expression after three and ten days of UUO
Relative crry gene expression in UUO and contralateral renal cortices was determined using rtPCR following three (A), five (B) and ten (C) days of UUO. mRNA expression was normalised to β-actin. Following five and ten days of UUO, Crry expression had decreased in the obstructed renal cortices of WT and $C3^{-/-}$ mice. Bars on graphs represent median values. rtPCR was performed in triplicate for each animal.

However, median DAF1 gene expression in obstructed WT kidneys was significantly higher than that seen for $C3^{-/-}$ kidneys after three days of UUO ($p<0.05$). Following five days of UUO, DAF1 mRNA expression in obstructed WT and $C3^{-/-}$ mouse kidneys was significantly lower compared with contralateral kidneys ($p<0.005$ respectively). Despite the median levels of DAF1 mRNA expression in WT UUO kidneys being more than twice as high than that observed in $C3^{-/-}$ UUO kidneys, this did not reach statistical significance (Figure 4.7B). After ten days, DAF1 gene expression remained significantly lower in the obstructed kidneys of both WT and $C3^{-/-}$ mice compared with their respective contralateral kidneys ($p<0.001$ respectively). Interestingly, DAF1 gene expression in $C3^{-/-}$ UUO kidneys was significantly lower than that observed in WT UUO kidneys ($p<0.05$; Figure 4.7C).

4.5.4 CD59a

CD59a inhibits formation of the MAC by binding to C5b678. This prevents the subsequent binding and polymerisation of C9. Following three days of ureteric obstruction, CD59a gene expression in WT UUO kidneys was significantly lower compared with contralateral kidneys ($p<0.05$). Conversely, there was no difference in CD59a mRNA expression in the renal cortices of obstructed $C3^{-/-}$ mice compared with contralateral renal cortices and CD59a expression was equivalent in the obstructed renal cortices of WT and $C3^{-/-}$ mice (Figure 4.8A). Five days following UUO, CD59a gene expression was significantly lower in obstructed kidneys of WT and $C3^{-/-}$ mice compared to their respective contralateral kidneys (Figure 4.8B).

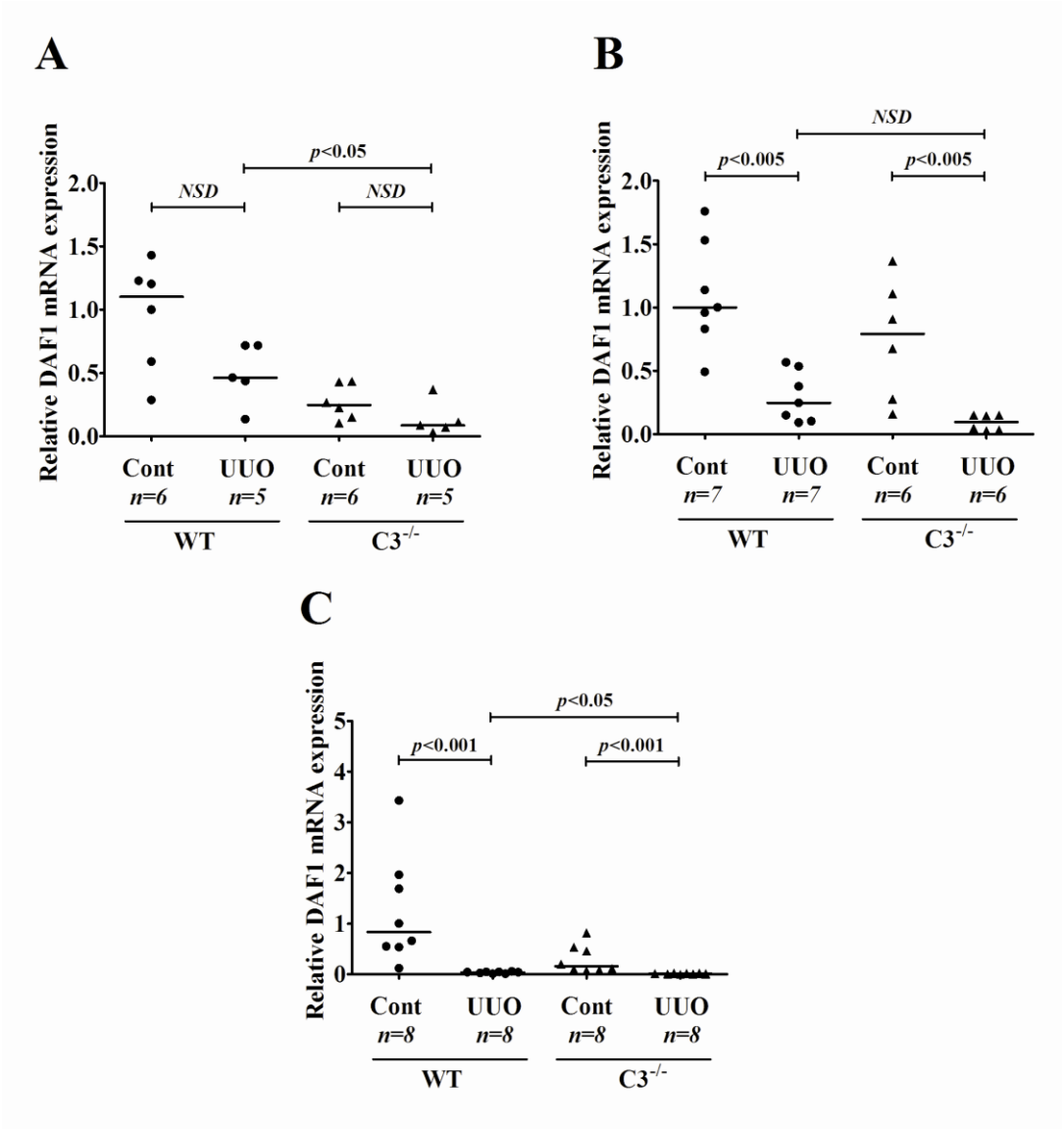

Figure 4.7. DAF1 gene expression after three, five and ten days of UUO
rtPCR was used to measure the relative gene expression of DAF1 mRNA in UUO and contralateral renal cortices after three (A), five (B) and ten (C) days of ureteric obstruction. mRNA expression was normalised to β-actin. After five and ten days of ureteric obstruction, DAF1 gene expression had decreased in the obstructed renal cortices of WT and $C3^{-/-}$ mice. Bars on graphs represent median values. rtPCR was performed in triplicate for each animal.

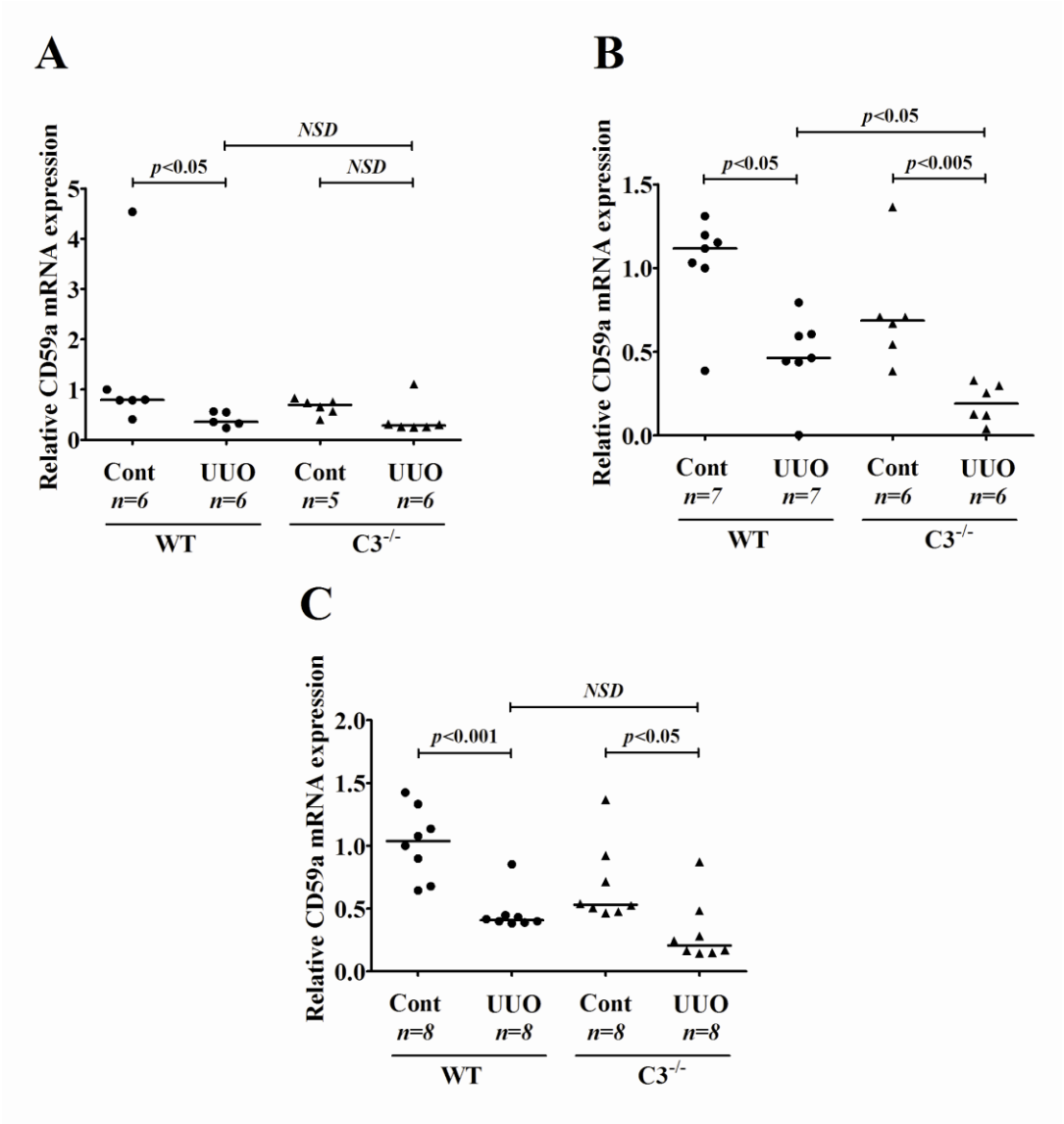

Figure 4.8. CD59a gene expression after three and ten days of UUO
Following three (A), five (B) and ten (C) days of ureteric obstruction, rtPCR was used to determine gene expression of CD59a in UUO and contralateral renal cortices. Gene expression of CD59a was normalised to β-actin. After ureteric obstruction, CD59a mRNA levels decreased in the day five and day ten obstructed renal cortices of WT and $C3^{-/-}$ mice. In addition, basal levels of CD59a in $C3^{-/-}$ contralateral kidneys were lower for all time points. Bars on graphs represent median values. rtPCR was performed in triplicate for each animal.

CD59a mRNA expression in UUO kidneys of $C3^{-/-}$ mice following five days of UUO was significantly lower than that observed in WT UUO kidneys ($p<0.05$). After ten days, CD59a gene expression remained lower in obstructed WT and $C3^{-/-}$ mouse kidneys (Figure 4.8C).

4.5.5 Factor B

Factor B (FB) is cleaved by FD to form Bb, the catalytic subunit which then associates with C3b to form the alternative pathway C3 convertase. After three days of ureteric obstruction, FB gene expression levels were comparable to contralateral kidneys in WT and $C3^{-/-}$ mice (Figure 4.9A). Five days post-UUO, median FB mRNA expression was significantly reduced in obstructed WT and $C3^{-/-}$ mouse kidneys compared with contralateral kidneys ($p<0.005$; Figure 4.9B). Interestingly, FB gene expression in $C3^{-/-}$ UUO kidneys following five days of UUO was significantly lower than that observed in WT UUO kidneys ($p<0.05$). After ten days of UUO FB gene expression was equivalent in obstructed kidneys of WT and $C3^{-/-}$ mice, but remained significantly lower compared to contralateral kidneys ($p<0.01$ and $p<0.001$ respectively; Figure 4.9C).

4.5.6 Factor H

Factor H (FH) regulates alternative complement activation by directing complement activation towards invading pathogens and away from host cells.

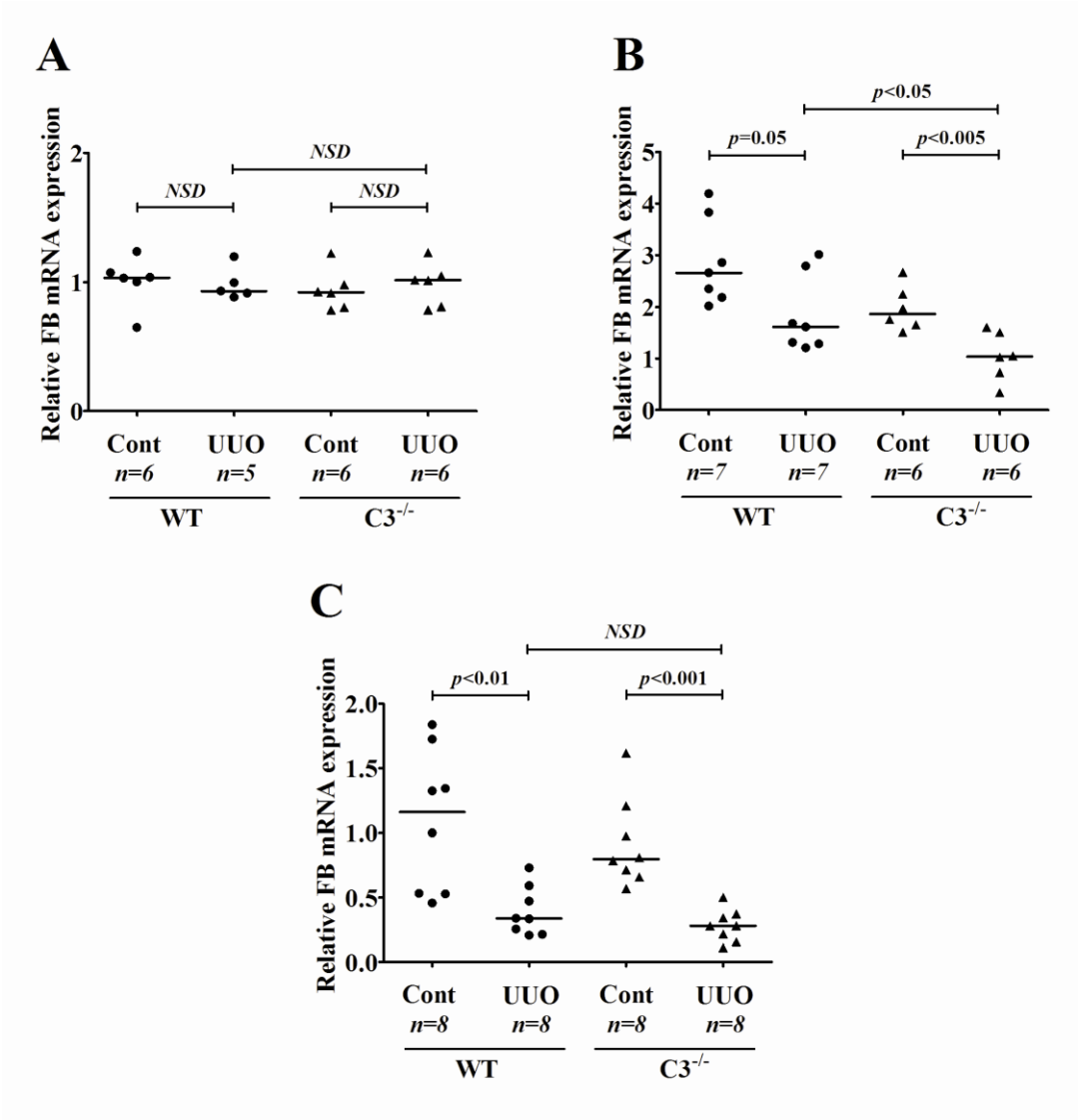

Figure 4.9. FB gene expression after three, five and ten days of UUO
rtPCR was used to measure FB gene expression in UUO and contralateral renal cortices three (A), five (B) and ten (C) days-post UUO. mRNA expression was normalised to β-actin. Following ureteric obstruction, FB mRNA expression gradually decreased in obstructed renal cortices of WT and $C3^{-/-}$ mice after three days of ureteric obstruction. Bars on graphs represent median values. rtPCR was performed in triplicate for each animal.

It also possesses cofactor activity for FI mediated C3b cleavage and accelerates decay of pre-formed C3bBb. There were no significant changes FH mRNA expression in the kidneys of obstructed WT and $C3^{-/-}$ mice after three days of ureteric obstruction (Figure 4.10A), however, after five days of UUO, FH gene expression in the obstructed kidneys of WT mice was significantly higher compared to unaffected WT kidneys and obstructed $C3^{-/-}$ mouse kidneys ($p<0.05$ and $p<0.01$ respectively; Figure 4.10B). FH mRNA expression in obstructed and contralateral $C3^{-/-}$ mouse kidneys was equivalent at day five UUO. Following ten days of UUO, FH gene expression in WT mice remained higher compared to WT contralateral kidneys ($p<0.001$). Interestingly, median FH mRNA expression in day ten obstructed $C3^{-/-}$ mouse renal cortices was significantly higher compared to contralateral $C3^{-/-}$ kidneys ($p<0.05$), but remained significantly lower compared to WT UUO kidneys ($p<0.001$; Figure 4.10C).

4.5.7 Factor I

Factor I regulates classical and alternative complement activation by cleaving C3b and C4b. In WT mice, FI expression was significantly higher in obstructed compared to contralateral kidneys after three and five days of UUO ($p<0.005$ and $p<0.001$ respectively; Figure 4.11A and B respectively). Although also elevated in obstructed $C3^{-/-}$ kidneys, this was only significant at day ten ($p<0.05$; Figure 4.11C). FI expression was significantly higher in obstructed WT kidneys compared to $C3^{-/-}$ kidneys throughout UUO.

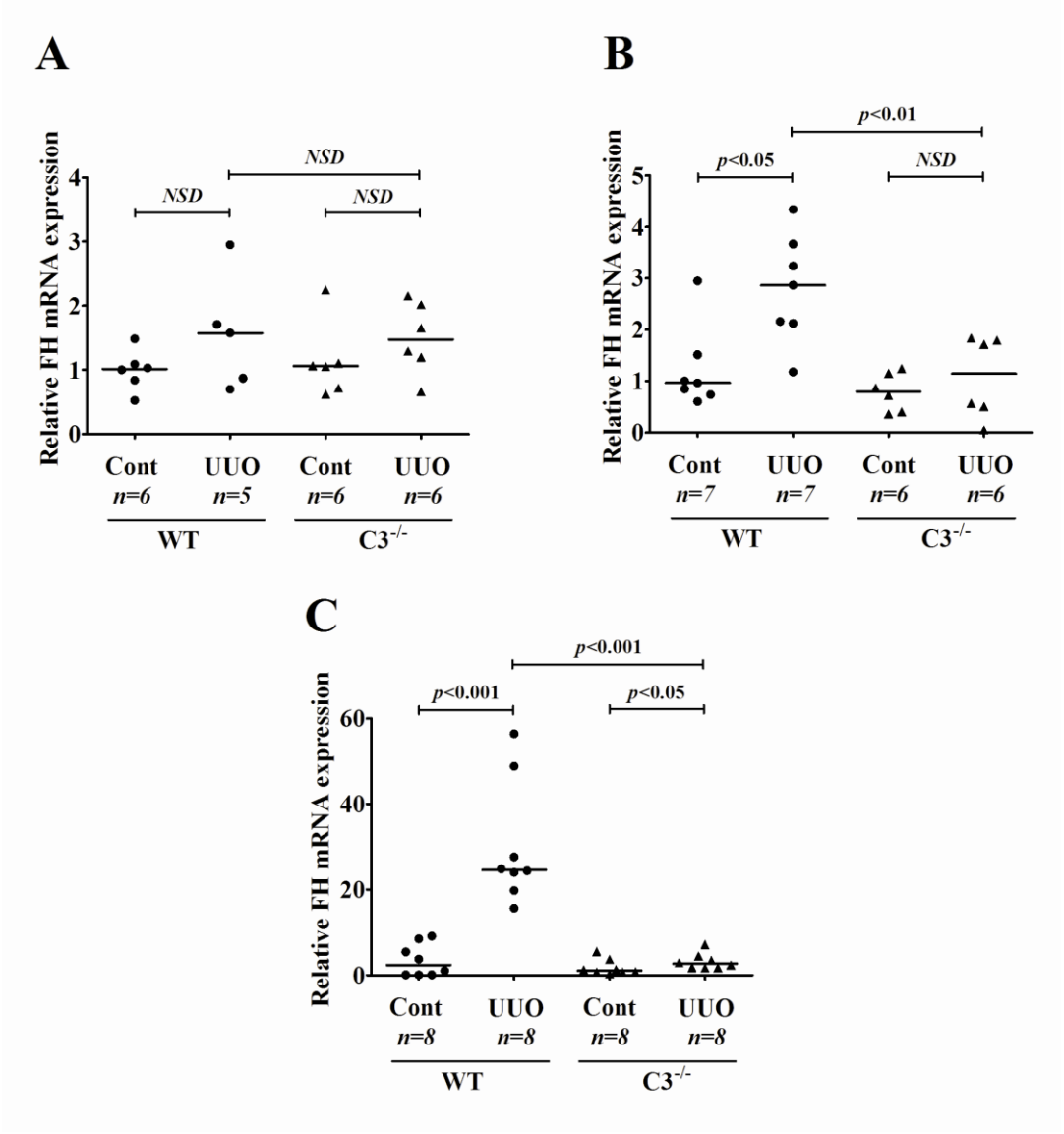

Figure 4.10 FH gene expression after three, five and ten days of UUO
Relative FH gene expression in UUO and contralateral renal cortices was measured by rtPCR three (A), five (B) and ten (C) days following ureteric obstruction. mRNA expression was normalised to β-actin. During the latter stages of ureteric obstruction, FH mRNA levels were only elevated in obstructed renal cortices of WT mice. Bars on graphs represent median values. rtPCR was performed in triplicate for each animal. rtPCR was performed in triplicate for each animal.

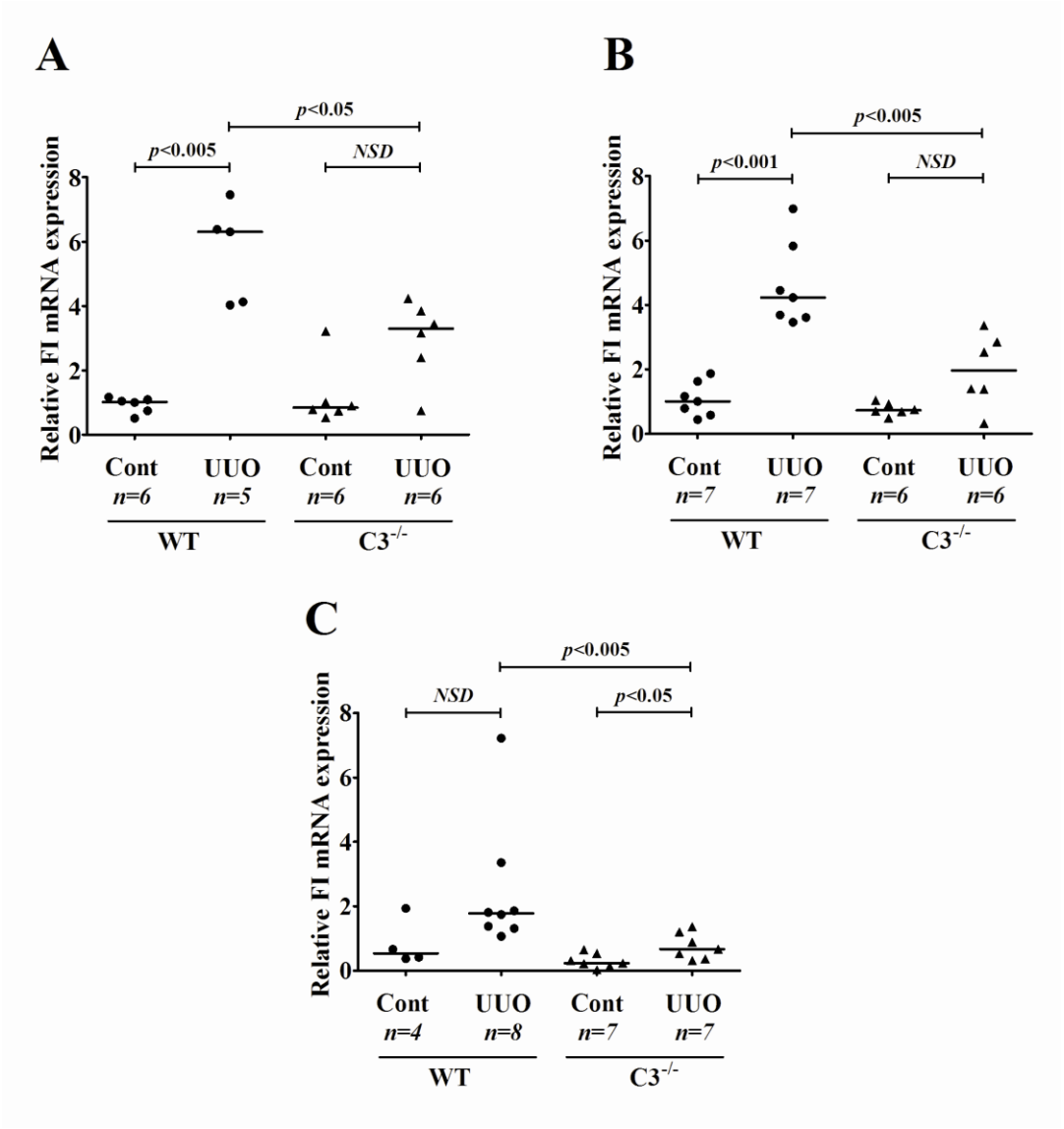

Figure 4.11. FI gene expression after three, five and ten days of UUO
Relative FI mRNA expression in UUO and contralateral renal cortices was measured by rtPCR following three (A), five (B) and ten (C) days of ureteric obstruction. Gene expression was normalised to β-actin. During the early stages of ureteric obstruction, FI gene expression was elevated in obstructed renal cortices of WT and $C3^{-/-}$ mice, but gradually declined during the course of UUO. Bars on graphs represent median values. rtPCR was performed in triplicate for each animal.

4.6 Complement activation in BUMPT cells

Chapters three and four of this thesis have demonstrated that complement is involved during the progression of UUO and that tubular epithelial cells appear to be the primary site for complement activation in the kidney. Since PTECs are known to synthesis C3, they are a potential source of complement in this disease model. Following on from these observations, the next part of this study sought to establish an *in vitro* model of complement activation in an established mouse PTEC cell line which could then be used to study the mechanisms of complement activation and assess the affect of knock down strategies on C3 gene expression. Complement activation in mouse BUMPT cells was stimulated using LPS, a known activator of the innate immune response. To establish optimum up-regulation of C3 mRNA, three different concentrations of LPS were tested at three different time points.

The amount of C3 protein produced by BUMPT cells post LPS stimulation was measured by ELISA. The concentration of C3 protein present in supernatant samples taken from BUMPT cells stimulated with 10, 100 and 1000ng/ml LPS for 12 hours was significantly elevated to mean values of $0.08\pm6x10^{-3}$µg/ml ($p<0.005$), $0.07\pm5x10^{-3}$µg/ml ($p<0.001$) and 0.08±0.02 µg/ml ($p<0.001$) respectively compared with a mean of $0.05\pm2x10^{-3}$µg/ml in unstimulated cells (Figure 4.12A). After 24 hours stimulation with 10 and 1000ng/ml LPS, the concentration of C3 in cell supernatents had significantly increased to mean values of 0.3±0.04µg/ml and 0.3±0.02µg/ml respectively compared with a mean value of 0.2±0.02µg/ml in un-stimulated BUMPT cells ($p<0.05$ respectively). C3 concentration in the supernatents of cells stimulated with 100ng/ml LPS was not significantly elevated (0.3±0.03µg/ml) compared to unstimulated cells (Figure 4.12B).

The concentration of C3 in BUMPT cell supernatents continued to increase significantly to mean values of 0.4±0.05, 0.4±0.02 and 0.4±0.04µg/ml following 48 hours LPS stimulation at concentrations of 10, 100 and 1000ng/ml respectively ($p<0.005$, $p<0.005$ and $p<0.01$ respectively) compared with a mean of 0.3±0.02µg/ml in unstimulated BUMPT cells (Figure 4.12C). C3 was also detected in the supernatants of unstimulated BUMPT cells that had been serum-starved. The concentration of C3 protein present in supernatant samples was determined by extrapolation from a standard curve of known C3 concentration (Figure 4.12D).

Up-regulation of C3 gene expression by BUMPT cells following stimulation with LPS was measured by rtPCR and normalised to the housekeeping gene β-actin. C3 gene expression in BUMPT cells stimulated for 12 hours with 10, 100 and 1000ng/ml LPS had significantly increased to mean values of 1.1±0.07 ($p<0.05$), 1.7±0.1 ($p<0.001$) and 1.8±0.2 ($p<0.001$) respectively compared with a mean of 0.98±0.02 in un-stimulated cells (Figure 4.13A). After 24 hours stimulation with 100 and 1000ng/ml LPS, C3 mRNA expression had significantly increased to mean values of 2.2±0.23 and 1.6±0.04 respectively compared with a mean value of 0.99±0.08 in un-stimulated BUMPT cells ($p<0.001$ and $p<0.005$ respectively).

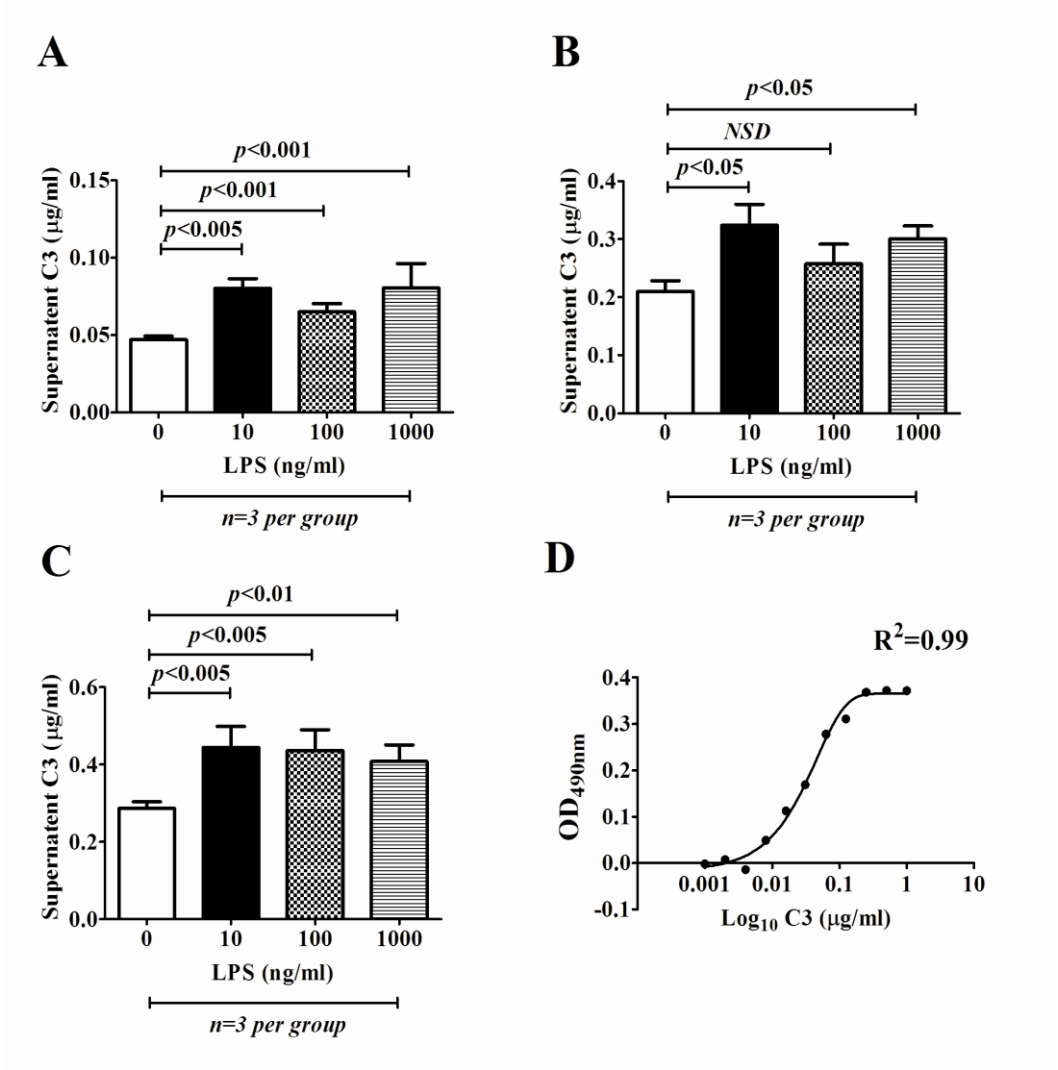

Figure 4.12. LPS-stimulated production of C3 by BUMPT cells
An ELISA assay was used to measure the concentration of C3 in supernatant taken from BUMPT cells that had been stimulated with LPS for 12 (A), 24 (B) and 48 (C) hours. Calculation of supernatent C3 concentrations was carried out using a standard curve of known C3 concentrations (D). Bars on graphs show mean values, error bars depict standard error (SEM).

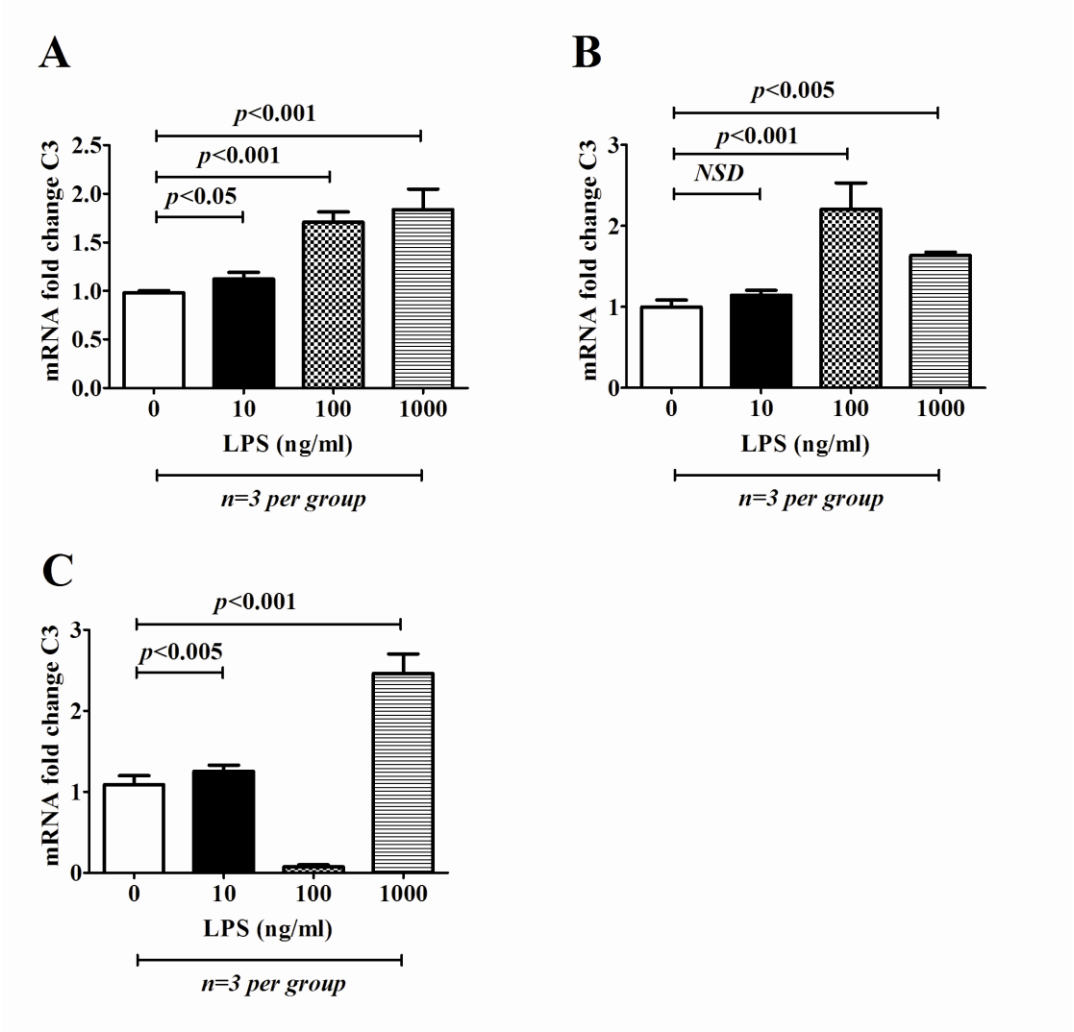

Figure 4.13. C3 mRNA expression in LPS-stimulated BUMPT cells
rtPCR was used to measure relative C3 gene expression in BUMPT cells stimulated with different concentrations of LPS for 12 (A), 24 (B) and 48 (C) hours. Coloured bars on graphs show mean values, error bars depict standard error.

C3 gene expression in cells stimulated with 10ng/ml LPS remained unchanged (Figure 4.13B). C3 mRNA expression in BUMPT cells continued to increase significantly to mean values of 1.3±0.08 and 2.5±0.2 following 48 hours LPS stimulation at concentrations of 10 and 1000ng/ml respectively ($p<0.005$ and $p<0.001$ respectively) compared with a mean of 1.1±0.11 in un-stimulated BUMPT cells (Figure 4.13C). After 48 hours of exposure to 100ng/ml LPS, C3 gene expression in BUMPT cells was not significantly up-regulated compared with un-stimulated cells.

Activation of complement following stimulation of BUMPT cells with LPS was determined by measuring the concentration of C3a protein present in the supernatant using an ELISA. After 12 hours stimulation with 10 and 100ng/ml LPS, the concentration of C3a in cell supernatents had increased to mean values of 161.8±73.8 and 96.5±19.4 respectively compared with a mean of 61.9±13.1ng/ml recorded in un-stimulated cells (Figure 4.14A). The mean C3a concentration present in cell supernatents exposed to 1000ng/ml LPS for 12 hours was lower than that detected for unstimlated cells (41.3±39.8ng/ml). C3a concentration in the supernatents of cells stimulated with 10ng/ml LPS was significantly elevated compared to unstimulated cells ($p<0.05$).

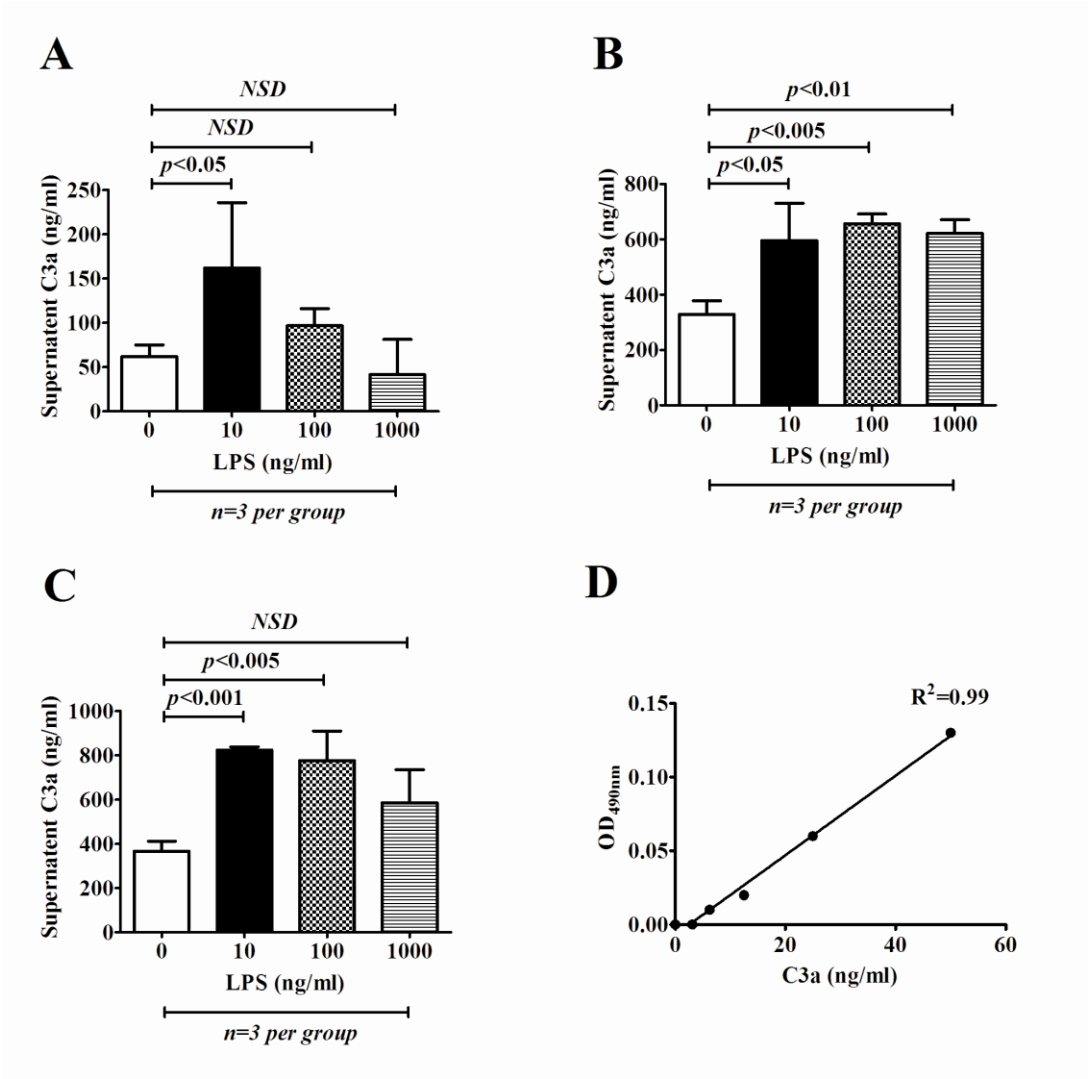

Figure 4.14. Production of C3a by BUMPT cells during LPS stimulation
Supernatent collected from LPS-stimulated BUMPT cells was analysed using by ELISA for the presence of C3a, a marker of complement activation. Concentration of C3a in supernatant taken from BUMPT cells stimulated with LPS for 12 (A), 24 (B) and 48 (C) hours. Calculation of supernatent C3a concentrations was carried out using a standard curve derived from known C3a concentrations (D). Coloured bars on graphs show mean values, error bars depict standard error (SEM).

The concentration of C3a present in the supernatants taken from cells stimulated with 10, 100 and 1000ng/ml LPS for 24 hours had significantly increased to mean values of 595.1±135.3ng/ml (p<0.05), 657.1±34.6ng/ml (p<0.005) and 621.7±48.6ng/ml (p<0.01) respectively compared with a mean of 328.5±49.15ng/ml in unstimulated cells (Figure 4.14B). Compared with the concentration of C3a in the supernatents of unstimulated cells (mean value of 366.1±45.6ng/ml), the concentration of C3a in cell supernatents had continued to increase significantly to mean values of 824.5±13.5 and 775.8±134.2ng/ml following 48 hours LPS stimulation at concentrations of 10 and 100ng/ml (p<0.001 and p<0.005 respectively). The concentration of C3a in cell supernatents stimulated with 1000ng/ml LPS for 48 hours had also increased (585.4±149.6), though this was not significant compared to unstimulated cells (Figure 4.14C). Interestingly, in the absence of FBS, C3a was detected in supernatants taken from 24 and 48 hour unstimulated BUMPT cells, suggesting that BUMPT cells are producing C3 and activating complement under basal conditions (Figure 4.14A-C). The concentration of C3a present in cell supernatents was calculated from a standard curve constructed using known concentrations of mouse C3a (Figure 4.14D).

4.7 Discussion

Following on from the previous chapter, this chapter sought to further explore the activity and distribution of C3 on a protein and molecular level during the progression of renal disease following ureteric obstruction in WT mice.

In the obstructed kidneys of WT mice, urinary C3a was significantly elevated indicating complement activation. The mechanism by which complement becomes activated under these circumstances is unclear. There is 'tick over' of the alternative complement pathway at the apical membrane of tubular epithelial cells (Zipfel, 2006) and it is plausible that injury to the tubular epithelium could cause up-regulation of complement protein synthesis by tubular epithelial cells, as reported previously (Timmerman et al., 1996; Ichida et al., 1994; Welch et al., 1993). This could be a major source of the complement activation protein C3a detected in urine taken from obstructed WT kidneys. Despite the presence of C3a, C5a was not present in urine taken from the renal pelvis of obstructed WT mice. A study by Boor *et al* demonstrated that C5aR was expressed on the apical and lateral membranes of tubular epithelial cells during UUO and that subsequent treatment with a C5aR antagonist ameliorated renal scarring. (Boor et al., 2007), suggesting a key role for C5a in the generation of disease in this animal model.

It is unclear why C5a was not detected in urine taken from obstructed kidneys. One possibility is that it may be below the level of detection (12.5ng/ml) in the assay. Alternatively, it may only be produced on the basolateral surface of cells or within the interstitium and would therefore not be present in urine. Another possibility is that C5a protein is not stable in the urine and is degraded. With this in mind, it would be interesting to study UUO in the absence of C5aR in future studies to determine the role of C5a signalling during the progression of renal fibrosis.

In other models of renal disease the presence of complement components in mouse urine has been demonstrated previously (Hsu and Couser, 2003). In the current study it would be interesting to investigate whether other complement components are present in mouse urine taken from obstructed kidneys. This may help to clarify the nature of complement activation during UUO.

Consistent with previous findings (Sheerin et al., 2008), C3 protein was present in abundance around the basolateral membrane of tubules in WT contralateral kidneys. After three days of ureteric obstruction less C3 was detected around tubules in WT mice and by day ten C3 staining was almost absent from tubular basolateral membranes. There did appear to be diffuse staining throughout the interstitium after ten days of UUO, but it was difficult to define the exact location of C3 protein at this time since renal morphology was markedly affected by persistent inflammation and fibrosis. Diffuse C3 staining in obstructed WT kidneys may be due to degradation of membrane bound C3 by proteases produced to allow ECM re-modelling. These observations contrast that of previous findings which reported an increase in tubular basal C3 protein expression during proteinuria (Sheerin et al., 2008). Similarly, in a rat model of protein overload, C3 is reported to be present at the apical membrane of tubular epithelial cells (Nangaku, 2004). C3 was not detected in obstructed or contralateral kidneys of $C3^{-/-}$ mice.

In this study, C3 gene expression was significantly up-regulated in WT renal cortices after three, five and ten days of UUO. In day three WT UUO kidneys, C3 mRNA was also detected by *in situ* hybridisation and was found to be present in some (but not all) renal tubules. This finding suggests that tubular epithelial cells are the main site of complement up-regulation during the early phases of obstructive nephropathy.

C3 gene expression was at its highest at day ten UUO and results from the previous chapter showed that lymphocytes and macrophages were present at this stage. It would be interesting to look at C3 mRNA distribution in day five and day ten WT UUO kidneys using *in situ* hybridisation to see if tubular epithelial cells remained the primary source of complement production as UUO progressed.

The observation that some renal tubules expressed C3 mRNA whilst others did not would suggest that only a specific portion of the nephron is up-regulating C3 during UUO. One potential site for C3 production could be the proximal tubule. Unfortunately immunostaining on *in situ* sections with the lectin from Lotus *tetragonobulus* (specific for the brush boarder of the proximal tubule) was unsuccessful in this study. In future work, other markers of the proximal tubule such as aquaporin-1 or glucose transporters could be identified by immunochemistry in obstructed kidneys following *in situ* hybridisation for C3 mRNA.

In mice crry is an important membrane bound regulator of complement activation. It prevents C3b deposition resulting from both alternative and classical complement activation and is critical for preventing autologous complement activation. In the unaffected kidneys of WT mice, crry is present at the tubular basolateral membrane. However during the course of UUO, a shift from membrane to cytoplasmic staining of crry occurs and crry gene expression declines simultaneously. Other studies have reported a similar loss of surface crry expression during disease progression (Thurman et al., 2006; Li et al., 1993). After three days of ureteric obstruction in WT and $C3^{-/-}$ mice, there were no changes in crry gene expression compared with unaffected kidneys. However at day five and day ten UUO, crry mRNA expression was significantly reduced in the obstructed kidneys of WT and $C3^{-/-}$ mice.

In comparison to obstructed WT mice, crry gene expression in obstructed $C3^{-/-}$ mouse kidneys was significantly lower. Crry is ubiquitously expressed in mice and is thought to be analogous to another complement regulator, membrane cofactor protein (CD46; (Foley et al., 1993)). In response to the altered haemodynamics ensuing from ureteric obstruction, blood flow to the kidney is restricted during the early stages of UUO, causing progressive ischaemia. In the mouse model of renal IRI, Li and co-workers reported that basolateral crry expression was disrupted during ischaemia and that the subsequent loss of surface crry permitted activation of the alternative complement pathway on tubular epithelial cells (Li et al., 1993). Another reason for declining crry could be due to the ECM re-modelling occurring within the cortical interstitium which may influence the expression of proteins at the basolateral membrane. In this study, crry gene expression was significantly reduced in obstructed kidneys. This could allow for increased complement activation which may in part explain the damage associated with complement activation described in chapter three.

After ten days of UUO, DAF1 gene expression was almost undetectable in obstructed WT and $C3^{-/-}$ mouse kidneys compared with respective contralateral kidneys. Compared with obstructed kidneys from WT mice, DAF1 mRNA was significantly lower in obstructed $C3^{-/-}$ mouse kidneys. The changes in gene expression observed for DAF1 follow a similar pattern to that of crry. DAF1 protects host cells from C3b and C5b-9 deposition on cell surfaces and inhibits formation of the C5 convertase, thus preventing MAC formation.

In mice, there are two DAF isoforms, DAF1 and DAF2. Of these, DAF1 is present in human and rat glomeruli and has been shown to protect against proteinuric renal injury during adriamycin nephropathy (Bao et al., 2002).

During the early stages of NTS nephropathy, DAF1 is critical in preventing induction of complement-mediated podocyte injury (Lin et al., 2002). In the absence of DAF1, proteinuria and glomerular C5b-9 deposition increase following induction of NTS nephritis (Lin et al., 2004). The present study has shown that, DAF1 and crry are both reduced in obstructed WT and $C3^{-/-}$ kidneys after ten days of ureteric obstruction. It would be interesting to see what the normal distribution of DAF1 is in mouse renal tissues and subsequently how this changes following ureteric obstruction. In this study, the role of DAF1 during UUO is unclear. Both crry and DAF1 are membrane bound regulators of complement activation and appear to behave similarly during UUO. This would increase the potential for complement activation and therefore tissue injury.

CD59a gene expression was reduced significantly in obstructed kidneys from WT and $C3^{-/-}$ mice. Generally, expression was lower in $C3^{-/-}$ mice compared to WT mice. In mice, two isoforms of CD59 exist, CD59a and CD59b (found only in testes). CD59a regulates the terminal complement pathway. Binding of CD59a to C5b678 prevents binding and polymerising of C9, inhibiting the formation of the MAC. Compared to WT mice, CD59a deficient mice have more severe PMN cell infiltration, greater tubular atrophy and increased deposition of C9 during renal IRI (Turnberg et al., 2006; Turnberg et al., 2004). Similarly, CD59a deficient mice had elevated glomerular deposition of C9 and increased expression of α-SMA during adriamycin nephropathy (Turnberg et al., 2006).

These studies suggest that CD59 restricts disease progression by preventing MAC formation. The role of CD59a during UUO has not been established. However, it would be interesting to see if urinary C5b-9 and renal C9 deposition increased in obstructed kidneys of WT and $C3^{-/-}$ mice at the same time as CD59a was in decline.

In the present study, the reason for a decline in membrane-bound regulators of complement is not clear. One possibility could be that a down regulation of membrane complement regulators on apoptotic cells allows increased deposition of C3b on apoptotic cell surfaces, making them a target for infiltrating macrophages.

At day five and day ten, FB had significantly decreased in the renal cortices of obstructed WT and $C3^{-/-}$ kidneys and was lower in the absence of C3. FB binds to surface-bound C3b to form C3bB, which is then cleaved by FD to form C3bBb, the catalytic subunit of the alternative pathway C3 convertase. The presence of Bb in urine is an indicator of alternative pathway activation and Bb is known to increase in patients with chronic renal failure however, this study did not measure urinary Bb. Future work addressing the complement activation pathway involved during UUO could look at measuring alternative and classical pathway components present in urine taken from the renal pelvis of obstructed kidneys. The alternative complement pathway is an important in mediator of renal injury characteristic of IRI. In a mouse model of renal IRI, FB deficient mice had fewer infiltrating neutrophils, less severe morphological injury and no C3/C9 staining compared with WT mice. During the later stages of UUO in this study, FB was equivalent in obstructed WT and $C3^{-/-}$ mouse kidneys (Lien et al., 2003; Thurman et al., 2003).

FH accelerates the dissociation of the C3 convertase during alternative complement pathway activation and also binds to glycosaminoglycans on host cell surfaces, thus protecting host cells by directing complement activation towards pathogens. One reason for the increase in FH expression in obstructed WT mouse kidneys at day five and day ten UUO could be to regulate complement activation by intrinsic renal cells and protect those cells from complement-mediated injury.

This is partly supported by a recent study in which Renner and co-workers demonstrated that binding of FH to tubular epithelial cells limited interstitial complement activation during renal IRI (Renner et al., 2011). The results from the first chapter of this thesis demonstrated that $F4/80^+$ cells are present in kidney cortices after five days of UUO and that T cells and $F4/80^+$ cells are present by day ten. Macrophages and T cells could be one source of increased FH at day five and day ten, since both are capable of producing significant amounts of complement. In this study, FH gene expression had also increased in the contralateral kidneys of WT mice ten days post-UUO. The reason for this in not clear, perhaps renal synthesis of C3 significantly elevated circulating C3 and triggered the activation of protective mechanisms in other organs to prevent complement activation on host cells.

FI promotes cleavage of cell bound and fluid phase C3b and C4b during alternative and classical complement activation respectively, reducing C3/C5 convertase activity and MAC formation. In mice, FI cleaves crry-bound C3b and C4b. FH also has co-factor activity for FI-mediated C3b cleavage during alternative pathway activation. An early increased in FI mRNA during UUO, suggests an attempt to regulate complement activity in WT mice, however FI gene expression declined during the course of UUO and was no longer significantly elevated in WT mice by day ten. In contrast to this, FH expression increased during the course of UUO, the reason for this is unclear.

LPS is an endotoxin derived from the outer cell wall of gram negative bacteria and is reported to activate the alternative complement pathway and induce the activation of several cytokines via toll-like receptor signalling (Fu et al., 2006; Kusner et al., 1991).

Following on from earlier work in this chapter which had demonstrated complement activation during ureteric obstruction, BUMPT cells were stimulated for different lengths of time with varying concentrations of LPS to induce synthesis of complement. Complement activation was assessed by measuring C3a protein in cell supernatants. The amount of C3a present increased in a time-dependent manner. Similarly, the amount of C3 protein in LPS-stimulated cell supernatents increased over time. C3 and C3a were also detected in the cell supernatents taken from unstimulated cells, suggesting that BUMPT cells are capable of producing and activating complement in the absence of serum and LPS. C3 mRNA was significantly up-regulated in BUMPT cells following stimulation with LPS. Higher concentrations of LPS yielded a greater fold change in C3 gene expression.

Up-regulation of C3 gene expression and production and activation of complement by BUMPT cells demonstrates a good *in vitro* model of complement activation which will be used to select antisense oligonucleotides capable of knocking down C3 mRNA expression *in vitro* in future work. When knock down of C3 gene expression *in vitro* has been achieved, the successful oligonucleotide will be modified for *in vivo* applications and tested during UUO.

The findings of this chapter support one hypothesis that local C3 production may be a contributing factor during the progression of fibrosis and inflammation in the mouse model of UUO. Work following on from this study will investigate C3 mRNA distribution at day five and day ten UUO and continue to focus on C3 as a target for therapeutic intervention. Extensive work is still required to establish which complement pathway is involved during the progression of UUO, though it is plausible that the alternative pathway is the most likely.

A key component for alternative pathway activation is FD, however the primers used to detect FD gene expression in this study did not detect FD mRNA taken from quiescent liver stellate cells, a positive control for FD expression. One way to determine alternative pathway activity in this disease model would be to induce UUO in mice lacking FB.

5 The role of nfκb1 in acute and chronic renal injury

5.1 Introduction

The first two results chapters of this thesis have already illustrated a role for complement in a model of unilateral obstructive nephropathy. The concluding part of this study sought to investigate the contribution of transcription factor nfκb1 towards the progression of acute and chronic renal diseases. The two animal models of renal disease selected for the final part of this study were UUO and NTS nephritis. They differ with respect to the factors driving disease progression; NTS nephritis is a complement-mediated model of acute renal nephropathy characterised by an early influx of neutrophils. Conversely, UUO is driven by an ANG-II mediated alteration to renal haemodynamics and wide-spread local complement activation, with progression towards wide-spread interstitial fibrosis and tubular atrophy and macrophage and T cell accumulation.

5.2 Scoring of histological injury in WT and *nfκb1*$^{-/-}$ mice following UUO

To investigate the effect of nfκb1 deficiency in chronic renal disease, periodic acid Schiff's histology was used to visualise interstitial expansion and tubular dilatation in renal tissues post-ureteric obstruction. Following three days of UUO some renal tubules were dilated and their epithelial cells had flattened and started to lose their brush boarder (Figure 5.1A and B). Unaffected (contralateral) kidneys in WT and *nfκb1*$^{-/-}$ mice showed normal renal morphology, with no interstitial expansion or tubular dilatation (Figure 5.1C).

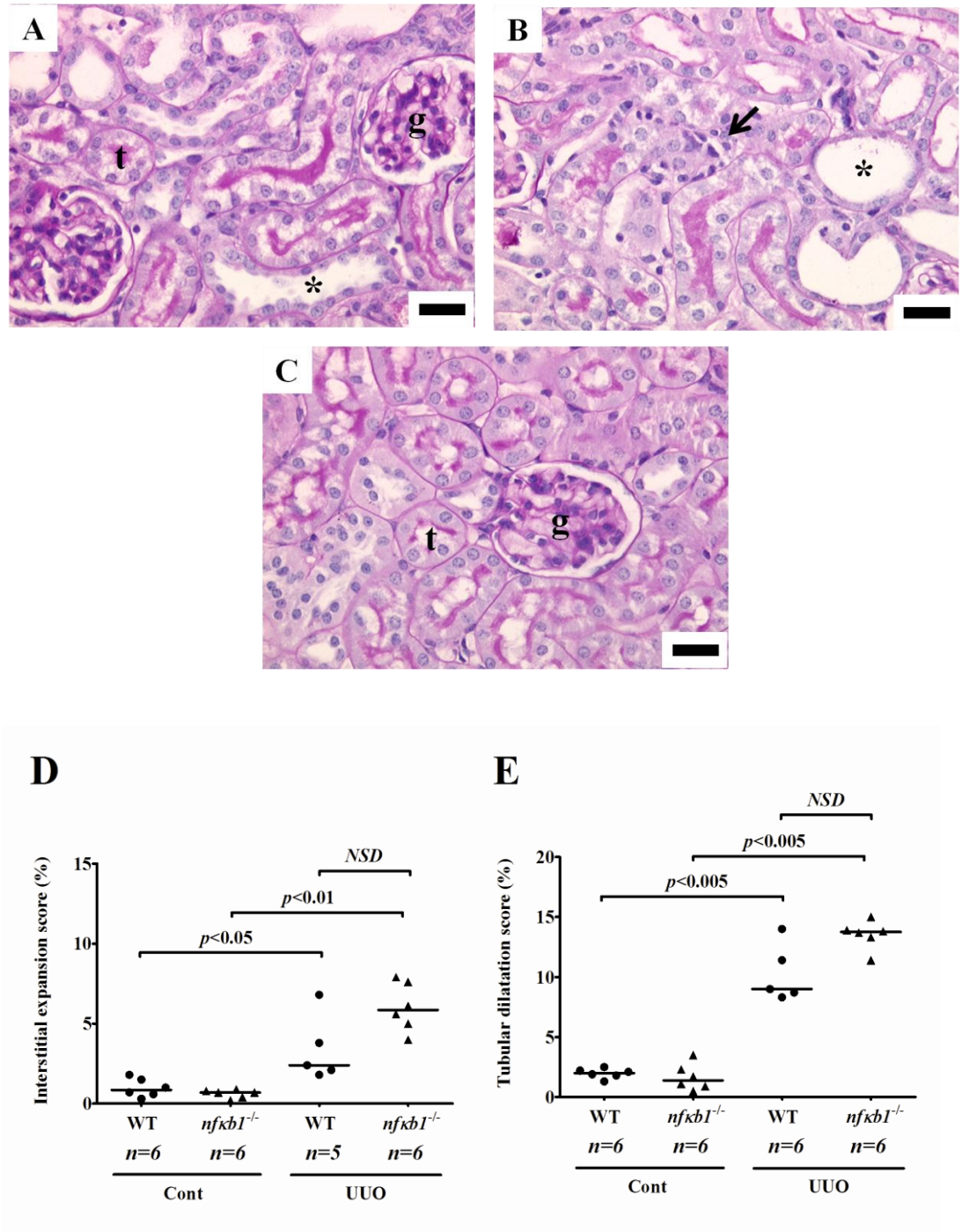

Figure 5.1. Histological injury at day three UUO
PAS-stained WT (A) and *nfκb1*$^{-/-}$ (B) renal cortices following three days of UUO. Contralateral kidneys showed normal renal morphology in WT and *nfκb1*$^{-/-}$ mice (C). Arrows highlight areas of interstitial expansion. Asterisks show dilated tubules. 't' represents a tubule and 'g' identifies a glomerulus. A grid-based counting method was used to score interstitial expansion (D) and tubular dilatation (E). Scale bars on A-C measure 20µm and bars on graphs D and E represent median values.

After three days of ureteric obstruction, median interstitial volume had significantly increased in WT and *nfκb1*$^{-/-}$ UUO kidneys compared with contralateral kidneys (2.40% vs. 0.85% and 5.85% vs. 0.70%; $p<0.05$ and $p<0.01$ respectively). Similarly, median interstitial expansion was significantly elevated in obstructed *nfκb1*$^{-/-}$ renal cortices compared to *nfκb1*$^{-/-}$ renal cortices from contralateral kidneys. Although the interstitial compartment of obstructed *nfκb1*$^{-/-}$ animals had expanded more than that of their WT counterparts, this difference was not statistically significant (Figure 5.1D). Compared with contralateral kidneys, tubular dilatation had increased significantly in day three obstructed WT and *nfκb1*$^{-/-}$ kidneys ($p<0.005$ for both). The extent of tubular dilatation was equivalent for both UUO groups (Figure 5.1E). Following ten days of UUO, interstitial expansion and tubular dilatation had continued to develop in the renal cortices of obstructed WT and *nfκb1*$^{-/-}$ mice (Figure 5.2A and B). WT and *nfκb1*$^{-/-}$ contralateral kidneys were normal at this time (Figure 5.2C). Compared with contralateral renal cortices, interstitial expansion had increased significantly in obstructed WT and *nfκb1*$^{-/-}$ groups ($p<0.001$ and $p<0.005$). Expansion of the cortical interstitial compartments of obstructed WT and *nfκb1*$^{-/-}$ kidneys remained equivalent (Figure 5.2D). Median tubular dilation continued to increase in WT and *nfκb1*$^{-/-}$ UUO mice compared with contralateral kidneys ($p<0.001$ and $p<0.005$). As with interstitial expansion, tubular dilatation in obstructed WT and *nfκb1*$^{-/-}$ groups was equivalent (Figure 5.2E).

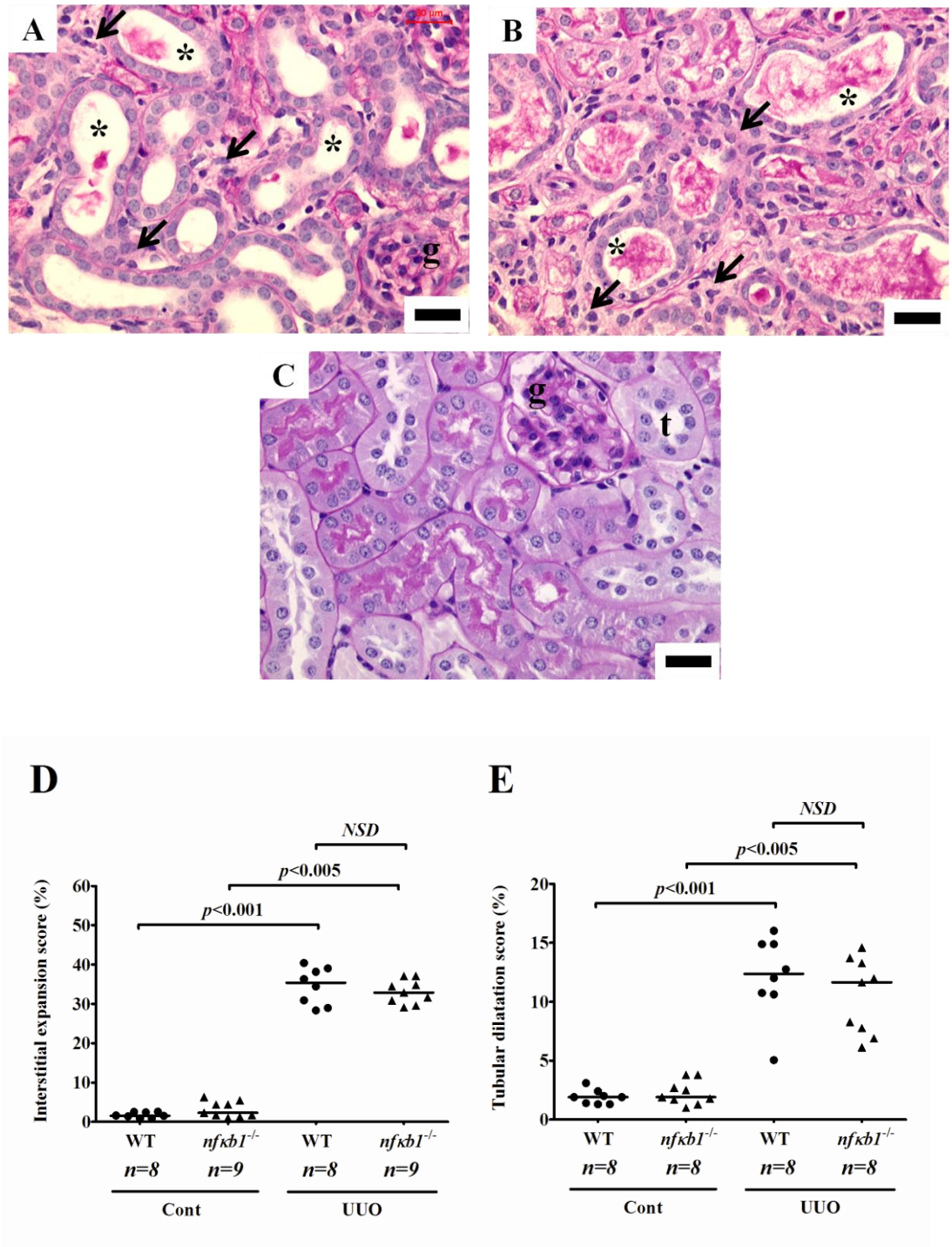

Figure 5.2. Histological injury at day ten UUO
Renal cortices of day ten WT UUO (A) and *nfκb1*$^{-/-}$ UUO (B) mice. A representative image of an unaffected contralateral kidney (C). Arrows show large and distinct areas of expanded interstitium. Asterisks high-light severely dilated tubules. 'g' identifies a glomerulus. 't' illustrates an intact tubule. Scoring of interstitial expansion (D) and tubular dilatation (E), was carried out using a grid-based counting method. Scale bars on A-C measure 20µm and bars on graphs represent median values.

5.3 Immunohistochemical analyses of infiltrating cells and collagen deposition during UUO

Infiltrating immune cells and extracellular matrix components present in tissues day ten post-ureteric obstruction were detected by IHC staining. Following ten days of ureteric obstruction, $CD4^+$ and $CD8^+$ T cell infiltrate counts were significantly elevated in WT ($p<0.001$ for both groups; Figure 5.3A and Figure 5.4A) and *nfκb1*$^{-/-}$ renal tissues ($p<0.001$ for both groups; Figure 5.3B and Figure 5.4B respectively). No $CD4^+$ and $CD8^+$ T cells were detected in unaffected kidneys (Figure 5.3C and Figure 5.4C respectively). The median number of infiltrating $CD4^+$ and $CD8^+$ cells was 11.45 and 4.65 per HPF and 14.10 and 3.10 per HPF in obstructed WT and *nfκb1*$^{-/-}$ mice respectively (Figure 5.3D and Figure 5.4D). The number of infiltrating $CD4^+$ and $CD8^+$ T cells was equivalent for WT and *nfκb1*$^{-/-}$ mice at this time.

$F4/80^+$ macrophages had infiltrated the renal interstitial compartment of WT and *nfκb1*$^{-/-}$ animals compared with unaffected kidneys ($p<0.005$ for both groups Figure 5.5A and B). No $F4/80^+$ cells were present in unaffected renal cortices (Figure 5.5C). Despite the median values for $F4/80^+$ infiltrate in WT and *nfκb1*$^{-/-}$ UUO mice being different this was not significant (Figure 5.5D). Extracellular matrix deposition of collagen I was significantly elevated in WT and *nfκb1*$^{-/-}$ UUO mouse kidneys ($p<0.001$ for both groups; Figure 5.6A and B), compared with contralateral kidneys (Figure 5.6C). Median deposition of α-SMA^+ myofibroblasts in WT and *nfκb1*$^{-/-}$ kidneys after ten days of UUO had increased to a similar level ($p<0.05$ for both groups compared with contralateral kidneys; Figure 5.7A-C).

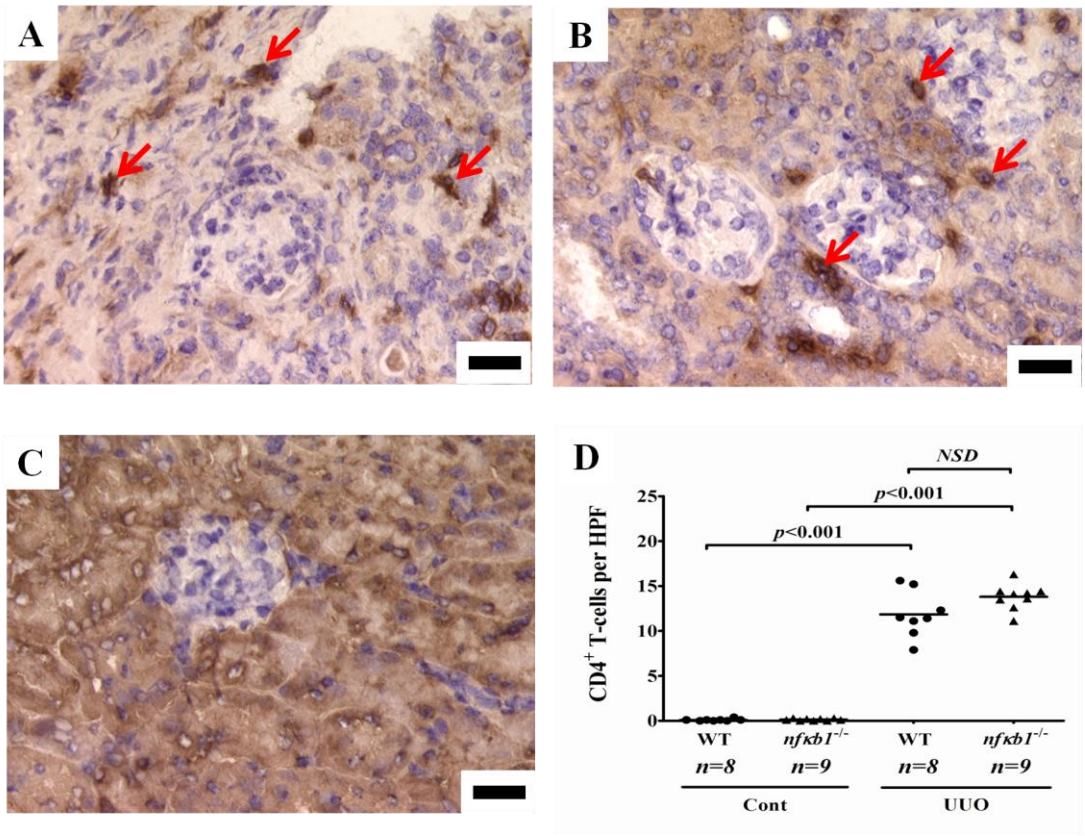

Figure 5.3. CD4$^+$ T cell infiltration at day ten UUO
WT obstructed (A), *nfκb1*$^{-/-}$ obstructed (B) and a representative contralateral kidney (C). Ten randomised HPFs were acquired for each animal. Positively stained cells present in each HPF field (indicated by red arrows), were counted manually and then graphed (D). The number of CD4$^+$ cells counted in WT and *nfκb1*$^{-/-}$ obstructed renal cortices, was equivalent. Bars on A-C measure 20µm. Bars on graph represent median values.

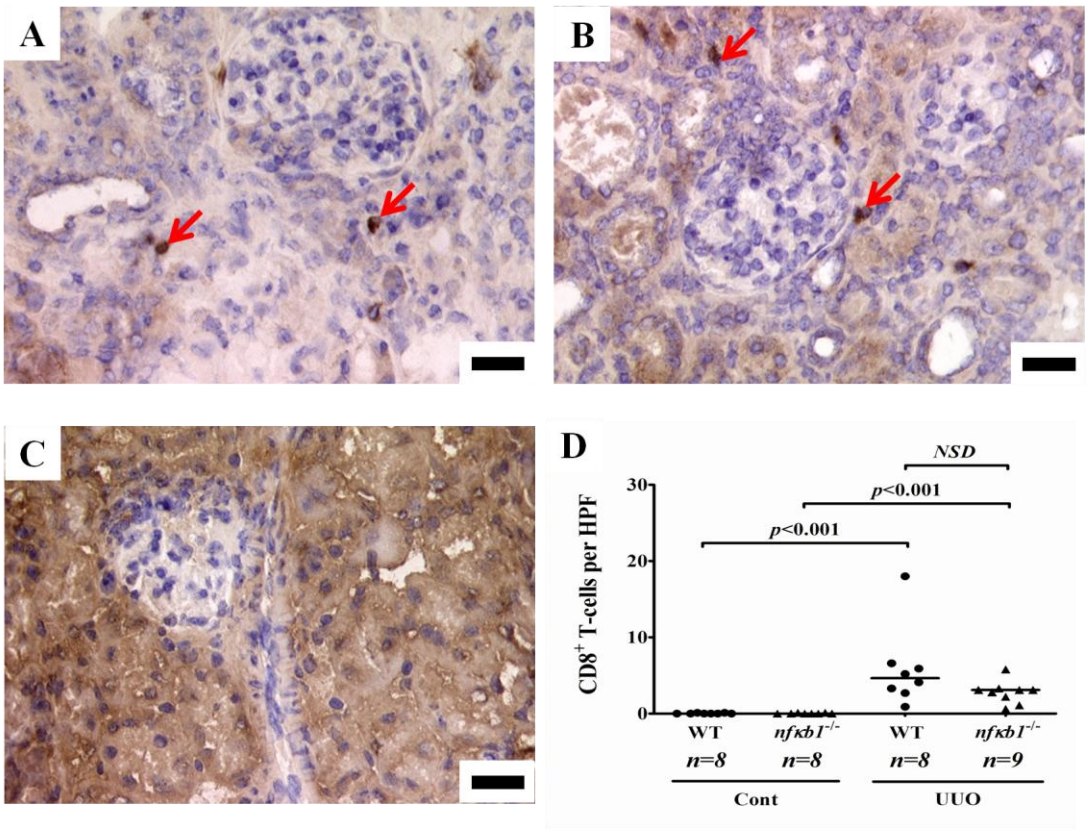

Figure 5.4. CD8$^+$ T cell infiltration at day ten UUO.
WT obstructed (A), *nfκb1*$^{-/-}$ obstructed (B) and a representative image of a contralateral kidney (C). Scale bars on A-C measure 20μm. Ten cortical HPFs were acquired at random for each animal. CD8$^+$ cells present in each HPF field (as indicated by red arrows), were manually counted and then graphed (D). CD8$^+$ cells were present in the obstructed kidneys WT and *nfκb1*$^{-/-}$ mice. Bars on graph represent median values.

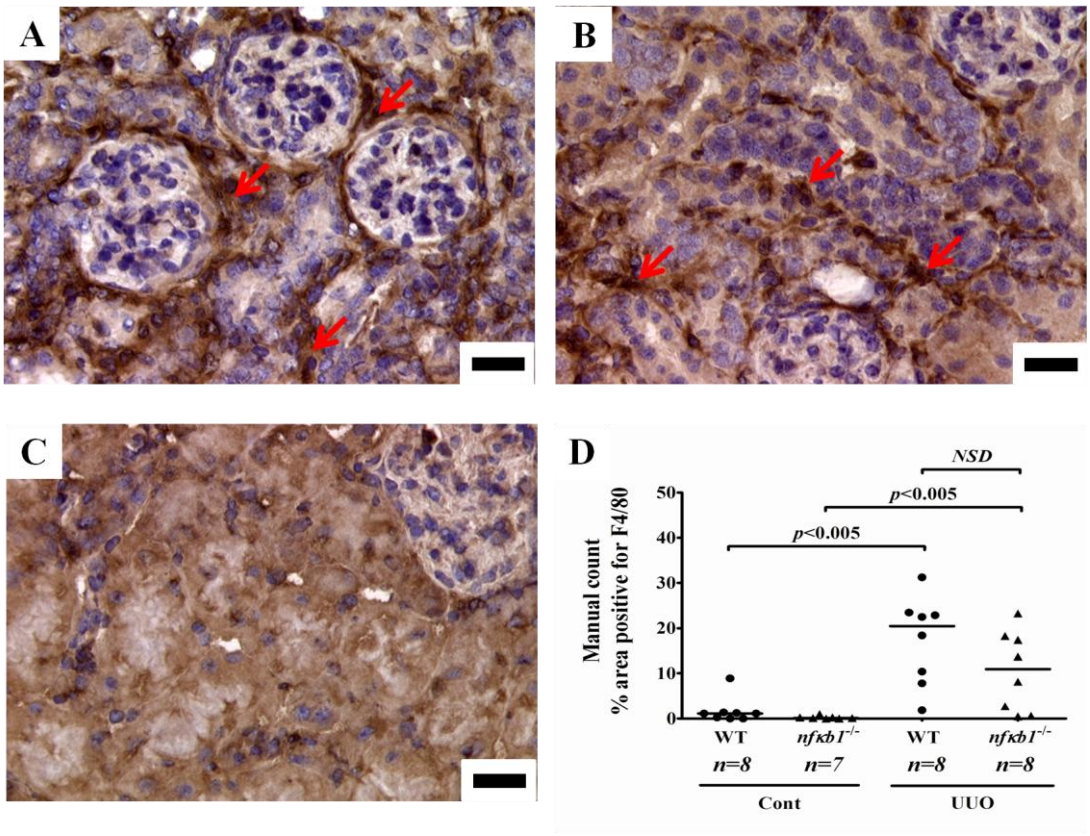

Figure 5.5. F4/80^{+} macrophage infiltration at day ten UUO
WT UUO (A), *nfκb1*$^{-/-}$ UUO mice (B) and a representative contralateral kidney (C) are shown. Scale bars on A-C measure 20µm. For each experimental group, ten randomised cortical HPFs were acquired for each animal. Areas of F4/80^{+} cells present in each HPF (as indicated by red arrows), were counted manually using a grid-based method (D). Equivalent numbers of F4/80^{+} macrophages were present in the renal cortices of WT and *nfκb1*$^{-/-}$ mice following UUO. Bars on graph represent median values.

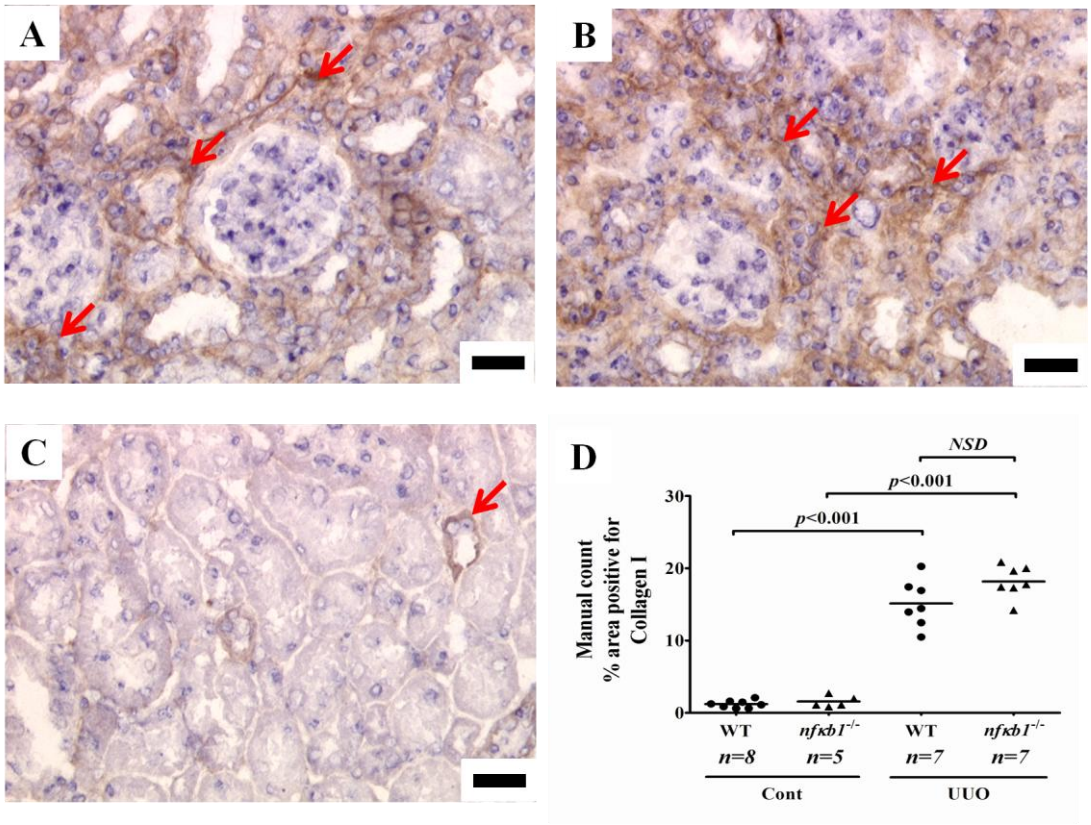

Figure 5.6. Collagen I deposition at day ten UUO
WT UUO (A), *nfκb1*$^{-/-}$ UUO mouse renal cortices (B) and a representative contralateral kidney (C). Scale bars on A-C measure 20µm. Ten randomised cortical HPFs were acquired for each experimental group. Collagen I positive staining within each HPF field (as indicated by red arrows) was measured using a grid-based method (D). Equivalent collagen I deposition was observed in the obstructed renal cortices of WT and *nfκb1*$^{-/-}$ mice. Bars on graph represent median values.

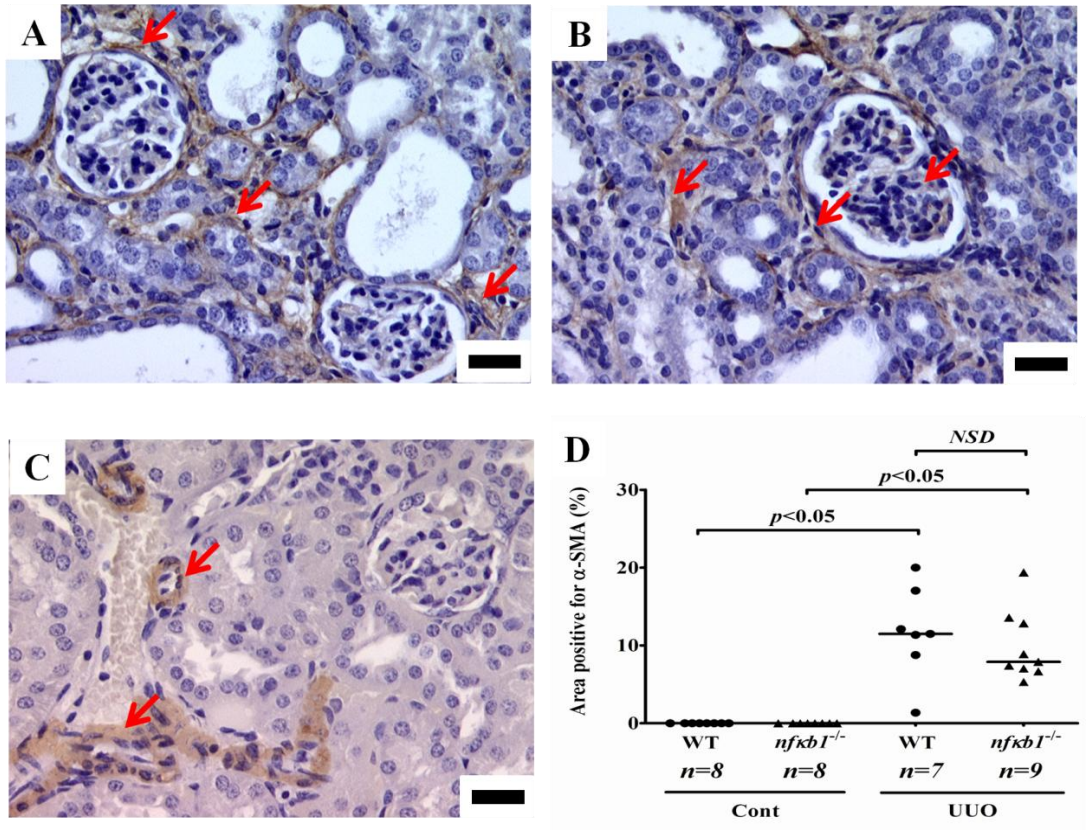

Figure 5.7. α-SMA^{+} myofibroblasts at day ten UUO
WT UUO (A), *nfκb1*$^{-/-}$ UUO mice (B) and a representative contralateral kidney (C). Scale bars on A-C measure 20μm. Ten cortical HPFs were acquired at random for each experimental group. Areas of α-SMA^{+} myofibroblasts (indicated by red arrows), were counted using a grid-based method (D). Myofibroblasts staining positive for α-SMA were observed in the obstructed renal cortices of WT and *nfκb1*$^{-/-}$ mice. Bars on graph represent median values.

5.4 rtPCR analyses of TNF-α, TGF-β and collagen mRNA expression during ureteric obstruction

Semi-quantitative rtPCR was used to measure the relative changes in gene expression of pro-inflammatory cytokine TNF-α. Following three days of ureteric obstruction median TNF-α mRNA expression was unchanged in obstructed WT and *nfκb1*$^{-/-}$ mouse kidneys. At day ten, median TNF-α gene expression in obstructed WT and *nfκb1*$^{-/-}$ kidneys remained significantly up-regulated compared with contralateral kidneys ($p<0.05$ and $p<0.001$ respectively). There were no significant differences in TNF-α expression observed in WT and *nfκb1*$^{-/-}$ obstructed kidneys at day three or day ten (Figure 5.8B). The expression of TGF-β mRNA in WT and *nfκb1*$^{-/-}$ obstructed kidneys was not significantly increased after three or ten days of UUO (Figure 5.9A and B).

Collagen I gene expression was not significantly up-regulated in WT or *nfκb1*$^{-/-}$ UUO renal cortices after three days of obstructive nephropathy (Figure 5.10A). Following ten days of UUO, median collagen I mRNA expression in obstructed WT mice had increased significantly compared with contralateral kidneys ($p<0.05$). Median expression of collagen I in day ten obstructed *nfκb1*$^{-/-}$ mice was equivalent to contralateral kidneys As observed at day three UUO, collagen I gene expression remained equivalent in the day 10 obstructed kidneys of WT and *nfκb1*$^{-/-}$ mice (Figure 5.10B).

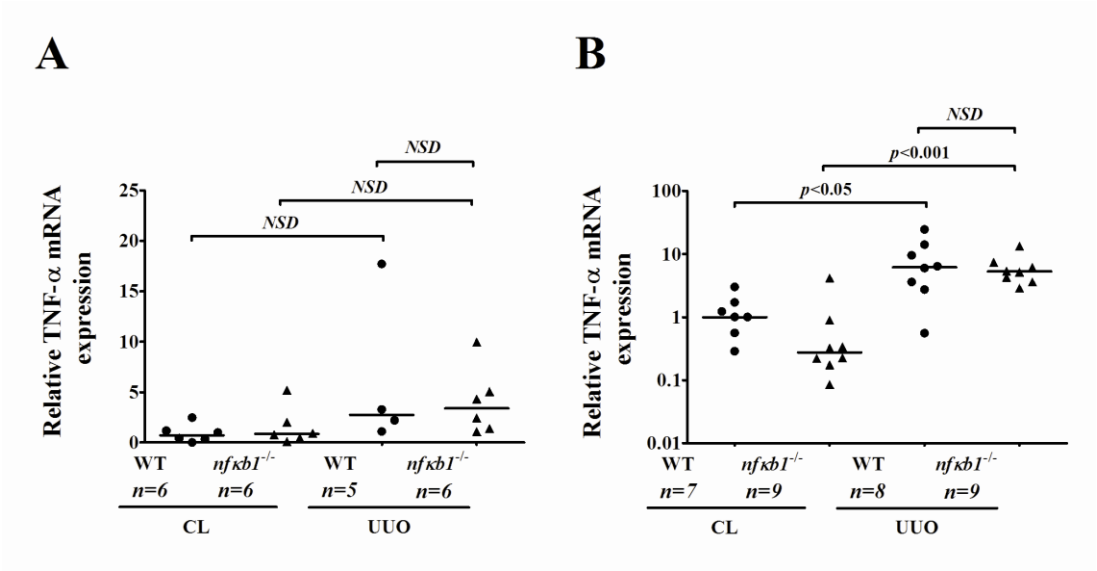

Figure 5.8. TNF-α gene expression at day three and day ten UUO
Relative gene expression of TNF-α in contralateral (CL) and UUO renal cortices three (A) and ten (B) days post-ureteric obstruction was semi-quantified by rtPCR. mRNA expression was first normalised to that of the house-keeping gene β-actin. After three days of UUO TNF-α gene expression was unchanged in the obstructed renal cortices of WT and *nfκb1*$^{-/-}$. By day ten, TNF-α expression was significantly up-regulated in WT and *nfκb1*$^{-/-}$ UUO mice. Bars on graphs represent median values. rtPCR was performed in triplicate for each animal.

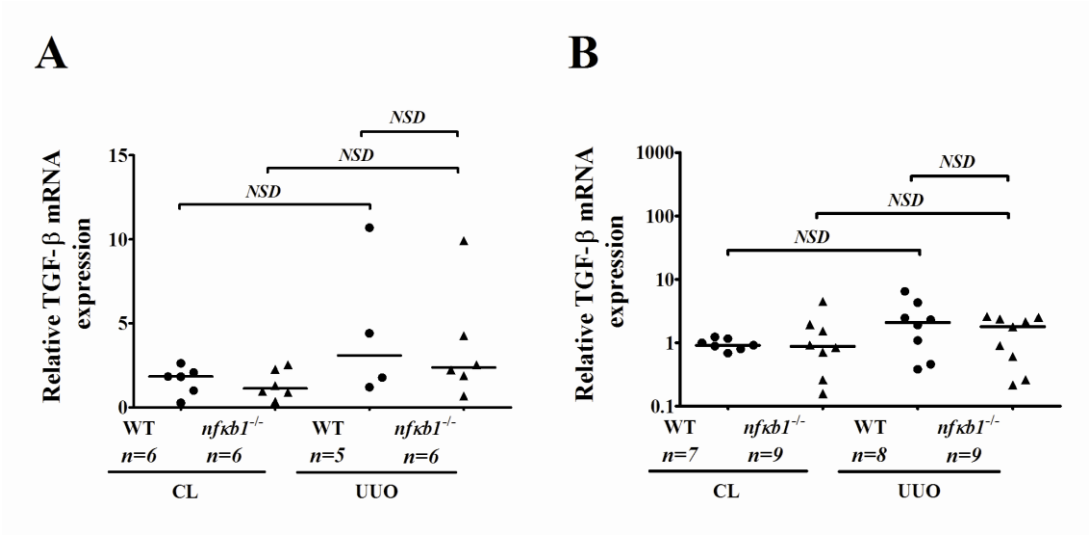

Figure 5.9. TGF-β gene expression at day three and day ten UUO
rtPCR was used to measure the relative mRNA expression of TGF-β in CL and UUO renal cortices three (A) and ten (B) days post-ureteric obstruction. There were no significant changes to the expression of TGF-β in obstructed WT and *nfκb1*$^{-/-}$ mouse kidneys after three and ten days of UUO. Bars on graphs represent median values. rtPCR was performed in triplicate for each animal.

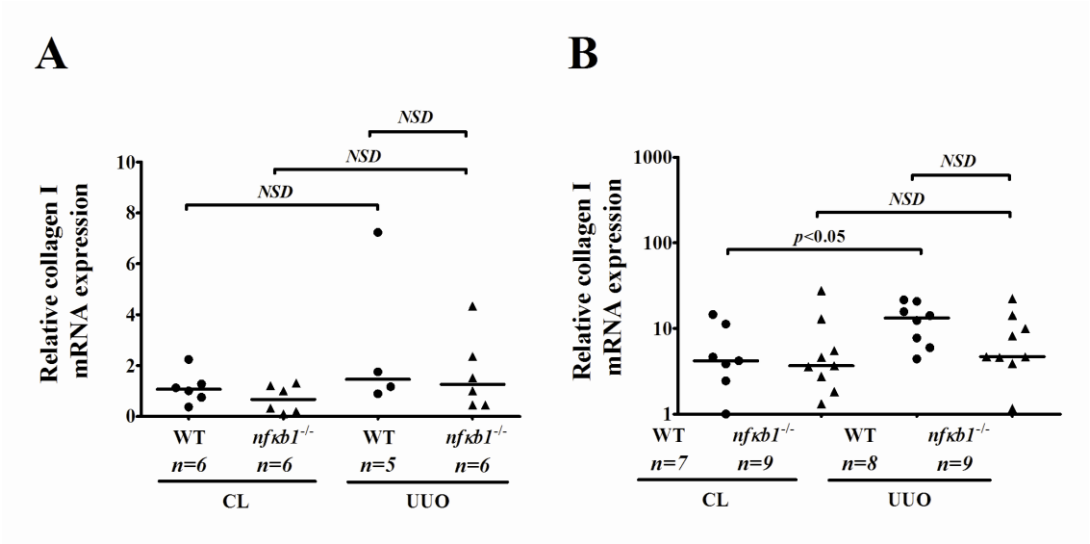

Figure 5.10. Collagen I gene expression at day three and day ten UUO
rtPCR was used to quantify collagen I in UUO and CL renal cortices three (A) and ten (B) days post-UUO. Gene expression was normalised to β-actin. Collagen I gene expression was not upregulated in WT or *nfκb1*$^{-/-}$ kidneys during the early stages of UUO, but was significantly elevated in obstructed kidneys of WT mice at day ten. Bars on graphs represent median values. rtPCR was performed in triplicate for each animal.

5.5 Glomerular injury and neutrophil infiltration in WT and *nfκb1*$^{-/-}$ mice after induction of NTS nephritis

Two hours after NTS injection, cells with multi-lobulated nuclei, characteristic of neutrophils, had infiltrated the glomeruli of WT and *nfκb1*$^{-/-}$ mice (Figure 5.11A and B respectively). The average number of neutrophils per glomerulus was statistically equivalent in WT and *nfκb1*$^{-/-}$ NTS-treated mice (2.73 and 2.00 respectively; Figure 5.11D). By 24 hours, glomerular injury was visibly apparent in WT and *nfκb1*$^{-/-}$ groups (Figure 5.12A and B respectively) and protein casts had started to form in some renal tubules. Glomerular injury was significantly higher in *nfκb1*$^{-/-}$ mice compared with WT mice at 24 hours (3.25 vs. 0.60; Figure 5.12D; $p<0.01$). Neutrophils and glomerular injury were not present in control kidneys (Figure 5.11C and Figure 5.12C).

The distribution of sheep anti-mouse anti-GBM antibody within the glomeruli two and 24 hours post-injection was visualised using a FITC-conjugated donkey anti-sheep antibody and quantified by measuring the fluorescence intensity of randomly selected glomeruli (Figure 5.13A-D). In WT and *nfκb1*$^{-/-}$ NTS groups, mean arbitary units for fluorescence intensity were 85.24±2.99 and 96.81±4.41 respectively at two hours and 88.80±0.61 and 88.95±1.28 respectively at 24 hours (Figure 5.13E).

5.6 Proteinuria in WT and *nfκb1*$^{-/-}$ mice

In addition to histological analyses of renal injury 24 hours following NTS injection, glomerular injury was also determined by measuring urinary albumin concentration using an immunodiffusion assay (Figure 5.14A-E).

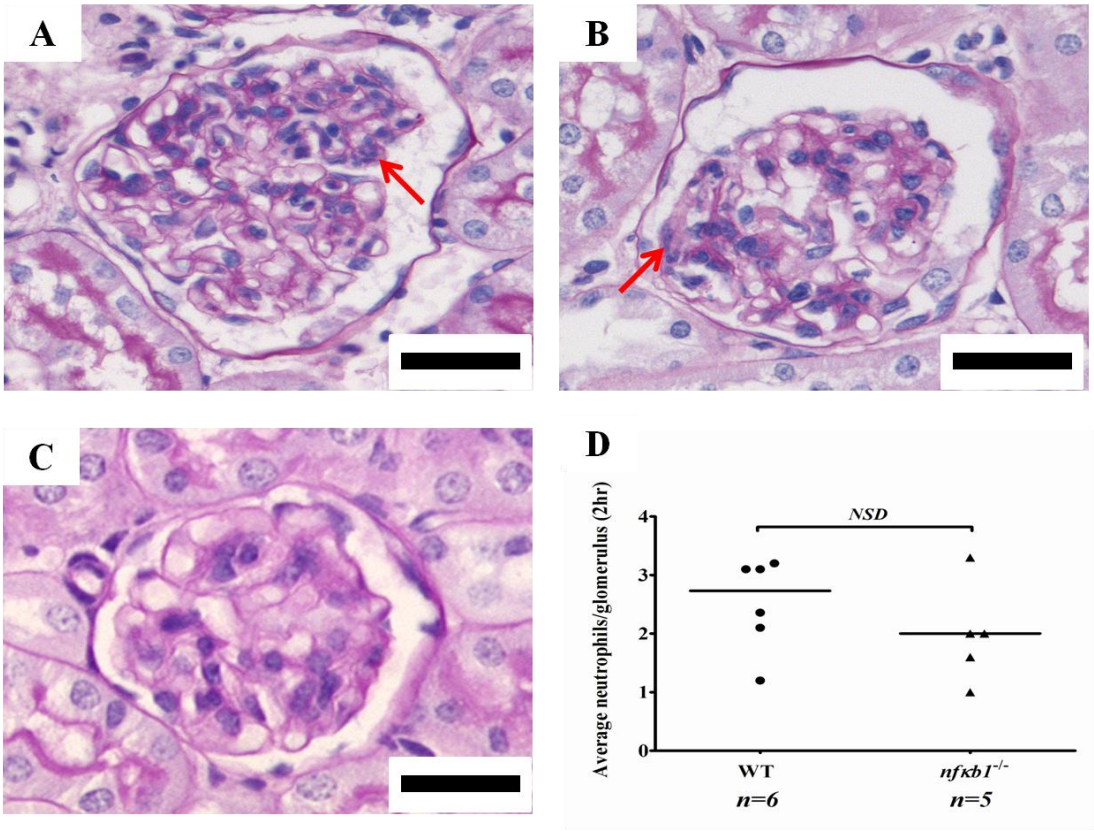

Figure 5.11. Neutrophil infiltration two hours after NTS injection
Following NTS injection, periodic acid Schiff's histology was used to identify infiltrating neutrophils present within the glomeruli of WT (A) and *nfκb1*$^{-/-}$ (B) mice. The average number of neutrophils present in randomly selected glomeruli was determined by counting muli-lobulated nuclei-containing cells in a blinded fashion. No neutrophils were present in the glomeruli of unaffected WT and *nfκb1*$^{-/-}$ mice (C). Scale bars on A-C represent 20µm. There were no differences in the number of infiltrating neutrophils in WT and *nfκb1*$^{-/-}$ tissues at two hours (D). Bars on graphs represent median values.

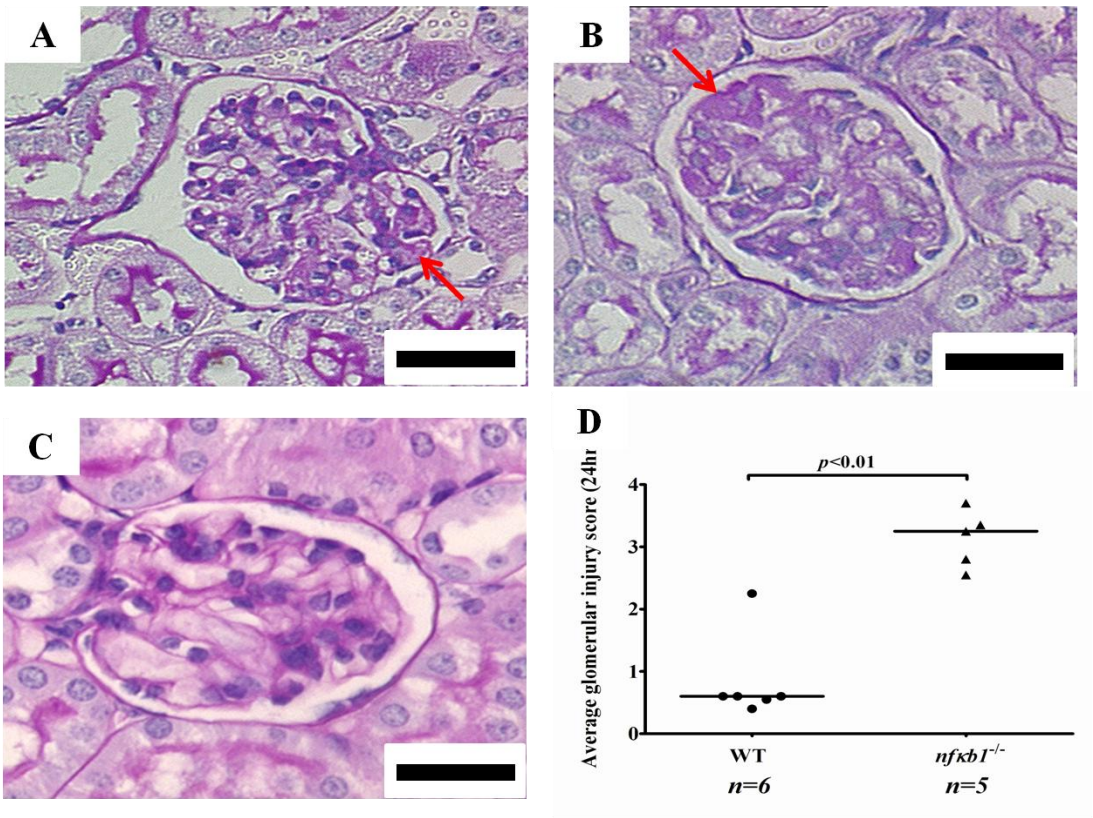

Figure 5.12. Glomerular injury 24 hours after NTS injection
Glomerular injury at 24 hours post-NTS injection was much less severe in WT mice (A) compared with *nfκb1*$^{-/-}$ mice (B). Control renal tissues displayed normal glomerular structure in WT and *nfκb1*$^{-/-}$ mice (C). Glomerular injury was measured using a +1 (<25% injury), +2 (25-50% injury), +3 (50-75% injury) and +4 (>75% injury) scoring system. A Mann-Whitney U-test showed that glomerular injury was significantly worse in *nfκb1*$^{-/-}$ mice (p<0.01) compared with WT mice. Scale bars on A-C represent 20µm. Bars on graphs represent median values.

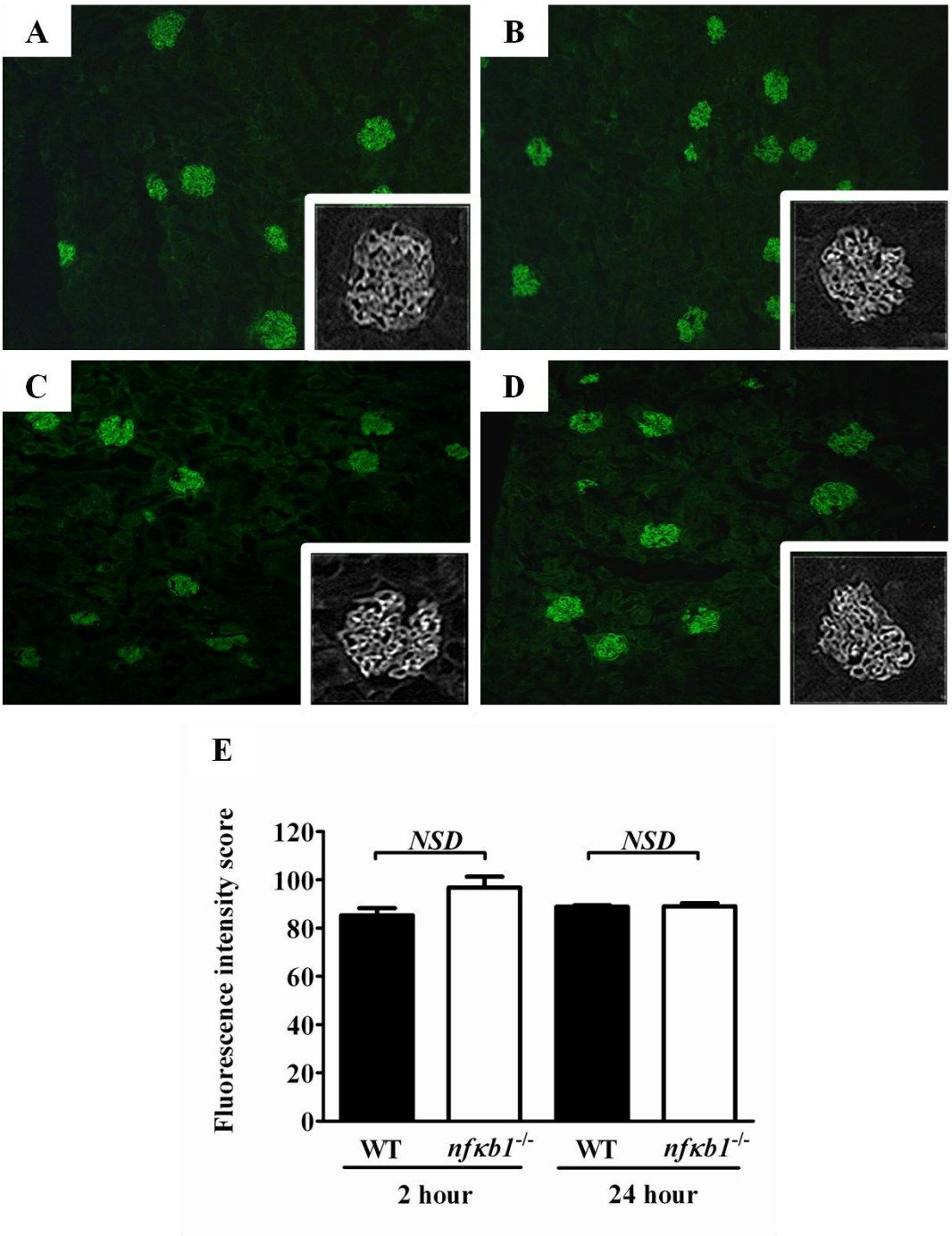

Figure 5.13. Anti-GBM antibody distribution in glomeruli post-NTS injection
FITC-stained glomeruli 2 and 24 hours post-NTS injection in WT mice (A and C respectively) and *nfκb1*$^{-/-}$ mice (B and D respectively). Fluorescence intensity scoring for glomerular-bound anti-GBM antibody (E). An unpaired t-test was performed and revealed no significant differences in mean fluorescence intensity of FITC-stained glomeruli between WT and *nfκb1*$^{-/-}$ groups at 2 and 24 hours post-injection. Bars on graph represent mean +SEM.

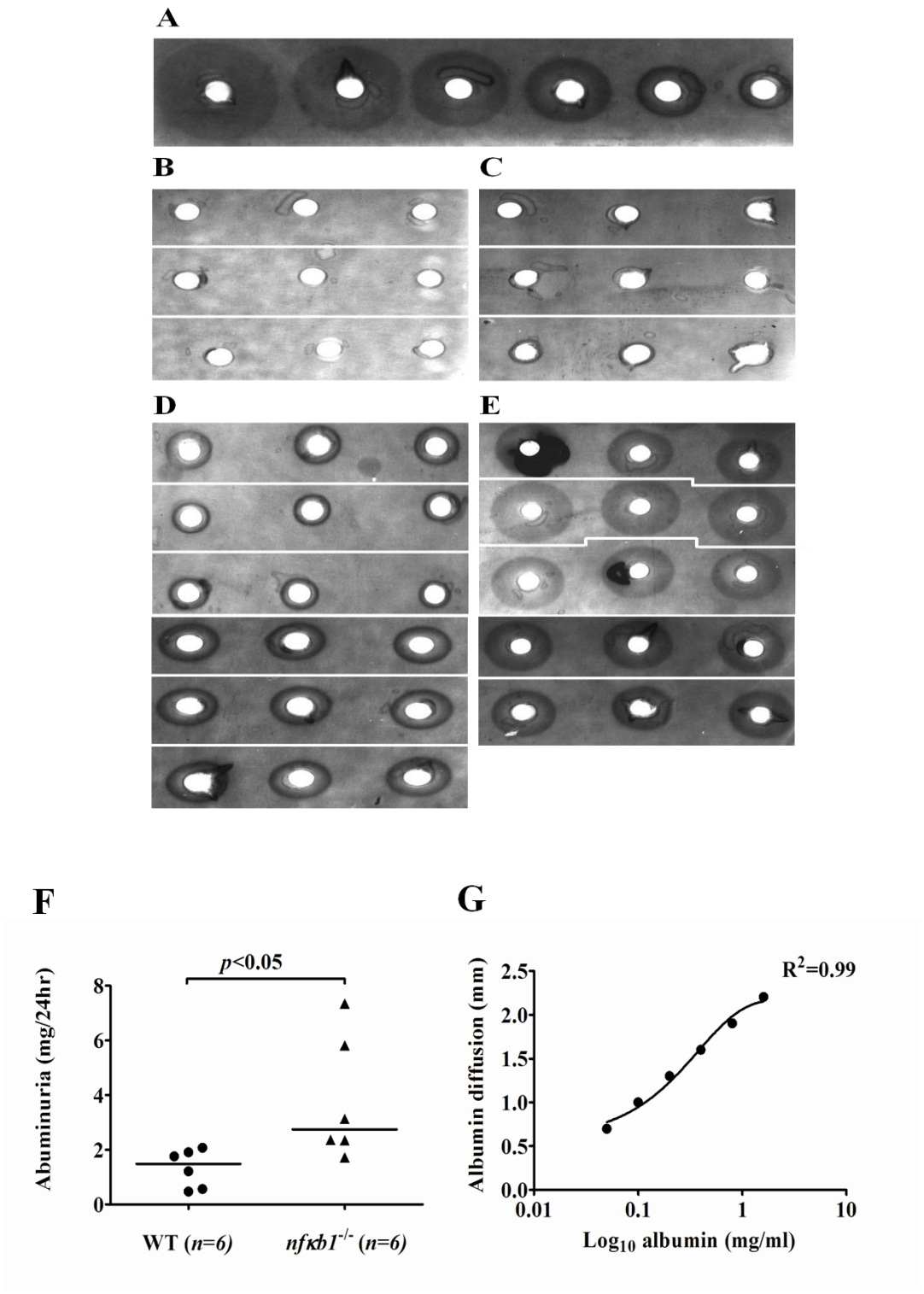

Figure 5.14. Urinary albumin concentration 24 hours after NTS injection
A standard control used for calculating urinary albumin measurements in the range 0.05-1.6mg/ml (A). No albumin was detected in the urine of WT (B) and *nfκb1*$^{-/-}$ (C) mice (n=6 for both groups, only 3 are illustrated). Albumin was detected in the urine collected from WT (D) and *nfκb1*$^{-/-}$ (E) mice 24 hours following NTS injection. Extrapolation of urinary albumin concentrations for WT and *nfκb1*$^{-/-}$ mice (F) using a standard curve of known albumin concentrations (G).

Albumin was present in urine collected from WT and *nfκb1*$^{-/-}$ animals at a median concentration of 1.48 and 2.74mg/24 hours respectively (p<0.05; Figure 5.14F). Albumin was not detected in urine collected from control mice. A standard curve of known albumin concentrations was used to extrapolate urinary albumin concentrations from NTS-injected WT and *nfκb1*$^{-/-}$ mice (Figure 5.14G).

5.7 Gene expression of pro-inflammatory mediators of glomerular injury

Changes in the relative gene expression of pro-inflammatory calcium binding proteins S100A8 and S100A9 were measured using rtPCR. S100A8 and S100A9 mRNA expression was significantly up-regulated two hours after NTS injection in WT and *nfκb1*$^{-/-}$ groups (p<0.005 for all analyses). S100A8 and S100A9 gene expression in WT and *nfκb1*$^{-/-}$ kidneys was equivalent 2 hours post-NTS injection (Figure 5.15Figure 5.16). By 24 hours, S100A8 mRNA levels remained significantly elevated by approximately 10 fold and 60 fold in affected WT and *nfκb1*$^{-/-}$ mouse kidneys respectively (p<0.005 for both groups; Figure 5.15). Interestingly, S100A8 gene expression in the kidneys of *nfκb1*$^{-/-}$ mice was significantly higher than that observed in WT mouse kidneys 24 hours following NTS injection (p<0.01). At 24 hours post-NTS treatment, S100A9 gene expression had fallen below baseline levels in WT kidneys (p<0.005), but remained significantly elevated in kidneys taken from *nfκb1*$^{-/-}$ mice (p<0.005). Compared to affected WT kidneys, S100A9 gene expression in affected *nfκb1*$^{-/-}$ mouse kidneys was significantly greater 24 hours post-NTS administration (p<0.01; Figure 5.16).

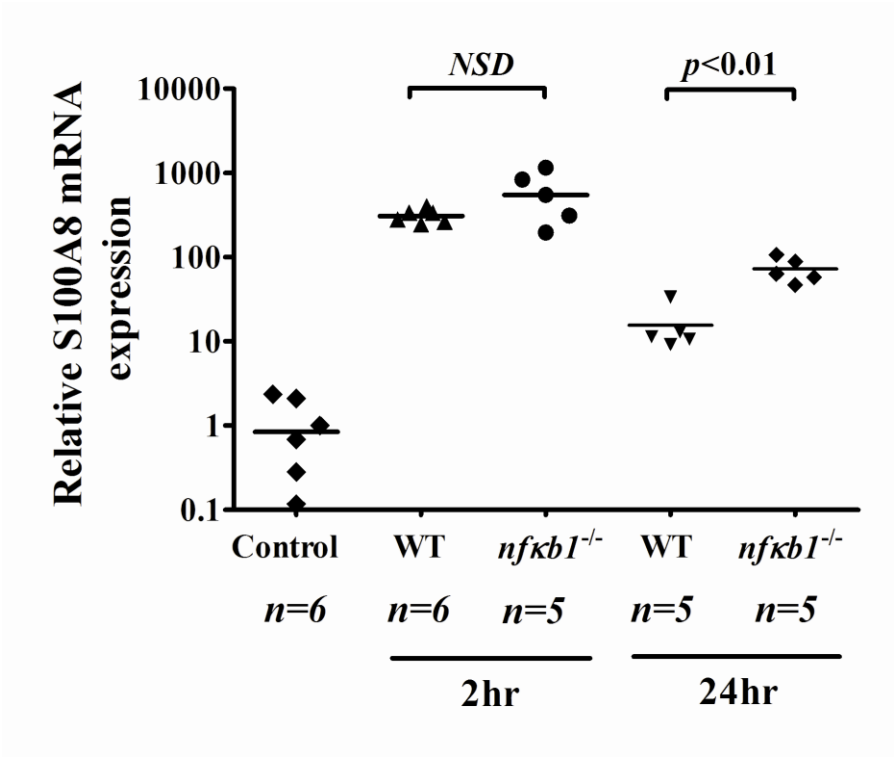

Figure 5.15. S100A8 gene expression two and 24 hours post-NTS injection
rtPCR was used to measure the relative gene expression of S100A8 in affected kidneys two and 24 hours following NTS injection. Gene expression was normalised to β-actin. Two and 24 hours following NTS injection, S100A8 mRNA expression had significantly increased in the kidneys of WT and *nfκb1*$^{-/-}$ mice. Bars on graphs represent median values. rtPCR was performed in triplicate for each animal.

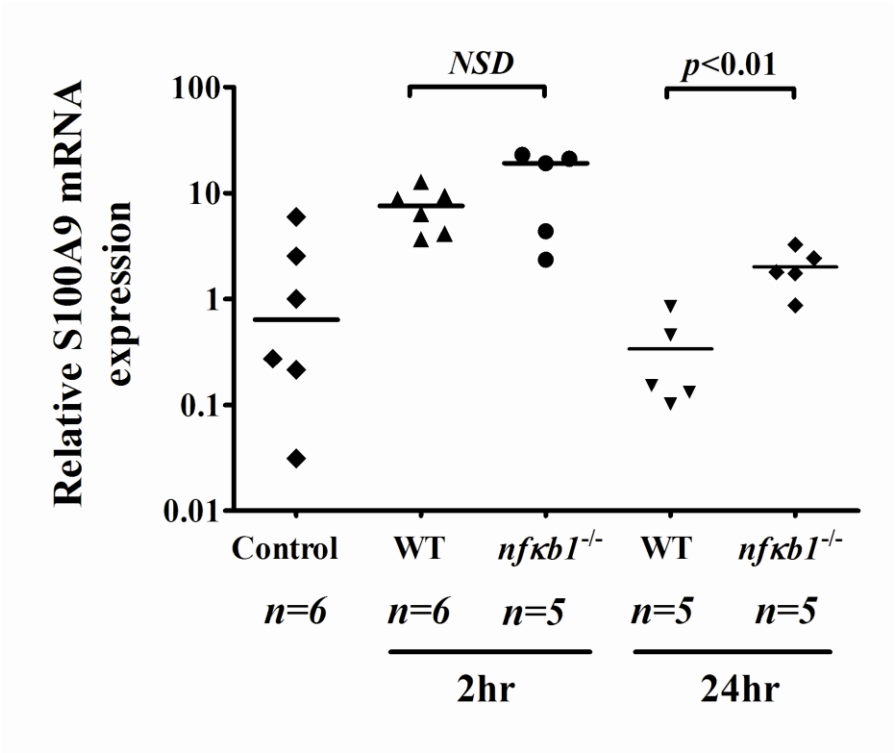

Figure 5.16. S100A9 gene expression two and 24 hours post-NTS injection
rtPCR was used to determine the relative mRNA expression of S100A9 in affected kidneys at two and 24 hours following NTS injection. S100A9 mRNA expression was calculated following gene expression normalisation to the house keeping gene β-actin. S100A9 gene expression was elevated in the kidneys of WT and *nfκb1*$^{-/-}$ mice two and 24 hours after NTS injection. Bars on graphs represent median values. rtPCR was performed in triplicate for each animal.

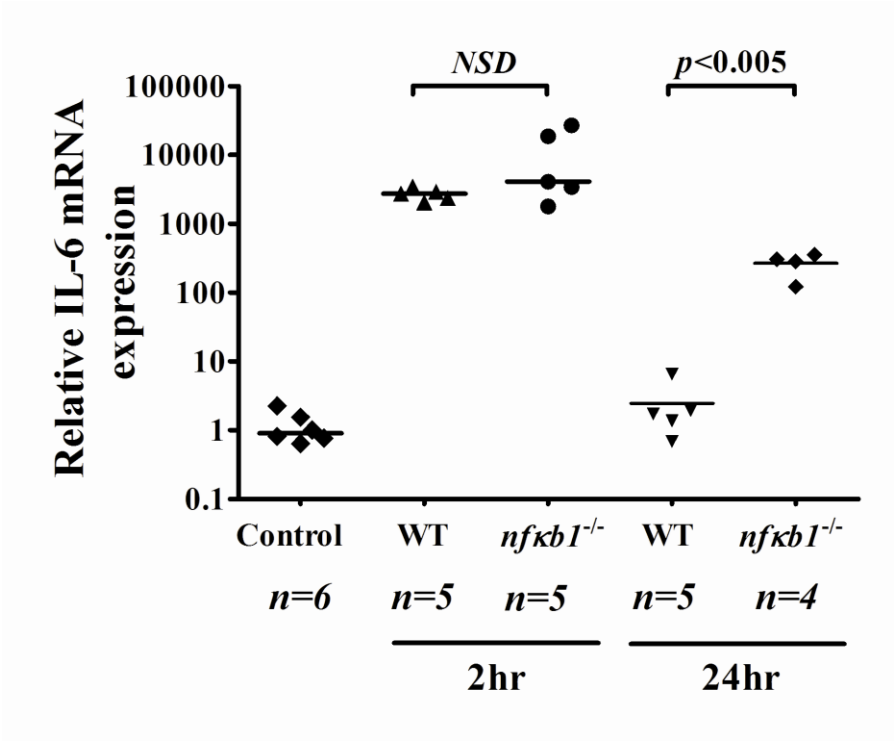

Figure 5.17. IL-6 gene expression two and 24 hours post-NTS injection
Relative IL-6 gene expression in affected kidneys two and 24 hours following NTS injection was measured by rtPCR. mRNA expression was normalised to that of the house keeping gene β-actin. Two hours after NTS treatment, IL-6 was up-regulated in the kidneys of WT and *nfκb1*$^{-/-}$ mice. IL-6 expression remained elevated in *nfκb1*$^{-/-}$ mice at 24 hours. Bars on graphs represent median values. rtPCR was performed in triplicate for each animal.

Two hours following NTS treatment, IL-6 gene expression was significantly up-regulated in WT and *nfκb1*$^{-/-}$ NTS-treated groups respectively (p<0.005 for all analyses). By 24 hours IL-6 gene expression had returned to normal levels in affected WT mouse kidneys, but remained elevated in *nfκb1*$^{-/-}$ renal tissues (p<0.01). 24 hours following NTS injection, IL-6 expression was significantly elevated in NTS-treated *nfκb1*$^{-/-}$ kidneys compared to WT kidneys (p<0.05; Figure 5.17).

TNF-α gene expression had increased by approximately 6 and 8 fold 2 hours after NTS was administered in WT and *nfκb1*$^{-/-}$ kidneys respectively (p<0.05 and p<0.005). The increase in TNF-α mRNA observed in WT and *nfκb1*$^{-/-}$ kidneys was equivalent two hours post-NTS treatment (Figure 5.18). 24 hours after NTS administration, TNF-α gene expression in WT kidneys was significantly elevated by approximately 3 fold (p<0.05), whereas TNF-α mRNA expression in *nfκb1*$^{-/-}$ kidneys had returned to normal levels There was no significant difference in TNF-α gene expression 24 hours post-NTS treatment in WT and *nfκb1*$^{-/-}$ mice (Figure 5.18).

5.8 Discussion

Recent studies have demonstrated that NF-κB activation is a common feature of renal pathophysiology, however, little is known about the contribution of individual NF-κB subunits during inflammation. To add to the complexity surrounding NF-κB, there is increasing evidence to suggest that NF-κB may exhibit both pro and anti-inflammatory actions depending upon the nature of activation. The last part of this thesis explored the contribution of nfκb1 towards inflammation and fibrosis during mouse models of acute and chronic renal disease.

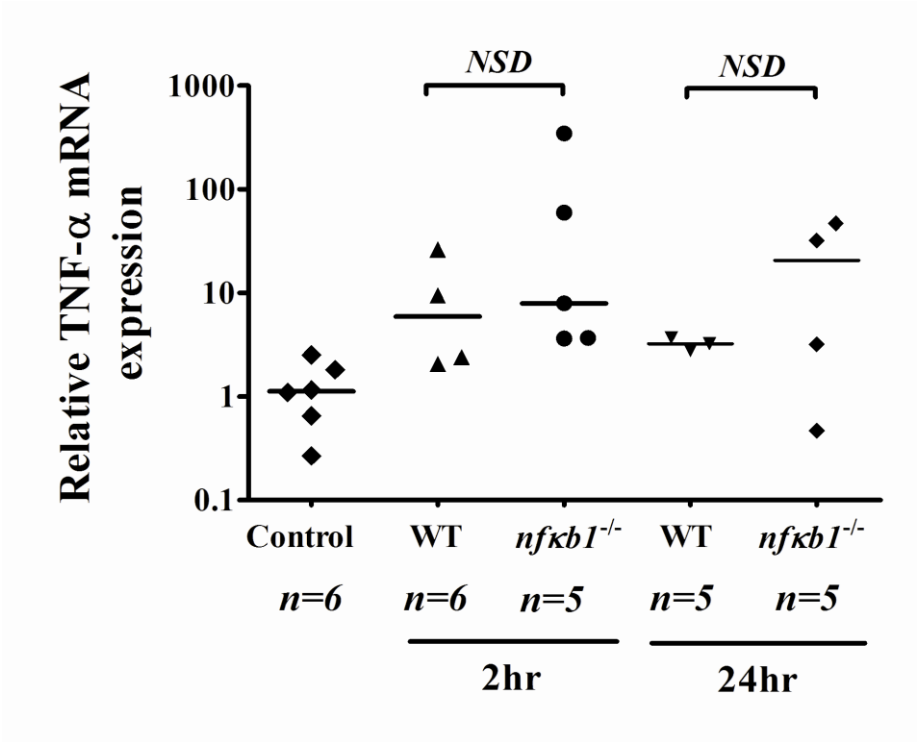

Figure 5.18. TNF-α gene expression two and 24 hours post-NTS injection
Relative gene expression for TNF-α at two and 24 hours after NTS injection was measured by rtPCR and the gene expression of TNF-α relative to that of the house keeping gene β-actin was calculated. Two hours after NTS treatment, TNF-α was significantly up-regulated in the obstructed kidneys of WT and *nfκb1*$^{-/-}$ mice. TNF-α mRNA expression remained significantly elevated in WT mice at 24 hours. Bars on graphs represent median values. rtPCR was performed in triplicate for each animal.

Compared with kidneys from WT mice, glomerular thrombosis was worse in *nfκb1*$^{-/-}$ mouse kidneys 24 hours after NTS injection. As a consequence of increased glomerular injury, *nfκb1*$^{-/-}$ mice developed more severe proteinuria compared with WT mice. Interestingly, the number of neutrophils present in glomeruli was equivalent in WT and *nfκb1*$^{-/-}$ mouse kidneys 2 hours post-NTS administration. Therefore, nfκb1 does not appear to mediate the recruitment of neutrophils into injured glomeruli. The level of neutrophil chemotaxis due to intrinsic cell signalling may be responsible for the exacerbated glomerular injury and proteinuria observed in *nfκb1*$^{-/-}$ mice.

In this study, two hours after NTS injection the expression of TNF-α mRNA had significantly increased in WT and *nfκb1*$^{-/-}$ mouse kidneys, but was equivalent. At 24 hours post-NTS injection, significant up-regulation of TNF-α gene expression was sustained in WT kidneys, but not in kidneys taken from *nfκb1*$^{-/-}$ mice. In animal models of NTS nephritis TNF-α has been shown to contribute towards glomerular injury and modulate the severity of inflammation during the heterologous phase of glomerular injury (Abbott et al., 1991; Hruby et al., 1990).

One study demonstrated that TNF-α deficient mice developed less severe NTS-induced nephritis (Ryffel et al., 1998). A second study showed that antibody blockade of TNF-α successfully reduced renal inflammation and scarring in a rat model of crescentic glomerulonephritis, thus preserving renal function (Khan et al., 2005). During NTS nephritis, intrinsic renal cells contribute towards the production of TNF-α (Timoshanko et al., 2003).

Although the present study only quantified infiltrating neutrophils, previous earlier work has demonstrated that macrophages and a small number of T cells also infiltrate the kidney during NTS nephritis, particularly when the model progresses beyond 24 hours (Kurts et al., 2007; Tesch et al., 1999). The changes in TNF-α gene expression observed in this study were relatively minor. One reason for this could be that the duration of the study was relatively short. Another reason could be that the tissue undergoing molecular analysis consisted of all components of the renal cortex, including the renal tubules, which will not have been significantly injured during disease induction. Considering the end-points used in this study, it is likely that the primary source of TNF-α would be the glomerulus, including mesangial cells, which in contrast to the surrounding tubular interstitium, are relatively few in number.

Interestingly, an *in vitro* study using human mesangial cell cultures demonstrated that TNF-α can stimulate the production of IL-6 and IL-8 (Abbott et al., 1991). As observed with TNF-α, IL-6 gene expression observed in the present study was significantly elevated, but equivalent in the kidneys of WT and *nfκb1*$^{-/-}$ mice two hours after NTS injection. Compared with kidneys taken from WT mice, the sustained elevation of IL-6 mRNA in *nfκb1*$^{-/-}$ mouse kidneys 24 hours post-NTS administration is consistent with a more severe disease phenotype in this group.

IL-6 is involved in the regulation of inflammatory responses and can also control the expression of other cytokines. However, there are mixed views on the contribution of IL-6 towards the development of renal injury, due to its pleiotropic activities. Although *in vitro* studies have demonstrated that human mesangial cells produce IL-6 in response to stimulation with TNF-α and that this in turn stimulates proliferation of mesangial cells, rodent models of mesangioproliferative glomerulonephritis have not found a role for IL-6 (Eitner et al., 1997).

In the present study, up-regulation of IL-6 gene expression persisted in *nfκb1*$^{-/-}$ mouse kidneys, contributing towards a more severe injury phenotype. This observation suggests that signalling by nfκb1 may be important for switching off IL-6 mediated pro-inflammatory activities. In addition to the roles of TNF-α and IL-6 during the progression of inflammation, cytoplasmic calcium-binding proteins S100A8 and S100A9 also act as pro-inflammatory mediators during acute and chronic inflammation. mRNA expression of S100A8 and S100A9 was equivalent in the kidneys of WT and *nfκb1*$^{-/-}$ mice two hours after NTS injection. Since S100A8 and S100A9 are expressed and secreted by neutrophils (Gebhardt et al., 2006), this observation was consistent with the presence of equivalent neutrophil numbers at two hours post-NTS administration. Previous studies have also demonstrated that blockade of S100A8 and S100A9 can reduce neutrophil migration (Ikemoto et al., 2007; Vandal et al., 2003). In the absence of nfκb1, persistent elevation of S100a8 and S100a9 24 hours after giving NTS was consistent with prolonged IL-6 elevation observed in *nfκb1*$^{-/-}$ mouse kidneys. Of further relevance to these observations are studies that have demonstrated up-regulation of S100A8, S100A9 and S100A8/A9 heterodimer mRNA expression to be stimulated by IL-6 production (Kim et al., 2012; Eggers et al., 2011).

Another study also reported that heterodimeric S100A8/A9 enhanced the production of IL-6 (Ehlermann et al., 2006), suggesting a positive reinforcement mechanism. In the present study, elevated IL-6, S100A8 and S100A9 gene expression in the absence of nfκb1 suggests interplay between these proteins that is normally controlled at least in part by nfκb1signalling. The findings of this study suggest that NF-κB signalling via the nfκb1 subunit may provide an important off-switch for the mechanisms that drive inflammation during NTS nephritis.

The precise mechanism by which this is achieved is unknown. One possibility is that other NF-κB pathways exist whereby NF-κB homodimers (including nfκb1) could translocate to the nucleus and inhibit inflammatory gene transcription via interactions with IκB proteins such as IκBζ. Similarly, the binding of nfκb1 homodimers to κB sites on activated genes may work to prevent activation by other pro-inflammatory NF-κB dimers. The observation that nfκb1 may have a protective role during injury is supported by a previous study of carbon tetrachloride liver necrosis in rodents (Oakley et al., 2005).

Other studies using rodent models of NTS nephritis have also demonstrated that activation of different NF-κB subunits takes place during disease progression and that this is responsible for the transcriptional activation of other inflammatory mediators such as IL-1β and IL-8 (Sakurai et al., 1997; Sakurai et al., 1996). The same studies showed that renal injury and proteinuria were both reduced in animals treated with NF-κB inhibitors. Based on the preliminary observations of this study, future work will address the relative contributions of intrinsic renal cells and circulating leukocytes towards the progression of NTS nephritis in the presence and absence of nfκb1 using bone marrow chimeric mice.

Support for this comes from a similar study by Timoshanko and co-workers who demonstrated that intrinsic renal cells were the primary source of TNF-α in a murine of crescentic glomerulonephritis (Timoshanko et al., 2003). Following on from the observation that nfκb1 appeared to assist with resolution from renal injury after NTS administration the final part of this chapter used the mouse model of UUO to determine if nfκb1 contributed to the development of chronic renal fibrosis.

Interstitial expansion and tubular dilatation increased significantly in the obstructed renal cortices of WT and *nfκb1*$^{-/-}$ mice, but was equivalent at day three and day ten UUO. After ten days of UUO, equivalent numbers of $CD4^+$ and $CD8^+$ cells and macrophages were observed in WT and *nfκb1*$^{-/-}$ mouse kidneys. Extracellular deposition of collagen I and accumulation of α-SMA^+ myofibroblasts within the renal interstitium of *nfκb1*$^{-/-}$ mice was equivalent to WT mice. These observations suggest that nfκb1 is not implicated in the recruitment of leukocytes and myofibroblasts during UUO and that nfκb1 does not influence ECM re-modelling with respect to collagen I accumulation.

Despite previous studies demonstrating TGF-β activity during ureteric obstruction (Moon et al., 2006; Wang et al., 2005b), TGF-β mRNA expression did not appear to change in WT or *nfκb1*$^{-/-}$ obstructed kidneys during the course of UUO in this study. It was expected that TGF-β mRNA expression would be detected in WT UUO mouse kidneys, since collagen I deposition and interstitial expansion increases. An explanation for the discrepancy in renal injury mediated by nfκb1 signalling during acute and chronic renal disease in this study remains incomplete. In the UUO model of chronic renal fibrosis, nfκb1 does not influence disease progression. Numerous articles in the literature highlight the multiple effects of NF-κB signalling during UUO.

During the early stages of ureteric obstruction, ANG II up-regulates NF-κB activation, which in turn activates other downstream inflammatory and fibrotic mediators such as TNF-α and TGF-β (Grande et al., 2010; Ucero et al., 2010; Misseri and Meldrum, 2005). The pivotal role for NF-κB in progression of UUO was shown in studies where administration of ACE inhibitors or blockade of angiotensin receptors limited NF-κB activation (Esteban et al., 2004).

Additionally, other studies showed that administration of pharmacological inhibitors of NF-κB reduced the number of infiltrating T cells and macrophages during ureteric obstruction (Nakatani et al., 2002). Although a promising strategy for reducing renal injury, pharmacological NF-κB inhibition lacks specificity and could have a negative impact on NF-κB mediated resolution from injury. There is also the possibility that other NF-κB subunits are predominantly involved with the progression of UUO or that in the absence of nfκb1, different NF-κB subunits become active to compensate. A more specific approach could be the development of gene therapy to target other NF-κB dimers that have been identified as behaving in a deleterious manner during disease states. However, with respect to the current study the relative contribution of different NF-κB dimers during UUO would first require additional exploration. Future studies could be directed towards investigating the relative contributions of different NF-κB subunits during ureteric obstruction and other renal diseases. Additionally, since nfκb1 is reportedly concerned with the limitation of inflammation during renal injury and other organ-specific models of disease, it may be interesting to investigate renal recovery from ureteric obstruction in *nfκb1*$^{-/-}$ mice, by surgically re-implanting the ureter into the bladder following an initial period of ureteric obstruction.

Depending upon the nature of activation, nfκb1 is known to form active homo or heterodimers, each with their own distinct κB binding sites. Of these dimers, the nfκb1 homodimer is thought to inhibit gene expression by binding to κB sites on activated genes, preventing further activation by other NF-κB dimmers (Gilmore, 2006). The results from this chapter demonstrate that nfκb1 is an important modifier of disease progression during acute glomerular nephritis, but not during obstructive nephropathy.

Future work will be directed towards exploring the participation of nfκb1 during recovery from UUO as well as establishing the relative contributions of intrinsic renal cells and circulating lymphocytes during NTS nephritis.

6 Conclusion

Data from this thesis has demonstrated a prominent role for the immune system in mediating the progression of renal disease in mice. During early experimental obstructive nephropathy, this study demonstrated complement activation and intrarenal complement synthesis by tubular epithelial cells. Exploration of the precise mechanisms by which complement activation occurs during UUO, were unfortunately beyond the time constraints of the present study. However, one possibility is that an accumulation of tubular debris and cellular waste within the renal tubule lumina may cause activation of complement at the apical brush boarder membrane. The abundance of C3a detected in urine extracted from the obstructed kidneys of WT mice certainly supports this idea, as do previous studies demonstrating 'tick over' of the alternative complement pathway at the apical membrane as well as the synthesis of complement proteins by tubular epithelial cells (Zipfel, 2006; Timmerman et al., 1996; Ichida et al., 1994).

An investigation into complement regulatory proteins during this study demonstrated a decrease in gene expression for the membrane-bound regulators crry, DAF1 and CD59a. Whilst interesting, this observation adds little to the current knowledge of complement regulatory mechanisms during ureteric obstruction without further analysis of crry, DAF1 and CD59a protein expression and deposition. The increase in FI and FH observed during UUO, would suggest an attempt to regulate complement activation, however FH and FI are concerned with the regulation of both alternative and classical complement pathways, so it is not possible to determine their precise roles or mechanisms in the context of the present study.

Li and co-workers demonstrated a loss of crry protein expression in the murine model of IRI (Li et al., 1993), in which activation of the alternative complement pathway is well characterised. However, activation of complement via the classical pathway cannot be excluded in the UUO model. Further studies into the expression of classical complement pathway proteins such as C1, C2 and C4 are needed to verify the nature of complement activation. These could take the form of measuring gene and protein expression in WT mouse obstructed kidneys used in the present study or by inducing UUO in mice lacking the classical pathway components C1q and C4 or the alternative complement pathway proteins FB and FD. Another approach to future work could be to measure complement components present in urine taken from obstructed mouse kidneys using ELISA or western blot analyses.

Overall, there were no significant differences in histological injury in $C3^{-/-}$ mouse renal cortices compared to WT mice in the present study. However this observation contrasted with the findings of a previous adriamycin nephropathy study in $C3^{-/-}$ mice, which demonstrated a reduction in tubulointerstitial injury (Turnberg et al., 2006). These differences are most likely due to the different mechanisms of injury in each of the experimental models.

Up-regulation of TGF-β gene expression has previously been shown to be an important contributor towards fibrosis in experimental models of renal injury (Ma et al., 2003; Oliver, 2002; Miyajima et al., 2000). During experimental obstructive nephropathy in this study, C3 enhanced TGF-β gene expression, which was most likely to have contributed towards the accumulation of activated myofibroblasts and interstitial deposition of collagen. Coinciding with C3-mediated activation and expression of TGF-β, collagen I and α-SMA mRNA expression were also increased after ten days of UUO in this study.

In addition to the documented changes in TGF-β mRNA expression in the present study, it would be interesting to measure TGF-β protein in obstructed renal tissues and urine and also TGF-β receptor expression within the renal cortices of UUO kidneys. T cells and macrophages can produce and activate TGF-β however $CD4^+$ T cell numbers were unchanged in the absence of C3. It could be that intrinsic renal cells are the main source of TGF-β during UUO, since elevated numbers of $CD8^+$ T cells and macrophages did not enhance TGF-β gene expression in the absence of C3. Although the gene expression patterns of collagen III were determined in this study, the presence and expression of other ECM proteins such as fibronectin, heparin sulphate and laminins was not explored. In addition to this, the activities of other growth factors such as platelet-derived growth factor, fibroblast growth factor and hepatocyte growth factor were not measured in this study, however previous work in this field has demonstrated activity of numerous growth factors in other animal models of renal disease (Matsumoto and Nakamura, 2001; Creely et al., 1990).

Quite unexpectedly and in contrast to the decrease in TGF-β, collagen I and α-SMA expression, the number of $CD8^+$ T cells and $F4/80^+$ macrophages counted in $C3^{-/-}$ mouse kidneys was significantly higher compared to those counted in WT mouse renal cortices. The exploration of different macrophage phenotypes was beyond the scope of this study however, it is plausible that the increase in $F4/80^+$ macrophages is due to a predominant expression of one phenotype and that complement expression influences macrophage phenotype to some degree during experimental obstructive nephropathy. An environment containing a higher number of cells which are responsible for the phagocytosis and subsequent removal of damaged cells may also reduce the inflammatory response and ensuing fibrosis that is characteristic of tubulointerstitial renal injury.

The presence of more $CD8^+$ T cells in the absence of C3 would suggest that $CD8^+$ T cells are not contributing towards fibrosis during obstructive nephropathy and that activation of complement might actually be regulating the trafficking or the proliferation of $CD8^+$ T cells during UUO. TNF-α and collagen III gene expression were also unusually high in $C3^{-/-}$ day ten UUO mouse kidneys compared with WT mice. One possible explanation for this could be that expression of collagen III in the absence of C3 is either dependent upon or controlled by TNF-α. This observation has not been reported elsewhere and additional work would be required to prove this theory. Another reason for the unexpected observations for TNF-α and collagen III gene expression in the C3 UUO study and the reduced expression of TNF-α, TGF-β and collagen I in the nfκb1 UUO study compared to the C3 UUO study could be due to minor alterations in mRNA expression for the housekeeping gene β-actin during renal fibrosis. Although no obvious differences were visualised by agarose gel electrophoresis resolution of rtPCR products, a better strategy for the future might be to implement the screening of multiple housekeeping genes in order to compare the expression of genes of interest to the average mRNA expression of a few different housekeeping genes.

The preliminary *in vitro* work using mouse PTECs presented in this thesis forms the basis for future work involving antisense silencing of C3 gene expression, but will need to be repeated in the future for the purpose of further optimisation and testing of candidate antisense oligonucleotides prior to any *in vivo* applications in the UUO mouse model. In the clinical setting, total inhibition of complement activation could predispose to infection and immune complex disease.

However, if tubular epithelial cells were the primary site of C3 production during ureteric obstruction, a strategy for inhibiting renal C3 synthesis could be used therapeutically in the future to delay the onset of ESRD. Aside from Boor and co-workers' demonstration of terminal complement pathway activation during UUO, the role of complement during ureteric obstruction remains relatively uncharacterised at the present time. Following on from this thesis, there is still much work to be done to begin to piece together a picture of the complement system's involvement during obstructive nephropathy.

The contribution of C3 during the development of injury following ureteric obstruction has been demonstrated in this thesis, but despite previous reports of TNF-α and ANG II mediated NF-κB activity in animal models of ureteric obstruction, the NF-κB subunit nfκb1 did not influence disease expression during UUO as measured within the parameters set out in this study (Guo et al., 2001; Satoh et al., 2001). This finding contrasted with a recent study of liver fibrosis by Oakley and co-workers, in which nfκb1 (p50) was shown to limit the amount of injury mediated by TNF-α dependent recruitment of inflammatory cells in the carbon tetrachloride model of chronic liver fibrosis (Oakley et al., 2005). It is interesting to note that this particular model of chronic hepatic fibrosis is neutrophil-driven, as is the NTS model of acute renal injury. Perhaps the nfκb1 subunit is specifically concerned with the mediation of neutrophil chemotaxis and activation as well as regulating the production of neutrophil-derived cytokines and signalling during inflammation. Future work could address this hypothesis by investigating the role of the nfκb1 subunit in other well characterised models of neutrophil-mediated injury in the kidney, for example, renal IRI.

nfκb1 does not contribute towards injury in the UUO model at the time points measured in this thesis however; it is possible that other NF-κB subunits play a more dominant role in macrophage and T cell mediated inflammation, or that the activities of different subunits dominate at distinct times during the development of injury in this particular model. The contribution of individual NF-κB subunits towards injury in the UUO model could be explored further using mice deficient in other NF-κB subunits, for example RelA. If resolution from injury was another factor mediated by nfκb1 signalling, then this could be investigated using a surgical technique to re-implant the ureter after a defined number of days of ureteric obstruction.

nfκb1 contributed towards the resolution of injury as demonstrated in the NTS nephritis model in the latter part of this study. Data from the final chapter of this thesis supports previous studies which have shown that the NF-κB subunit nfκb1 plays an important role in mediating the recovery from renal injury during NTS nephritis (Panzer et al., 2009; Kim et al., 2004; Sakurai et al., 1996). This further supports the idea of nfκb1 being associated with exerting anti-inflammatory activity during the resolution of injury and was demonstrated in this study. nfκb1 prevented the persistent up-regulation of gene expression of the pro-inflammatory mediators IL-6, TNF-α, S100A8 and S100A9. In the presence of nfκb1, proteinuria and glomerular injury were also reduced. Following on from the preliminary NTS nephritis model data presented in this thesis, ongoing work in the lab is now addressing the relative contributions of both intrinsic renal cells and infiltrating cells using bone marrow chimeric mice.

Although NF-κB inhibitors and antioxidant compounds have been used experimentally to ameliorate NF-κB activity in various disease models, a clearer understanding of the role of specific NF-κB subunits and the mechanisms by which they become activated during disease states, may provide more suitable targets for future therapies.

The present study focused on the individual contributions of complement component C3 during UUO and nfκb1 during the progression of UUO and NTS nephritis however, there is increasing evidence to suggest that NF-κB signalling may actually regulate complement activation. In a recent study, Gancz and colleagues used mouse embryonic fibroblasts prepared from RelA and IKKα deficient mice to demonstrate that the NF-κB pathway promoted cell survival by contributing towards cell resistance to C5b-9 induced injury (Gancz et al., 2012). The authors speculated that their findings suggested crosstalk between NF-κB and c-jun terminal kinase (JNK) pathways and that NF-κB signalling may either directly activate the synthesis of C5b-9 elimination proteins or counteract the damaging effects of C5b-9. Prior to their 2012 study, the lead author had also demonstrated that JNK participated during the MAC-induced signalling cascade, resulting in rapid necrotic cell injury (Gancz et al., 2009).

Cancer resistance to complement-dependent cytotoxicity was reviewed by Gancz and Fishelson around the same time (Gancz and Fishelson, 2009). The significance of this review is two-fold; firstly, NF-κB signalling has been shown previously to occur during periods of chronic inflammation which precede the development of cancer and secondly, NF-κB stimulates the expression of anti-apoptotic factors promoting tumour cell survival (Karin, 2006; Mann and Oakley, 2005).

With this in mind, it would be interesting to expand upon the role of the terminal complement pathway during UUO, by looking at cell surface expression of C5b-9 and other complement regulatory proteins. In addition, NF-κB signalling mediated by different NF-κB subunits in the presence and absence of C3 could be measured.

Data from this thesis suggests that the specific targeting of locally produced C3 and individual NF-κB subunits may potentially provide effective therapeutic strategies for reducing renal injury and delaying the progression to ESRD in the future.

7 Abstracts

7.1 Publications

Fearn A, Fox C, Wilson C, O'Boyle G, Oakley F, Mann D, Robson M and Sheerin NS: **NFκB1 is protective against acute but not chronic inflammatory renal disease.** Manuscript in preparation

Fearn A, Lisgo, S and Sheerin NS: **Complement C3 contributes towards tubulointerstitial fibrosis during ureteric obstruction.** Manuscript in preparation

7.2 Abstracts

Fearn A, Fox C, Wilson C, O'Boyle G, Oakley F, Mann D, Robson M and Sheerin NS: **NFκB1 is protective against acute but not inflammatory renal disease.** Oral presentation at the Renal Association Annual Meeting, Newcastle-Gateshead, UK, June 2012.

Fearn A, Sheerin NS: **Complement activation drives interstitial inflammation and fibrosis in models of kidney disease.** Poster presentation at the Creative Advances in Fibrosis Therapy (CRAFT) Symposium, UK, November 2011.

Fearn A, Lisgo S, Darby S and Sheerin NS: **The influence of complement activation on chronic renal inflammation and fibrosis.** Poster presentation at the 13th Annual European Meeting on Complement in Human Disease, Netherlands, August 2011.

Fearn A, Lisgo S, Darby S, and Sheerin NS: **The influence of complement activation on chronic renal inflammation and fibrosis.** Poster presentation at the Renal Association Annual Meeting, Birmingham, UK, June 2011.

Fearn A, Oakley F, Mann D Sheerin NS: **Tubulointerstitial inflammation and fibrosis is not influenced by deficiency of the regulatory transcription factor NFκB1**. Poster presentation at the Renal Association Annual Meeting, Liverpool, UK, April 2009.

8 Bibliography

Abbott, F., Ryan, J. J., Ceska, M., Matsushima, K., Sarraf, C. E. and Rees, A. J. (1991) 'Interleukin-1-Beta Stimulates Human Mesangial Cells to Synthesize and Release Interleukin-6 and Interleukin-8', *Kidney International,* 40, (4), pp. 597-605.

Anderson, J. and Glynn, L. G. (2011) 'Definition of chronic kidney disease and measurement of kidney function in original research papers: a review of the literature', *Nephrology Dialysis Transplantation,* 26, (9), pp. 2793-U1503.

Atkinson, J. P. (1988) 'COMPLEMENT DEFICIENCY - PREDISPOSING FACTOR TO AUTOIMMUNE SYNDROMES', *American Journal of Medicine,* 85, (6A), pp. 45-47.

Bao, L. H., Spiller, O. B., St John, P. L., Haas, M., Hack, B. K., Ren, G. H., Cunningham, P. N., Doshi, M., Abrahamson, D. R., Morgan, B. P. and Quigg, R. J. (2002) 'Decay-accelerating factor expression in the rat kidney is restricted to the apical surface of podocytes', *Kidney International,* 62, (6), pp. 2010-2021.

Blobe, G. C., Schiemann, W. P. and Lodish, H. F. (2000) 'Mechanisms of disease: Role of transforming growth factor beta in human disease', *New England Journal of Medicine,* 342, (18), pp. 1350-1358.

Bonizzi, G. and Karin, M. (2004) 'The two NF-kappa B activation pathways and their role in innate and adaptive immunity', *Trends in Immunology,* 25, (6), pp. 280-288.

Boor, P., Konieczny, A., Villa, L., Schult, A. L., Bucher, E., Rong, S., Kunter, U., van Roeyen, C. R. C., Polakowski, T., Hawlisch, H., Hillebrandt, S., Lammert, F., Eitner, F., Floege, J. and Ostendorf, T. (2007) 'Complement C5 mediates experimental tubulointerstitial fibrosis', *Journal of the American Society of Nephrology,* 18, (5), pp. 1508-1515.

Bottinger, E. P. and Bitzer, M. (2002) 'TGF-beta signaling in renal disease', *Journal of the American Society of Nephrology,* 13, (10), pp. 2600-2610.

Brooimans, R. A., Stegmann, A. P. A., Vandorp, W. T., Vanderark, A. A. J., Vanderwoude, F. J., Vanes, L. A. and Daha, M. R. (1991) 'INTERLEUKIN-2 MEDIATES STIMULATION OF COMPLEMENT-C3 BIOSYNTHESIS IN HUMAN PROXIMAL TUBULAR EPITHELIAL-CELLS', *Journal of Clinical Investigation,* 88, (2), pp. 379-384.

Bucala, R., Spiegel, L. A., Chesney, J., Hogan, M. and Cerami, A. (1994) 'Circulating Fibrocytes Define a New Leukocyte Subpopulation That Mediates Tissue-Repair', *Molecular Medicine,* 1, (1), pp. 71-81.

Buraczynska, M., Jozwiak, L., Ksiazek, P., Borowicz, E. and Mierzicki, P. (2007) 'Interleukin-6 gene polymorphism and faster progression to end-stage renal failure in chronic glomerulonephritis', *Translational Research,* 150, (2), pp. 101-105.

Carroll, M. C. (2004) 'The complement system in regulation of adaptive immunity', *Nature Immunology,* 5, (10), pp. 981-986.

Caskey, F., Dawnay, A., Farrington, K., Feest, T., Fogarty, D., Inward, C. and Tomson, C. R. V. (2011) *Nephron Clinical Practice.* Bristol, UK: UK Renal Registry (13).

Chen, F., Castranova, V. and Shi, X. L. (2001) 'New insights into the role of nuclear factor-kappa B in cell growth regulation', *American Journal of Pathology,* 159, (2), pp. 387-397.

Chen, S. M., Mukoyama, T., Sato, N., Yamagata, S. I., Arai, Y., Satoh, N. and Ueda, S. (2002) 'Induction of nephrotoxic serum nephritis in inbred mice and suppressive effect of colchicine on the development of this nephritis', *Pharmacological Research,* 45, (4), pp. 319-324.

Cirillo, M. (2010) 'Evaluation of glomerular filtration rate and of albuminuria/proteinuria', *Journal of Nephrology,* 23, (2), pp. 125-132.

Creely, J. J., Dimari, S. J., Howe, A. M., Hyde, C. P. and Haralson, M. A. (1990) 'Effects of Epidermal Growth-Factor on Collagen-Synthesis by an Epithelioid Cell-Line Derived from Normal Rat-Kidney', *American Journal of Pathology,* 136, (6), pp. 1247-1257.

Daha, M. R. and van Kooten, C. (2000) 'Is there a role for locally produced complement in renal disease?' *Nephrology Dialysis Transplantation,* 15, (10), pp. 1506-1509.

Dendooven, A., Ishola, D. A., Nguyen, T. Q., Van der Giezen, D. M., Kok, R. J., Goldschmeding, R. and Joles, J. A. (2010) 'Oxidative stress in obstructive nephropathy', *International Journal of Experimental Pathology,* 92, (3), pp. 202-210.

Dinh, D. T., Frauman, A. G., Johnston, C. I. and Fabiani, M. E. (2001) 'Angiotensin receptors: distribution, signalling and function', *Clinical Science,* 100, (5), pp. 481-492.

Eggers, K., Sikora, K., Lorenz, M., Taubert, T., Moobed, M., Baumann, G., Stangl, K. and Stangl, V. (2011) 'RAGE-Dependent Regulation of Calcium-Binding Proteins S100A8 and S100A9 in Human THP-1', *Experimental and Clinical Endocrinology & Diabetes,* 119, (6), pp. 353-357.

Ehlenberger, A. G. and Nussenzweig, V. (1977) 'ROLE OF MEMBRANE RECEPTORS FOR C3B AND C3D IN PHAGOCYTOSIS', *Journal of Experimental Medicine,* 145, (2), pp. 357-371.

Ehlermann, P., Eggers, K., Bierhaus, A., Most, P., Weichenhan, D., Greten, J., Nawroth, P. P., Katus, H. A. and Remppis, A. (2006) 'Increased proinflammatory endothelial response to S100A8/A9 after preactivation through advanced glycation end products', *Cardiovascular Diabetology,* 5, pp. 9.

Eitner, F., Westerhuis, R., Burg, M., Weinhold, B., Grone, H. J., Ostendorf, T., Ruther, U., Koch, K. M., Rees, A. J. and Floege, J. (1997) 'Role of interleukin-6 in mediating mesangial cell proliferation and matrix production in vivo', *Kidney International,* 51, (1), pp. 69-78.

Esteban, V., Lorenzo, O., Ruperez, M., Suzuki, Y., Mezzano, S., Blanco, J., Kretzler, M., Sugaya, T., Egido, J. and Ruiz-Ortega, M. (2004) 'Angiotensin II, via AT(1) and AT(2) receptors and NF-kappa B pathway, regulates the inflammatory response in unilateral ureteral obstruction', *Journal of the American Society of Nephrology,* 15, (6), pp. 1514-1529.

Fischer, M. B., Goerg, S., Shen, L. M., Prodeus, A. P., Goodnow, C. C., Kelsoe, G. and Carroll, M. C. (1998) 'Dependence of germinal center B cells on expression of CD21/CD35 for survival', *Science,* 280, (5363), pp. 582-585.

Foley, S., Li, B., Dehoff, M., Molina, H. and Holers, V. M. (1993) 'Mouse Crry/P65 Is a Regulator of the Alternative Pathway of Complement Activation', *European Journal of Immunology,* 23, (6), pp. 1381-1384.

Frank, M. M. and Fries, L. F. (1991) 'THE ROLE OF COMPLEMENT IN INFLAMMATION AND PHAGOCYTOSIS', *Immunology Today,* 12, (9), pp. 322-326.

Fu, Y. Y., Xie, C., Chen, J. L., Zhu, J. K., Zhou, H., Thomas, J., Zhou, X. J. and Mohan, C. (2006) 'Innate stimuli accentuate end-organ damage by nephrotoxic antibodies via Fc receptor and TLR stimulation and IL-1/TNF-alpha production', *Journal of Immunology,* 176, (1), pp. 632-639.

Gancz, D., Donin, N. and Fishelson, Z. (2009) 'Involvement of the c-jun N-terminal kinases JNK1 and JNK2 in complement-mediated cell death', *Molecular Immunology,* 47, (2-3), pp. 310-317.

Gancz, D. and Fishelson, Z. (2009) 'Cancer resistance to complement-dependent cytotoxicity (CDC): Problem-oriented research and development', *Molecular Immunology,* 46, (14), pp. 2794-2800.

Gancz, D., Lusthaus, M. and Fishelson, Z. (2012) 'A Role for the NF-kappa B Pathway in Cell Protection from Complement-Dependent Cytotoxicity', *Journal of Immunology,* 189, (2), pp. 860-866.

Gebhardt, C., Nemeth, J., Angel, P. and Hess, J. (2006) 'S100A8 and S100A9 in inflammation and cancer', *Biochemical Pharmacology,* 72, (11), pp. 1622-1631.

Ghosh, S., May, M. J. and Kopp, E. B. (1998) 'NF-kappa B and rel proteins: Evolutionarily conserved mediators of immune responses', *Annual Review of Immunology,* 16, pp. 225-260.

Gilmore, T. D. (2006) 'Introduction to NF-kappa B: players, pathways, perspectives', *Oncogene,* 25, (51), pp. 6680-6684.

Grande, M. T., Perez-Barriocanal, F. and Lopez-Novoa, J. M. (2010) 'Role of inflammation in tubulo-interstitial damage associated to obstructive nephropathy', *Journal of Inflammation-London,* 7, pp. 14.

Grygielko, E. T., Martin, W. M., Tweed, C., Thornton, P., Harling, J., Brooks, D. P. and Laping, N. J. (2005) 'Inhibition of gene markers of fibrosis with a novel inhibitor of transforming growth factor-beta type I receptor kinase in puromycin-induced nephritis', *Journal of Pharmacology and Experimental Therapeutics,* 313, (3), pp. 943-951.

Guijarro, C. and Egido, J. (2001) 'Transcription factor-kappa B (NF-kappa B) and renal disease', *Kidney International,* 59, (2), pp. 415-424.

Guo, G. J., Morrissey, J., McCracken, R., Tolley, T. and Klahr, S. (1999) 'Role of TNFR1 and TNFR2 receptors in tubulointerstitial fibrosis of obstructive nephropathy', *American Journal of Physiology-Renal Physiology,* 277, (5), pp. F766-F772.

Guo, G. J., Morrissey, J., McCracken, R., Tolley, T., Liapis, H. and Klahr, S. (2001) 'Contributions of angiotensin II and tumor necrosis factor-alpha to the development of renal fibrosis', *American Journal of Physiology-Renal Physiology,* 280, (5), pp. F777-F785.

Guzik, T. J. and Harrison, D. G. (2007) 'Endothelial NF-kappa B as a mediator of kidney damage the missing link between systemic vascular and renal disease?' *Circulation Research,* 101, (3), pp. 227-229.

Harris, R. C. and Neilson, E. G. (2006) 'Toward a unified theory of renal progression', *Annual Review of Medicine,* 57, pp. 365-380.

Hayden, M. S. and Ghosh, S. (2004) 'Signaling to NF-kappa B', *Genes & Development,* 18, (18), pp. 2195-2224.

Hayden, M. S. and Ghosh, S. (2008) 'Shared principles in NF-kappa B signaling', *Cell,* 132, (3), pp. 344-362.

Hebert, M. J., Takano, T., Papayianni, A., Rennke, H. G., Minto, A., Salant, D. J., Carroll, M. C. and Brady, H. R. (1998) 'Acute nephrotoxic serum nephritis in complement knockout mice: relative roles of the classical and alternate pathways in neutrophil recruitment and proteinuria', *Nephrology Dialysis Transplantation,* 13, (11), pp. 2799-2803.

Henke, N., Schmidt-Ullrich, R., Dechend, R., Park, J. K., Qadri, F., Wellner, M., Obst, M., Gross, V., Dietz, R., Luft, F. C., Scheidereit, C. and Muller, D. N. (2007) 'Vascular endothelial cell-specific NF-kappa B suppression attenuates hypertension-induced renal damage', *Circulation Research,* 101, (3), pp. 268-276.

Hruby, Z. W., Cybulsky, A. V. and Lowry, R. P. (1990) 'Effects of Tumor-Necrosis-Factor on Glomerular Mesangial and Epithelial-Cells in Culture', *Nephron,* 56, (4), pp. 410-413.

Hsu, S. I. H. and Couser, W. G. (2003) 'Chronic progression of tubulointerstitial damage in proteinuric renal disease is mediated by complement activation: A therapeutic role for complement inhibitors?' *Journal of the American Society of Nephrology,* 14, (7), pp. S186-S191.

Ichida, S., Yuzawa, Y., Okada, H., Yoshioka, K. and Matsuo, S. (1994) 'Localization of the Complement Regulatory Proteins in the Normal Human Kidney', *Kidney International,* 46, (1), pp. 89-96.

Ikemoto, M., Murayama, H., Itoh, H., Totani, M. and Fujita, M. (2007) 'Intrinsic function of S100A8/A9 complex as an anti-inflammatory protein in liver injury induced by lipopolysaccharide in rats', *Clinica Chimica Acta,* 376, (1-2), pp. 197-204.

Ishidoya, S., Morrissey, J., McCracken, R. and Klahr, S. (1996) 'Delayed treatment with enalapril halts tubulointerstitial fibrosis in rats with obstructive nephropathy', *Kidney International,* 49, (4), pp. 1110-1119.

Iwano, M. and Neilson, E. G. (2004) 'Mechanisms of tubulointerstitial fibrosis', *Current Opinion in Nephrology and Hypertension,* 13, (3), pp. 279-284.

Iwano, M., Plieth, D., Danoff, T. M., Xue, C., Okada, H. and Neilson, E. G. (2002) 'Evidence that fibroblasts derive from epithelium during tissue fibrosis', *Journal of Clinical Investigation,* 110, (3), pp. 341-350.

Jacquiersarlin, M. R., Gabert, F. M., Villiers, M. B. and Colomb, M. G. (1995) 'MODULATION OF ANTIGEN-PROCESSING AND PRESENTATION BY COVALENTLY-LINKED COMPLEMENT C3B FRAGMENT', *Immunology,* 84, (1), pp. 164-170.

Kaneto, H., Morrissey, J., McCracken, R., Reyes, A. and Klahr, S. (1994) 'Enalapril Reduces Collagen Type-Iv Synthesis and Expansion of the Interstitium in the Obstructed Rat-Kidney', *Kidney International,* 45, (6), pp. 1637-1647.

Kaneto, H., Ohtani, H., Fukuzaki, A., Ishidoya, S., Takeda, A., Ogata, Y., Nagura, H. and Orikasa, S. (1999) 'Increased expression of TGF-beta 1 but not of its receptors contributes to human obstructive nephropathy', *Kidney International,* 56, (6), pp. 2137-2146.

Karin, M. (2006) 'Nuclear factor-kappa B in cancer development and progression', *Nature*, 441, (7092), pp. 431-436.

Karin, M. and Delhase, M. (2000) 'The I kappa B kinase (IKK) and NF-kappa B: key elements of proinflammatory signalling', *Seminars in Immunology,* 12, (1), pp. 85-98.

Kayama, F., Yoshida, T., Kodama, Y., Matsui, T., Matheson, J. M. and Luster, M. I. (1997) 'Pro-inflammatory cytokines and interleukin 6 in the renal response to bacterial endotoxin', *Cytokine,* 9, (9), pp. 688-695.

Khalil, K. I., Shokeir, A. A., Wafa, E. W., Gad, G. E., Helmy, S. A., Nour, E. M. and Sarhan, M. (2012) 'Renoprotection against complete unilateral ureteric obstruction: Is there an ultimate choise?' *Arab Journal of Urology*, 10, pp. 199-206.

Khan, S. B., Cook, H. T., Bhangal, G., Smith, J., Tam, F. W. K. and Pusey, C. D. (2005) 'Antibody blockade of TNF-alpha reduces inflammation and scarring in experimental crescentic glomerulonephritis', *Kidney International,* 67, (5), pp. 1812-1820.

Kielar, M. L., John, R., Bennett, M., Richardson, J. A., Shelton, J. M., Chen, L. Y., Jeyarajah, D. R., Zhou, X. J., Zhou, H., Chiquett, B., Nagami, G. T. and Lu, C. Y. (2005) 'Maladaptive role of IL-6 in ischemic acute renal failure', *Journal of the American Society of Nephrology,* 16, (11), pp. 3315-3325.

Kim, J. H., Ha, I. S., Hwang, C. I., Lee, Y. J., Kim, J., Yang, S. H., Kim, Y. S., Cao, Y. A., Choi, S. and Park, W. Y. (2004) 'Gene expression profiling of anti-GBM glomerulonephritis model: The role of NF-kappa B in immune complex kidney disease', *Kidney International,* 66, (5), pp. 1826-1837.

Kim, J. H., Oh, S. H., Kim, E. J., Park, S. J., Hong, S. P., Cheon, J. H., Kim, T. I. and Kim, W. H. (2012) 'The role of myofibroblasts in upregulation of S100A8 and A9 and the differentiation of myeloid cells in the colorectal cancer microenvironment', *Biochemical and Biophysical Research Communications,* 423, (1), pp. 60-66.

Klahr, S. (2000) 'Obstructive nephropathy', *Internal Medicine,* 39, (5), pp. 355-361.

Klahr, S. and Morrissey, J. (2002a) 'Comparative effects of ACE inhibition and angiotensin II receptor blockade in the prevention of renal damage', *Kidney International,* 62, pp. S23-S26.

Klahr, S. and Morrissey, J. (2002b) 'Obstructive nephropathy and renal fibrosis', *American Journal of Physiology-Renal Physiology,* 283, (5), pp. F861-F875.

Klahr, S. and Morrissey, J. J. (1998) 'The role of growth factors, cytokines, and vasoactive compounds in obstructive nephropathy', *Seminars in Nephrology,* 18, (6), pp. 622-632.

Klahr, S. and Purkerson, M. L. (1994) 'THE PATHOPHYSIOLOGY OF OBSTRUCTIVE NEPHROPATHY - THE ROLE OF VASOACTIVE COMPOUNDS IN THE HEMODYNAMIC AND STRUCTURAL ABNORMALITIES OF THE OBSTRUCTED KIDNEY', *American Journal of Kidney Diseases,* 23, (2), pp. 219-223.

Kriz, W., Gretz, N. and Lemley, K. V. (1998) 'Progression of glomerular diseases: Is the podocyte the culprit?' *Kidney International,* 54, (3), pp. 687-697.

Kucharczak, J., Simmons, M. J., Fan, Y. J. and Gelinas, C. (2003) 'To be, or not to be: NF-kappa B is the answer - role of Rel/NF-kappa B in the regulation of apoptosis', *Oncogene,* 22, (56), pp. 8961-8982.

Kuncio, G. S., Neilson, E. G. and Haverty, T. (1991) 'Mechanisms of Tubulointerstitial Fibrosis', *Kidney International,* 39, (3), pp. 550-556.

Kurts, C., Heymann, F., Lukacs-Kornek, V., Boor, P. and Floege, J. (2007) 'Role of T cells and dendritic cells in glomerular immunopathology', *Seminars in Immunopathology,* 29, (4), pp. 317-335.

Kusner, D. J., Luebbers, E. L., Nowinski, R. J., Konieczkowski, M., King, C. H. and Sedor, J. R. (1991) 'Cytokine-Induced and Lps-Induced Synthesis of Interleukin-8 from Human Mesangial Cells', *Kidney International,* 39, (6), pp. 1240-1248.

Lange-Sperandio, B., Cachat, F., Thornhill, B. A. and Chevalier, R. L. (2002) 'Selectins mediate macrophage infiltration in obstructive nephropathy in newborn mice', *Kidney International,* 61, (2), pp. 516-524.

Lawrence, T. and Fong, C. (2010) 'The resolution of inflammation: Anti-inflammatory roles for NF-kappa B', *International Journal of Biochemistry & Cell Biology,* 42, (4), pp. 519-523.

Lawrence, T., Gilroy, D. W., Colville-Nash, P. R. and Willoughby, D. A. (2001) 'Possible new role for NF-kappa B in the resolution of inflammation', *Nature Medicine,* 7, (12), pp. 1291-1297.

Lemley, K. V. and Kriz, W. (1991) 'Anatomy of the Renal Interstitium', *Kidney International,* 39, (3), pp. 370-381.

Lesher, A. M. and Song, W. C. (2010) 'Review: Complement and its regulatory proteins in kidney diseases', *Nephrology,* 15, (7), pp. 663-675.

Levey, A. S., Astor, B. C., Stevens, L. A. and Coresh, J. (2010) 'Chronic kidney disease, diabetes, and hypertension: what's in a name?' *Kidney International,* 78, (1), pp. 19-22.

Levey, A. S. and Coresh, J. (2012) 'Chronic kidney disease', *Lancet,* 379, (9811), pp. 165-180.

Li, B., Sallee, C., Dehoff, M., Foley, S., Molina, H. and Holers, V. M. (1993) 'Mouse Crry/P65 - Characterization of Monoclonal-Antibodies and the Tissue Distribution of a Functional Homolog of Human Mcp and Daf', *Journal of Immunology,* 151, (8), pp. 4295-4305.

Lien, Y. H. H., Lai, L. W. and Silva, A. L. (2003) 'Pathogenesis of renal ischemia/reperfusion injury: lessons from knockout mice', *Life Sciences,* 74, (5), pp. 543-552.

Lin, F., Emancipator, S. N., Salant, D. J. and Medof, M. E. (2002) 'Decay-accelerating factor confers protection against complement-mediated podocyte injury in acute nephrotoxic nephritis', *Laboratory Investigation,* 82, (5), pp. 563-569.

Lin, F., Salant, D. J., Meyerson, H., Emancipator, S., Morgan, B. P. and Medof, M. E. (2004) 'Respective roles of decay-accelerating factor and CD59 in circumventing glomerular injury in acute nephrotoxic serum nephritis', *Journal of Immunology,* 172, (4), pp. 2636-2642.

Liszewski, M. K., Farries, T. C., Lublin, D. M., Rooney, I. A. and Atkinson, J. P. (1996) 'Control of the complement system', in *Advances in Immunology, Vol 61.* Vol. 61 San Diego: Academic Press Inc, pp. 201-283.

Ma, L. J., Yang, H. C., Gaspert, A., Carlesso, G., Barty, M. M., Davidson, J. M., Sheppard, D. and Fogo, A. B. (2003) 'Transforming growth factor-b-dependent and -independent pathways of induction of tubulointerstitial fibrosis in beta 6-/- mice', *American Journal of Pathology,* 163, (4), pp. 1261-1273.

Mann, D. A. and Oakley, F. (2005) 'NF-kappa B: a signal for cancer', *Journal of Hepatology,* 42, (4), pp. 610-611.

Marsh, J. E., Zhou, W. D. and Sacks, S. H. (2001) 'Local tissue complement synthesis - Fine tuning a blunt instrument', *Archivum Immunologiae Et Therapiae Experimentalis,* 49, pp. S41-S46.

Massy, Z. A., Guijarro, C., O'Donnell, M. P., Kim, Y. K., Kashtan, C. E., Egido, J., Kasiske, B. L. and Keane, W. F. (1999) 'The central role of nuclear factor-kappa B in mesangial cell activation', *Kidney International,* 56, pp. S76-S79.

Matsumoto, K. and Nakamura, T. (2001) 'Hepatocyte growth factor: Renotropic role and potential therapeutics for renal diseases', *Kidney International,* 59, (6), pp. 2023-2038.

Misseri, R., Meldrum, D. R., Dinarello, C. A., Dagher, P., Hile, K. L., Rink, R. C. and Meldrum, K. K. (2005) 'TNF-alpha mediates obstruction-induced renal tubular cell apoptosis and proapoptotic signaling', *American Journal of Physiology-Renal Physiology,* 288, (2), pp. F406-F411.

Misseri, R. and Meldrum, K. K. (2005) 'Mediators of Fibrosis and Apoptosis in obstructive Uropathies', *Current Urology Reports,* 6, pp. 140-145.

Miyajima, A., Chen, J., Lawrence, C., Ledbetter, S., Soslow, R. A., Stern, J., Jha, S., Pigato, J., Lemer, M. L., Poppas, D. P., Vaughan, E. D. and Felsen, D. (2000) 'Antibody to transforming growth factor-beta ameliorates tubular apoptosis in unilateral ureteral obstruction', *Kidney International,* 58, (6), pp. 2301-2313.

Moon, J. A., Kim, H. T., Cho, I. S., Sheen, Y. Y. and Kim, D. K. (2006) 'IN-1130, a novel transforming growth factor-beta type I receptor kinase (ALK5) inhibitor, suppresses renal fibrosis in obstructive nephropathy', *Kidney International,* 70, (7), pp. 1234-1243.

Morgan, B. P. and Walport, M. J. (1991) 'COMPLEMENT DEFICIENCY AND DISEASE', *Immunology Today,* 12, (9), pp. 301-306.

Morris, K. M., Aden, D. P., Knowles, B. B. and Colten, H. R. (1982) 'COMPLEMENT BIOSYNTHESIS BY THE HUMAN HEPATOMA-DERIVED CELL-LINE HEPG2', *Journal of Clinical Investigation,* 70, (4), pp. 906-913.

Morrissey, J. J. and Klahr, S. (1997) 'Enalapril decreases nuclear factor kappa B activation in the kidney with ureteral obstruction', *Kidney International,* 52, (4), pp. 926-933.

Muller, D. N., Dechend, R., Mervaala, E. M. A., Park, J. K., Schmidt, F., Fiebeler, A., Theuer, J., Breu, V., Ganten, D., Haller, H. and Luft, F. C. (2000a) 'NF-kappa B inhibition ameliorates angiotensin II-induced inflammatory damage in rats', *Hypertension,* 35, (1), pp. 193-201.

Muller, G. A., Zeisberg, M. and Strutz, F. (2000b) 'The importance of tubulointerstitial damage in progressive renal disease', *Nephrology Dialysis Transplantation,* 15, pp. 76-77.

Nakatani, T., Tamada, S., Asai, T., Iwai, Y., Kim, T., Tsujino, T., Kumata, N., Uchida, J., Tashiro, K., Kuwabara, N., Komiya, T., Sumi, T., Okamura, M. and Miura, K. (2002) 'Role of renin-angiotensin system and nuclear factor-kappa B in the obstructed kidney of rats with unilateral ureteral obstruction', *Japanese Journal of Pharmacology,* 90, (4), pp. 361-364.

Nangaku, M. (2004) 'Mechanisms of tubulointerstitial injury in the kidney: Final common pathways to end-stage renal failure', *Internal Medicine,* 43, (1), pp. 9-17.

Naughton, M., Botto, M., Carter, M., Alexander, G., Goldman, J. and Walport, M. J. (1996) 'Extrahepatic secreted complement C3 contributes to circulating C3 levels in humans', *British Journal of Rheumatology,* 35, (ABSTR. SUPPL. 1), pp. 66.

Nielsen, C. H., Fischer, E. M. and Leslie, R. G. Q. (2000) 'The role of complement in the acquired immune response', *Immunology,* 100, (1), pp. 4-12.

Oakley, F., Mann, J., Nailard, S., Smart, D. E., Mungalsingh, N., Constandinou, C., Ali, S., Wilson, S. J., Millward-Sadler, H., Iredale, J. P. and Mann, D. A. (2005) 'Nuclear factor-kappa beta 1 (p50) limits the inflammatory and fibrogenic responses to chronic injury', *American Journal of Pathology,* 166, (3), pp. 695-708.

Oliver, J. A. (2002) 'Unexpected news in renal fibrosis', *Journal of Clinical Investigation,* 110, (12), pp. 1763-1764.

Panzer, U., Steinmetz, O. M., Turner, J. E., Meyer-Schwesinger, C., von Ruffer, C., Meyer, T. N., Zahner, G., Gomez-Guerrero, C., Schmid, R. M., Helmchen, U., Moeckel, G. W., Wolf, G., Stahl, R. A. K. and Thaiss, F. (2009) 'Resolution of renal inflammation: a new role for NF-kappa B1 (p50) in inflammatory kidney diseases', *American Journal of Physiology-Renal Physiology,* 297, (2), pp. F429-F439.

Perkins, N. D. (2006) 'Post-translational modifications regulating the activity and function of the nuclear factor kappa B pathway', *Oncogene,* 25, (51), pp. 6717-6730.

Perkins, N. D. (2007) 'Integrating cell-signalling pathways with NF-kappa B and IKK function', *Nature Reviews Molecular Cell Biology,* 8, (1), pp. 49-62.

Perkins, N. D. and Gilmore, T. D. (2006) 'Good cop, bad cop: the different faces of NF-kappa B', *Cell Death and Differentiation,* 13, (5), pp. 759-772.

Picard, N., Baum, O., Vogetseder, A., Kaissling, B. and Le Hir, M. (2008) 'Origin of renal myofibroblasts in the model of unilateral ureter obstruction in the rat', *Histochemistry and Cell Biology,* 130, (1), pp. 141-155.

Pratt, J. R., Basheer, S. A. and Sacks, S. H. (2002) 'Local synthesis of complement component C3 regulates acute renal transplant rejection', *Nature Medicine,* 8, (6), pp. 582-587.

Pueyo, M. E., Gonzalez, W., Nicoletti, A., Savoie, F., Arnal, J. and Michel, J. (2000) 'Angiotensin II stimulates endothelial vascular cell adhesion molecule-1 via nuclear factor-κB activation induced by intracellular oxidative stress', *Arteriosclerosis Thrombosis and Vascular Biology,* 20, pp. 645-651.

Quigg, R. J. (2003) 'Complement and the kidney', *Journal of Immunology,* 171, (7), pp. 3319-3324.

Rangan, G. K., Pippin, J. W. and Couser, W. G. (2004) 'C5b-9 regulates peritubular myofibroblast accumulation in experimental focal segmental glomerulosclerosis', *Kidney International,* 66, (5), pp. 1838-1848.

Renner, B., Ferreira, V. P., Cortes, C., Goldberg, R., Ljubanovic, D., Pangburn, M. K., Pickering, M. C., Tomlinson, S., Holland-Neidermyer, A., Strassheim, D., Holers, V. M. and Thurman, J. M. (2011) 'Binding of factor H to tubular epithelial cells limits interstitial complement activation in ischemic injury', *Kidney International,* 80, (2), pp. 166-174.

Robertson, H., Ali, S., McDonnell, B. J., Burt, A. D. and Kirby, J. A. (2004) 'Chronic renal allograft dysfunction: The role of T cell-mediated tubular epithelial to mesenchymal cell transition', *Journal of the American Society of Nephrology,* 15, (2), pp. 390-397.

Ruiz-Ortega, M., Lorenzo, O., Ruperez, M. and Egido, J. (2000) 'ACE inhibitors and AT(1) receptor antagonists - beyond the haemodynamic effect', *Nephrology Dialysis Transplantation,* 15, (5), pp. 561-565.

Ruiz-Ortega, M., Lorenzo, O., Ruperez, M., Suzuki, Y. and Egido, J. (2001) 'Angiotensin II activates nuclear transcription factor-kappa B in aorta of normal rats and in vascular smooth muscle cells of AT(1) knockout mice', *Nephrology Dialysis Transplantation,* 16, pp. 27-33.

Ryffel, B., Eugster, H., Haas, C. and Le Hir, M. (1998) 'Failure to induce anti-glomerular basement membrane glomerulonephritis in TNF alpha/beta deficient mice', *International Journal of Experimental Pathology,* 79, (6), pp. 453-460.

Saccani, S., Marazzi, I., Beg, A. A. and Natoli, G. (2004) 'Degradation of promoter-bound p65/RelA is essential for the prompt termination of the nuclear factor kappa B response', *Journal of Experimental Medicine,* 200, (1), pp. 107-113.

Sacks, S. H., Zhou, W., Pani, A., Campbell, R. D. and Martin, J. (1993) 'COMPLEMENT C3 GENE-EXPRESSION AND REGULATION IN HUMAN GLOMERULAR EPITHELIAL-CELLS', *Immunology,* 79, (3), pp. 348-354.

Sakurai, H., Hisada, Y., Ueno, M., Sugiura, M., Kawashima, M. and Sugita, T. (1996) 'Activation of transcription factor NF-kappa B in experimental glomerulonephritis in rats', *Biochimica Et Biophysica Acta-Molecular Basis of Disease,* 1316, (2), pp. 132-138.

Sakurai, H., Shigemori, N., Hisada, Y., Ishizuka, T., Kawashima, K. and Sugita, T. (1997) 'Suppression of NF-kappa B and AP-1 activation by glucocorticoids in experimental glomerulonephritis in rats: molecular mechanisms of anti-nephritic action', *Biochimica Et Biophysica Acta-Molecular Basis of Disease,* 1362, (2-3), pp. 252-262.

Sanz, A. B., Sanchez-Nino, M. D., Ramos, A. M., Moreno, J. A., Santamaria, B., Ruiz-Ortega, M., Egido, J. and Ortiz, A. (2010) 'NF-kappa B in Renal Inflammation', *Journal of the American Society of Nephrology,* 21, (8), pp. 1254-1262.

Satoh, M., Kashihara, N., Yamasaki, Y., Maruyama, K., Okamoto, K., Maeshima, Y., Sugiyama, H., Sugaya, T., Murakami, K. and Makino, H. (2001) 'Renal interstitial fibrosis is reduced in angiotensin II type 1a receptor-deficient mice', *Journal of the American Society of Nephrology,* 12, (2), pp. 317-325.

Sha, W. C., Liou, H. C., Tuomanen, E. I. and Baltimore, D. (1995) 'Targeted Disruption of the P50 Subunit of Nf-Kappa-B Leads to Multifocal Defects in Immune-Responses', *Cell,* 80, (2), pp. 321-330.

Sheerin, N. S., Risley, P., Abe, K., Tang, Z. Y., Wong, W. L., Lin, T. and Sacks, S. H. (2008) 'Synthesis of complement protein C3 in the kidney is an important mediator of local tissue injury', *Faseb Journal,* 22, (4), pp. 1065-1072.

Sheerin, N. S., Zhou, W., Adler, S. and Sacks, S. H. (1997) 'TNF-alpha regulation of C3 gene expression and protein biosynthesis in rat glomerular endothelial cells', *Kidney International,* 51, (3), pp. 703-710.

Sjoberg, A. P., Trouw, L. A. and Blom, A. M. (2009) 'Complement activation and inhibition: a delicate balance', *Trends in Immunology,* 30, (2), pp. 83-90.

Springall, T., Sheerin, N. S., Abe, K., Holers, V. M., Wan, H. and Sacks, S. H. (2001) 'Epithelial secretion of C3 promotes colonization of the upper urinary tract by Escherichia coli', *Nature Medicine,* 7, (7), pp. 801-806.

Stahl, P. J. and Felsen, D. (2001) 'Transforming growth factor-beta, basement membrane, and epithelial-mesenchymal transdifferentiation - Implications for fibrosis in kidney disease', *American Journal of Pathology,* 159, (4), pp. 1187-1192.

Staniszewski, W. (2009) 'Virtual microscopy, data management and image analysis in Aperio ScanScope system', *Folia Histochemica Et Cytobiologica,* 47, (4), pp. 699-701.

Stevens, P. E., O'Donoghue, D. J., de Lusignan, S., Van Vlymen, J., Klebe, B., Middleton, R., Hague, N., New, J. and Farmer, C. K. T. (2007) 'Chronic kidney disease management in the United Kingdom: NEOERICA project results', *Kidney International,* 72, (1), pp. 92-99.

Strutz, F., Zeisberg, M., Hemmerlein, B., Sattler, B., Hummel, K., Becker, V. and Muller, G. A. (2000) 'Basic fibroblast growth factor expression is increased in human renal fibrogenesis and may mediate autocrine fibroblast proliferation', *Kidney International,* 57, (4), pp. 1521-1538.

Strutz, F., Zeisberg, M., Ziyadeh, F. N., Yang, C. Q., Kalluri, R., Muller, G. A., Neilson, E. G., Renziehausen, A. and Sisic, Z. (2002) 'Role of basic fibroblast growth factor-2 in epithelial-mesenchymal transformation', *Kidney International,* 61, (5), pp. 1714-1728.

Tang, S., Zhou, W. D., Sheerin, N. S., Vaughan, R. W. and Sacks, S. H. (1999) 'Contribution of renal secreted complement C3 to the circulating pool in humans', *Journal of Immunology,* 162, (7), pp. 4336-4341.

Tang, Z. Y., Lu, B., Hatch, E., Sacks, S. H. and Sheerin, N. S. (2009) 'C3a Mediates Epithelial-to-Mesenchymal Transition in Proteinuric Nephropathy', *Journal of the American Society of Nephrology,* 20, (3), pp. 593-603.

Tapmeier, T. T., Fearn, A., Brown, K., Chowdhury, P., Sacks, S. H., Sheerin, N. S. and Wong, W. (2010) 'Pivotal role of CD4(+) T cells in renal fibrosis following ureteric obstruction', *Kidney International,* 78, (4), pp. 351-362.

Tesch, G. H., Schwarting, A., Kinoshita, K., Lan, H. Y., Rollins, B. J. and Kelley, V. R. (1999) 'Monocyte chemoattractant protein-1 promotes macrophage-mediated tubular injury, but not glomerular injury, in nephrotoxic serum nephritis', *Journal of Clinical Investigation,* 103, (1), pp. 73-80.

Thiel, S., VorupJensen, T., Stover, C. M., Schwaeble, W., Laursen, S. B., Poulsen, K., Willis, A. C., Eggleton, P., Hansen, S., Holmskov, U., Reid, K. B. and Jensenius, J. C. (1997) 'A second serine protease associated with mannan-binding lectin that activates complement', *Nature,* 386, (6624), pp. 506-510.

Thurman, J. M., Ljubanovic, D., Edelstein, C. L., Gilkeson, G. S. and Holers, V. M. (2003) 'Lack of a functional alternative complement pathway ameliorates ischemic acute renal failure in mice', *Journal of Immunology,* 170, (3), pp. 1517-1523.

Thurman, J. M., Ljubanovic, D., Royer, P. A., Kraus, D. M., Molina, H., Barry, N. P., Proctor, G., Levi, M. and Holers, V. M. (2006) 'Altered renal tubular expression of the complement inhibitor Crry permits complement activation after ischemia/reperfusion', *Journal of Clinical Investigation,* 116, (2), pp. 357-368.

Timmerman, J. J., vanderWoude, F. J., vanGijlswijkJanssen, D. J., Verweij, C. L., vanEs, L. A. and Daha, M. R. (1996) 'Differential expression of complement components in human fetal and adult kidneys', *Kidney International,* 49, (3), pp. 730-740.

Timoshanko, J. R., Sedgwick, J. D., Holdsworth, S. R. and Tipping, P. G. (2003) 'Intrinsic renal cells are the major source of tumor necrosis factor contributing to renal injury in murine crescentic glomerulonephritis', *Journal of the American Society of Nephrology,* 14, (7), pp. 1785-1793.

Truong, L. D., Petrusevska, G., Yang, G. A., Gurpinar, T., Shappell, S., Lechago, J., Rouse, D. and Suki, W. N. (1996) 'Cell apoptosis and proliferation in experimental chronic obstructive uropathy', *Kidney International,* 50, (1), pp. 200-207.

Turnberg, D., Botto, M., Lewis, M., Zhou, W. D., Sacks, S. H., Morgan, B. P., Walport, M. J. and Cook, H. T. (2004) 'CD59a deficiency exacerbates ischemia-reperfusion injury in mice', *American Journal of Pathology,* 165, (3), pp. 825-832.

Turnberg, D., Lewis, M., Moss, J., Xu, Y. Y., Botto, M. and Cook, H. T. (2006) 'Complement activation contributes to both glomerular and tubulointerstitial damage in adriamycin nephropathy in mice', *Journal of Immunology,* 177, (6), pp. 4094-4102.

Ucero, A. C., Goncalves, S., Benito-Martin, A., Santamaria, B., Ramos, A. M., Berzal, S., Ruiz-Ortega, M., Egido, J. and Oritz, A. (2010) 'Obstructive renal injury: from fluid mechanics to molecular cell biology', *Opern Access Journal of Urology,* 2, pp. 41-55.

Vandal, K., Rouleau, P., Boivin, A., Ryckman, C., Talbot, M. and Tessier, P. A. (2003) 'Blockade of S100A8 and S100A9 suppresses neutrophil migration in response to lipopolysaccharide', *Journal of Immunology,* 171, (5), pp. 2602-2609.

Vassalotti, J. A., Stevens, L. A. and Levey, A. S. (2007) 'Testing for chronic kidney disease: A position statement from the national kidney foundation', *American Journal of Kidney Diseases,* 50, (2), pp. 169-180.

Wan, F. Y. and Lenardo, M. J. (2009) 'Specification of DNA Binding Activity of NF-kappa B Proteins', *Cold Spring Harbor Perspectives in Biology,* 1, (4), pp. 16.

Wang, W. S., Huang, X. R., Li, A. G., Liu, F., Li, J. H., Truong, L. D., Wang, X. J. and Lan, H. Y. (2005a) 'Signaling mechanism of TGF-beta l in prevention of renal inflammation: Role of Smad7', *Journal of the American Society of Nephrology,* 16, (5), pp. 1371-1383.

Wang, W. S., Koka, V. and Lan, H. Y. (2005b) 'Transforming growth factor-beta and Smad signalling in kidney diseases', *Nephrology,* 10, (1), pp. 48-56.

Welch, T. R. (2001) 'The complement system in renal diseases', *Nephron,* 88, (3), pp. 199-204.

Welch, T. R., Beischel, L. S. and Witte, D. P. (1993) 'Differential Expression of Complement C3 and C4 in the Human Kidney', *Journal of Clinical Investigation,* 92, (3), pp. 1451-1458.

Welch, T. R. and Blystone, L. W. (2009) 'Renal disease associated with inherited disorders of the complement system', *Pediatric Nephrology,* 24, (8), pp. 1439-1444.

Welch, T. R., Frenzke, M. and Witte, D. (2000) 'Evidence of a role for local complement expression in a murine model of progressive glomerulonephritis', *Pediatric Research,* 48, (2), pp. 200-205.

Wessels, M. R., Butko, P., Ma, M. H., Warren, H. B., Lage, A. L. and Carroll, M. C. (1995) 'Studies of Group-B Streptococcal Infection in Mice Deficient in Complement Component C3 or C4 Demonstrate an Essential Role for Complement in Both Innate and Acquired-Immunity', *Proceedings of the National Academy of Sciences of the United States of America,* 92, (25), pp. 11490-11494.

Wetsel, R. A. (1995) 'Structure, Function and Cellular Expression of Complement Anaphylatoxin Receptors', *Current Opinion in Immunology,* 7, (1), pp. 48-53.

Wynn, T. A. (2004) 'Fibrotic disease and the T(H)1/T(H)2 paradigm', *Nature Reviews Immunology,* 4, (8), pp. 583-594.

Yamamoto, T., Noble, N. A., Miller, D. E. and Border, W. A. (1994) 'Sustained Expression of Tgf-Beta-1 Underlies Development of Progressive Kidney Fibrosis', *Kidney International,* 45, (3), pp. 916-927.

Yang, J. W. and Liu, Y. H. (2002) 'Blockage of tubular epithelial to myofibroblast transition by hepatocyte growth factor prevents renal interstitial fibrosis', *Journal of the American Society of Nephrology,* 13, (1), pp. 96-107.

Yeh, C. H., Chiang, H. S., Lai, T. Y. and Chien, C. T. (2011) 'Unilateral Ureteral Obstruction Evokes Renal Tubular Apoptosis via the Enhanced Oxidative Stress and Endoplasmic Reticulum Stress in the Rat', *Neurourology and Urodynamics,* 30, (3), pp. 472-479.

Zhang, Q. L. and Rothenbacher, D. (2008) 'Prevalence of chronic kidney disease in population-based studies: Systematic review', *Bmc Public Health,* 8, pp. 13.

Zhang, W. R., Wang, W., Yu, H., Zhang, Y. J., Dai, Y. B., Ning, C., Tao, L. J., Sun, H., Kellems, R. E., Blackburn, M. R. and Xia, Y. (2012) 'Interleukin 6 Underlies Angiotensin II-Induced Hypertension and Chronic Renal Damage', *Hypertension,* 59, (1), pp. 136-U321.

Zheng, X. F., Zhang, X. S., Sun, H. T., Feng, B. A., Li, M., Chen, G., Vladau, C., Chen, D., Suzuki, M., Min, L., Liu, W. H., Zhong, R., Garcia, B., Jevnikar, A. and Min, W. P. (2006) 'Protection of renal ischemia injury using combination gene silencing of complement 3 and caspase 3 genes', *Transplantation,* 82, (12), pp. 1781-1786.

Zhou, W. D., Marsh, J. E. and Sacks, S. H. (2001) 'Intrarenal synthesis of complement', *Kidney International,* 59, (4), pp. 1227-1235.

Zipfel, P. F. (2006) *Complement and Kidney Disease.*

Zipfel, P. F. and Skerka, C. (2009) 'Complement regulators and inhibitory proteins', *Nature Reviews Immunology,* 9, (10), pp. 729-740.

Zoccali, C., Kramer, A. and Jager, K. J. (2010) 'Chronic kidney disease and end-stage renal disease - a review produced to contribute to the report 'the status of health in the European union: towards a healthier Europe", *Nephrology Dialysis Transplantation*, 3, pp. 213-224.